DISSERTATION

DEVELOPMENT OF AN EXPERIMENTAL MODEL OF PALMAR OSTEOCHONDRAL DISEASE AND REPETITIVE STRESS INJURY IN THE EQUINE METACARPOPHALANGEAL JOINT

Submitted by

Lauren Eileen Smanik

Department of Microbiology, Immunology, and Pathology

In partial fulfillment of the requirements

For the Degree of Doctor of Philosophy in Pathology

Colorado State University

Fort Collins, Colorado

Fall 2025

Doctoral Committee:

Advisor: Kelly S. Santangelo
Co-Advisor: Christopher E. Kawcak

Kurt T. Selberg
Dan Regan
Steve Simske

ABSTRACT

DEVELOPMENT OF AN EXPERIMENTAL MODEL OF PALMAR OSTEOCHONDRAL DISEASE AND REPETITIVE STRESS INJURY IN THE EQUINE METACARPOPHALANGEAL JOINT

Palmar osteochondral disease (POD) is a traumatic fatigue injury of the subchondral bone of the palmaro/plantarodistal third metacarpal/metatarsal (MC3/MT3) condyles that has a wide spectrum of disease severity and is highly prominent amongst the racehorse population. The development and progression of this disease tend to be unpredictable, with the time to lesion progression, the degree and timing of clinical effects, and the severity of disease varying between individual horses. A prominent feature of early POD is trabecular and subchondral bone sclerosis, microcrack formation, and osteocyte necrosis, often visible on advanced diagnostic imaging as a bone marrow lesion (BML). BMLs have been shown to precede and be associated with fatigue injury and structural deterioration in the subchondral bone. A successful model for inducing POD, or repetitive stress injury in general, does not yet exist. Most experimental research involves the use of impact devices that diffusely injure the articular cartilage, serving as a catalyst for disease progression without persistent BMLs. Since there is little to no overlying cartilage damage in the early stages of POD, a technique that produces subchondral bone changes, in a minimally-invasive manner, without diffusely affecting cartilage at the time of lesion induction is critical. An experimental model that would allow researchers to study the progression in a controlled, prospective manner would open the doors for future studies on

variables that may affect lesion severity, as well as an individual horse's risk of injury, and facilitate development of an optimized treatment plan.

This dissertation describes a pilot study focused on the initial development of an experimental model of POD, or maladaptive stress remodeling, in horses. This research evaluated the potential of a previously validated pin penetration model developed by Stewart et al. to create BMLs in the distal third metacarpal condyles of horses. By combining this model with a high-speed treadmill exercise protocol previously shown to induce subchondral bone remodeling, the goal was to induce lesions similar to those in the earlier stages of POD, and to evaluate lesion progression and host response. The results of this pilot study confirmed that the pin penetration model – which involved using a 1.1 mm Steinmann pin to create an osteochondral defect that extended approximately 8 mm from the articular surface into the trabecular bone – combined with 6 months of high-speed treadmill exercise, consistently resulted in BMLs in the palmarodistal MC3 condyles of horses that persisted throughout the study.

The first portion of this work (chapter 3) describes the clinical effects of this experimental model including lameness evaluation and synovial fluid analysis. Similar to POD, this model induced a dynamic, mild to moderate, bilateral forelimb lameness that persisted, though to variable degrees. This corresponded to an increased response to flexion, increased joint effusion and a reduction in range of motion. When evaluating the response using synovial fluid analysis, the total nucleated cell counts and total protein were near or below the upper limits of the reference interval (1,000 cells/uL and 2.5g/dL, respectively). Findings from this experimental model were consistent with a primarily mononuclear response, indicative of a non-inflammatory arthropathy such as that from degenerative or traumatic joint diseases. These results demonstrated why it is critical to pair synovial fluid analysis with clinical examination, as

degenerative processes affecting joints can have minimal to no inflammation reflected in the synovial fluid, with overlap between cell counts from normal and osteoarthritic joints.

The next section (chapter 4) describes the appearance and progression of the experimentally-induced BMLs using digital radiography, magnetic resonance imaging (MRI), and computed tomography (CT). Modifications to both the subchondral and trabecular bones were observed without evidence of significant articular cartilage degeneration on advanced diagnostic imaging. Importantly, the BMLs induced using this model changed over time. While histopathology was not performed until the end of the study period, the combined information obtained from MRI, CT, and the initial study by Stewart et al. allow some assumptions to be made about lesion composition; this would need to be confirmed in future research with earlier histologic evaluation. The initial composition when imaged after 4 weeks was consistent with hemorrhage and edema within the marrow spaces, at which point the BML occupied the greatest percentage of the condylar area. This fluid signal decreased significantly by week 12 and was no longer significantly different compared to baseline. Bone sclerosis was present by week 4 and remained unchanged in size throughout the remainder of the study period; however, these lesions subjectively became more defined by weeks 12 and 24. Resorptive lesions were also observed on CT and MRI near the tip of the pin tract. While the study by Stewart et al., in which the model was developed in the medial femoral condyles of sheep, reported that the trabecular bone must be damaged in addition to the subchondral plate for BMLs to persist, it is possible that a shallower pin tract would allow resorption to occur closer to the subchondral bone, as occurs in clinical POD, with the addition of high-speed treadmill exercise allowing for lesion persistence.

The final portion of this research (chapter 5) describes the characteristics of the BMLs on post-mortem examination at the end of the 24-week study. This was performed via gross

evaluation, microcomputed tomography (microCT), and histopathology. Gross abnormalities were consistent with pathologies of the MC3 condyles shown to be associated with POD including wear lines, subchondral bone bruising visible through the articular cartilage, cartilage loss and ulceration, marginal remodeling of the proximal sesamoid bones, dorsal impact injury, and linear fissures. In support of the diagnostic imaging findings, microCT showed marked and extensive subchondral and trabecular bone sclerosis throughout the palmarodistal condyles in all horses, with density patterns similar to previous reports. Histopathology confirmed the presence of a larger volume of less mineralized bone closer to the articular surface, characterized by regionally extensive thickening of the cancellous trabeculae with variable immature, woven bone in the region surrounding the pin tracts. Additional changes included cavitation of the articular cartilage and subchondral bone plate, extensive myelofibrosis, cellular debris within marrow spaces, and fibroplasia within the tract. While the osseous changes were more extensive, degenerative changes were also observed in the articular cartilage in the regions overlying and immediately adjacent to the pin tracts; however, distant articular cartilage was within normal limits. Based on the results by Stewart et al., this degeneration is suspected to be a result of the extensive subchondral bone damage, similar to clinical disease, and prolonged treadmill exercise.

The results of this pilot study have provided in vivo proof-of-concept that the pin penetration technique combined with high-speed treadmill exercise will produce significant BMLs in the palmar third metacarpal condyles, similar to those seen in the early stages of POD. While further research is still required, this pilot study will provide a foundation for future studies bridging the gap between descriptive, associative, and predictive factors for the progression of POD-type lesions, as well as studies on how to better optimize treatment.

ACKNOWLEDGEMENTS

There were many people involved in the success of this pilot research, none of which would have been possible without their contributions and support. First, I would like to thank the members of my graduate committee. To Dr. Chris Kawcak, thank you for your unwavering support and mentorship throughout this doctoral journey, and for always challenging me to think critically and improve. I am forever grateful that you agreed to take me on as your graduate student – even after serving as my resident advisor and working with me for three years as a surgery resident, fully knowing what you were getting into. Thank you for encouraging me to pursue a research topic I was passionate about and for giving me the opportunity to make it my own. You trusted me and gave me independence, but you were always there to support and guide me when I needed it. I appreciate your support in my (perhaps overly ambitious) decision to take on a clinical faculty role while completing my PhD. Your confidence in my ability to manage both has been both humbling and motivating. You have set an example that I strive to follow – not only in your work as an equine surgeon and as a researcher, but also in how you support and lead those around you. I cannot fully express the impact you have had on me throughout this process, and I feel lucky to have you as my mentor and emotional support faculty. To Dr. Kelly Santangelo, thank you for stepping in as one of my advisors when my faculty role required me to change departments, as well as for your support of my unconventional path through this PhD. Your willingness to support me during a challenging transition made all the difference, and I'm incredibly grateful for the guidance and encouragement you have provided since then. I especially appreciate your help in navigating the difficult process of shaping this dissertation. You had a unique ability to bring improved clarity to my writing, sharing lessons from your mentors and helping me focus on what mattered. Your guidance has been an essential part of my

progress, and I truly appreciate it. To Dr. Kurt Selberg, thank you for putting up with this surgeon's attempts at learning diagnostic imaging, first over my three years as a surgery resident and now my four years as a PhD student. I am happy to say you have certainly taught me a few things, though I think we can both agree that it is still best to have a trusted radiologist on call for assistance. You have also taught me the importance of having fun despite the chaos. I certainly could not have completed this work without your knowledge, help, and support. To Dr. Steve Simske, thank you for your support, guidance, and seemingly constant level of optimism and enthusiasm. You helped me see the importance of and relationship between the immune system and bone remodeling, which will certainly serve me well in the planning of future research. I appreciate the time you spent exploring potential machine learning opportunities using this data in future research, as well as helping me prepare for my preliminary examination. And to Dr. Dan Regan, thank you for joining my committee and helping me navigate the transition to MIP, as well as supporting me in my less-than-traditional path to a PhD. You contributed more to this process than you may realize, and I was glad to have you as part of my team. Thank you for helping me grow and improve as a clinician scientist.

Next, I want to thank those beyond my graduate committee that made this research possible. Of course, this research would not have been possible without the generous funding that was provided. Thank you to the Grayson-Jockey Club Research Foundation and the Graduate Student Research Grant through the American Association of Equine Practitioners Foundation for the Horse for providing financial support for this pilot study, and for your continued contributions to help improve the health of our equine partners.

Thank you to Dr. Holly Stewart. Words cannot express my gratitude for your support throughout this journey. You were a necessary support system for me, helping me learn how to

navigate life as a graduate student. You set an incredible example for me to follow and I am always impressed by what you are able to accomplish. Furthermore, without your incredible and groundbreaking work developing the pin penetration model for your own doctoral work, the research described in this dissertation would not exist. Thank you for helping me apply what you built to an equine model. I look forward to our continued collaborations and friendship in the future. Thank you to everyone involved in the Equine Orthopaedic Research Center, especially Jen Daniels, Natalie Lombard, Ryan Shelton, Dr. Katie Seabaugh, Nikki Phillips, and all the hourlies that helped care for the research horses. Your love and care towards each one of them is unmatched. None of this would have happened, or been even remotely organized, if I did not have such a rockstar team working alongside me. Thank you to Dr. Kelly Zersen for keeping my research horses safe under general anesthesia, and to the imaging technicians in the Translational Medicine Institute for facilitating the hours of advanced diagnostic imaging required in this study. Thank you to Laura Aston for allowing me to be a part of the processing of my research samples for histopathology. This gave me a true appreciation for the difficulties associated with bone research and the immense skill required to make it possible. Thank you to Dr. Mac Harris for your expertise, guidance, and help with the histopathologic evaluations; to Lucas Nakamura for microCT and guiding me on how to perform the analysis; to Dr. Russel Moore for performing the cytologic evaluations for the synovial fluid analysis; and to Dr. Lynn Pezzanite and the Dow Lab for assistance and guidance with the cytokine and Nanostring analyses. Thank you to Amartya Maulik and Tianjian Zhou for your help and guidance through the statistical analysis, including my numerous questions and multiple requests to perform further analysis on an already significant amount of data. Thank you for making sure I understood the process and tests being performed, and for allowing me to be involved. I truly could not have managed this data set

without your assistance. Lastly, thank you to my colleagues in the Johnson Family Equine Hospital and Veterinary Teaching Hospital for your support throughout this doctoral process, without which juggling this program alongside my role as faculty would not have been possible.

Finally, thank you to my friends and family for supporting me throughout every stage of my career, including this one. Thank you to my support system and those special to me in this profession and in life including Dr. KT Steward, Meredith Park, and Dr. Drew Koch. Thank you to Drs. Alicia Bertone and Jennifer Dulin for igniting my passion for equine surgery and orthopedic research as a veterinary student, and setting the foundation for the start of my career. Thank you to my family – my parents, Susan and Jim, and my sister, Katie. Thank you for loving me unconditionally as I pursue my goals, and for always being my biggest cheerleaders. Most of all, thank you to my husband, Kyle. Thank you for supporting me and standing beside me through the ups and downs of this process, and for always being there for me. I wouldn't have been able to do this without you.

TABLE OF CONTENTS

CHAPTER 1:

A REVIEW OF MALADAPTIVE STRESS REMODELING IN THE EQUINE METACARPOPHALANGEAL JOINT

1.1 Introduction

Deterioration of the osteochondral unit, which includes the articular cartilage and the bone beneath it (subchondral bone), secondary to injury is a well-recognized cause of osteoarthritis (OA).[1–3] OA is a progressive, debilitating disease that impacts human and veterinary species alike. OA affects an estimated 32.5 million adults in the United States alone,[4] with an estimated 535-656 million people affected on a global scale (6.8-8.4% of the global population).[5] Not only is there a significant patient burden secondary to the pain, fatigue, and physical limitations, but OA and allied disorders also have a substantial economic impact with over $486 billion in annual costs (direct and indirect).[6,7] The prevalence of OA is only expected to increase and similar trends are occurring in veterinary medicine. OA is the cause of up to 60% of clinical lameness cases in equine athletes, accounting for the greatest single economic loss to the horse industry with an estimated cost of up to $15,000 per year per horse.[8–10] While OA is a collection of overlapping etiologies all sharing a common end-stage, in equine athletes it is most commonly attributed to pathologic and clinical states that develop secondary to acute or chronic trauma.[11]

With the occurrence of catastrophic musculoskeletal injuries placing the racehorse industry under heightened scrutiny, increased efforts are being made to mitigate injury risk and optimize treatment in these animals. Because of the high incidence of injury in the racehorse population, the industry's social license to operate is at risk. A social license to operate (SLO) is

the ongoing acceptance and approval of an industry or organization's activities by the general public. It is a process by which a community grants or withholds permission to an industry to conduct its business. In the context of the racehorse industry, the SLO is closely tied to public perceptions of animal welfare, ethical treatment, and the industry's overall transparency and accountability. If these concerns are not addressed meaningfully, the racehorse industry may face greater regulatory scrutiny, declining public interest, reduced sponsorship, and ultimately, a revocation of its social license—threatening its long-term viability. Probably one of the most important issues affecting racehorse injury rates is chronic trauma resulting in bone fatigue or repetitive stress injury due to continuous cyclical loading and performance at high speeds.[12] This cyclic loading results in microdamage at areas of stress concentration and, with enough time and loading, eventually can result in catastrophic failure. The cost of poor performance and injury has been reported to have a large detrimental impact on sport horse industries. Racehorse injuries in particular have quite devastating effects, both on industry economics and the health of the athletes, contributing to the poor public perception and to increases in both racehorse death and jockey injury and death.[13,14] Economic wastage has been previously reported as $81 million per month nationally, based on a loss of 3% of horses from racing each month and median yearling auction price.[13] Furthermore, median financial return for yearling Thoroughbreds in training that lost 13 to 108 days of training was $23,000 less compared to those that only lost 1 to 11 days.[13,15] The economic, social, and physical impacts of OA and related diseases extend across multiple species and, as such, it has become a heavily researched area in both human and veterinary medicine.[5,7,8,10,13,16–20]

As will be described later in this chapter, the equine metacarpophalangeal joint is at the highest risk of repetitive stress injury in the racehorse,[11,12] with the initiation of disease focused

primarily around derangements in the subchondral bone. Of particular importance in the racehorse industry is palmar osteochondral disease (POD), one of many significant contributors to the development of OA in racehorses. POD is a traumatic fatigue injury of the subchondral bone of the medial and lateral palmar/plantar distal third metacarpal/metatarsal condyles of Thoroughbred racehorses. It is a well-documented disease that still requires further research to fully understand the course of progression, as well as to optimize treatment and minimize loss of racing and training days. As a result, the focus of this dissertation will be on the development of an experimental model to help us continue researching this disease, and other forms of maladaptive stress remodeling, in a controlled, prospective manner.

The joint is considered an organ and all tissues associated with the joint can be injured. When pathologic states arise, it is usually because of dysfunction of one or more of these components; the reaction in the various joint-associated tissues cannot be considered in isolation.[11] Because the health of the joint depends on the sum of its parts to be working in unison, all components must be functional. Derangements in the subchondral bone, such as in cases of POD, and its relationship to the articular cartilage have been recognized to play a critical role in the initiation of osteochondral insufficiency and progression of OA.[21–24] While addressing changes in both the subchondral bone and articular cartilage (collectively termed osteochondral tissues) has become increasingly important for the treatment of joint disease, successful long-term treatment options are currently limited as there are no treatments available that can completely prevent degeneration beyond the innate healing capabilities of the various tissues.

In order to reduce the risk of catastrophic injury in the racehorse population, it is critical to understand the pathophysiology behind repetitive stress injury in the equine metacarpophalangeal joint, and which factors affect an individual horse's risk for injury. We can

then apply this knowledge to develop preventative management strategies and optimize our treatment plans. That being written, one must first have an understanding of the normal anatomy and physiology of the joint tissues being affected, and how they respond to the forces applied to them. In the case of POD, such comprehension begins with the osteochondral unit.

1.2 Anatomy and Physiology of the Osteochondral Unit

1.2.1 Anatomy of the Osteochondral Unit

The osteochondral unit is a critical anatomical and functional component of the whole joint organ, consisting of the trabecular bone, articular cartilage, and the interface between them including the calcified cartilage and the subchondral bone (Figure 1.1). These components are essential for the function and biomechanics of synovial joints, where they play a significant role in load distribution, shock absorption, and the movement of the bony components in relation to each other.

Articular Cartilage

The articular cartilage is the most superficial layer of the osteochondral unit. It consists of hyaline cartilage that covers the articular surface of bones and provides a smooth, sliding surface for joint movement. Articular cartilage is avascular and aneural, with nutrients supplied via diffusion from the synovial fluid.[25,26] The primary cell type in articular cartilage is the chondrocyte, a cell of mesenchymal origin that accounts for 1-12% of the total cartilage volume.[25] The morphology and metabolism of chondrocytes vary according to their depth within the cartilage. The remainder of the total cartilage volume is the extracellular matrix (ECM).

Chondrocytes are located within lacunae in the ECM. The ECM consists of three main components, the first two of which are produced by the chondrocytes: collagen, proteoglycan,

and water (70-80% of the wet weight). On a dry weight basis, the ECM is composed of approximately 50% collagen, 35% proteoglycans, 10% glycoproteins, 3% minerals, 1% lipids, and 1% miscellaneous substances.[25,26] Collagen provides the structural framework for articular cartilage and its remaining matrix components, functioning to counteract the tensile stresses seen at the articular surface.[26] The articular cartilage is composed of primarily type II collagen (90% to 95%).[26,27] Additional types of collagen found in articular cartilage include types III, VI, IX, X, XI, XII, and XIV. Types IX and XI are intimately associated with and provide mechanical stability to the type II collagen network.[26] Proteoglycan molecules are a combination of a core protein and attached glycosaminoglycans. Aggrecan makes up about 85% of the proteoglycans and helps provide resistance to compressive forces. Collectively, these unique structures act to entrap and retain water.

There are four distinct zones that make up the articular cartilage: the superficial zone, intermediate zone, deep zone, and calcified zone. The superficial zone, making up approximately 10% to 20% of the cartilage volume,[28] is characterized by flattened chondrocytes and densely packed collagen fibers that are aligned parallel to the articular surface, providing resistance to shear forces.[25,28] This is where the water content and the chondrocyte density are the highest, the latter being critical for maintaining the integrity of the articular cartilage and protecting the deeper layers from stress.[28] The high-water content also creates a compressible material that can deform under load and redistribute the resulting forces, providing shock absorption at the joint surface. The intermediate zone, representing 40% to 60% of the articular cartilage volume,[28] has randomly arranged collagen fibers, irregularly dispersed, rounded chondrocytes, and a higher proteoglycan content that helps absorb compressive forces.[25] The deep zone, representing approximately 30% of the cartilage volume,[28] contains large chondrocytes and a low collagen

content consisting of large, thick collagen fibers, both of which are aligned perpendicular to the articular surface and contribute to the cartilage's tensile strength.[25] This is where the proteoglycan – particularly aggrecan – content is the highest, and by providing cartilage with its osmotic properties, offers the greatest amount of resistance to compressive forces.[28] The benefits of this inverse gradient between chondrocyte density and proteoglycan content are discussed in section 1.2.2.

Calcified Cartilage

The calcified zone, or calcified cartilage, consists of mineralized cells and matrix that anchor the cartilage to the subchondral bone, ensuring the structural integrity of the joint. The interface between the articular cartilage and the subchondral bone is a complex structure that allows the effective transfer of mechanical forces between the two tissues. It consists of an intermediate zone of calcified cartilage, where cartilage is mineralized to a degree that facilitates anchorage of the collagen fibrils of the deep zone of cartilage to the subchondral bone.[28] It is defined from the articular cartilage by the "tidemark", the interface between the calcified and non-calcified cartilage, and from the subchondral bone plate by a "cement line," marking the point where cartilage tissue transitions into bone.[25,29] Perforations in the tidemark allow for direct contact between the hyaline component of the articular cartilage and the subchondral bone.[30] While the tidemark is crossed by collagen fibers that create a secure link between the calcified cartilage and the articular cartilage, the cement line lacks that same continuity in collagen fibers; therefore, this osteochondral junction creates an important point of weakness in the osteochondral unit.[29] This interface is also important for nutrient exchange and the overall health of the joint, which will be discussed further in section 1.2.2.

Subchondral Bone

Subchondral bone lies beneath the articular cartilage, providing contour to the joint surface and playing a crucial role in load-bearing and stability of the overlying cartilage. It is composed of a dense cortical bone layer (subchondral bone plate) that is connected to the articular cartilage through the anchored collagen fibers within the calcified cartilage layer, providing firm support to the joint surface. In contrast to diaphyseal cortical bone in which the haversian system is perpendicular to the joint surface, the haversian system of the subchondral bone plate runs parallel.[26] This parallel alignment allows it to better disperse axial loads across the joint, further protecting the articular cartilage and providing stability to the joint surface. There is also an underlying spongy (trabeculae or subarticular spongiosa[29]) bone layer that contributes to the elasticity of the joint surface and is contiguous with the medullary cavity. Trabeculae run perpendicular to the joint surface with finer trabeculae forming a complex network between them.[29]

The thickness of the subchondral bone plate will vary depending on location and the magnitude of load, ranging from 10 um to 3 mm in humans and up to 4 mm in horses, with thickness increasing with intense excercise.[25,31,32] The thinner areas of subchondral bone consist of mostly appositional layers that are continuous with trabeculae and have fewer Haversian canals, whereas thicker regions are primarily made up of a network of osteons.[24] The subchondral bone is highly vascularized, allowing for the additional supply of nutrients to the deeper cartilage layers through vascular channels in the bone-cartilage interface. This attributes to the ability of the subchondral bone to respond to both physiologic and pathologic stimuli.[25] The subchondral bone is also highly innervated, with injury to this area being a known source of pain in OA.[16,33]

The subchondral bone is composed of both inorganic and organic components. The inorganic component is made up of hydroxyapatite crystals that impart the subchondral bone with its rigidity.[34] The organic component, the bone extracellular matrix, is made up of predominantly type I collagen, as well as proteoglycan, glycosaminoglycans and water, and provides elasticity and resiliency.[34] While both type I and type II collagen are fibril-forming and serve a structural role, type II collagen can form complex extracellular scaffolds with its other proteins and proteoglycans to bear mechanical forces applied to the joint surface, maintain physiological homeostasis, and provide anchoring sites for chondrocytes, ECM molecules, and growth factors.[35] In contrast, type I collagen – synthesized predominantly by fibroblasts and osteoblasts – is densely packed and its differing composition provides better structure to bones, tendons, ligaments, and many interstitial connective tissues.[35] The composition of subchondral bone is what allows it to effectively disperse axial loads across the articular surface, helping to protect the articular cartilage layer.[36–40]

1.2.2 Physiology of the Osteochondral Unit

The osteochondral unit is a complex and dynamic system where bone, cartilage, and their interface work together to maintain joint function. The articular cartilage covering the joint surface enables smooth, low-friction movement, while each layer of the osteochondral unit both contributes to the joint's mechanical stiffness and experiences varying degrees of strain during movement.[41] This intricate system’s ability to absorb shock, distribute forces, and facilitate nutrient exchange ensures the smooth operation of joints under various mechanical loads. The physiological processes that govern the osteochondral unit are multifactorial, involving biomechanics, cellular activities, and biochemical processes.

Load Distribution and Shock Absorption

The primary physiological function of the osteochondral unit is to distribute loads across the joint and absorb shock during movement. Articular cartilage plays a pivotal role in this process. As mentioned above, the high-water content in cartilage creates a compressible material that can deform under load and redistribute the resulting forces, providing shock absorption at the joint surface. Next, there is a distinct gradient where chondrocyte density increases towards the superficial layer, while the proteoglycan content increases toward the deeper layer. This orientation reflects the specialized functions of the different cartilage zones. The high density of flattened chondrocytes and tightly packed collagen fibers within the superficial zone are designed to protect the deeper layers and withstand sheer stresses. This layer is responsible for most of the tensile properties of cartilage, allowing it to resist the tensile, sheer and compressive forces applied to it during locomotion.[28] The deeper layers, rich in proteoglycans, provide the bulk of the cartilage's compressive strength. Furthermore, the chondrocytes within articular cartilage have cytoplasmic processes that extend into the interterritorial region and sense the biochemical and biomechanical environment, allowing them to respond to articular cartilage loading and appropriately adjust their metabolic processes in response to various anabolic and catabolic growth factors.[25] This function is essential for joint health, particularly in high-impact activities.

The biomechanical behavior of articular cartilage can be further understood when the tissue is viewed as a biphasic medium consisting of a fluid phase, the principal component of which is water, and a solid phase characterized by the permeable ECM.[28] Synovial fluid, which is produced outside of the osteochondral unit by the synovium, also assists with joint biomechanics and is essential for the lubrication of the articular cartilage, reducing friction and

wear during joint movement. The primary boundary lubricants within synovial fluid are hyaluronan and lubricin, which play a key role in reducing friction by adhering to apposing articular surfaces and forming a protective layer that reduces wear and tear of the articular cartilage.[42] Boundary lubrication, while it helps minimize adhesion formation and abrasions between articulating surfaces, is relatively ineffective at physiologic loads.[43] Low friction movement during loading is more likely afforded by fluid-film lubrication, in which a wedge of fluid is created between the two surfaces such that they remain separated.[25,26] This is accomplished through several mechanisms including hydrodynamic, elastohydrodynamic, squeeze film, and hydrostatic lubrication.[25] Referring back to the biphasic nature of the articular cartilage, when load is applied to the articular surface, there is an immediate increase in interstitial fluid pressure and fluid extravasates from the ECM of the articular cartilage, separating the articulating surfaces. As that load decreases, the fluid is resorbed by the cartilage in part due to the attraction between water and aggrecan molecules.[43] Through the interaction between aggrecan and water, offset by the constraints of the collagen network, the articular cartilage is able to maintain a balance of pressure.[26]

The subchondral bone, in turn, provides resistance to excessive deformation, helping to maintain the mechanical properties of the articular cartilage. It also has an unparalleled ability to quickly respond to both the loads placed on it, such as those applied during training, as well as to injury.[44] This is in part due to the proteoglycan content of the bone matrix, which affords it with flexibility and resilience, and the expression of cytokines by cells within the matrix that are critical in cell signaling pathways.[45] Given its relatively low elastic modulus and greater abundance relative to the articular cartilage, most of the shock absorption for the joint is provided by the subchondral bone.[39,40,44] As previously mentioned, forces are transferred and

transformed from the articular cartilage down to the subchondral bone. The calcified cartilage layer assists in creating a continuum of increasing stiffness to minimize the shear stress between these two layers. This, in combination with the irregular contour of the calcified cartilage interface, helps with the transition of shear forces applied to the joint surface to compressive and tensile forces at the level of the subchondral bone.[46] Disruption of this interface, such as in joint injuries or degenerative diseases, can lead to significant biomechanical issues. The compliant trabecular structure of subchondral bone aids in the distribution and dissipation of these forces across the joint,[24] further enhancing the shock-absorbing capacity of the cartilage. In a normal joint environment, there must be a balance between the strength of the subchondral bone and its ability to cushion the joint surface.[44,47]

Each part of the osteochondral unit supports its adjacent structures and, as such, the osteochondral unit is able to compensate for the rate and strength of forces applied during joint loading. This is largely in part to the subchondral bone being in a constant state of bone remodeling,[48] responding to the forces applied to it in accordance with Wolff's Law. This will be discussed further in section 1.3 of this chapter.

Nutrient Exchange and Waste Removal

As articular cartilage is avascular, its nutritional needs are met through the diffusion of nutrients and metabolites from the synovial fluid.[49,50] The nutritional solutes diffuse through the intimal layer of the synovium into the synovial fluid via subintimal vessels, then through the articular cartilage matrix to reach the chondrocytes.[26] The architecture and biomaterials of the chondrocytes support a diffusion gradient from superficial to deep layers. This exchange occurs during the loading and unloading of joints, as just described for lubrication. Conversely, metabolic waste products are removed in a similar fashion.

In addition to serving as a biomechanical coupler between articular cartilage and subchondral bone, the calcified cartilage layer also has an important role in nutrient exchange and biochemical communication. The calcified cartilage acts as a barrier that limits diffusion and restrains vascular invasion from the subchondral bone to the hypoxic environment of the articular cartilage; however, it still permits transport of smaller solutes from the subchondral bone and contributes to the nourishment of the deeper zone of articular cartilage.[51] This has a significant impact on the crosstalk between the articular cartilage and the subchondral bone.

1.3 Response of the Subchondral Bone to Exercise

The avascular nature of cartilage, in addition to the limited proliferation capacity of chondrocytes, results in a limited capacity for intrinsic repair. Collagen turnover tends to be slower than that of other components of the ECM, and the inability to restore the collagen network further limits the ability of articular cartilage to fully repair itself.[26] In response to damage, the body attempts to form a structurally inferior fibrocartilage, resulting in altered joint function and biomechanics. In contrast, the vascularized subchondral bone can contribute to healing by forming new bone in response to injury. Through the process of bone remodeling, subchondral bone, like diaphyseal cortical bone, has the capacity to remove and replace defective bone in order to adapt to changing biomechanical stresses. Mild, subclinical damage that resolves without remodeling induces trabecular thickening and subchondral sclerosis, increasing the strength, stiffness, and fatigue life of the bone.[12,13,52] Under well-adapted circumstances, this reduces damage; however, as will be discussed throughout this section, the levels of microdamage vary and if exercise intensity is not adjusted to allow the body time to properly remove and replace devitalized bone, the damage can be catastrophic.

The response of subchondral bone to mechanical loading can influence both the structure of the bone and the health of the overlying cartilage. The forces incurred by the articular cartilage are transmitted across the calcified cartilage to the subchondral bone, which helps maintain cartilage integrity by serving as a buffer between the articular surface and the underlying tissues. The calcified cartilage layer helps to effectively minimize shear stresses and transfer mechanical forces between the articular cartilage and the subchondral bone through an undulating association with each.[53] The spongy, more elastic underlying trabecular bone further assists with deformation and dissipation of energy across the osteochondral unit, likely also assisting with joint congruency.[34] Each part of the osteochondral unit supports its adjacent structures and as such, it is able to compensate for the rate and strength of forces applied to it. In a normal joint environment, there must be a balance between the strength of the subchondral bone and its ability to cushion the joint surface.[44,47]

Joint motion is determined and restricted by both joint shape and the extraarticular soft tissue support structures, primarily the ligamentous attachments.[34] This, in turn, affects the response within the subchondral bone. The response to loading is also influenced by the associated muscle and tendon groups. Surface loads are generated across the joint to counteract the rotational forces resulting from the ground reaction force acting on the limb's moment arm.[54,55] The muscles and tendons that span the particular joint are the primary contributors to that surface load.[54] Since the moment arm of the tendon is shorter than that of the limb, the tendon-generated forces are much larger than the ground reaction forces; therefore, contact forces within the joint and subchondral bone are amplified.[55]

The skeleton has the ability to adapt to external forces by altering its morphology and metabolism in order to meet different needs.[56] Like other bones in the body, subchondral bone

responds to mechanical loading through mechanotransduction, where mechanical signals such as stress and strain are converted into biochemical signals. Subchondral bone has been shown to be approximately 10 times more deformable than the cortical shaft of long bones,[57] providing it with an inherent capacity to exhibit a variety of responses to both acute and more prolonged, chronic stresses within the joint. As such, changes in the rigidity of the subchondral bone can have repercussions for the mechanical loading of articular cartilage, with subchondral sclerosis being considered an initiating factor rather than secondary sign of OA.[25,53]

The rich vascularization and innervation of the subchondral bone allows it to adapt to the repetitive stresses applied to the joint during locomotion by modeling and remodeling in accordance with Wolff's law. This law states that bone will adapt to the loading to which it is subjected, with bone aligning along the line of principal stress. How the integrity of the bone is altered will depend on the duration, magnitude, and rate of forces applied to the bone.[58] The primary cell types responsible for these processes include osteoblasts and osteoclasts.

Osteoblasts are responsible for the synthesis of new organic bone matrix components (osteoid production via rapid deposition of type I collagen) and the regulation of its mineralization.[45] In normal, adult bone, matrix production and mineralization occur at the same rate. These cells are derived from self-renewing, multipotent mesenchymal stem cells that give rise to osteoprogenitor cells, which differentiate into preosteoblasts and then mature into osteoblasts.[45,58] Osteoclasts are giant, multinucleated cells derived from mononuclear precursor cells of the hematopoietic monocyte-macrophage lineage.[45] These cells originate in the bone marrow and their function is regulated by locally acting cytokines and systemic hormones. Under the stimulation of macrophage colony–stimulating factor (M-CSF), monocytes and osteoclast precursors in the peripheral blood migrate to a specific location within the bone, differentiate into

tissue-specific macrophages, and then fuse with each other to form mature osteoclasts. Another important cytokine produced by stromal cells and osteoblasts, receptor activator of nuclear factor-κB ligand (RANKL), triggers osteoclast formation.[26] The protein osteoprotegerin (OPG) binds RANKL to prevent osteoclast activation,[59] with the ratio of RANKL to OPG determining the balance of bone resorption and bone remodeling. This delicate, dynamic balance is necessary for the maintenance of normal bone morphology.

Bone modeling is defined as the simultaneous but independent formation and resorption of bone at anatomically discrete sites to produce a functional and mechanically purposeful architecture.[55,60] This results in a change in bone shape both microscopically through trabecular thickening, and macroscopically through the endosteal and periosteal formation of new bone.[24] This change in bone shape and volume makes it possible to maintain strains within the bone at a safe level when the loading environment of the bone changes in magnitude.[12,61–63] An increase in loading will result in the net formation of bone, thus strengthening the subchondral bone plate and underlying trabecular bone, while a decrease in loading will cause these layers to weaken through stimulation of bone resorption.[58] This response to exercise is demonstrated in the third metacarpal bones of Thoroughbred racehorses in active race training, characterized by an increase in diaphyseal cortical thickness and in the percent bone volume of the subchondral bone of the distal third metacarpal condyles.[61,64,65] This reaction increases both the stiffness of the subchondral bone and the monotonic yield stress.[66] In contrast, a reduction in diaphyseal bone density and an increase in the porosity of the condylar subchondral bone are observed in horses rested from race training, reducing its ability to handle mechanical stress.[67–69] Net bone resorption in response to reduced loading is also seen in humans.[70,71]

Bone remodeling, also known as bone turnover, is the process of removing bone and replacing it with new bone through the temporally and spatially coupled activation of osteoclasts and osteoblasts, respectively. This process is a defined, synchronized sequence of removal and replacement that proceeds through defined stages of activation, resorption, and formation.[12] This is critical for both bone metabolism and the bone's ability to respond to trauma. In healthy adult humans, this sequence of activation through formation takes approximately 4 months to complete,[72] with the resorption phase alone requiring 6-7 weeks.[73] The duration of the resorption phase is unknown in horses.[12]

Subchondral bone plays a crucial role in joint biomechanics, and its response to exercise can significantly impact overall joint health and function. This process of subchondral bone modeling and remodeling is driven by bone strain, with resorption occurring below the minimum threshold and formation occurring above the maximum threshold; however, the mechanism by which this occurs is unknown.[44,60] Exercise-induced mechanical loading has a profound impact on the remodeling of subchondral bone, leading to changes in bone density, microarchitecture, and strength that improve its ability to distribute loads. This occurs particularly in regions of the subchondral bone that experience the greatest mechanical load. It is critical that a balance between the resorption and formation processes be maintained, as excessive or inappropriate loading can have significant, negative consequences.

1.4 Anatomy and Biomechanics of the Equine Fetlock Joint

The kinematics of a particular joint are a function of both the geometry of the joint surface, major players of which are the articular cartilage and the subchondral bone, and the periarticular supporting structures such as the joint capsule, tendons, ligaments, and muscles.[26] The equine fetlock joint (metacarpophalangeal/metatarsophalangeal joint) is a high-motion,

monoaxial, diarthrodial joint composed of articulations between the distal third metacarpal/metatarsal bone (MC3/MT3), the proximal aspect of the first phalanx, and the medial and lateral proximal sesamoid bones (Figure 1.2). It is a hinge-type joint that is primarily restricted to movement in the sagittal plane. More specifically, there are individual articulations between the distal aspect of MC3/MT3 and the first phalanx, and between the palmar/plantar aspect of the distal MC3/MT3 and the proximal sesamoid bones. The distal end of the MC3/MT3 is made up of the medial and lateral condyles, separated on midline by the mid-sagittal ridge. On either side of the mid-sagittal ridge are the medial and lateral parasagittal grooves. The condyles are responsible for transmitting load from MC3/MT3 to the first phalanx.[74,75] The mid-sagittal ridge is supported by its articulation with the corresponding sagittal groove in the proximal articular surface of the first phalanx. This articulation limits forces to flexion and extension, permitting rotation around the center of the distal end of MC3/MT3 in just the sagittal plane.[76] The fetlock joint is extended in the normal standing position and hyperextended during high speed gaits; therefore, the dorsal surface of the distal MC3/MT3 primarily articulates with the proximal first phalanx, while the palmar/plantar surface articulates with the proximal sesamoid bones.[77]

The medial and lateral proximal sesamoid bones are a pair of triangular or pyramidal shaped bones in which the dorsal articular surface of each articulates with the palmar/plantar aspect of the medial and lateral MC3/MT3 condyles, respectively.[76] This dorsal surface contains both an abaxial and axial portion, the former comprising a significant majority of the articular surface. The abaxial portion of the dorsal articular surface articulates with the respective condyle, while the axial portion is angled at approximately 50° palmar/plantar in the abaxial-to-axial direction, allowing it to match the conformation of the parasagittal grooves and mid-sagittal

ridge of MC3/MT3.[76] Between and connecting the proximal sesamoid bones is the intersesamoidean ligament.

The remaining surfaces of the proximal sesamoid bones are embedded in numerous ligamentous attachments, forming a critical component of the suspensory apparatus.[78] The suspensory apparatus consists of the suspensory ligament, the medial and lateral extensor branches of the suspensory ligament, and the proximal sesamoid bones. The functional continuations of the suspensory apparatus are the distal sesamoidean ligaments (from superficial to deep: straight, oblique, paired cruciate, paired short), which originate and extend distad from the base of the medial and lateral proximal sesamoid bones.[79] The function of the suspensory apparatus is to provide support and stabilization to the fetlock joint both when weight-bearing and during locomotion.[79]

In the normal weight-bearing/standing position, the fetlock joint is in extension. With an increase in ground reaction forces and weight-bearing during locomotion, an increased amount of load is transferred to the first phalanx.[75] Additionally, the palmar/plantar soft tissues, including those of the suspensory apparatus, are stretched. As a result of the collagen arrangement and recruitment, this applied stress is stored in these soft tissue structures as elastic strain energy.[34] When the limb is unloaded during the breakover phase of the stride, the stored energy is returned. This results in flexion of the fetlock joint and assists in limb advancement and forward motion.[76,80,81] This passive energy return also helps reduce the energy expenditure during galloping by up to 50%.[76,82,83]

The fetlock joint, particularly in the forelimbs (metacarpophalangeal joint), is highly susceptible to injury in racehorses because: it has a relatively small surface area with respect to body size; relative to other joints, it has the greatest range of motion of any of the limb joints; it

sustains the greatest forces of acceleration; and in racehorses, all of the weight is transmitted through a single front fetlock joint during one phase of the stride.[77] There is also an abrupt change in the articular surface curvature just beyond the transverse ridge, which is the junction between the dorsal and palmar/plantar aspects of the MC3/MT3 condyles. This transverse ridge becomes more accentuated with racing and race training.[84] It is critical to consider muscle-tendon wrapping when assessing joint load in the equine fetlock, as the joint reaction forces resulting from the wrapping of tendons around the proximal sesamoid bones is of similar magnitude to the forces between the long bones at each joint in the forelimb.[54] Between the ground reaction and muscle forces that are applied to the fetlock joint during locomotion, it undergoes five to seven times its body weight in stress.[85]

During periods of maximal weight-bearing (full stance), the fetlock reaches a state of hyperextension with MC3/MT3 and the first phalanx approaching a right angle.[76] The dorsal surface of the first phalanx becomes compressed by the dorsal articular surface of distal MC3/MT3, while the tensile forces in the suspensory apparatus press the proximal sesamoids and the intersesamoidean ligament against its palmar/plantar aspect.[75,76] Even just during walking, the force exerted on the palmar/plantar MC3/MT3 has been reported to be 35% greater compared to that placed on the dorsal aspect by the first phalanx.[86] Through the resulting compressive and shear forces,[87] a greater percentage of the load is absorbed over a smaller surface area by the proximal sesamoid bones compared to the first phalanx,[74,86] thus predisposing the parasagittal grooves, condyles, and proximal sesamoid bones to injury.

During both early development and race training, MC3/MT3 undergoes bone remodeling in order to manage the loads associated with exercise.[31,62,76,87–90] In fact, controlled exercise has been shown to be modestly beneficial at an early stage, with one study showing that young,

untrained horses (18 months) subjected to exercise had fewer gross fetlock lesions and a higher rate of bone formation when compared to their non-exercised (pastured) counterparts, with no evidence of musculoskeletal damage.[91] According to the pattern of sclerosis seen on diagnostic imaging, mechanical load has been proposed to run obliquely from the palmar/plantar apex of the condyles to the dorsoproximal aspect of the distal epiphysis.[31,62,76,89] Subchondral bone sclerosis is also denser beneath the palmar/plantar articular surface of MC3/MT3 than it is beneath the dorsal aspect, which suggests the biomechanical interactions between the palmar/plantar articular surface and the proximal sesamoid bones are of a higher magnitude of loading than between the dorsal condyles and the proximal first phalanx.[77,86] It is suggested that excessive, repetitive loading and inadequate remodeling contribute to injuries in these more predisposed areas.[76,77,85,87,90,92]

1.5 Pathophysiology of Repetitive Stress Injury in the Equine Fetlock Joint

The properties of subchondral bone are dictated by the stresses experienced by the limb.[55] Racehorses undergo a unique range of musculoskeletal injuries, particularly injuries involving bone. Many of these injuries result from repetitive loading during high-speed work, leading to the gradual accumulation of damage and material fatigue in the bone.[12] The fetlock experiences the highest joint loads and is the most common site for subchondral bone injuries in racehorses. In a study of 2-year-old Thoroughbred racehorses monitored over their first year of race training, a longitudinal change in subchondral bone morphology was observed on CT imaging including a significant increase in subchondral bone sclerosis in the distal MC3/MT3 condyles and parasagittal grooves.[93] The presence of subchondral bone pathology also increased significantly over time in the palmar/plantar condyle, lateral parasagittal groove, medial dorsal condyle, and

medial and lateral ridges of the first phalanx. This repeated high-intensity loading can inevitably result in weakening of the bone and possible catastrophic failure.[94–96]

Joint functionality depends on homeostasis of the osteochondral tissues, which in turn affects the mechanical interactions between and responses of both cartilaginous and mineralized tissues.[41,97,98] The ability of the osteochondral unit to compensate for the rate and coordinated loading of the joint is key for the bone to properly respond to imposed stresses. While the exact factors influencing tissue homeostasis and mechanical response are not fully understood, research suggests that changes in tissue strain can have an impact on certain biochemical signals.[41,99,100] In general, the etiologic mechanisms for OA can be broken down into either abnormal loading on normal cartilage or normal loading on abnormal cartilage.[101] When abnormal tissue characteristics are present within a joint, there is a significant effect on the dissipation of ground reaction forces and their transmission up the limb. Traumatic events or conditions like OA disrupt strain distribution, negatively affecting the biochemical signals that regulate cellular functions[41,102] and altering the structure and composition of the osteochondral unit.[41,103–105] Joint degeneration and OA can occur secondary to damage or disease affecting any one of the articular structures – subchondral bone, synovium, fibrous joint capsule, peri-articular support structures, or articular cartilage – all of which contribute to overall joint dysfunction. In particular, changes in the composition or architecture of the subchondral bone, such as the development of sclerosis and microcracks, can be a significant mediator of OA due to alterations in its mechanical properties. Not only does this change its response to loading, but it can also be a source of inflammatory mediators with degradation of the deeper articular cartilage layers.[106,107]

The limbs in racehorses undergo continuous cyclic loading or repetitive stress. When excessively high loads applied to a joint cause the rate of damage to exceed the bone's ability to repair itself, the decreased compliance of the sclerotic bone results in microtrabecular damage that often progresses to fatigue injuries or insufficiency fractures within the subchondral bone.[95] Fatigue microcrack generation is also seen following prolonged, repetitive loading that exceeds physiological strain levels.[108] This is commonly observed in Thoroughbred and Standardbred racehorses as a repetitive stress or chronic fatigue injury of the subchondral bone – i.e. subchondral bone disease.[55] Subchondral bone disease represents a spectrum of pathologic changes within the subchondral bone that occur when the ability of the bone to compensate for excessive stress is surpassed. The response to repetitive stress transforms into injury once clinical disease becomes apparent.[55] In cases of severe subchondral bone disease, the subchondral bone plate tends to be weaker and the trabecular bone stronger compared to cases of mild disease.[66] As will be discussed throughout this dissertation, the tolerance of these changes by horses varies greatly depending on the individual, with similar lesions resulting in different responses. As such, it is difficult to determine at what stage these lesions become pathologic or at the very least, clinically significant. Typically, by the time clinical signs of injury become apparent, more advanced or gross damage to the joint has already occurred.[109] Additionally, the spectrum of disease and injuries experienced by racehorses may be the result of primary subchondral bone disease, or secondary to more complex injury of the whole joint organ.

As previously discussed, subchondral bone has the capacity to acclimate to changing biomechanical stresses through repeated cycles of adaptive bone modeling and reparative bone remodeling. This is part of the normal adaptive process and enhances its ability to handle the applied mechanical loads during locomotion. This is initially accomplished through the

deposition of new bone, with microcrack removal being delayed by deferred resorption.[108] Repetitive, high-speed exercise impairs these normal repair processes, which are necessary to maintain a structurally and functionally robust bone, favoring net bone formation as osteoclastic resorption is inhibited.[67,84,108] In the equine metacarpus, remodeling is thus reduced during periods of training and racing when microdamage is accumulating.[110] With the inhibition of this remodeling process, the dominant mechanism for maintaining the strength of and strains within the bone is adaptive bone modeling.[12,67] This is suggested to be the reason behind the high density of the subchondral bone of the distal MC3/MT3 condyles in racehorses, with increased bone deposition within the marrow spaces and increased bone volume fraction of the distal subchondral trabecular bone (Figure 1.3a,b).[12,61,64,65,67,108] This is seen on diagnostic imaging as focal areas of subchondral and trabecular bone sclerosis. Unfortunately, the resulting sclerotic bone may contain poorer mineral quality and integrity,[108] with further alterations in both vascular perfusion and nutrient delivery.[111] Subchondral bone sclerosis also reduces the abilities of the subchondral bone to absorb energy during locomotion, thus increasing the risk of abnormal shear forces and tensile failure in the articular cartilage.[53] Despite this exercise-induced reduction in subchondral remodeling, it has been shown that focal remodeling can still occur once failure develops in the subchondral bone. Whitton et al. demonstrated that fatigued subchondral bone in the MC3 condyles is focally remodeled in proportion to the modeling of the surrounding trabecular bone, with focal areas of porosity observed at sites of fatigue failure.[112] In this study, bone eroded surface was two-fold greater per unit area in association with fatigue fractures with an increased volume of surrounding trabecular bone, suggesting that trabecular modeling allows the remodeling and repair of subchondral bone by focally unloading the damaged tissue.

Once the bone remodeling process is eventually initiated, the body must first remove the damaged bone and fatigued matrix through resorption. The reparative actions of bone remodeling are accelerated during periods of rest. This has been demonstrated in equids by a decrease in bone density of the MC3 diaphysis and an increase in porosity of the distal MC3 condyles during rest from training(Figure 1.3c).[12,67–69] Actively remodeling bone is at some structural risk after the initiation of the remodeling process, before maximum replacement and mineralization. During this stage, bone is resorbed faster than it is replaced, leaving it more susceptible to injury due to the increase in porosity. The newly deposited, less mineralized bone also has a relatively low elastic modulus, making it transiently vulnerable to changes in stress and more susceptible to failure.[113] This is especially true in racehorses when repetitive or excessive stress is applied to the remodeling bone during continued training and racing, without giving it the appropriate amount of time to complete this process. Furthermore, until proper integration between the old, highly-mineralized bone and newly formed, lower density bone is achieved, that particular site is predisposed to failure, especially if there is a disparity in their mineral properties as there is no mechanical interlock between these layers.[108]

It is important to note that due to differences in stiffness between bone specimens, there is an inherent variability in the likelihood and timing of injury occurrence not only between individuals, but also between different anatomical locations in the same bone.[12] This inherent variability is also associated with difference in bone porosity, mineralization, and trabecular orientation.[114] It is because of a gradient in mechanical properties of subchondral bone in the MC3 condyles, characterized by a gradient in both bone density and microstructure across the width of the condyles, that condylar fractures occur as an end result of fatigue damage.[66] This is coupled with a steep gradient at the level of the parasagittal grooves. In the distal MC3/MT3

condyles of exercising racehorses, the bone of the distal condyles has a higher stiffness, toughness, yield stress, and reduced porosity relative to that of the mid-sagittal ridge secondary to extensive new bone formation at areas of greater mechanical loading.[66,108] This is consistent with work published by Muir et al. in which microcracking was increased in the condylar grooves of racing Thoroughbreds compared to both other joint regions and to non-racehorses.[115] There is also evidence that this mechanical gradient extends further proximad in the distal condyles in horses with more severe subchondral bone disease.[66] This disparity in bone properties concentrates strain within the parasagittal grooves where bone material density is lower, contributing to a complex process resulting in microcrack formation within the calcified cartilage and subchondral bone layers and eventually, catastrophic injury.[88,96]

The mechanisms through which continuous cyclic loading may progress to repetitive or chronic stress injury include 1) microdamage formation that stimulates a tissue response either resulting in injury repair or disease progression, 2) biomechanical and tissue responses – with or without microdamage – creating an area of weakness, thus predisposing the tissue to injury, or 3) adaptive responses that lead to chronic tissue fatigue, changes in the tissue's material properties, and inevitably to repetitive stress injury.[111] Even though subchondral bone sclerosis may not itself be a problem, it has been associated with the presence of microdamage and may prompt the modification of a horse's training regimen.[116] The likelihood of injury is multifactorial but the magnitude of mechanical loading and the number of loading cycles are believed to play an important role. Bone fatigue is the degradation of a bone's material properties when it is repetitively loaded with forces that are less than the monotonic force required to cause catastrophic failure.[12] Cyclic loading results in microdamage at areas of stress concentration and with enough time and loading, eventually can result in catastrophic failure.[12,44] A structure can

only withstand a certain number of loading cycles, or finite fatigue life, before the cyclic stress results in failure.

The length of a bone's fatigue life decreases exponentially with increasing loads per cycle, the latter also occurring with increasing speeds.[12,117,118] The microcracks that form in the subchondral bone, particularly in the fetlock joint where intra-articular fractures and repetitive stress injuries such as palmar osteochondral disease occur, are similar to the fatigue damage detected experimentally after repeated loading of bone.[12] The microdamage observed in the subchondral bone of the distal MC3/MT3 condyles appears to accumulate throughout a horse's racing career. It has been recommended that in order to limit the risk of fatigue injury in racehorses, the intensity and duration of training and racing should be reduced and/or the duration of rest periods should be increased.[116] In contrast, there are several risk factors associated with an increased risk of chronic fatigue (including % fatigue life accumulated per start) or repetitive stress injury in horses, fractures and other musculoskeletal injuries included – less than 1 or greater than 5 years of active racing,[119–121] increasing age,[116,122–124] starting a racing career at an older age,[125,126] smaller ratio of lateral to medial condyle width,[127] intact males,[128] female,[124] firmer track surfaces potentially resulting in higher speeds,[122–124,129] better finishing position,[124] longer distance races,[120,124,129] and higher rates of accumulation of distance.[130–133] The exact reasons why some of these factors increase a horse's risk for injury are poorly understood; however, it is clear that there is an association between microdamage accumulation and chronic, high-intensity, repetitive loading. That being said, there is support for the benefits of early adaptation to work at high speeds over a minimum cumulative distance below the threshold for detrimental fatigue damage.[12]

In an experimental equine model involving controlled treadmill exercise, subchondral bone microdamage was an early development in exercising horses and was similar, albeit milder, compared to clinical observations.[95] Compared to controls, exercising horses exhibited increased radiopharmaceutical uptake in the distal MC3 condyles with an associated increase in subchondral bone density. Postmortem evaluation of the fetlock joints of racehorses has revealed a wide spectrum of disease processes ranging from articular cartilage fibrillation to subchondral bone sclerosis, necrosis, and collapse.[87] Microscopic changes have also included abnormal subchondral bone matrix, atypical osteocyte morphology, increased osteocyte necrosis, and microcracks co-localized with blood vessels and osteocytic resorption spaces.[115] While subchondral bone injury can occur in the face of an intact, viable articular cartilage surface, the chronic fatigue injuries identified in the fetlock joints of racehorses typically also result in changes to other joint tissues.

Norrdin et al. found that at sites of overload where mechanical trauma is greatest, such as the palmar/plantar apex of the distal MC3/MT3, the height of the calcified cartilage tended to be decreased and the interface irregularity increased. The authors suggested that this was indicative of extension of subchondral bone remodeling to the calcified layer, but that the thickness and irregularity of the calcified cartilage were not consistently related to current subchondral remodeling.[46] These microscopic changes may also vary based on the intensity of exercise, rather than just the duration or total load. While low- to moderate-intensity exercise has been shown to stimulate proteoglycan synthesis, increased cartilage thickness, and increased glycosaminoglycan content, high-intensity exercise – or a supraphysiologic mechanical environment – can have a negative effect on chondrocyte metabolism with proteoglycan depletion, destruction of the collagen framework, reduced vascularization to the articular

cartilage, and increased tissue permeability.[41,115,134–138] Over time, these changes in the subchondral bone and articular cartilage degrade the mechanical behavior of the osteochondral unit, further exacerbating alterations in strain levels[139] and leading to changes beyond the recovery capabilities of the joint tissues.[41] Despite the knowledge that has been gained in this area, there is still much left to learn about the pathophysiology of repetitive stress injury in the equine fetlock joint. In particular, factors affecting the injury risk in an individual horse, as well as the clinical significance of various lesions and the point at which recovery is still possible.

1.6 Palmar Osteochondral Disease (POD)

Palmar osteochondral disease (POD) is a traumatic fatigue injury of the subchondral bone of the medial and lateral palmar/plantar distal third metacarpal/metatarsal condyles of Thoroughbred racehorses. Not only does it limit an equine athlete's potential, but it can also result in chronic pain and OA secondary to a reduction in the structural ability of the subchondral bone to withstand high-intensity exercise.[140] POD has also been associated with progression of generalized joint disease.[141] It has been reported that POD lesion severity is higher in the forelimbs compared to the hind limbs,[77,141,142] and that the medial condyle tends to be more severely affected in the forelimb while the lateral condyle is predominantly affected in the hind limb.[109,141] In contrast, another publication found no significant difference in the distribution of POD lesions between forelimbs and hind limbs, or between lateral versus medial condyles when examined overall and separately within the forelimbs and hind limbs.[143] This is in agreement with another study that found no difference in lesion severity between medial and lateral condyles within forelimbs; although, POD grades were higher in the lateral condyle compared to the medial condyle when examining hind limbs.[144] There appears to be no significant difference

between the right and left limbs when examined overall and separately within the forelimbs and hind limbs.[141–144]

There is a wide spectrum of disease severity, from subtle alterations in bone remodeling to complete collapse of the articular surface.[145] While the true prevalence of POD is unknown, studies have reported that 67-90% of racehorses exhibit POD lesions of some grade,[140,141,143] with 14-30% having lesions of moderate or marked severity.[141,143,144] As a result, POD has been a significant contributor to days lost from training.[146,147] Evidence also suggests that progression is by no means predictable or linear. This section of Chapter 1 will discuss the pathophysiology, clinical signs, diagnosis, and treatment of POD; the appearance of these lesions on postmortem examination will be discussed further in Chapter 5.

1.6.1 Pathophysiology

Through training and racing, racehorses subject their fetlock joints to repetitive overload at high speeds, resulting in subsequent areas of focal fatigue damage to the subchondral bone palmar/plantar to the transverse ridge of the condyles. POD is considered a manifestation of traumatic overload arthrosis, though there is a complexity to the role of subchondral adaptation that requires continued investigation.[143] This hypothesis that the disease is due to repetitive loading is supported by a study on risk factors for POD, which found that cumulative racing exposure and training intensity were associated with higher POD grades.[94] Longer between-race intervals (> 16 weeks) and increased time since racing were associated with lower POD grades. In general, POD begins with microcrack formation and focal sclerosis in younger animals, progressing to severe subchondral bone collapse and lesion formation in the articular cartilage with increasing age and athletic activity (Figure 1.4).[148] It is important to note that age at first race has not been shown to be associated with POD grade,[94] and while the severity or likelihood

of fatigue injury can rise with increasing age, cumulative exercise over a longer career duration is more important and significant than age alone.[94,144]

As previously discussed in section 1.5, the articulation between the palmar/plantar MC3/MT3 condyles and the proximal sesamoid bones during hyperextension is highly predisposed to chronic stress remodeling and subchondral bone injury due to the nature of the forces applied in that area. During a high-speed gallop, the movement of the proximal sesamoid bones against the palmar/plantar condyles creates an articular incongruity that results in the abnormal distribution of stress, contributing to the occurrence of these focal subchondral bone lesions as well as fractures of the proximal sesamoid bones.[149] The potential for alterations in blood supply to the palmar/plantar condyle has also been examined as a contributing factor in the etiopathogenesis of this disease process.[150] A cadaver study performed by Alber et al.[150] found that perfusion to the palmar condyle was significantly decreased when the fetlock was placed in maximal extension compared to passive flexion, with the medial axial and medial middle regions of the condyles being the most vulnerable to maximal extension. Additionally, perfusion was greater in the dorsal condyle compared to the palmar condyle in 78% of specimens in flexion and 92% of specimens in extension. While a cause-and-effect relationship cannot be determined based on this single study, the observed effects of maximal extension on vascular perfusion should be considered as a contributing factor in POD susceptibility – especially with the chronic, repetitive hyperextension observed in racehorses.

A prominent feature of POD is the subchondral bone change that occurs (Figure 1.5). It begins with sclerosis of the subchondral bone of the palmar/plantar condyles in response to repetitive loading.[77] This is followed by microcrack formation, increased microfracture density, and osteocyte necrosis within the subchondral bone plate, as well as thickening and sclerosis of

the surrounding trabecular bone.[144,151] With continued racing, focal areas of sclerotic subchondral bone on the palmar/plantar condyle undergo ischemic necrosis, while the overlying articular cartilage, which derives its nutrition from synovial fluid, remains viable.[77,152] As the body attempts to remodel the damaged subchondral bone, there is an invasion of granulation tissue and increased vascularity at the periphery of the lesion.[77] Deep to this area of necrosis is a zone of new bone formation producing a sclerotic barrier in an attempt to compensate for the biomechanical dysfunction of the lesion.[153] During this time of active remodeling, the subchondral bone is more susceptible to failure until complete replacement and mineralization has occurred.[113] As peripheral resorption occurs around the POD lesion, the support for the overlying articular cartilage is lost and the articular surface of the lesion collapses.[77] Findings associated with an increased extent of articular surface collapse include inward collapse of the calcified cartilage, an increase in which is associated with more microfractures in the calcified cartilage and superficial subchondral bone layers, and reduced porosity of the deep bone layers (6-10mm).[151] Unfortunately, the time for POD lesions to progress to this stage is unknown and seems to vary between individuals. Additionally, it is unknown at which stage these lesions are no longer able to fully remodel and heal under the intact articular surface.

Articular surface collapse appears to be an important step in the progression of POD because, prior to this event, the overlying articular cartilage remains viable. Early POD lesions often have no or minimal grossly visible evidence of overlying cartilage damage, despite the presence of gross pathologic lesions of the subchondral bone. While it has been reported that it is likely changes in bone turnover and the resulting subchondral bone injury that lead to articular cartilage damage, gene expression analysis has shown that changes in cartilage microstructure (ex: decreased proteoglycan anabolism) and gene expression are still detectable in the early

stages.[154] With progression of disease, eventual subchondral bone resorption and displacement results in complete cartilage loss.[141,143,151] Unfortunately, the reparative response of the articular cartilage is limited, with a distinguishable layer of fibrous tissue seen at the articular surface above sites of severe subchondral bone collapse.[148]

While focal resorption of the subchondral bone may contribute to the collapse of the articular surface, there is a theory that greater bone resorption during periods of rest from training is more likely since bone resorption has been shown to be inhibited in equine subchondral bone with the repetitive loading of race training.[67,110] In cases with joint surface incongruity, findings have included inward collapse of the calcified cartilage with extensive microfracturing of the subchondral bone; an increased prevalence of collapse was associated with an increased number of microfractures and with more career starts.[151] Bone eroded surface and subchondral bone porosity were greater when horses changed to a lower exercise level, with focal articular cartilage undermining observed in several of these cases.[151] When comparing horses in active training versus those being rested from training, horses in training have a lower eroded bone surface in the subchondral bone of both the parasagittal groove and condyle, a higher bone area fraction (lower porosity) in the condylar subchondral bone, and a higher osteoid perimeter in the parasagittal groove.[110]

It may not be the sole contributing factor, but it is possible that articular surface collapse could be exacerbated by the acceleration of subchondral resorption during rest from training. It is currently unknown whether lesion size, morphology, degree of bone loss, or a combination of these is most clinically significant and predictive of future collapse. Nevertheless, the transcriptional response of the articular cartilage in the early stages of POD – when only microscopic evidence of cartilage degeneration is detectable – is supportive of the recognized

role of the biomechanical and biochemical relationship between the subchondral bone and articular cartilage in the development of POD.[154]

1.6.2 Clinical Signs

Unfortunately, the clinical impact of varying grades of POD on performance is still not fully understood; however, horses with higher grades of POD are more likely to be presented with a fetlock joint issue while training compared to those without POD.[141] POD primarily presents as a variable, performance-limiting lameness secondary to pain associated with chronic subchondral bone disease in the distal MC3/MT3 condyles. This lameness may not be readily identified in the early stages, especially since this is commonly a bilateral or even quadrilateral disease that can make it more difficult to notice an overt lameness. Lameness may be acute and severe after training/racing and improve with rest, or intermittent lameness and poor performance may linger for weeks to months.[155]

As with many disease processes that begin within the subchondral bone, there may be minimal or no specific localizing clinical signs of disease in the fetlock joint such as joint effusion and swelling or pain on palpation.[85,155,156] In particular, joint effusion is typically absent in early POD due to the lack of articular cartilage involvement and tends to only develop as cartilage damage progresses.[155–158] In a postmortem study of horses with POD, many horses were performing well with no reported signs of lameness prior to presentation.[144] A caveat to this is that lameness may be difficult to identify due to the frequently bilateral and symmetrically distributed lesions that often occur with POD.[144] The lameness can present as a bilateral forelimb or hind limb lameness, or as a short, choppy gait suggestive of disease in all four limbs. The degree of lameness is typically mild to moderate in the early stages (grade 2 out of 5 on the American Association of Equine Practitioners lameness scale[159]), with a reported 60% being

positive to flexion of the fetlock joint.[109] This lameness becomes more severe with advanced disease.

Poor performance is a commonly cited manifestation of POD in racehorses, though there is conflicting evidence in the literature and the question as to whether it is statistically associated with poor performance is still unanswered.[145,160] There is also a poor correlation between the degree of lameness and macroscopic findings.[161] POD lesions are regularly identified on postmortem examination in limbs without catastrophic injury, suggesting that racehorses are capable of training and racing despite these degenerative lesions.[84] It has also been reported that some horses with POD may plateau or even demonstrate continual improvement in clinical signs without treatment and whilst continuing with race training.[145] The individual response to lesion severity is highly variable, with the same lesion causing no negative effects on performance in one horse but proving to be career-ending in another.

1.6.3 Principles of Diagnosis

Detection of SCB disease is a clinical challenge, especially in the early stages where therapeutic intervention may be most beneficial[143,162]; therefore, this is becoming an important focus for future research. POD is a fatigue injury that occurs at an articular site subjected to extreme loads. This has made it difficult to diagnose clinically before the end stages of disease as early radiographic changes compatible with the development of POD are also changes that we see as being characteristic of adaptation to high intensity exercise. The difficulty in diagnosing POD is further compounded by inconsistent blocking patterns[156] and the inability to access the predilection site arthroscopically. At the point of diagnosis (when structural changes have occurred), the disease becomes irreversible and less responsive to therapy, or it remains progressive despite supportive treatment.[143] This emphasizes the importance of prompt

diagnosis, though a definitive diagnosis of early POD lesions is difficult without the use of advanced imaging modalities.[94]

Due to the primary pathology being in the subchondral bone, perineural anesthesia of the palmar/plantar metacarpal/metatarsal nerves has been found to be more useful in cases of POD when compared to intra-articular anesthesia of the metacarpo/metatarsophalangeal joints.[109] In many cases, there will be a dramatic improvement in lameness following a low four-point block; however, more proximal anesthesia of the palmar/plantar metacarpal/metatarsal nerves may be needed for complete resolution.[156] More severe cases in which there is an overlying full-thickness cartilage lesion are more likely to experience improvement in lameness following intra-articular anesthesia as the local anesthetic has access to the primary site of disease.[156]

Digital radiography alone is not a sensitive modality for identification of changes in the quality of the subchondral bone, as bone loss of 30% or greater is typically needed before lesions can be identified.[163,164] This degree of bone change required for radiographic detection combined with a limited ability to isolate the condyles without superimposition makes radiographs unreliable in the detection of POD.[85] As such, negative radiological findings do not rule out POD as a source of pain.[157] Specialized radiographic views have been developed to help improve examination of the palmar aspect of the distal MC3 condyles, including the flexed dorsopalmar, dorsal 125° distal-palmaroproximal (D125Di-PaPr or 125° DP),[92,165,166] and the 10° proximodistal 45° dorsomedial/lateral-palmarolateral/medial obliques (10° DMPLO and DLPMO).[85] Despite these additional views, there are still limitations in the use of radiography to evaluate this area; however, given the ease of access to a majority of equine practitioners and the ease of acquisition, it is often the first-line diagnostic imaging modality for lameness localized to the fetlock. Radiographic indicators of POD commonly include sclerosis, disruption of the

outline of the subchondral bone, focal flattening of the palmar/plantarodistal condyles, and osteophytosis (Figure 1.6).[167] In more severe cases, a central region of radiolucency within the area of sclerosis can be seen, potentially indicative of subchondral bone lysis and localized collapse of the articular cartilage.[85,87,167] Research by Davis et al. has shown that radiography is useful in the later stages of POD, but not for the early diagnosis.[167] If findings on digital radiographs are vague or negative, either repeat radiographs (at least 10-14 days later) or more advanced diagnostic imaging should be considered.

Nuclear scintigraphy is a commonly utilized imaging modality for the detection of fetlock disease in racehorses given its wide availability and primary use as a screening tool. In the palmar condyles of the forelimbs, increased radiotracer uptake (IRU) is most commonly identified biaxially or isolated to the medial condyle; however, in the plantar condyles of the hind limbs, IRU is more common in the lateral condyle.[155,168,169] Despite its popularity and high sensitivity, nuclear scintigraphy has been recognized as a poorly specific diagnostic modality for fetlock joint pathology[169,170] since radiotracer uptake is a measure of osteoblastic activity and blood flow, not a direct indicator of pathology. This is especially true in the equine distal metacarpal/metatarsal condyles due to the substantial amount of adaptive stress remodeling that occurs in the subchondral and trabecular bone,[44,155] making it necessary to distinguish these adaptive changes from pathologic damage (Figure 1.7).[85] Approximately 20-50% of horses with IRU in the fetlock joint will have no radiographic abnormalities.[155,168,171,172] In racehorses, bilateral IRU in the fetlock joint has been identified in 62% of forelimbs and 69% of hind limbs of Thoroughbreds, 73% of forelimbs and 76% of hind limbs of Standardbreds, and in all 4 fetlocks in 28%.[155,171–173] One study even showed a similar pattern of IRU in the fetlocks of both the lame and contralateral limbs of unilaterally lame horses, both in the forelimbs and the hind

limbs.[174] Results are often equivocal unless there is marked asymmetry in IRU between condyles or limbs.[76] Additionally, there is conflicting reports on the correlation between the degree of uptake and prognosis for racing.[143,169] For these reasons, magnetic resonance imaging (MRI) and computed tomography (CT) are becoming more popular and are improving our knowledge on the response of subchondral bone to training and trauma.

MRI is useful as it provides superior anatomic detail and can demonstrate occult bone bruises (bone edema-like signal [hyperintense] on fluid-sensitive sequences), bone sclerosis (hypointense signal), and clinically silent subchondral bone lesions before the obvious loss of articular cartilage. Changes identified on low-field MRI in association with POD include increased signal within the superficial subchondral bone surrounded by an area of low signal (bone mineral densification), on all sequences (Figure 1.8).[175] In 52% of cases, these changes were surrounded by bone marrow lesions (BMLs) in the deeper trabecular bone (Figure 1.8).[175] Diffuse changes indicative of BML formation have been identified associated with the early stages of the disease prior to collapse of the articular surface, with some suggesting that this may be an initial MRI finding. With the use of high-field MRI, these changes can be evaluated in addition to the extent of damage in the articular cartilage. MRI is considered the gold standard for diagnosing early changes in humans with femoral head osteonecrosis, a disease with lesions similar to that of horses with advanced POD, as it is more sensitive than radiography, CT, and nuclear scintigraphy for the diagnosis of early osteonecrosis.[176] That being said, it must still be interpreted with caution as signal changes may be non-specific. For example, areas of apparent sclerosis may just be representative of an increased volume of lower density bone.[177] Despite its potential for diagnosing radiographically-silent bone lesions, particularly in the early stages of

disease, the use of MRI can be limited by expense, limited availability, and a need for anesthesia if a standing unit is not available.

CT imaging has been increasing in popularity due to the ability to perform imaging without general anesthesia, to evaluate the bone in three dimensions, and for the superior level of trabecular bone detail and high spatial resolution for more comprehensive evaluation of stress remodeling within the subchondral bone.[85] In addition, CT has improved diagnostic sensitivity of risk assessment in horses at a higher risk of injury compared to digital radiography.[178] Both fan-beam and cone-beam CT have been validated for detection of pathologic lesions in the fetlock joint of horses,[93,162,179,180] helping to identify subchondral bone pathology not detected on radiographs and characterize additional subchondral bone pathologies in cases with abnormalities identified on other imaging modalities.[162] CT has the capability to detect a spectrum of changes within the subchondral bone of racehorses, from adaptive sclerosis to collapse of the articular surface (Figure 1.9). When compared with macroscopic evaluation, the sensitivity and specificity of diagnosis of POD is 95.8% and 63.6% for fan-beam CT, 85.4% and 81.8% for cone-beam CT, and 69% and 71.4% for MRI.[180] Quantitative CT also shows good correlation with bone density measurement in this region.[181] When evaluating gross POD lesions, one study observed articular surface collapse in only 6/36 condyles while some degree of articular surface collapse was present on 21/36 condyles using high-resolution quantitative CT.[151] With continued research, there is potential for CT, especially standing units, to be applied clinically for earlier recognition of subchondral bone pathology prior to more serious injury. In particular, algorithms are being developed that can more specifically identify early-stage changes in trabecular architecture, thus providing tools for identifying early disease states.[182,183]

As part of the continued effort to prevent or reduce the risk of catastrophic injury in the racehorse population, optimization of diagnostic imaging modalities is an increasing topic of research. A more recent imaging modality with the potential to improve diagnosis of subchondral bone injury and POD in horses is positron emission tomography (PET). A common tracer used for PET imaging of bone is ^{18}F-sodium fluoride (NaF). ^{18}F-NaF, the fluoride in particular, is incorporated in hydroxyapatite crystals at sites of osteoblastic activity, making it an excellent marker of active bone turnover.[184,185] In contrast to other currently-utilized modalities, PET can identify which lesions are actively trying to remodel, giving it the potential to be instrumental in the detection and monitoring of subchondral bone injuries in racehorses, POD included. Previous research has shown that PET is able to identify additional lesions in fetlock joints that were not visible on other modalities such as nuclear scintigraphy, standing MRI and CT, with superior anatomical localization compared to nuclear scintigraphy (Figure 1.10).[170,185] One study also found a significant correlation between PET scores and lameness, something that was not observed for CT imaging.[170] As a functional form of imaging, PET could be particularly useful as a screening tool in racehorses to prevent catastrophic breakdown by helping to distinguish normal adaptive responses from pathologic remodeling, in addition to determining the clinical significance of abnormalities.[170] That being said, in one pilot study of 20 Thoroughbred fetlocks, 13 out of 17 fetlocks without history of lameness showed IRU on PET, some of similar severities to the 3 fetlocks with a history of lameness.[170] This modality has the potential to be a useful imaging technique for determining the significance of POD lesions in racehorses, as well as for studying the changes in metabolic activity of lesions in horses actively working versus resting. But until our ability to establish reference images discriminating between physiologic adaptation

from pathologic remodeling is improved, the clinical significance of findings on PET must be interpreted with caution.[186]

1.6.4 Principles of Treatment

The goals of treating any form of subchondral bone disease are to restore subchondral bone function and prevent progression to bone failure.[55] One significant limitation in the management of POD is the scarcity of research on effective treatment strategies. Several treatment options for POD have been reported but with inconsistent results. The response to intra-articular medications including corticosteroids, hyaluronic acid, and polysulphated glycosaminoglycan has historically been inconsistent or poor.[168] Medications such as isoxsuprine[168] and acetylsalicylic acid[187] have been prescribed to increase blood flow to the sclerotic subchondral bone; however, there is no scientific evidence of their effectiveness for treatment of this particular disease process. A more effective and supported treatment method is active rest to allow time for bone remodeling to occur.[116,144,151]

Treatment typically involves 60-90 days of rest from race training, allowing some horses to return to racing.[109,175] When given an appropriate amount of time for the subchondral bone to remodel and heal, lameness in the early stages of POD may improve with proper rest from training.[153] One study even demonstrated lower POD grades in horses that had been retired from racing for at least 2 months prior to post-mortem examination, and those with a history of extended rest due to other injury.[141] It is likely that rest is most effective, with the highest possibility for lesion healing, in the early stages of POD.[94,109] It must also be considered, however, that during this time of rest the subchondral bone plate weakens and lameness has been reported to recur when horses resume training at faster paces.[12,110,151] These periods of rest are useful to allow for bone healing but have also been shown to result in serious clinical

deterioration with subchondral bone resorption, subsequent collapse of the overlying articular surface, and eventual articular cartilage degeneration.[151] This leads to the development of significant OA and a career-ending lameness.

This condition is difficult to treat in later stages once the bony changes have become extensive; therefore, efforts at early detection and rest from training with paddock exercise are important.[153] Surgical access to the palmar/plantar region of the distal metacarpus/metatarsus is also limited, further complicating treatment. While there is still much information left to be gained in this area, it is likely that the prognosis following rest depends on the severity of loss in the normal subchondral bone architecture and the amount of structural damage to the overlying articular cartilage.[156] Additionally, given the individual variability in clinical response to and progression of these lesions, treatment should be tailored to the individual horse. In order to improve treatment of this disease, further research into the influence of individual risk factors is needed.

1.7 Palmar Osteochondral Disease as a Translational Model

Human research has demonstrated the importance of the subchondral bone in OA[21–23,188] and the horse is considered one of the best and most challenging models for studying orthopedic ailments.[8,189,190] The clinical importance of OA is remarkably similar between the human and equine species, which helps drive the use of the horse as an important research model. Of the animal models used for studying OA in humans, equine articular cartilage has the most similar cellular structure, biochemical makeup, and biomechanical properties to human cartilage, with the cartilage of the equine stifle being the most similar to the human knee.[191] Risk factors for OA development in both species can be attributed to adverse effects of abnormal loading on normal cartilage or normal loading on abnormal cartilage.[192] Additionally, there has been a substantial

effort to develop advanced diagnostic imaging techniques and identify biomarkers of disease in equine.[193–198]

Similar to human athletes, both primary OA and post-traumatic (PT)OA occur in the horse as a result of athletic use.[191] The Thoroughbred racehorse, in particular, is a model in which adaptive failure and associated development of stress fracture is common. Given the multitude of locations and manifestations of subchondral bone disease in these horses, they are also a well-studied model for repetitive stress injury. Similar to human athletes, naturally-occurring OA depends on the use of the horse (ex. carpal and fetlock joints in racehorses vs stifles in western performance horses),[8,191] and it can occur at an early age or later in older horses.[44,96,199] The most recognized locations in racehorses are the palmar/plantar MC3/MT3 condyles,[8,111,200] which are more vulnerable to injury for the reasons discussed in section 1.4 of this chapter. In both species, the response of bone to repetitive stress is the same, with similar risk factors identified in humans as in equine.[201] Higher rates of stress fracture occur in endurance athletes,[202] with an increase in frequency, duration or intensity of training load,[203] and when training on hard surfaces.[203] The horse provides a naturally-occurring model of repetitive stress injury that can be used to help us better understand similar diseases in humans. It must be considered, however, that despite altered regulation of several well-established markers of OA, there is limited activation of proinflammatory and catabolic genes with POD, which suggests a distinct molecular phenotype compared to PTOA.[154]

Subchondral bone injury is a frequent cause of pain causing lameness in horses.[204–206] Early disease within the subchondral bone has been shown to precede more significant disease, both in animals and humans. The bone changes associated with the early stages of POD are similar to those in humans with subchondral attrition in the knee.[151,207] These early stages of

subchondral bone disease have been associated with and preceded by the presence of bone marrow lesions (BML) diagnosed on MRI, representing a generalized term that corresponds to areas of trabecular abnormalities such as hemorrhage, edema, necrosis, and fibrosis. In Thoroughbred racehorses, these BMLs are seen most commonly in association with POD.[208] BMLs have been associated with a variety of disease processes; however, the presence of BMLs on MRI has been strongly associated with the presence and severity of knee pain in humans,[33] and is predictive of and precedes subchondral bone attrition,[24,95,207,209] loss of cartilage volume,[210] and progression of OA.[22,211] In horses, they have been observed in multiple locations within the limb, and may or may not be associated with pain and lameness.[208,212–214] In humans, subchondral bone attrition has been shown to be more likely to occur in joint compartments that experience greater mechanical loads, resulting in increased forces transmitted to the cartilage due to an alteration in subchondral bone, and with increased bone mineral density.[209] As previously described, this same event occurs in repetitive stress injury of the distal MC3/MT3 condyles of the equine fetlock joint, such as POD.

Another human disease process similar to POD is femoral head necrosis. A prospective study on steroid-induced (atraumatic) osteonecrosis of the femoral head found that BMLs on the initial MRI were highly correlated with the onset of hip pain and subsequent collapse of the femoral head,[215] and are considered a marker for potential progression to more advanced disease.[215,216] Several other studies have described MRI evidence of diffuse bone marrow edema in the marrow of the femoral head and neck in early stages of osteonecrosis, with a change to more focal abnormalities occurring with progression.[217–219] That being said, it is possible that the initial MRIs in these studies were acquired later in the disease process. Importantly, similar to POD, it is suspected that abnormal mechanical stress has an important role in the development of

BMLs as opposed to them being representative of ischemic change[215]; however, there is evidence to suggest that ischemic change may occur as an end result. While the etiology of traumatic osteonecrosis of the femoral head may share more similarities to POD than atraumatic osteonecrosis, the imaging appearances and end stage of all three processes are similar.

Reported origins of avascular necrosis are numerous but include traumatic and atraumatic causes – the former consistent with repetitive, forceful athletic activity – after which the final mechanism is critical ischemia.[220,221] The initial BMLs are insidiously symptomatic and primarily responsible for pain early in the disease process, with progression to subchondral bone collapse, degenerative arthritis, and chronic pain.[222,223] Various theories on the pathophysiology exist including vascular disruption secondary to direct trauma or repetitive microdamage, as well as intraosseous vascular compression secondary to BML formation, increased intraosseous pressure, and lastly decreased blood flow within vascular channels.[220,224] Repetitive and excessive loads result in microdamage with vascular disruption, marrow edema with increased intraosseous extravascular pressure, osteocyte necrosis, and lastly, an attempt to remodel the damaged bone. As with POD, the initial lamination of new bone is followed by subchondral bone resorption that exceeds new bone formation, thus resulting in compromise of the structural integrity of the subchondral trabecular bone, loss of support to the subchondral plate, subchondral bone fracture, and focal collapse of the articular surface.[220,224,225]

Based on these similarities, there is a unique opportunity to not only utilize the data on repetitive stress injury and POD in equine athletes to help advance our knowledge on similar diseases in humans, but to also use the data in humans to help study potential treatment options for more advanced cases of equine disease. With the development of a prospective model of

disease in equine, there is a greater chance of this testing being accomplished with the hope of preserving and improving the athletic careers of these animals.

1.8 Experimental Fetlock Trauma Models in the Current Literature

Chronic subchondral bone fatigue injury was first described in clinical cases of injured racehorses.[77] It has since been validated and studied further through numerous clinical studies and experimental equine models.[12,46,87,95,148] Norrdin et al.[87] performed a postmortem histological comparison between limbs from Thoroughbred and Quarter Horse racehorses without histories of lameness euthanized at the track, and limbs from Quarter Horses crosses exercised on a treadmill for 2 months for a study on carpal healing. This study proposed that controlled treadmill exercise, resulting in milder evidence of subchondral bone overload compared to racehorses, may provide a possible model to continue studying the pathogenesis of subchondral bone fatigue injury. Changes in the calcified cartilage layer were described in the metacarpal condyles following 2 months of treadmill exercise, indicating that activated subchondral bone remodeling extends into this calcified layer.[46] Further evaluation of the effects of treadmill exercise on the subchondral bone of both carpal and metacarpophalangeal joints in 2-year-old horses was later performed by Kawcak et al.,[95] comparing 6 months of treadmill exercise to 6 months of hand walking. Exercised horses were significantly lamer at the end of the study, had gross damage in both joints, and had greater IRU and higher subchondral bone density in the metacarpal condyles. This study showed that treadmill exercise can induce adaptive changes in the subchondral bone within 6 months, even in normal horses without disease. Mathematical modelling has been applied to investigate the pathophysiology of bone fatigue and stress fractures, as well as how different mechanisms of failure interact, but with limited validation.[12]

Despite these initial models, much of our information on subchondral bone disease is from postmortem analysis of racehorse cadaver samples. While naturally-occurring models of subchondral bone injury and joint disease are more likely to mimic pathological lesions in degenerative joints of humans,[8] their use is limited by an inconsistency in the level of disease both between individual horses and between individual joints from the same horse.[154] There is further variation in the time to disease development, which is often unknown for horses in these studies, and the stage of disease at the time of death or euthanasia. Where we are particularly lacking in an effective model for research is POD. An experimental technique that produces subchondral bone changes without affecting the articular cartilage at the time of lesion induction is critical for modeling the early stages of POD. Ideally, the progression of these lesions to collapse of the articular surface occurs with intense exercise and maladaptive subchondral bone remodeling without articular lesions serving as a catalyst for progression. Additionally, the model should be reliable and minimally-invasive. A successful model for inducing POD does not yet exist and most research involves the use of impact devices that injure the articular cartilage. Furthermore, these single-impact models are better suited for studying PTOA rather than POD.

Rickey et al.[226] evaluated the efficacy of a single contusive impact injury for inducing POD in the metacarpophalangeal joints of horses. These horses were a variety of breeds and ages. A hand-held spring driven impactor with a 6.5-mm-diameter tip was used through a fluoroscopic and arthroscopic approach to create four impact injuries of 80MPa on the palmarodistal aspect of the medial metacarpal condyles in each treatment limb. This pressure was selected as the optimal pressure required in a preliminary cadaver study to induce chondrocyte death into the deep zone without causing macroscopic damage to the cartilage. The contralateral limb was assigned as a sham limb for comparison, including insertion of the

impactor device without creating lesions. When examined up to 10 months later, this method caused mild, inconsistent, focal osteoarthritic lesions without progressing to POD. There was no significant difference in lameness, radiographic scores, or synovial fluid variables between impact-treated and sham-control limbs. Since there was no difference in lameness scores between limbs, it was likely that the soft tissue damage caused by insertion of the impactor device through the instrument portal was a significant contributor to lameness in these horses. There was also a wide variation in the location, extent, and depth of the impact lesions between condyles, with no significant difference in the area of cartilage disruption within the medial metacarpal condyle between impact-treated and control limbs. The overall results of this study suggested that cartilage damage, not subchondral bone injury, initiated the development of OA.

A more invasive approach to lesion creation was performed by Rice et al.[227] in which a dorsal arthrotomy was performed to access the palmar medial condyle of MC3 with a 1-cm-diameter, rubber-tipped, compressed-air driven device at 27.6MPa. Impact lesions could be seen grossly and on post-procedure MRI in all cases. Interestingly, despite the impact be of lower pressure compared to the previous study, macroscopic evidence of cartilage damage was still present. It is unknown whether, had the horses been exercised rather than euthanized following lesion induction, subchondral bone injury would be apparent. Additionally, due to the maximally invasive nature of the approach, soft tissue trauma in surgery would likely be a contributing factor in the development of post-operative disease. The point of this study was to assess a potential treatment option for more advanced POD rather than study disease progression; however, it highlights the disadvantages of impact devices for creation of POD-like lesions, as well as the need for improved, less invasive models.

Other models published for the induction of OA in the equine fetlock joint include osteochondral chip fragmentation models in the proximodorsal proximal phalanx,[228–232] thus making them inappropriate for the study of subchondral bone injury. In theory, the use of an impact model is appropriate for the induction of subchondral bone injury; however, a model of POD is restricted to models that induce subchondral bone damage without disease progression being initiated by articular cartilage damage. In addition, it is unlikely that a single impact will result in the same degree of subchondral bone changes as chronic, repetitive loading. Access to the palmaro/plantarodistal condyles is limited by the small joint volume, thick periarticular soft tissues of the palmaro/plantarodistal aspect of the joint, limited access for arthroscopic evaluation of that area, and a curved condylar geometry which could create instability of the impactor device.[226] Further research is required to develop a more consistent, reliable, minimally-invasive method for disease induction in the palmar/plantar condyles.

1.9 Purpose of Study

POD is a fatigue injury of the subchondral bone that is highly prominent amongst the racehorse population. There is a wide spectrum of disease severity ranging from subtle alterations in bone remodeling to subchondral attrition and complete collapse of the articular surface. Subchondral BMLs have been shown to be predictive of subchondral attrition, and to precede and be associated with fatigue injury in the subchondral bone.[24,95,207] Targeting treatment to the subchondral bone in the early stages of POD, prior to articular surface collapse, may enhance the local therapeutic effects and improve support to the articular surface. Before we can effectively test this hypothesis, we must first improve our understanding of the progression of POD – which is precisely the goal of this dissertation work.

Evidence shows that the prediction and prognostication of POD progression in horses rests on further disease characterization. The development and progression of this disease tend to be unpredictable, with the time to lesion progression, the degree and timing of clinical effects, and the severity of the disease process varying between individual horses. In clinical practice, horses diagnosed with BMLs in the third metacarpal condyles are treated with 60-90 days of active rest from training. In some cases, this will result in resolution of the BML. In a subset of horses, the lesion returns or progresses once the horse returns to training, with the severity and clinical significance of lesion progression varying between individuals. Unfortunately, many of the current publications on POD are limited by potentially biased samples and small numbers.[145] They are further limited by non-standardized training and rest protocols as the anatomical site and severity of lesions, and rate of joint injury varies significantly between trainers.[142] Additionally, much of the information we have on POD is from postmortem analysis. A successful experimental model for inducing POD lesions does not yet exist and most involve the use of impact devices that injure articular cartilage.[226,227] Since there is little to no overlying cartilage damage in the early stages of POD,[152] an experimental technique that produces subchondral bone changes without affecting cartilage at the time of lesion induction is critical. Furthermore, the model should be reliable and minimally-invasive.

The development of an experimental model of POD, or repetitive stress injury in general, that would allow researchers to study the progression in a controlled, prospective manner would open the doors for future studies on variables that may affect an individual horse's risk of injury and facilitate development of an optimized treatment plan. A reliable, minimally-invasive pin penetration model has been developed to induce BMLs in the femoral condyles of sheep[233] and rats with minimal damage to the articular cartilage and surrounding structures. Further details on

this technique will be provided in Chapter 2. As a novel extension of this work, the purpose of this pilot study was to provide *in vivo* proof of concept of this previously validated pin penetration model, combined with 6-months of high-speed treadmill exercise, in the distal MC3 condyles of horses. The central objective was to develop an experimental model of repetitive stress injury in horses that mimics the early stages of clinical disease. To address this objective, the following specific aims and hypotheses were developed.

1.10 Specific Aims and Hypothesis

An *in vivo* pilot study evaluating the ability to induce early POD lesions in horses has been performed. Based on our findings in other animal models, our central hypothesis was that this technique would consistently induce subchondral bone changes similar to those seen in the early stages of POD and repetitive stress injury, and in humans with subchondral attrition, thus allowing us to potentially improve our understanding of disease progression and develop suitable treatment strategies. Future testing of disease progression and treatment first requires evaluation of the efficacy of this experimental model.

1.10.1 Specific Aim 1 (Chapter 2: Development of an Experimental Model of Palmar Osteochondral Disease in the Equine Metacarpophalangeal Joint)

Before we can design future studies on injury risk and disease progression, we first need an experimental model in the horse that mimics the early stages of disease, particularly the changes in the subchondral bone, without injury to other tissues serving as a catalyst for progression. The specific aim of this chapter was to design a comprehensive model for the induction of lesions consistent with the early stages of POD in horses that could be performed in a minimally-invasive manner. Lesions were created in the distal MC3 condyles of adult horses,

bilaterally and biaxially, and lesion progression and host response were monitored postoperatively. All horses were treadmill-exercised to simulate active race training. It was hypothesized that this pin penetration model would be a simple, minimally-invasive, and reproducible experimental technique for the induction of BMLs in the distal MC3 condyles in horses.

1.10.2 Specific Aim 2 (Chapters 3 through 5)

Once we have a model that induces subchondral bone changes, it is critical to examine the effects of this model in comparison to clinical disease. The specific aim of chapters 3 through 5 was to evaluate lesion progression and host response to the pin penetration model. This was done using clinical examination (Chapter 3), synovial fluid analysis (Chapter 3), and diagnostic imaging (Chapter 4; digital radiography, MRI, CT) of the front fetlock joints over a 6-month period. Gross evaluation of each condyle was performed postmortem at the end of the study period, followed by microCT and histopathology to examine the microscopic effects of the model and to allow for improved comparison to the published literature (Chapter 5). It was hypothesized that the host response and progression of disease would be similar to that published for horses with POD, with clinical examination and advanced diagnostic imaging being suitable to monitor disease progress.

1.11 Figures

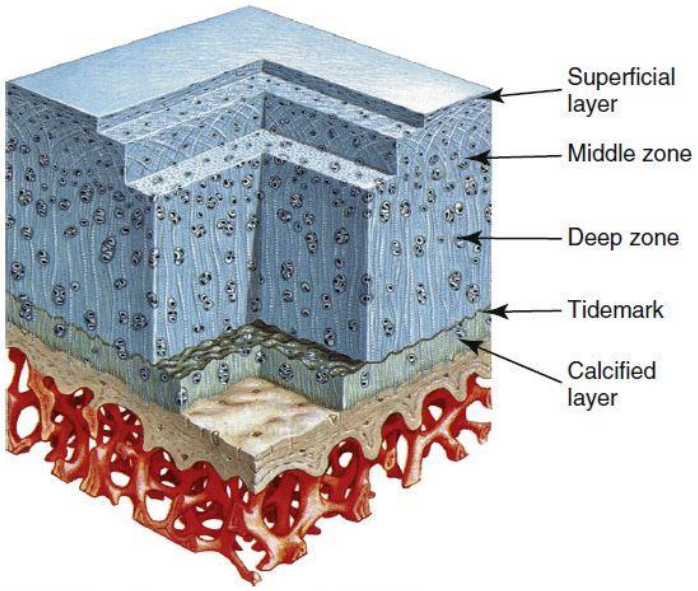

Figure 1.1 – Semischematic drawing of the zonal composition of articular cartilage, sitting on the compact subchondral plate and the underlying trabecular bone. *Reprinted from McIlwraith CW, et al. Joint Disease in the Horse (Second Edition), 2016:1-24, with permission from Elsevier.*

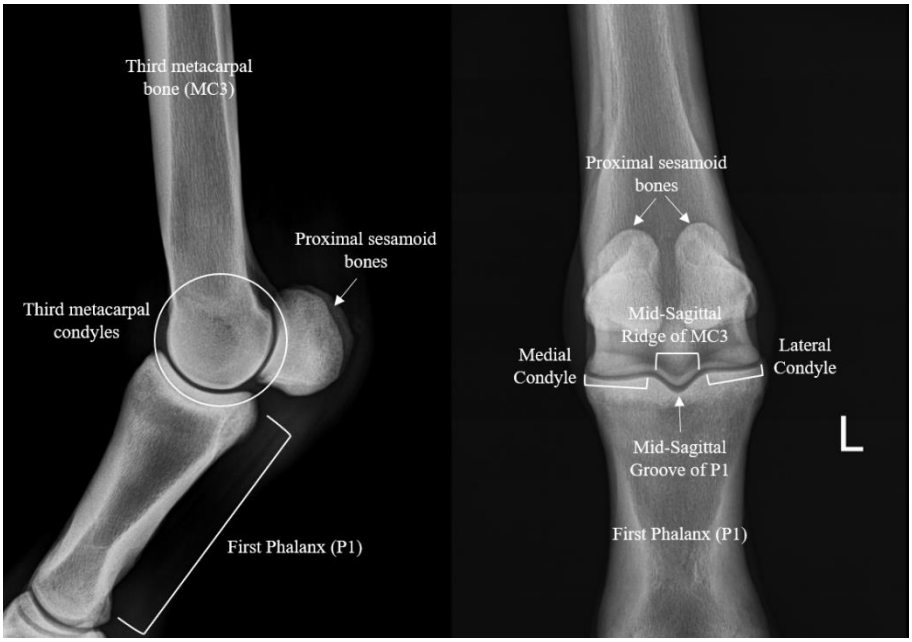

Figure 1.2 – Lateromedial and dorsopalmar radiographs showing the anatomy of the equine metacarpophalangeal (front fetlock) joint in a neutral standing position. The anatomy of the metatarsophalangeal (hind fetlock) joint is identical.

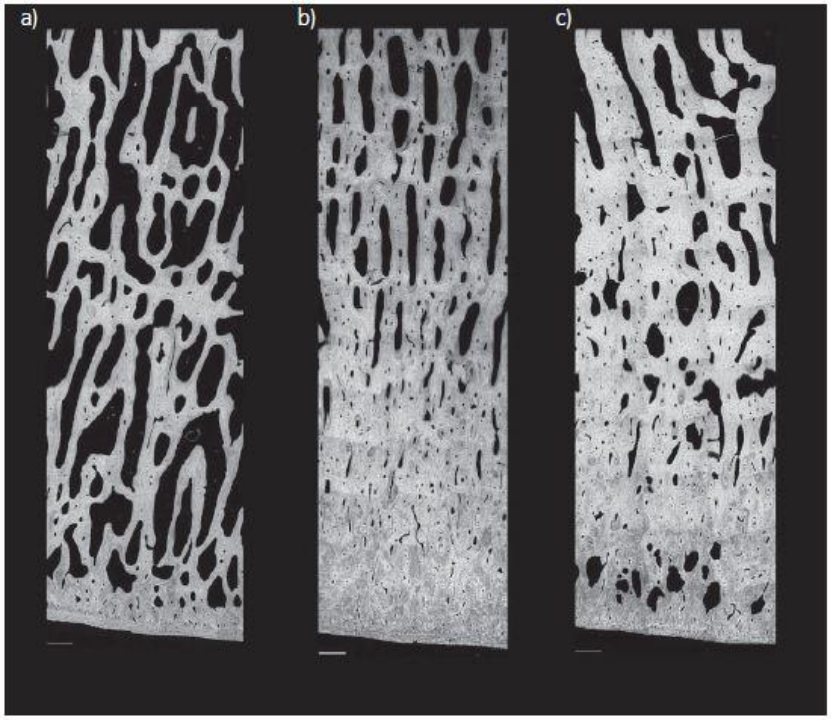

Figure 1.3 – Back-scattered electron microscopy images of the subchondral bone in the palmar aspect of the metacarpal condyle in Thoroughbred racehorses. The articular surface is to the bottom of the images. A) Unraced 2-year-old horse with well-defined trabecular bone underlying the subchondral plate. B) Mature horse in race training. There is infilling of marrow spaces in response to training. C) Mature racehorse that has been resting from training for 9 weeks. Detraining results in increased porosity of the sclerotic subchondral bone. Bars 0.5mm. *Reprinted from Martig S, et al. Bone fatigue and its implications for injuries in racehorses. Equine Vet J. 2014;46:408-415, with permission from John Wiley and Sons.*

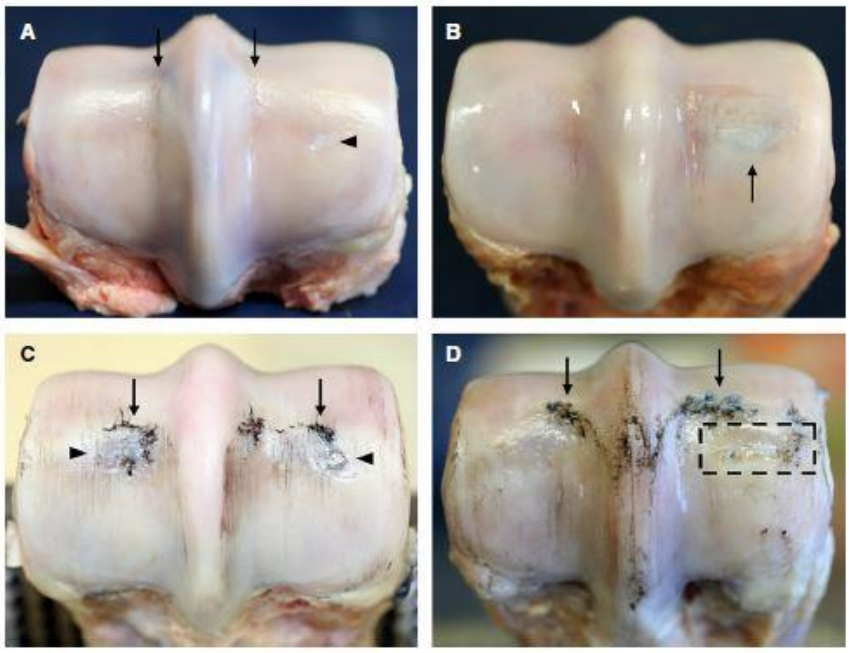

Figure 1.4 – Macroscopic images of the distal end of MC3 from younger (A,B) and older (C,D) animals. Lateral is to the left in all images with India ink staining to define cartilage damage. A) Horse 5 showing an intact cartilage surface except for very slight linear fissures in the parasagittal grooves (see arrows). Note the small oval-shaped area of opaque white cartilage visible in the center of the medial condyle region (see arrowhead). B) Horse 4 with a slightly darkened region beneath undisrupted cartilage (see arrow). C) Horse 14 showing minor wear lines, significant disruption at the transverse ridges (see arrows), and some darkening beneath the cartilage in the central condylar regions (see arrowheads), especially laterally. D) Horse 13 showing a further example of cartilage disruption at the transverse ridge (see arrows). There is an area of the mid-condylar region where the joint surface is noticeably sunken in i.e. collapse of the articular surface (boxed region). *Reprinted from Turley S, et al. Microstructural changes in cartilage and bone related to repetitive overloading in an equine athlete model. J Anat. 2014;224:647-658, with permission from John Wiley and Sons.*

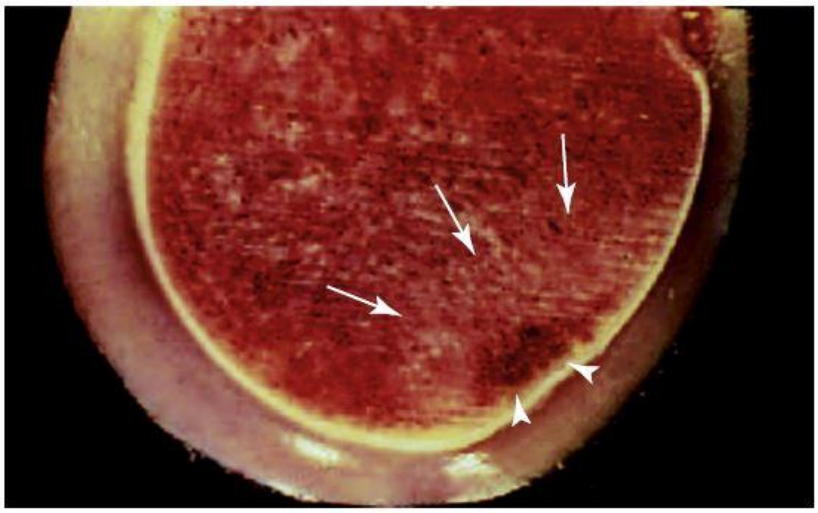

Figure 1.5 – Postmortem sample of a distal metacarpus from the leg opposite to that suffering a catastrophic injury in a racehorse. Although there is intact articular cartilage, subchondral bone necrosis (arrowheads) and sclerosis (arrows) can be seen. *Reprinted from McIlwraith CW, et al. Joint Disease in the Horse (Second Edition), 2016:33-48, with permission from Elsevier.*

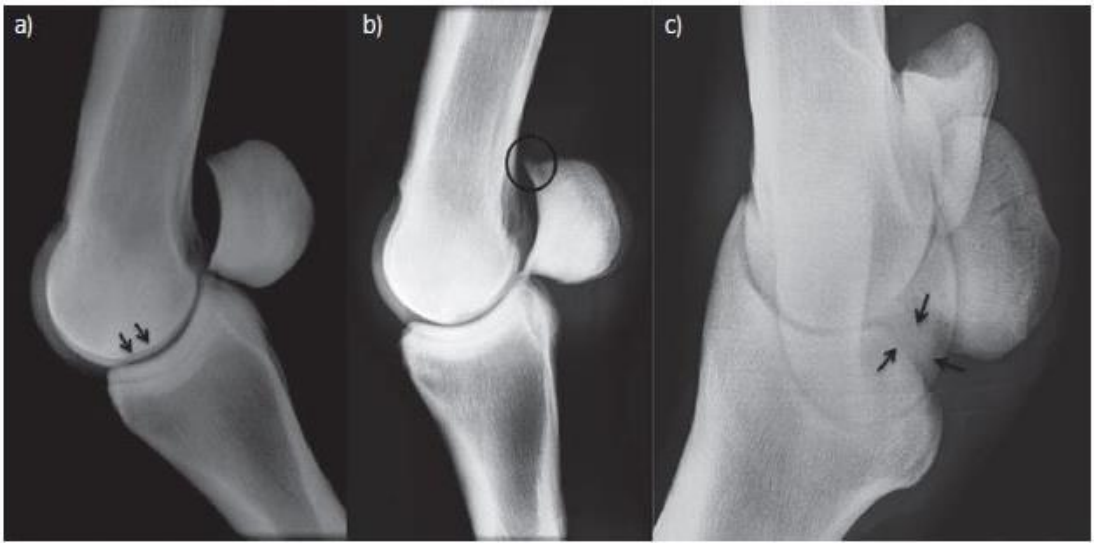

Figure 1.6 – Radiographs illustrating the radiological features included in the final model for diagnosing palmar osteochondral disease: a) Flattening of the palmar condyles, b) Apical osteophyte on the proximal sesamoid bone and c) Sclerosis of the palmar condyles. *Reprinted from Davis A, et al. Improved radiological diagnosis of palmar osteochondral disease in the Thoroughbred racehorse. Equine Vet J. 2017;49:454-460, with permission from John Wiley and Sons*.

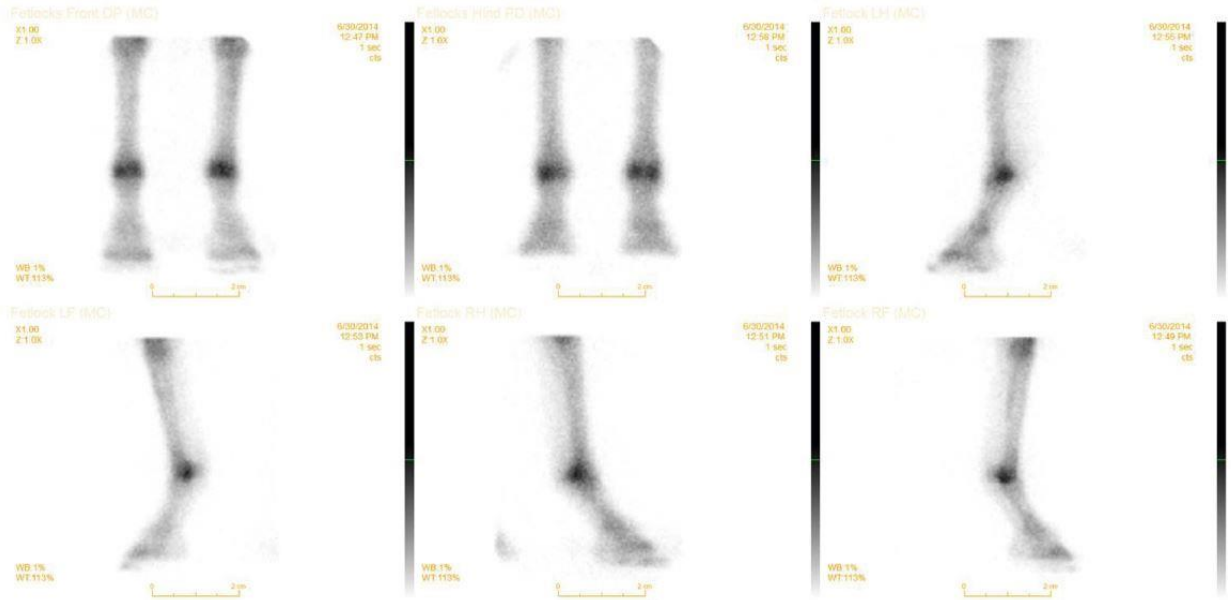

Figure 1.7 – Scintigraphic images of all four fetlocks of a 3-year-old Thoroughbred colt with a short choppy gait and bilateral hind limb lameness that improves to a lateral plantar metatarsal nerve block. Radiographs were unremarkable. There is significant increased radiopharmaceutical uptake affecting the palmar/plantar condyles of all four fetlock joints. (Images courtesy of Dr. Michael Ross, University of Pennsylvania New Bolton Center). *Reprinted from McIlwraith CW, et al. Joint Disease in the Horse (Second Edition), 2016:302-317, with permission from Elsevier.*

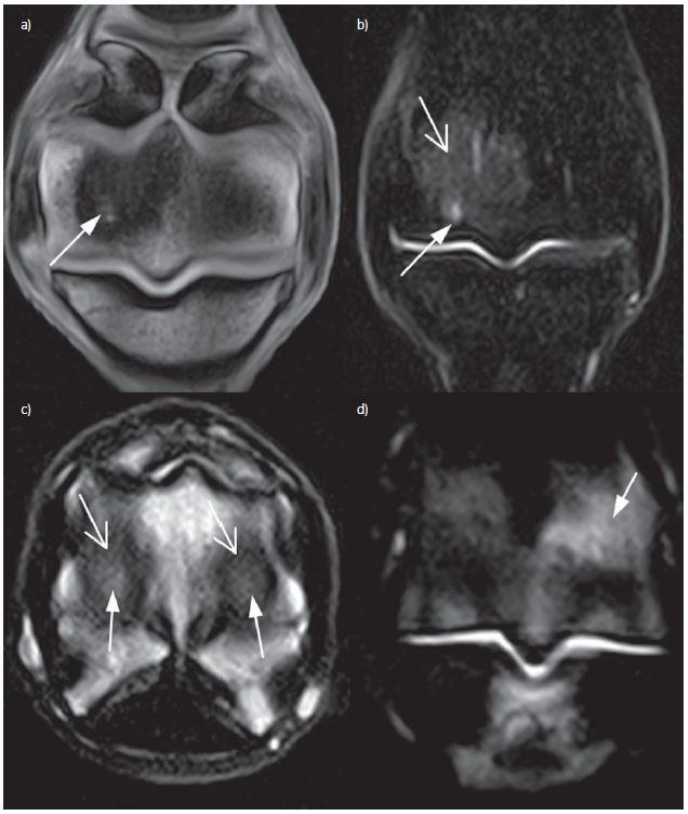

Figure 1.8 – a) T1 GRE dorsal oblique MR image of the same joint. Lateral is to the left. A uniaxial palmar osteochondral disease (POD) lesion is present in the lateral condyle (white arrow). On this sequence the surrounding hypointensity within the trabecular bone could represent the presence of bone mineral densification, fluid or both. b) STIR FSE front image of the same joint. The POD lesion is focally hyperintense at the joint margin (closed white arrow) with generalized STIR hyperintensity within the surrounding bone (open white arrow). c) T2 FSE transverse MR image shows focal, circular hyperintense regions are present at the joint margins (closed white arrows) surrounded by hypointense rim of bone mineral densification (open white arrows). d) The STIR FSE dorsal image reveals generalized hyperintensity within the cancellous bone of the third metatarsal condyles, predominantly the lateral condyle (closed white arrow). *Reprinted from Powell S. Low-field standing magnetic resonance imaging findings of the metacarpo/metatarsophalangeal joint of racing Thoroughbreds with lameness localized to the region: A retrospective study of 131 horses. Equine Vet J. 2012;44:169-177, with permission from John Wiley and Sons*.

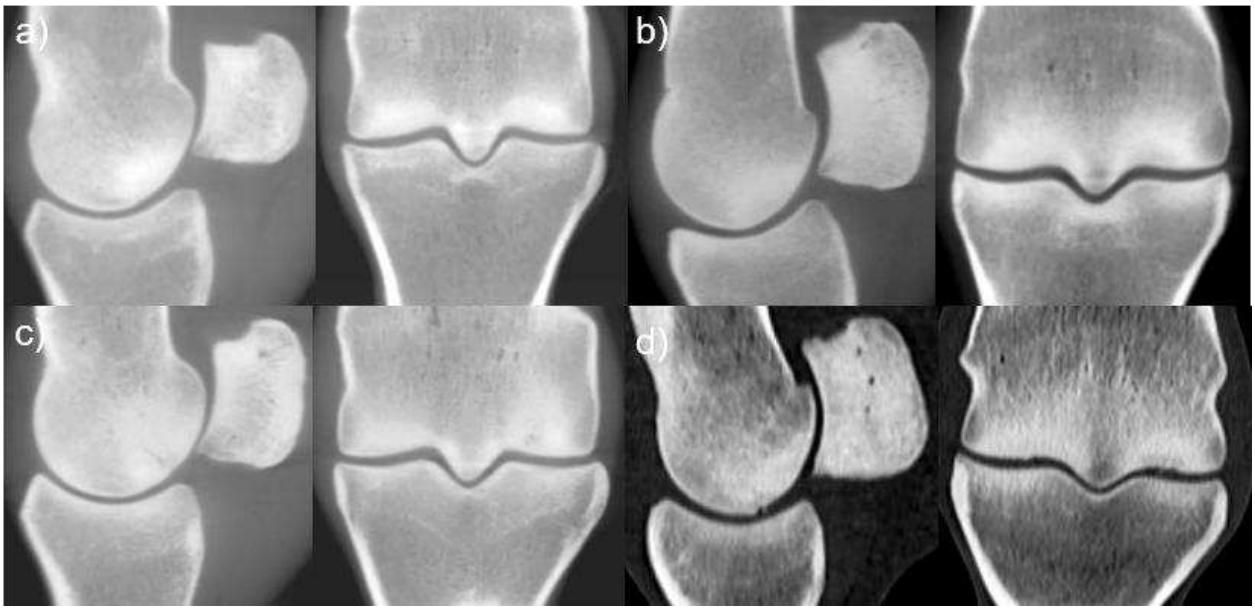

Figure 1.9 – Sagittal (left) and frontal (right) computed tomographic images of the metacarpophalangeal joints of Thoroughbred racehorses demonstrating the range of findings in the various stages of POD. Abnormalities in the palmar aspect of the third metacarpal (MC3) condyles can range from focal sclerosis without evidence of subchondral bone lysis (a), to focal sclerosis surrounding a focal hypointensity suggestive of various degrees of subchondral bone lysis (b, c), to marked focal sclerosis with lysis and collapse of the subchondral plate (d).

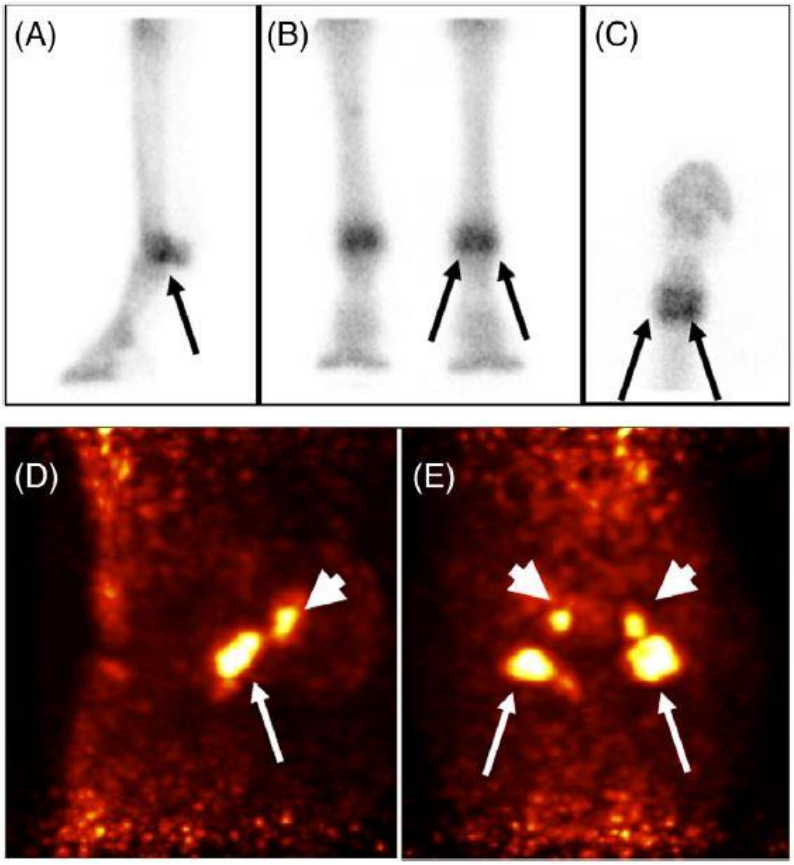

Figure 1.10 – Lateral (A), dorsal (B) and palmar (C) 99mTc-MDP scintigraphic images and lateral (D) and dorsal (E) maximal intensity projection of 18F-NaF PET data of the left front fetlock of a Thoroughbred racehorse. Lateral is to the right on the dorsal images. Increased radiopharmaceutical uptake was recognized in both metacarpal condyles both on scintigraphy and PET imaging (arrows). Focal IRU was also identified biaxially at the dorsal aspect of the proximal sesamoid bones (arrowheads), which was not detected on scintigraphic images. (Scintigraphic images were obtained with a 60-second acquisition and displayed in an arbitrary window width. The PET data were acquired using a 4-minute acquisition and a 12-cm axial field of view and are displayed here as a maximal intensity projection with a window ranging from 0 to 15 standardized uptake values). *Reprinted from Spriet M, et al. Comparison of skeletal scintigraphy and standing 18F-NaF positron emission tomography for imaging of the fetlock in 33 Thoroughbred racehorses. Vet Radiol Ultrasound. 2023;64:123-130, with permission from John Wiley and Sons*.

1.12 References

1. Cicuttini F, Ding C, Wluka A, Davis S, Ebeling PR, Jones G. Association of cartilage defects with loss of knee cartilage in healthy, middle-age adults: A prospective study. *Arthritis Rheum*. 2005;52(7):2033-2039. doi:10.1002/art.21148

2. Davies-Tuck M, Wluka A, Wang Y, et al. The natural history of cartilage defects in people with knee osteoarthritis. *Osteoarthr Cartil*. 2008;16(3):337-342.

3. Ding C, Cicuttini F, Scott F, Boon C, Jones G. Association of prevalent and incident knee cartilage defects with loss of tibial and patellar cartilage: A longitudinal study. *Arthritis Rheum*. 2005;52(12):3918-3927. doi:10.1002/art.21474

4. Cisternas M, Murphy L, Sacks J, Solomon D, Pasta D, Helmick C. Alternative methods for defining osteoarthritis and the impact on estimating prevalence in a US population-based survery. *Arthritis Care Res (Hoboken)*. 2016;68(5):574-580.

5. Steinmetz JD, Culbreth G, Haile L, et al. Global, regional, and national burden of osteoarthritis, 1990-2020 and projections to 2050: a systematic analysis for the Global Burden of Disease Study 2021. *Lancet Rheumatol*. 2023;5(9):e508-e522.

6. United States Bone and Joint Initiative: The Burden of Musculoskeletal Diseases in the United States (BMUS), Fourth Edition, Forthcoming Rosemont, IL.

7. Osteoarthritis Action Alliance. Cost of Osteoarthritis. https://oaaction.unc.edu/policy/cost-of-osteoarthritis/. Published 2024. Accessed February 12, 2025.

8. McIlwraith CW, Frisbie DD, Kawcak CE. The horse as a model of naturally occurring osteoarthritis. *Bone Joint Res*. 2012;1(11):297-309. doi:10.1302/2046-3758.111.2000132

9. Caron J. Osteoarthritis. In: ROSS M, Dyson S, eds. *Diagnosis and Management of Lameness in the Horse*. 2nd ed. St. Louis, Missouri: Elsevier; 2011:655-668.

10. Oke S, McIlwraith C. Review of the Economic Impact of Osteoarthritis and Oral Joint-Health Supplements in Horses. In: *Proceedings of the American Association of Equine Practitioners*. ; 2010.

11. McIlwraith C. Traumatic Arthritis and Posttraumatic Osteoarthritis in the Horse. In: McIlwraith C, Frisbie D, Kawcak C, van Weeren PR, eds. *Joint Disease in the Horse*. Second edi. St. Louis, Missouri: Elsevier; 2016:33-48.

12. Martig S, Chen W, Less P, Whitton RC. Bone fatigue and its implications for injuries in racehorses. *Equine Vet J*. 2014;46:408-415.

13. Stover S. Skeletal Injuries in Equine Athletes - Pathogenesis and Training Concepts for Injury Prevention. In: *Proceedings of the 68th Annual Convention of the American Association of Equine Practitioners*. ; 2022:95-104.

14. Rossdale P, Hopes R, Digby N, Offord K. Epidemiological study of wastage among racehorses 1982 and 1983. *Vet Rec*. 1985;116(3):66-69.

15. Hernandez J, Hawkins D. Training failure among yearling horses. *Am J Vet Res*. 2001;62:1418-1422.

16. Saltzman BM, Riboh JC. Subchondral Bone and the Osteochondral Unit: Basic Science and Clinical Implications in Sports Medicine. *Sport Heal A Multidiscip Approach*. 2018;10(5):412-418. doi:10.1177/1941738118782453

17. Lepage S, Robson N, Gilmore H, et al. Beyond cartilage repair: the role of the osteochondral unit in joint health and disease. *Tissue Eng Part B Rev*. January 2019:ten.TEB.2018.0122. doi:10.1089/ten.TEB.2018.0122

18. Bland S. Canine osteoarthritis and treatments: a review. *Vet Sci Dev*. 2015;5:5931:84-89.

19. Lacourt M, Gao C, Li A, et al. Relationship between cartilage and subchondral bone lesions in repetitive impact trauma-induced equine osteoarthritis. *Osteoarthr Cartil*. 2012;20(6):572-583.

20. Stover S. The epidemiology of Thoroughbred racehorse injuries. *Clin Tech Equine Pract*. 2003;2(4):312-322.

21. Sharkey P, Cohen S, Leinberry C, Parvizi J. Subchondral bone marrow lesions associated with knee osteoarthritis. *Am J Orthop*. 2012;41(9):413-417.

22. Tanamas SK, Wluka AE, Pelletier J-P, et al. Bone marrow lesions in people with knee osteoarthritis predict progression of disease and joint replacement: a longitudinal study. *Rheumatology*. 2010;49(12):2413-2419. doi:10.1093/rheumatology/keq286

23. Gomoll AH, Madry H, Knutsen G, et al. The subchondral bone in articular cartilage repair: current problems in the surgical management. *Knee Surgery, Sport Traumatol Arthrosc*. 2010;18(4):434-447. doi:10.1007/s00167-010-1072-x

24. Stewart HL, Kawcak CE. The importance of subchondral bone in the pathophysiology of osteoarthritis. *Front Vet Sci*. 2018;5:178. doi:10.3389/fvets.2018.00178

25. van Weeren PR. General Anatomy and Physiology of Joints. In: McIlwraith C, Frisbie DD, Kawcak C, van Weeren PR, eds. *Joint Disease in the Horse*. Second Edi. St. Louis, Missouri: Elsevier; 2016:1-24.

26. Frisbie D, Johnson S. Synovial Joint Biology and Pathobiology. In: Auer J, Stick J, Kummerle J, Prange T, eds. *Equine Surgery*. 5th ed. St. Louis, Missouri: Elsevier; 2019:1326-1348.

27. Vachon A, Keeley F, McIlwraith C, Chapman P. Biochemical analysis of normal articular cartilage in horses. *Am J Vet Res*. 1990;51(12):1905-1911.

28. Fox A, Bedi A, Rodeo S. The Basic Science of Articular Cartilage. *Sports Health*. 2009;1(6):461-468.

29. Madry H, van Dijk C, Mueller-Gerbl M. The basic science of the subchondral bone. *Knee Surgery, Sport Traumatol Arthrosc*. 2012;18(4):419-433.

30. Lyons T, McClure S, Stoddart R, McClure J. The normal human chondro-osseous junctional region: evidence for contact of uncalcified cartilage with subchondral bone and marrow spaces. *BMC Musculoskelet Disord*. 2006;7(1):52.

31. Murray RC, Vedi S, Birch H, Lakhani K, Goodship A. Subchondral bone thickness, hardness and remodelling are influenced by short-term exercise in a site-specific manner. *J Orthop Res*. 2001;19(6):1035-1042.

32. Branch M, Murray R, Dyson S, Goodship A. Is there a characteristic distal tarsal subchondral bone plate thickness pattern in horses with no history of hindlimb lameness? *Equine Vet J*. 2005;37(5):450-455.

33. Felson D, Chaisson C, Hill C, et al. The association of bone marrow lesions with pain in knee osteoarthritis. *Ann Intern Med*. 2001;134(7):541-549.

34. Kawcak C. Biomechanics in Joints. In: McIlwraith C, Frisbie DD, Kawcak C, van Weeren PR, eds. *Joint Disease in the Horse*. Second edi. St. Louis, Missouri: Elsevier; 2016:25-32.

35. Alcaide-Ruggiero L, Molina-Hernandez V, Granados M, Dominguez J. Main and Minor Types of Collagens in the Articular Cartilage: The Role of Collagens in Repair Tissue Evaluation in Chondral Defects. *Int J Mol Sci*. 2021;22(24):13329.

36. Radin E, Paul I. Response of joints to impact loading: I. In vitro wear. *Arthritis Rheum*. 1971;14(3):356-362.

37. Simon S, Radin E, Paul I, Rose R. The response of joints to impact loading - II In vivo behavior of subchondral bone. *J Biomech*. 1972;5:267-272.

38. Radin E, Parker H, Pugh J, Steinberg R, Paul I, Rose R. Response of joints to impact loading: III. Relationship between trabecular microfractures and cartilage degeneration. *J Biomech*. 1973;6(1):51-57.

39. Radin E, Paul I. Importance of bone in sparing articular cartilage from impact. *Clin Orthop*. 1971;78:342-344.

40. Radin E, Paul I, Lowy M. A comparison of the dynamic force transmitting properties of subchondral bone and articular cartilage. *J Bone Jt Surg*. 1970;52(3):444-456.

41. Berni M, Marchiori G, Massimiliano B, Gianluca G, Lopoma N. Biomechanics of the human osteochondral unit: A systematic review. *Materials (Basel)*. 2024;17(7):1698-.

42. Walker P, Dowson D, Longfield M, Wright V. “Boosted lubrication” in synovial joints by fluid entrapment and enrichment. *Ann Rheum Dis*. 1968;27(6):512-520.

43. Ekman L, Nilsson G, Persson L, Lumsdan J. Volume of the synovia in certain joint cavities in the horse. *Acta Vet Scand*. 1981;22(1):23-31.

44. Kawcak C, McIlwraith C, Norrdin R, Park R, James S. The role of subchondral bone in joint disease: a review. *Equine Vet J*. 2001;33(2):120-126.

45. Lopez M. Bone Biology and Fracture Healing. In: Auer J, Stick J, Kummerle J, Prange T, eds. *Equine Surgery*. 5th ed. St. Louis, Missouri: Elsevier; 2019:1255-1269.

46. Norrdin R, Kawcak C, Capwell B, McIlwraith C. Calcified Cartilage Morphometry and Its Relation to Subchondral Bone Remodeling in Equine Arthrosis. *Bone*. 1999;24(2):109-114.

47. Kobayashi S, Takei T. Mechanical role of subchondral bone in protecting overlying articular cartilage. *Trans Orthop Res Soc*. 1991;37:73.

48. Clark J, Huber J. The structure of the human subchondral plate. *J Bone Jt Surg*. 1990;72:866-873.

49. Akkiraju H, Nohe A. Role of Chondrocytes in Cartilage Formation, Progression of Osteoarthritis and Cartilage Regeneration. *J Dev Biol*. 2015;3(4):177-192.

50. Poole C. Articular cartilage chondrons: Form, function and failure. *J Anat*. 1997;191(Pt 1):1–13.

51. Wang W, Ye R, Xie W, et al. Roles of the calcified cartilage layer and its tissue engineering reconstruction in osteoarthritis treatment. *Front Bioeng Biotechnol*. 2022;10:911281.

52. Martig S, Hitchens P, Lee P, Whitton R. The relationship between microstructure, stiffness and compressive fatigue life of equine subchondral bone. *J Mech Behav Biomed Mater*. 2020;101:103439.

53. Radin E, Rose R. Role of subchondral bone in the initiation and progression of cartilage damage. *Clin Orthop Relat Res*. 1986;213:34-40.

54. Merritt J, Davies H, Burvill C, Pandy M. Influence of muscle-tendon wrapping on calculations of joint reaction forces in the equine distal forelimb. *J Biomed Biotechnol*. 2008;2008(Article ID 165730):1-9.

55. Smith MRW, Kawcak C, McIlwraith C. Science in brief: Report on the Havemeyer Foundation workshop on subchondral bone problems in the equine athlete. *Equine Vet J*. 2016;48:6-8.

56. Yavropoulou M, Yovos J. The molecular basis of bone mechanotransduction. *J*

Musculoskelet Neuronal Interact. 2016;16(3):221-236.

57. Mankin H, Radin E. Structure and function of joints. In: McCarthy D, ed. *Arthritis and Allied Conditions: A Textbook of Rheumatology*. 12th ed. Philadelphia, PA: Lea & Febiger; 1993:189.

58. Rowe P, Koller A, Sharma S. Physiology, Bone Remodeling. In: *StatPearls [Internet]*. StatPearls. Treasure Island (FL): StatPearls Publishing; 2023.

59. Blair H, Athanasou N. Recent advances in osteoclast biology and pathological bone resorption. *Histol Histopathol*. 2004;19:189-199.

60. Frost H. Skeletal structural adaptations to mechanical usage (SATMU): 2. Redefining Wolff's Law: The remodeling problem. *Anat Rec*. 1990;226(4):414-422.

61. Riggs C, Boyde A. Effect of exercise on bone density in distal regions of the equine third metacarpal bone in 2-year-old thoroughbreds. *Equine Vet J*. 1999;31(S30):555-560.

62. Firth E, Rogers C, Doube M, Jopson N. Musculoskeletal responses of 2-year-old Thoroughbred horses to early training. 6. Bone parameters in the third metacarpal and third metatarsal bones. *N Z Vet J*. 2005;53(2):101-112.

63. Burr D, Schaffler M, Yang K, et al. Skeletal changes in response to altered strain environments: is woven bone a response to elevated strain? *Bone*. 1989;10:223-233.

64. Boyde A, Riggs C, Firth E. Densification by infilling marrow space in response to exercise in thoroughbred horse distal cannon bone. *Bone*. 2001;28:S110-S110.

65. Nunamaker D. Relationships of exercise regimen and racetrack surface to modeling/remodeling of the third metacarpal bone in two year old Thoroughbred racehorses. *Vet Comp Orthop Traumatol*. 2002;15:195-199.

66. Rubio-Martinez L, Cruz A, Gordon K, Hurtig M. Mechanical properties of subchondral bone in the distal aspect of third metacarpal bones from Thoroughbred racehorses. *Am J Vet Res*. 2008;69(11):1423-1433.

67. Whitton R, Trope G, Ghasem-Zadeh A, et al. Third metacarpal condylar fatigue fractures in equine athletes occur within previously modelled subchondral bone. *Bone*. 2010;47(4):826-831.

68. Firth E, Rogers C, van Weeren PR, et al. The effect of previous conditioning exercise on diaphyseal and metaphyseal bone to imposition and withdrawal of training in young Thoroughbred horses. *Vet J*. 2012;192:34-40.

69. Porr C, Kronfeld D, Lawrence L, Pleasant R, Harris P. Deconditioning reduces mineral content of the third metacarpal bone in horses. *J Anim Sci*. 1998;76:1875-1879.

70. Rittweger J, Simunic B, Bilancio G, et al. Bone loss in the lower leg during 35 days of bed

rest is predominantly from the cortical compartment. *Bone*. 2009;44:612-618.

71. Vogel J, Whittle M. Bone mineral changes: the second manned Skylab mission. *Aviat Sp Environ Med*. 1976;47:396-400.

72. Frost H. Transient-steady state phenomena in microdamage physiology: a proposed algorithm for lamellar bone. *Calcif Tissue Int*. 1989;44:367-381.

73. Schaffler M. Bone fatigue and remodeling in the development of stress fractures. In: Burr D, Milgrom C, eds. *Musculoskeletal Fatigue and Stress Fractures*. London: CRC Press; 2001:161-182.

74. Easton K, Kawcak C. Evaluation of increased subchondral bone density in areas of contact in the metacarpophalangeal joint during joint loading in horses. *Am J Vet Res*. 2007;68(8):816-821.

75. Brama P, Karssenberg D, Barneveld A, van Weeren PR. Contact areas and pressure distribution on the proximal articular surface of the proximal phalanx under sagittal plane loading. *Equine Vet J*. 2001;33:26-32.

76. Santschi E. Articular Fetlock Injuries in Exercising Horses. *Vet Clin Equine*. 2008;24:117-132.

77. Pool R, Meagher D. Pathologic findings and pathogenesis and racetrack injuries. *Vet Clin North Am - Equine Pract*. 1990;6(1):1-30.

78. Weaver J, Stover S, O'Brien T. Radiographic anatomy of soft tissue attachments in the equine metacarpophalangeal and proximal phalangeal region. *Equine Vet J*. 1992;24(4):310-315.

79. Fails AD. Functional Anatomy of the Equine Musculoskeletal System. In: Baxter GM, ed. *Equine Surgery*. Seventh Ed. Hoboken, NJ: John Wiley & Sons, Inc.; 2020:1-66.

80. Wilson A, McGuigan M, Su A, van den Bogert A. Horses damp the spring in their step. *Nat*. 2001;414(6866):895-899.

81. Wilson A, Watson J, Lichtwark G. A catapult action for rapid limb protraction. *Nat*. 2003;421(6918):35-36.

82. Dimery N, Alexander R, Ker R. Elastic extension of leg tendons in the locomotion of horses (Equus caballus). *J Zool*. 1987;210(3):415-425.

83. Minetti A, Ardigo L, Reinach E, Saibene F. The relationship between mechanical work and energy expenditure of locomotion in horses. *J Exp Biol*. 1999;202(17):2329-2338.

84. Janes J, Kennedy L, Garrett K, Engiles J. Common lesions of the distal end of the third metacarpal/metatarsal bone in racehorse catastrophic breakdown injuries. *J Vet Diagnostic Investig*. 2017;29(4):431-436.

85. Kawcak C, Barrett MF. Fetlock. In: McIlwraith C, Frisbie D, Kawcak C, van Weeren PR, eds. *Joint Disease in the Horse*. Second Edi. St. Louis, Missouri: Elsevier; 2016:302-317.

86. Lewis C, Williamson A, Chen A, et al. Evaluation of subchondral bone mineral density associated with articular cartilage structure and integrity in healthy equine joints with different functional demands. *Am J Vet Res*. 2005;66(10):1823-1829.

87. Norrdin R, Kawcak C, Capwell B, McIlwraith C. Subchondral bone failure in an equine model of overload arthrosis. *Bone*. 1998;22:133-139.

88. Riggs C, Whitehouse G, Boyde A. Structural variation of the distal condyles of the third metacarpal and third metatarsal bones. *Equine Vet J*. 1999;31:130-139.

89. Reilly G, Currey J, Goodship A. Exercise of young Thoroughbred horses increases impact strength of the third metacarpal bone. *J Orthop Res*. 1997;15:862-868.

90. Radtke C, Danova N, Scollay M, et al. Macroscopic changes in the distal ends of the third metacarpal and metatarsal bones of Thoroughbred racehorses with condylar fractures. *Am J Vet Res*. 2003;64(9):1110-1116.

91. Kawcak C, McIlwraith C, Firth E. Effects of early exercise on metacarpophalangeal joints in horses. *Am J Vet Res*. 2010;71(4):405-411.

92. Kawcak C, Bramlage L, Embertson R. Diagnosis and management of incomplete fracture of the distal palmar aspect of the third metacarpal bone in five horses. *J Am Vet Med Assoc*. 1995;206(3):335-337.

93. Ciamillo S, Wulster K, Gassert T, et al. Prospective, longitudinal assessment of subchondral bone morphology and pathology using standing, cone-beam computed tomography in fetlock joints of 2-year-old Thoroughbred racehorses in their first year of training. *Equine Vet J*. 2025;57:126-139.

94. Pinchbeck G, Clegg P, Boyde A, Barr E, Riggs C. Horse-, training- and race-level risk factors for palmar/plantar osteochondral disease in the racing Thoroughbred. *Equine Vet J*. 2013;45:582-586.

95. Kawcak C, McIlwraith C, Norrdin R, Park R, Steyn P. Clinical effects of exercise on subchondral bone of carpal and metacarpophalangeal joints in horses. *Am J Vet Res*. 2000;61(10):1252-1258.

96. Riggs C, Whitehouse G, Boyde A. Pathology of the distal condyles of the third metacarpal and third metatarsal bones. *Equine Vet J*. 1999;31:140-148.

97. Zhou X, Cao H, Yuan Y, Wu W. Biochemical Signals Mediate the Crosstalk between Cartilage and Bone in Osteoarthritis. *Biomed Res Int*. 2020;2020:1-8.

98. Yuan X, Meng H, Wang Y, et al. Bone–Cartilage Interface Crosstalk in Osteoarthritis: Potential Pathways and Future Therapeutic Strategies. *Osteoarthr Cartil*. 2014;22:1077-

1089.

99. Leong D, Hardin J, Cobelli N, Sun H, Zaidi M. Mechanotransduction and Cartilage Integrity. *Ann New York Acadamy Sci*. 2011;1240(1):32-37.

100. Teichtahl A, Wluka A, Wijethilake P, Wang Y, Ghasem-Zadeh A, Cicuttini F. Wolff's Law in Action: A Mechanism for Early Knee Osteoarthritis. *Arthritis Res Ther*. 2015;17(1):207.

101. Goldring M, Goldring S. Osteoarthritis. *J Cell Physiol*. 2007;213:626-634.

102. Theocharis A, Skandalis S, Gialeli C, Karamanos N. Extracellular Matrix Structure. *Adv Drug Deliv Rev*. 2016;97:4-27.

103. Sanchez C, Pesesse L, Gabay O, et al. Regulation of Subchondral Bone Osteoblast Metabolism by Cyclic Compression. *Arthritis Rheum*. 2012;64(4):1193-1203.

104. Massicotte F, Aubry I, Martel-Pelletier J, Pelletier J, Fernandes J, Lajeunesse D. Abnormal Insulin-like Growth Factor 1 Signaling in Human Osteoarthritic Subchondral Bone Osteoblasts. *Arthritis Res Ther*. 2006;8(6):R177.

105. Zhang L, Wen C. Osteocyte Dysfunction in Joint Homeostasis and Osteoarthritis. *Int J Mol Sci*. 2021;22(12):6522.

106. Berenbaum F. Osteoarthritis as an inflammatory disease (osteoarthritis is not osteoarthrosis!). *Osteoarthr Cartil*. 2013;21:16-21.

107. Kapoor M, Martel-Pelletier J, Lajeunesse D, Pelletier J, Fahmi H. Role of proinflammatory cytokines in the pathophysiology of osteoarthritis. *Nat Rev Rheumatol*. 2011;7:33-42.

108. Boyde A. The real response of bone to exercise. *J Anat*. 2003;203:173-189.

109. Tull T, Bramlage L. Racing prognosis after cumulative stress-induced injury of the distal portion of the third metacarpal and third metatarsal bones in Thoroughbred racehorses: 55 cases (2000-2009). *J Am Vet Med Assoc*. 2011;238:1316-1322.

110. Holmes J, Mirams M, Mackie E, Whitton R. Thoroughbred horses in race training have lower levels of subchondral bone remodelling in highly loaded regions of the distal metacarpus compared to horses resting from training. *Vet J*. 2014;202:443-447.

111. Kawcak C. Pathologic Manifestations of Joint Disease. In: McIlwraith C, Frisbie D, Kawcak C, van Weeren PR, eds. *Joint Disease in the Horse*. 2nd ed. St. Louis, Missouri: Elsevier; 2016:49-56.

112. Whitton R, Mirams M, Mackie E, Anderson G, Seeman E. Exercise-induced inhibition of remodelling is focally offset with fatigue fracture in racehorses. *Osteoporos Int*. 2013;24:2043-2048.

113. Yeh P-H. Traumatic osteochondrosis of the third metacarpal condyle in Thoroughbred racehorses - Gross, histological, high detail radiographic, microradiographic and magnetic resonance imaging findings and their relationship with exercise history. *ProQuest Diss Publ*. 2004:20.

114. Lee T, O'Brien F, Taylor D. The nature of fatigue damage in bone. *Int J Fatigue*. 2000;22:847-853.

115. Muir P, Peterson A, Sample S, Scollay M, Markel M, Kalscheur V. Exercise-induced metacarpophalangeal joint adaptation in the Thoroughbred racehorse. *J Anat*. 2008;213:706-717.

116. Whitton R, Ayodele B, Hitchens P, Mackie E. Subchondral bone microdamage accumulation in distal metacarpus of Thoroughbred racehorses. *Equine Vet J*. 2018;50:766-773.

117. Carter D, Caler W, Spengler D, Frankel V. Uniaxial fatigue of human cortical bone. The influence of tissue physical characteristics. *J Biomech*. 1981;14:461-470.

118. Dendorfer S, Maier H, Taylor D. Anisotropy of the fatigue behaviour of cancellous bone. *J Biomech*. 2008;41:636-641.

119. Parkin T, Clegg P, French N, et al. Horse-level risk factors for fatal distal limb fracture in racing Thoroughbreds in the UK. *Equine Vet J*. 2004;36:513-519.

120. Parkin T, Clegg P, French N, et al. Risk factors for fatal lateral condylar fracture of the third metacarpus/metatarsus in UK racing. *Equine Vet J*. 2005;37:192-199.

121. Vallance S, Entwistle R, Hitchens P, Gardner I, Stover S. Case-control study of high-speed exercise history of Thoroughbred and Quarter Horse racehorses that died related to a complete scapular fracture. *Equine Vet J*. 2013;45:284-292.

122. Bailey C, Reid S, Hodgson D, Bourke J, Rose R. Flat, hurdle and steeple racing: risk factors for musculoskeletal injury. *Equine Vet J*. 1998;30:498-503.

123. Williams R, Harkins L, Hammond C, Wood J. Racehorse injuries, clinical problems and fatalities recorded on British racecourses from flat racing and National Hunt racing during 1996, 1997 and 1998. *Equine Vet J*. 2001;33:478-486.

124. Morrice-West A, Hitchens P, Walmsley E, et al. Relationship between Thoroughbred workloads in racing and the fatigue life of equine subchondral bone. *Sci Rep*. 2022;12(1):11528.

125. Tanner J, Rogers C, Firth E. The association of 2-year-old training milestones with career length and racing success in a sample of Thoroughbred horses in New Zealand. *Equine Vet J*. 2013;45:20-24.

126. Velie B, Knight P, Thomson P, Wade C, Hamilton N. The association of age at first start

with career length in the Australian Thoroughbred racehorse population. *Equine Vet J*. 2013;45:410-413.

127. Kawcak C, Zimmerman C, Easton K, McIlwraith C, Parkin T. Effects of third metacarpal geometry on the incidence of condylar fractures in Thoroughbred racehorses. In: *Proceedings American Association of Equine Practitioners*. ; 2009:197.

128. Estberg L, Stover S, Gardner I, et al. Fatal musculoskeletal injuries incurred during racing and training in Thoroughbreds. *J Am Vet Med Assoc*. 1996;208:92-96.

129. Parkin T, Clegg P, French N, et al. Race- and course-level risk factors for fatal distal limb fracture in racing Thoroughbreds. *Equine Vet J*. 2004;36:521-526.

130. Estberg L, Stover S, Gardner I, Drake C, Johnson B, Ardans A. High-speed exercise history and catastrophic racing fracture in Thoroughbreds. *Am J Vet Res*. 1996;57:1549-1555.

131. Estberg L, Gardner I, Stover S, Johnson B, Case J, Ardans A. Cumulative racing-speed exercise distance cluster as risk factor for fatal musculoskeletal injury in Thoroughbred racehorses in California. *Prev Vet Med*. 1995;24:253-263.

132. Cogger N, Perkins N, Hodgson D, Reid S, Evans D. Risk factors for musculoskeletal injuries in 2-year-old Thoroughbred racehorses. *Prev Vet Med*. 2006;74:36-43.

133. Reed S, Jackson B, Wood J, Price J, Verheyen K. Exercise affects joint injury risk in young Thoroughbreds in training. *Vet J*. 2013;196:339-344.

134. van Weeren PR, Brama P. Effects of Loading/Exercise on Articular Tissues and Developmental Aspects of Joints. In: McIlwraith C, Frisbie D, Kawcak C, van Weeren PR, eds. *Joint Disease in the Horse*. 2nd ed. St. Louis, Missouri: Elsevier; 2016:105-118.

135. Sun H. Mechanical Loading, Cartilage Degradation, and Arthritis. *Ann New York Acadamy Sci*. 2010;1211:37-50.

136. Singh P, Marcu K, Goldring M, Otero M. Phenotypic Instability of Chondrocytes in Osteoarthritis: On a Path to Hypertrophy. *Ann New York Acadamy Sci*. 2019;1442:17-34.

137. Goldring M. Articular Cartilage Degradation in Osteoarthritis. *HSS J*. 2012;8:7-9.

138. Waldstein W, Perino G, Gilbert S, Maher S, Windhager R, Boettner F. OARSI Osteoarthritis Cartilage Histopathology Assessment System: A Biomechanical Evaluation in the Human Knee. *J Orthop Res*. 2016;34:135-140.

139. Peters A, Akhtar R, Comerford E, Bates K. The Effect of Ageing and Osteoarthritis on the Mechanical Properties of Cartilage and Bone in the Human Knee Joint. *Sci Rep*. 2018;8:5931-13.

140. Davis A, Fan X, Shen L, Robinson P, Riggs C. Improved radiological diagnosis of palmar

osteochondral disease in the Thoroughbred racehorse. *Equine Vet J*. 2017;49:454-460.

141. Pinchbeck G, Clegg P, Boyde A, Riggs C. Pathological and clinical features associated with palmar/plantar osteochondral disease of the metacarpo/metatarsophalangeal joint in Thoroughbred racehorses. *Equine Vet J*. 2013;45:587-592.

142. Reed S, Jackson B, McIlwraith C, et al. Descriptive epidemiology of joint injuries in Thoroughbred racehorses in training. *Equine Vet J*. 2012;44:13-19.

143. Barr E, Pinchbeck G, Clegg P, Boyde A, Riggs C. Post mortem evaluation of palmar osteochondral disease (traumatic osteochondrosis) of the metacarpo/metatarsophalangeal joint in Thoroughbred racehorses. *Equine Vet J*. 2009;41:366-371.

144. Bani Hassan E, Mirams M, Mackie E, Whitton RC. Prevalence of subchondral bone pathological changes in the distal metacarpi/metatarsi of racing Thoroughbred horses. *Aust Vet J*. 2017;95:362-369.

145. Ramzan PH. Mind the gaps: The science of POD and the racehorse fetlock. *Equine Vet J*. 2021;53:217-220.

146. Dyson P, Jackson B, Pfeiffer D, Price J. Days lost from training by two- and three-year-old Thoroughbred horses: a survey of seven UK training yards. *Equine Vet J*. 2008;40:650-657.

147. Bailey C, Reid S, Hodgson D, Rose R. Impact of injuries and disease on a cohort of two- and three-year-old thoroughbreds in training. *Vet Rec*. 1999;145:487-493.

148. Turley S, Thambyah A, Riggs C, Firth E, Broom N. Microstructural changes in cartilage and bone related to repetitive overloading in an equine athlete model. *J Anat*. 2014;224:647-658.

149. Shaffer S, Sachs N, Garcia T, Fyhrie D, Stover S. In vitro assessment of the motion of equine proximal sesamoid bones relative to the third metacarpal bone under physiologic midstance loads. *Am J Vet Res*. 2021;82(3):198-206.

150. Alber M, Brown M, Merritt K, Trumble T. Vascular perfusion of the palmar condyles of the equine third metacarpal bone: A possible contributing factor to palmar osteochondral disease? *Osteoarthr Cartil*. 2014;22:S128-S129.

151. Bani Hassan E, Mirams M, Ghasem-Zadeh A, Mackie E, Whitton RC. Role of subchondral bone remodelling in collapse of the articular surface of Thoroughbred racehorses with palmar osteochondral disease. *Equine Vet J*. 2016;48:228-233.

152. Nixon A. Palmar/plantar metacarpal/metatarsal fragmentation. In: Auer J, Stick J, Kummerle J, Prange T, eds. *Equine Surgery*. 5th ed. St. Louis, Missouri: Elsevier, Inc.; 2019:1601-1603.

153. Brokken M, Bertone A. The Fetlock. In: Baxter GM, ed. *Adams and Stashak's Lameness*

in Horses. Seventh Ed. Hoboken, NJ: John Wiley & Sons, Inc.; 2020:541-562.

154. Turlo A, McDermott B, Barr E, et al. Gene expression analysis of subchondral bone, cartilage, and synovium in naturally occurring equine palmar/plantar osteochondral disease. *J Orthop Res*. 2021:1-9.

155. Davidson E, Ross M. Clinical recognition of stress-related bone injury in racehorses. *Clin Tech Equine Pract*. 2003;2(4):296-311.

156. Richardson D, Dyson S. The Metacarpophalangeal Joint. In: Ross M, Dyson S, eds. *Diagnosis and Management of Lameness in the Horse*. St. Louis, Missouri: Elsevier Saunders; 2011:394-410.

157. Arthur R, Blea J, Ross M, Moloney P, Cheney M. The North American Thoroughbred. In: Ross M, Dyson S, eds. *Diagnosis and Management of Lameness in the Horse*. 2nd Ed. St. Louis, Missouri: Elsevier Saunders; 2011:977-993.

158. Pilsworth R. The European Thoroughbred. In: Ross M, Dyson S, eds. *Diagnosis and Management of Lameness in the Horse*. 2nd Ed. St. Louis, Missouri: Elsevier Saunders; 2011:994-1013.

159. American Association of Equine Practitioners. Definition and classification of lameness. In: *Veterinarian's Guide to Equestrian Competition Official Duties*. Lexington, KY: American Association of Equine Practitioners; 2020:8.

160. Walmsley E, Jackson M, Wells-Smith L, Whitton R. Solar angle of the distal phalanx is associated with scintigraphic evidence of subchondral bone injury in the palmar/plantar aspect of the third metacarpal/tarsal condyles in Thoroughbred racehorses. *Equine Vet J*. 2019;51:720-726.

161. Riggs C. Osteochondral injury and joint disease in the athletic horse. *Equine Vet Educ*. 2006;18:100-112.

162. Curtiss A, Ortved K, Dallap-Schaer B, et al. Validation of standing cone beam computed tomography for diagnosing subchondral fetlock pathology in the Thoroughbred racehorse. *Equine Vet J*. 2021;53:510-523.

163. Harris W, Heaney R. Skeletal renewal and metabolic bone disease. *N Engl J Med*. 1969;280:193-202.

164. Greenfield G. Analytical approach to bone radiology. In: Greenfield G, ed. *Radiology of Bone Diseases*. Philadelphia, PA: JB Lippincott Co; 1986:7.

165. Hogan P. Nonstandard Radiographic Techniques for the Equine Practitioner. In: *Proceedings of the Annual Convention of the American Association of Equine Practitioners*. ; 1997:141-144.

166. Hornof W, O'Brien T. Radiographic evaluation of the palmar aspect of the equine

metacarpal condyles: a new projection. *Vet Radiol*. 1980;21(4):161-167.

167. Davis A, Fan X, Shen L, Robinson P, Riggs C. Improved radiological diagnosis of palmar osteochondral disease in the Thoroughbred racehorse. *Equine Vet J*. 2017;49:454-460.

168. Ross M. Scintigraphic and clinical findings in the Standardbred metatarsophalangeal joint: 114 cases (1993-1995). *Equine Vet J*. 1998;30(2):131-138.

169. Trope G, Anderson G, Whitton RC. Patterns of scintigraphic uptake in the fetlock joint of Thoroughbred racehorses and the effect of increased radiopharmaceutical uptake in the distal metacarpal/tarsal condyle on performance. *Equine Vet J*. 2011;43:509-515.

170. Spriet M, Espinosa-Mur P, Cissell D, et al. 18F-sodium fluoride positron emission tomography of the racing Thoroughbred fetlock: validation and comparison with other imaging modalities in nine horses. *Equine Vet J*. 2019;51(3):375-383.

171. Ehrlich P, Dohoo I, O'Callaghan M. Results ofbone scintigraphy in racing Standardbred horses: 64 cases (1992-1994). *J Am Vet Med Assoc*. 1999;215:982-991.

172. Martinelli M, Chambers M, Baker G, Semevolos S. A retrospective study of increased bone scintigraphic uptake in the palmar-plantar fetlock and its relationship to performance: 50 horses (1989-1993). In: *Proceedings of the 40th Annual Meeting of the American Association of Equine Practitioners*. ; 1994:53-54.

173. Arthur R, Constantinide D. Results of 428 nuclear scintigraphic examinations of the musculoskeletal system at a Thoroughbred racetrack. In: *Proceedings of the 41st Annual Meeting of the American Association of Equine Practitioners*. ; 1995:84-87.

174. Biggi M, Dyson S, Murray R. Scintigraphic assessment of the metacarpophalangeal and metatarsophalangeal joints of horses with joint pain. *Vet Radiol Ultrasound*. 2009;50(5):536-544.

175. Powell S. Low-field standing magnetic resonance imaging findings of the metacarpo/metatarsophalangeal joint of racing Thoroughbreds with lameness localized to the region: A retrospective study of 131 horses. *Equine Vet J*. 2012;44:169-177.

176. Mitchell M, Kundal H, Steinberg M, Kressel H, Alavi A, Axel L. Avascular necrosis of the hip: comparison of MR, CT, and scintigraphy. *Am J Roentgenol*. 1986;147:67-71.

177. Stewart H. Dissertation: Evaluation of bone marrow lesions as a manifestation of subchondral bone disease. 2021.

178. Irandoust S, O'Neil L, Stevenson C, et al. Comparison of radiography and computed tomography for identification of third metacarpal structural change and associated assessment of condylar stress fracture risk in Thoroughbred racehorses. *Equine Vet J*. 2024:1-14.

179. Stewart H, Siewerdsen J, Nelson B, Kawcak C. Use of cone-beam computed tomorgraphy

for advanced imaging of the equine patient. *Equine Vet J*. 2021;53:872-885.

180. Lin S-T, Bolas N, Peter V, et al. Comparison of cone-beam and fan-beam computed tomography and low-field magnetic resonance imaging for detection of palmar/plantar osteochondral disease in Thoroughbred horses. *Equine Vet J*. 2024;56:999-1007.

181. Drum M, Les C, Park R, Norrdin R, McIlwraith C, Kawcak C. Correlation of quantitative computed tomographic subchondral bone density and ash density in horses. *Bone*. 2009;44(2):316-319.

182. Brehler M, Thawait G, Shyr W, Ramsay J, Siewerdsen J, Zbijewski W. Atlas-based automatic measurements of the morphology of the tibiofemoral joint. *Proc SPIE Int Soc Opt Eng*. 2017;10137:101370E. doi:10.1117/12.2255566

183. Cao Q, Sisniega A, Stayman J, Yorkston J, Siewerdsen J, Zbijewski W. Quantitative cone-beam CT of bone mineral density using model-based reconstruction. *Proc SPIE Int Soc Opt Eng*. 2019;10948:109480Y. doi:10.1117/12.2513216

184. Even-Sapir E, Mishani E, Flusser G, Metser U. 18F-fluoride positron emission tomography and positron emission tomography/computed tomography. *Semin Nucl Med*. 2007;37:462-469.

185. Spriet M, Arndt A, Pige C, et al. Comparison of skeletal scintigraphy and standing 18F-NaF positron emission tomography for imaging of the fetlock in 33 Thoroughbred racehorses. *Vet Radiol Ultrasound*. 2023;64:123-130.

186. Denoix J-M, Coudry V. Clinical insights: Imaging of the equine fetlock in Thoroughbred racehorses: Identification of imaging changes to predict catastrophic injury. *Equine Vet J*. 2020;52:342-343.

187. Parker R, Bladon B, Parkin T, Fraser B. Quantitative evaluation of subchondral bone injury of the plantaro-lateral condyles of the third metatarsal bone in Thoroughbred horses identified using nuclear scintigraphy: 48 cases. *Equine Vet J*. 2010;42:552-557.

188. Hu W, Chen Y, Dou C, Dong S. Microenvironment in subchondral bone: predominant regulator for the treatment of osteoarthritis. *Ann Rheum Dis*. 2020;80(4):413-422. doi:10.1136/annrheumdis-2020-218089. Online ahead of print.

189. McIlwraith C, Fortier L, Frisbie D, Nixon A. Equine models of articular cartilage repair. *Cartilage*. 2011;2:317-326.

190. Moran C, Ramesh A, Brama P, O'Byrne J, O'Brien F, Levingstone T. The benefits and limitations of animal models for translational research in cartilage repair. *J Exp Orthop*. 2016;3:1.

191. McCoy A. Animal Models of Osteoarthritis: Comparisons and Key Considerations. *Vet Pathol*. 2015;52(5):803-818.

192. McIlwraith C. Frank Milne Lecture: From arthroscopy to gene therapy: 30 years of looking in joints. *Am Assoc Equine Pract*. 2005;51:65-113.

193. Frisbie D, Al-Sobayil F, Billinghurst R, Kawcak C, McIlwraith C. Changes in synovial fluid and serum biomarkers with exercise and early osteoarthritis in horses. *Osteoarthr Cartil*. 2008;16(10):1196-1204.

194. Kawcak C, Frisbie D, Werpy N, Park R, McIlwraith C. Effects of exercise vs experimental osteoarthritis on imaging outcomes. *Osteoarthr Cartil*. 2008;16(12):1519-1525.

195. Menendez M, Clark D, Carlton M, et al. Direct delayed human adenoviral BMP-2 or BMP-6 gene therapy for bone and cartilage regeneration in a pony osteochondral model. *Osteoarthr Cartil*. 2011;19(8):1066-1075.

196. Trumble T, Brown M, Merritt K, Billinghurst R. Joint dependent concentrations of bone alkaline phosphatase in serum and synovial fluids of horses with osteochondral injury: an analytical and clinical validation. *Osteoarthr Cartil*. 2008;16(7):779-786.

197. Frisbie D, Ray C, Ionescu M, Poole A, Chapman P, McIlwraith C. Measurement of synovial fluid and serum concentrations of the 846 epitope of chondroitin sulfate and of carboxy propeptides of type II procollagen for diagnosis of osteochondral fragmentation in horses. *Am J Vet Res*. 1999;60(3):306-309.

198. Fuller C, Barr A, Sharif M, Dieppe P. Cross-sectional comparison of synovial fluid biochemical markers in equine osteoarthritis and the correlation of these markers with articular cartilage damage. *Osteoarthr Cartil*. 2001;9:49-55.

199. McIlwraith C. Current concepts in equine degenerative joint disease. *J Am Vet Med Assoc*. 1982;180:239-250.

200. Norrdin R, Stover S. Subchondral bone failure in overload arthrosis: a scanning electron microscopic study in horses. *J Musculoskelet Neuronal Interact*. 2006;6(3):251-257.

201. Aicale R, Tarantino D, Maffulli N. Overuse injuries in sport: a comprehensive overview. *J Orthop Surg Res*. 2018;13:309.

202. Rizzone K, Ackerman K, Roos K, Dompier T, Kerr Z. Epidemiology of stress fractures in collegiate student-athletes, 2004-2005 through 2013-2014 academic years. *J Athl Train*. 2017;52(10):966-975.

203. Johanson M. Contributing factors in microtrauma injuries of the lower extremity. *J Back Musculoskelet Rehabil*. 1992;2(4):12-25.

204. King J, Zubrod C, Schneider R, Sampson S, Roberts G. MRI findings in 232 horses with lameness localized to the metacarpo(tarso)phalangeal region and without a radiographic diagnosis. *Vet Radiol Ultrasound*. 2013;54:36-47.

205. Gonzalez L, Schramme M, Robertson I, Thrall D, Redding R. MRI features of metacarpo(tarso)phalangeal region lameness in 40 horses. *Vet Radiol Ultrasound*. 2010;51:404-414.

206. Dyson S, Murray R. Osseous trauma in the fetlock region of mature sports horses. In: *Proceedings American Association of Equine Practitioners*. ; 2006:443-456.

207. Roemer F, Neogi T, Nevitt M, et al. Subchondral bone marrow lesions are highly associated with, and predict subchondral bone attrition longitudinally: the MOST study. *Osteoarthr Cartil*. 2010;18(1):47-53.

208. Guio C, Segard-Weisse E, Thomas-Cancian A, Schramme M. Bone marrow lesions of the distal condyles of the third metacarpal bone are common and not always related to lameness in sports and pleasure horses. *Vet Radiol Ultrasound*. 2019;60(2):167-175.

209. Neogi T, Nevitt M, Niu J, et al. Subchondral bone attrition may be a reflection of compartment-specific mechanical load: the MOST Study. *Ann Rheum Dis*. 2010;69(5):841-844.

210. Wluka AE, Wang Y, Davies-Tuck M, English DR, Giles GG, Cicuttini FM. Bone marrow lesions predict progression of cartilage defects and loss of cartilage volume in healthy middle-aged adults without knee pain over 2 yrs. *Rheumatology*. 2008;47(9):1392-1396. doi:10.1093/rheumatology/ken237

211. Scher C, Craig J, Nelson F. Bone marrow edema in the knee in osteoarthrosis and association with total knee arthroplasty within a three-year follow-up. *Skeletal Radiol*. 2008;37(7):609-617. doi:10.1007/s00256-008-0504-x

212. Olive J, Mair TS, Charles B. Use of standing low-field magnetic resonance imaging to diagnose middle phalanx bone marrow lesions in horses. *Equine Vet Educ*. 2009;21(3):116-123. doi:10.2746/095777309X383612

213. Biggi M, Zani DD, De Zani D, Di Giancamillo M. Magnetic resonance imaging findings of bone marrow lesions in the equine distal tarsus. *Equine Vet Educ*. 2012;24(5):236-241. doi:10.1111/j.2042-3292.2011.00288.x

214. Barrett MF, Selberg KT, Johnson SA, Hersman J, Frisbie DD. High field magnetic resonance imaging contributes to diagnosis of equine distal tarsus and proximal metatarsus lesions: 103 horses. *Vet Radiol Ultrasound*. 2018;59(5):587-596. doi:10.1111/vru.12659

215. Iida S, Harada Y, Shimizu K, et al. Correlation between bone marrow edema and collapse of the femoral head in steroid-induced osteonecrosis. *Am J Roentgenol*. 2000;174:735-743.

216. Joint Surgery Group of the Orthopaedic Branch of the Chinese Medical Association. Guideline for Diagnostic and Treatment of Osteonecrosis of the Femoral Head. *Orthop Surg*. 2015;7(3):200-207.

217. Mitchell D, Rao V, Dalinka M, et al. Femoral head avascular necrosis: correlation of MR imaging, radiographic staging, radionuclide imaging, and clinical findings. *Radiology*. 1987;162(3):709-715.

218. Turner D, Templeton A, Selzer P, Rosenberg A, Petasnick J. Femoral capital osteonecrosis: MR finding of diffuse marrow abnormalities without focal lesions. *Radiology*. 1989;171(1):135-140.

219. Li K, Hiette P. Contrast-enhanced fat saturation magnetic resonance imaging for studying the pathophysiology of osteonecrosis of the hips. *Skeletal Radiol*. 1992;21:375-379.

220. Wells M, Dunn J. Pathophysiology of Avascular Necrosis. *Hand Clin*. 2022;38:367-376.

221. Mont M, Cherian J, Sierra R, Jones L, Lieberman J. Nontraumatic Osteonecrosis of the Femoral Head: Where Do We Stand Today? *J Bone Jt Surgery-American Vol*. 2015;97-A(19):1604-1627.

222. Aaron R, Dyke J, Ciombor D, et al. Perfusion Abnormalities in Subchondral Bone Associated with Marrow Edema, Osteoarthritis, and Avascular Necrosis. *Ann New York Acadamy Sci*. 2007;1117(1):124-137.

223. Afshar A, Tabrizi A. Avascular Necrosis of the Carpal Bones Other Than Kienböck Disease. *J Hand Surg Am*. 2020;45(2):148-152.

224. Shah K, Racine J, Jones L, Aaron R. Pathophysiology and risk factors for osteonecrosis. *Curr Rev Musculoskelet Med*. 2015;8:201-209.

225. Bain G, MacLean S, Yeo C, Perilli E, Lichtman D. The Etiology and Pathogenesis of Kienböck Disease. *J Wrist Surg*. 2016;5(4):248-254.

226. Rickey EJ, Cruz A, Trout D, McEwen B, Hurtig M. Evaluation of experimental impact injury for inducing post-traumatic osteoarthritis in the metacarpophalangeal joints of horses. *Am J Vet Res*. 2012;73(10):1540-1552.

227. Rice H, Brokken M, Hostnik E, Bertone A. Evaluation of a novel bone substitute injection technique for potential treatment of impact injury to the equine palmar metacarpal condyle. *Vet Comp Orthop Traumatol*. 2019;32(6):447-453.

228. Bertoni L, Jacquet-Guibon S, Branly T, et al. An experimentally induced osteoarthritis model in horses performed on both metacarpophalangeal and metatarsophalangeal joints: Technical, clinical, imaging, biochemical, macroscopic and microscopic characterization. *PLoS One*. 2020;15(6):e0235251.

229. Boyce M, Trumble T, Carlson C, Groschen D, Merritt K, Brown M. Non-terminal animal model of post-traumatic osteoarthritis induced by acute joint injury. *Osteoarthr Cartil*. 2013;21(5):746-755.

230. Kawcak C, McIlwraith C. Proximodorsal first phalanx osteochondral chip fragmentation

in 336 horses. *Equine Vet J*. 1994;26:392-396.

231. Yovich J, McIlwraith C. Arthroscopic surgery for osteochondral fractures of the proximal phalanx of the metacarpophalangeal and metatarsophalangeal (fetlock) joints in horses. *J Am Vet Med Assoc*. 1986;188:273-279.

232. Broeckx S, Pille F, Buntinx S, et al. Evaluation of an osteochondral fragment–groove procedure for induction of metacarpophalangeal joint osteoarthritis in horses. *Am J Vet Res*. 2019;80(3):246-258.

233. Stewart HL, Easley JT, Selberg KT, et al. Experimental models of bone marrow lesions in ovine femoral condyles. *Vet Surg*. 2023;52:284-298.

CHAPTER 2:

DEVELOPMENT OF AN EXPERIMENTAL MODEL OF PALMAR OSTEOCHONDRAL DISEASE IN THE EQUINE METACARPOPHALANGEAL JOINT

2.1 Introduction

Palmar osteochondral disease (POD) is a traumatic fatigue injury of the subchondral bone of the palmar distal third metacarpal/metatarsal condyles that is suspected to affect up to 90% of racehorses. Not only does it limit an equine athlete's potential, but it can also result in chronic pain and osteoarthritis secondary to a reduction in the structural ability of the subchondral bone to withstand high-intensity exercise.[1] There is a wide spectrum of disease severity, from subtle alterations in bone remodeling to complete collapse of the articular surface.[2] Evidence also suggests that progression is by no means predictable or linear. It is currently unknown whether lesion size, morphology, degree of bone loss, or a combination of these is most clinically significant and predictive of future collapse.

Evidence shows that the prediction and prognostication of POD progression in horses rests on further disease characterization. In clinical practice, horses diagnosed with subchondral bone marrow lesions (BMLs) in the third metacarpal condyles are treated with 60-90 days of active rest from training. In some cases, this will result in resolution of the BML. In a subset of horses, the lesion returns or progresses once the horse returns to training, with the severity and clinical significance of lesion progression varying between individuals. Many of the current publications on POD are limited by potentially biased samples, small numbers, non-standardized training and rest protocols, and much of this information is from post-mortem analysis.[2,3] A successful experimental model for inducing POD lesions does not yet exist and most involve the

use of impact devices that injure articular cartilage.[4,5] Since there is little to no overlying cartilage damage in the early stages of POD,[6] a reliable, minimally-invasive model that produces changes in the subchondral bone without affecting the articular cartilage is crucial. The investigators believe that targeting treatment to the subchondral bone in the early stages of POD, prior to articular surface collapse, will enhance the local therapeutic effects of treatment and provide better support to the articular surface. Before we can test this hypothesis, we must first establish a reproducible experimental model for POD.

The horse is considered one of the best and most challenging models for studying orthopedic ailments,[7–9] providing a naturally-occurring model of repetitive stress injury. There is a unique opportunity to not only utilize the data on repetitive stress injury and POD in equine athletes to help advance our knowledge on similar diseases in humans, such as subchondral bone attrition, subchondral bone injury in long distance athletes, and femoral head necrosis, but to also use the data in humans to help study potential treatment options for more advanced cases of equine disease. With the development of a prospective model of disease in equine, there is a greater chance of this testing being accomplished with the hope of preserving and improving the athletic careers of these animals. The development of an experimental model of POD, or repetitive stress injury in general, would make it possible to study the progression in a controlled, prospective manner, thus opening the doors for future studies on variables that may affect an individual horse's risk of injury and facilitate development of an optimized treatment plan. BMLs have been shown to be predictive of subchondral bone attrition, and to precede and be associated with fatigue injury in the subchondral bone.[10–12] A reliable, minimally-invasive pin penetration model has been developed to induce BMLs in the femoral condyles of sheep[13] and rats with minimal damage to the articular cartilage and surrounding structures. In this chapter,

the details of this recent research and how it led to the development of a model of repetitive stress injury in the equine metacarpophalangeal (front fetlock) joint will be discussed. Additionally, the details of this model provided in this chapter will be the basis for the data provided in chapters 3-5 of this dissertation.

2.2 An Experimental Model of Bone Marrow Lesions in the Ovine Femoral Condyle

There is an increasing amount of research being performed on subchondral bone disease due to its recent recognition as a significant player in the pathogenesis and progression of osteoarthritis (OA). A focus of this research has been the detection of early changes within the subchondral bone, with reports citing BMLs as early indicators of maladaptive remodeling and structural deterioration. As part of her post-doctoral work, Dr. Holly Stewart sought to develop a comprehensive model to help improve our understanding of the biological behavior of BMLs, as well as to optimize their detection using advanced diagnostic imaging techniques. The work performed and published by Stewart et al. investigating a pin penetration model to induce BMLs in the femoral condyles of sheep[13] served as the foundation and inspiration for the equine work presented in this dissertation.

In this randomized, prospective experimental study, BMLs were reliably induced in the medial condyle of the distal femur in 18 skeletally-mature Dorper cross ewes,[13] with a similar appearance on MRI to those observed in clinical cases.[14–16] In this study, one randomly-selected medial femoral condyle was penetrated to one of four possible depths with a 1.1mm Steinmann pin. Penetration depths included 1 mm through the articular and into the calcified cartilage layer (P_1), 2 mm through the articular and calcified cartilage layers and into the subchondral bone plate (P_2), and 8 mm through the articular and calcified cartilage layers, subchondral bone plate, and into the underlying trabecular bone (P_8). There was a fourth group in which the pin was advanced

from an extraarticular, abaxial approach from the level of the cranial margin of the origin of the medial collateral ligament of the femorotibial joint distally to the subchondral bone plate in the center of the condyle (P_E). The contralateral medial femoral condyle of each animal was treated with extracorporeal shockwave (ESW) – 10,000 pulses at 8 Hz and an energy of 0.39 ± 0.04 mJ/mm^2 applied at 240-360 pulses/minute using either a 20 mm or 35 mm trode. In addition to model development, this work also focused on imaging optimization for detection of BMLs in sheep; therefore, all stifle joints were monitored throughout the 12-week study period using both computed tomography (CT) and high-field 3-Tesla magnetic resonance imaging (MRI).

BMLs were not observed on MRI for any of the 18 medial femoral condyles treated with ESW application. BMLs were also not observed on MRI in limbs from the P_1 or P_E groups – groups in which either just the articular and calcified cartilage layers or just the trabecular bone and subchondral bone plate were penetrated. In groups P_2 and P_8, in which both the cartilage and subchondral bone layers were involved, BMLs were present on MRI beginning 2 weeks post-operatively. These BMLs remained visible though progressively decreased in volume through week 8 in the P_2 group, and throughout the entire study in the P_8 group. Two of the 5 animals in the latter group also developed a circular-to-ovoid pattern on MRI similar in appearance to a cyst-like lesion. Serial MRI images of a single animal in the P_8 group are shown in Figure 2.1. Serial imaging allowed the investigators to follow the changes in the appearance of BMLs over the study period, which were similar in appearance to POD-associated BMLs (See Figure 1.8 from Chapter 1).[17]

Histologically, the pin entry point from the articular cartilage was covered by fibrocartilaginous tissue within 30 days. Early degenerative changes were visible histologically only within the subchondral tissues, with minimal changes to the articular cartilage after 90 days.

Histological findings in the P_2 and P_8 groups were indicative of a dynamic, active bone remodeling process with a mixed inflammatory cell infiltrate that was greatest at 4 weeks and continued throughout the study period. The periphery of the pin tracts was lined with dense, fibrous tissue and in some sections, there was a central, amorphous area of cellular debris within the pin tract that became a necrotic sequestrum by 12 weeks (Figure 2.2). The mechanism of this necrotic foci was believed to be secondary to changes such as impaired blood flow, increased intraosseous pressure and local tissue hypoxia, similar to that reported for POD and avascular necrosis as discussed in Chapter 1. The marrow spaces also contained changes consistent with fluid accumulation or bone marrow edema, with increased cartilaginous matrix within the tissue adjacent to the pin tracts. There was no significant difference in chondrocyte density or cell cloning compared to controls for either group.

Changes in the subchondral bone were present histologically in these two groups. Both had an increased thickness of the subchondral bone plate and increased bone volume/tissue volume ratio relative to the controls, and changes for group P_8 were significantly greater than P_2. There was also evidence of osteochondral ossification in the tissue adjacent to the pin tracts in group P_8. Additional changes in the P_8 group included duplication of the tidemark, the presence and penetration of blood vessels into the subchondral bone plate, subchondral bone remodeling, and osteochondral splitting. Lastly, histomorphometry of the P_8 group revealed a decreasing percentage of bone with an increasing percentage of fibrosis from the 4-week to 12-week timepoints, with the end-of-study composition consisting of 16.75% bone and 73% fibrosis adjacent to the pin tract.

Data from this study demonstrated that damage to the cartilage or bone layers alone is not enough to induce a BML. This emphasized that the integrity of the cartilage-bone interface is

critical in the pathophysiology of BML formation and suggested that the depth of osteochondral damage may be the most important factor to distinguish and predict BML persistence. This study also suggested that BMLs will regress when damage extends to, but not beyond, the subchondral bone plate; however, damage extending from the articular cartilage into the trabecular bone will result in persistent or progressive BMLs. Furthermore, this study demonstrated the dynamic nature of BMLs, further validating the need for serial advanced diagnostic imaging to appropriately interpret and prognosticate BMLs.

This work enabled our team to optimize MRI and CT for BML detection in animal models and provided additional data to understand the changes within the subchondral bone of the medial femoral condyle associated with the presence of a BML. Based on the observations from Dr. Stewart's research, and given the reliable and minimally-invasive nature of the model, we believed that this had the potential to initiate a model of repetitive stress injury and POD in the equine fetlock, particularly if using a penetration depth of 8 mm. As such, this study served as the foundation for the post-doctoral research presented in this dissertation.

2.3 Preliminary Work

Preliminary work testing the feasibility of the pin penetration model was initially performed in the distal third metatarsal (MT3) condyles of eight equine cadaver limbs. Hind limbs were selected for this preliminary work instead of forelimbs based on cadaver availability; however, procedural differences were not expected between hind limbs compared to forelimbs. This work yielded promising results and allowed for optimization of the technique to be used in live horses. Following identification of the ideal entry point through the skin on ultrasound, a 1.1 mm Steinmann pin was directed to the plantarodistal aspect of the mid-medial third metatarsal condyle under ultrasound-guidance until it was felt contacting the articular surface. The location

was confirmed radiographically, after which the pin was drilled through the articular surface and into the subchondral and trabecular bone to a depth of 8 mm. Depending on the degree of subchondral sclerosis in each cadaver limb, there were initial issues with pin breakage and/or bending. This occurred using both 1.1-mm- and 1.6-mm-diameter pins. To reduce pin cycling and provide the pin with added stability as it was advanced through the subchondral plate, the technique was modified such that a 14-gauge, 1.5-inch hypodermic needle was ultrasound-guided to the desired location on the condyle and used as a cannula for the 1.1 mm pin during drilling (Figure 2.3). This successfully prevented breakage of the pin.

Preliminary work confirmed that a 1.1 mm Steinman pin could be successfully placed into the medial metatarsal condyle of equine cadaver limbs. Figure 2.4 shows the point of entry of the pin in three of the condyles, within the ideal location based on clinical POD lesions. In order to get the tip of the pin in the proper location on the condyle, while avoiding the superficial and deep digital flexor tendons, the medial oblique sesamoidean ligament was penetrated just distal to its origin on the base of the medial proximal sesamoid bone. Upon gross examination of the cadavers, the pin tract through the ligament could not be identified.

Additional preliminary work was performed on cadaver limbs to continue refining the technique. In a group of 12 horses evaluated from birth to 18-months of age, in which six were raised on pasture and six were subjected to an additional training regimen, changes in cartilage biomechanical, structural, and biochemical properties consistent with early cartilage degeneration were present in this region of the metacarpophalangeal joint without detectable effects of exercise training.[18] Based on this evidence of cartilage compromise even prior to training combined with the preliminary studies performed at this institution, the creation of a 1.1 mm pin tract through the articular cartilage was not expected to create any significant pathologic

changes. Furthermore, the lack of significant damage identified to the associated soft tissue structures meant that this model could induce changes in the subchondral bone without damage to the remainder of the joint serving as a catalyst for progression. As such, the research progressed to a pilot study performed in live horses.

2.4 Overview of Model Development

Based on the results of the research performed by Stewart et al. and the consistent ability to access the region of interest on the palmar/plantar condyles with the Steinmann pin, a prospective, experimental pilot study was performed in live horses. Throughout this section, the details of the horses and protocols used in the live-horse pilot study are described. Details of the methods used for monitoring host response will be provided in the appropriate chapters (Chapter 3: lameness examinations, synovial fluid analysis; Chapter 4: diagnostic imaging; Chapter 5: postmortem evaluation).

2.4.1 Horses

Three healthy, skeletally-mature horses (2-3 years old) that had no perceptible lameness at a walk or trot (grade 0 out of 5 on the American Association of Equine Practitioners [AAEP] Lameness Scale),[19] palpable effusion within the metacarpophalangeal joint of either front fetlock, or radiographic evidence of fetlock disease or condylar sclerosis were used. The horses included one mare and two geldings, all of which were Quarter Horse crosses (weight, 360 kg to 420 kg). While the use of Thoroughbreds would have been ideal for developing a model of POD, Quarter Horse crosses were selected based on horse availability and are similar to those used in prior studies.[4,20–23] In a study utilizing Quarter Horses and Quarter Horse crosses, treadmill exercise alone induced increased radioisotope uptake in the palmarodistal MC3 condyles on nuclear scintigraphy, as well as increased subchondral bone density in that region.[20] As they were

similarly light-breed horses to Thoroughbreds, no dramatic differences in outcome were expected. POD is viewed as a manifestation of large volumes of high-speed exercise,[2,24–27] and it has been identified grossly in Quarter Horse racehorses on postmortem examination at this institution. Multiple conformational characteristics have been identified in horses to alter the mechanical distribution of forces and their predisposition to specific injuries,[28–32] and it could be argued that there would likely be generic differences in limb conformation between Thoroughbreds and Quarter Horse crosses; however, the same argument could be made for individual horses within the same breed. At this stage, the goal was to perform the pilot study in a group of similar horses for more uniform outcomes. Nevertheless, differences in breed characteristics and individual horse variability cannot be ruled out as a factor affecting this study. All horses underwent intake physical examinations and complete bloodwork (complete blood count and equine biochemistry panel) upon admission, the results of which were within the normal reference ranges. Research performed for this study was approved by the Institutional Animal Care and Use Committee at Colorado State University (#2514).

2.4.2 Study Design

This was an experimental, prospective pilot study utilizing a biaxial, bilateral forelimb model. It has been reported that POD lesion severity is higher in the forelimbs compared to the hind limbs[3,26,33]; therefore, only forelimbs were used for the purposes of this pilot study. It has also been reported that the medial condyle tends to be more severely affected in the forelimb while the lateral condyle is predominantly affected in the hind limb.[26,34] In contrast, other publications found no significant difference between lateral versus medial condyles when examined overall or separately within the forelimbs.[25,35] As clinical POD is a biaxial and bilateral disease, BMLs were induced in the medial and lateral third metacarpal condyles of both

forelimbs, resulting in 4 identically-induced lesions per horse. The horses were exercised over the course of 6 months post-operatively, with serial evaluations performed using various methods as discussed below.

2.4.3 Study Timeline

A visual timeline of the study period is provided in Figure 2.5. A 2-week quarantine and acclimation period took place following horse acquisition, including routine anthelminthic treatment and vaccination, farriery, and serial fecal culture, followed by a 2-week training period for treadmill exercise. All horses underwent baseline lameness exams, synovial fluid aspiration and analysis, radiographs and radiographic arthrography within the week prior to surgery. On day 0, horses were placed under general anesthesia for baseline MRI and CT, including arthrography, of both front fetlocks. Following MRI and CT, surgery with biaxial, bilateral lesion induction was performed. Horses remained on box stall rest for two weeks post-operatively. On Day 14, horses began treadmill exercise, which was performed as described in section 2.4.6, for 6 months. Follow-up lameness evaluations, synovial fluid aspiration and analysis, and radiographs (with and without intra-articular contrast) were collected at weeks 2, 4, 8, 12, 16, 20, and 24 post-operatively. Follow-up MRI and CT (with and without contrast) were performed under general anesthesia at weeks 4, 12, and 24 post-operatively. Horses were humanely euthanized at the end of the 6-month study period for post-mortem analysis.

2.4.4 Surgical Technique

All 3 horses underwent general anesthesia for lesion induction. Routine pre-operative bloodwork (complete blood count and equine biochemistry panel) was performed prior to surgery and was within normal reference ranges for all horses. All horses had an intravenous catheter placed in the jugular vein on the morning of surgery. Peri-operative antimicrobials

(cefazolin 11 mg/kg bwt, gentamicin 6.6 mg/kg bwt) and an anti-inflammatory (phenylbutazone 4.4 mg/kg) were administered, intravenously, at the time of surgery. Once anesthetized, each horse was placed in right lateral recumbency on a padded surgical table, with the forelimbs positioned such that the front fetlocks could be extended as needed throughout surgery. This was done immediately following advanced diagnostic imaging, performed as described in Chapter 4. Both front fetlocks were then clipped free of hair and cleaned circumferentially using standard aseptic technique, then draped routinely.

Using standard aseptic technique and with the fetlock held in moderate extension, an ultrasound examination was performed to identify the palmarodistal surface of each distal third metacarpal condyle through a space between the palmar eminence of the proximal first phalanx and the distal margin of each proximal sesamoid bone in the longitudinal plane. A 14-gauge, 1.5-inch sterile hypodermic needle was advanced at a 45° angle through the skin, between the straight and oblique distal sesamoidean ligaments and just abaxial to the deep digital flexor tendon, until it reached the articular surface of the condyle using ultrasound-guidance. Lateromedial and dorsopalmar radiographs were taken intraoperatively to confirm proper needle placement, with the ideal location of the needle tip being at the mid-to-slightly axial aspect of the palmarodistal surface of the condyle. Once positioning of the needle was confirmed, a 1.1 mm Steinmann pin was inserted through the needle and drilled to a depth of 8 mm, attempting to be positioned as close to parallel to the sagittal plane as possible; however, each needle was angled to a degree in an abaxial-to-axial direction. The pin was marked with a sterile permanent marker once it was secure within the needle and prior to drilling to ensure accuracy of depth. Additional intraoperative radiographs were taken to document the final pin location, after which the pin was removed. The same procedure was performed in each of the four metacarpal condyles and

surgery was performed by a single board-certified equine surgeon (LES) for all cases. A light bandage consisting of antimicrobial-impregnated gauze (Kerlix AMD) and adhesive tape (Elastikon) was placed on both front fetlocks prior to recovery from general anesthesia. All three horses recovered from general anesthesia without incident.

2.4.5 Postoperative Care

The bandage placed at surgery was removed after 24 hours. Due to the minimally-invasive nature of the procedure, intravenous antimicrobials were not continued postoperatively. Oral phenylbutazone (4.4 mg/kg bwt) was administered every 24 hours for 5 days, postoperatively. All horses were kept on box stall rest for 14 days and monitored daily for signs of acute lameness. No postoperative complications were encountered during this 14-day period.

2.4.6 Treadmill Exercise

The pin penetration model was intended to "fast forward" the disease process to the point of subchondral bone damage and BML development. In order to better simulate the chronic, repetitive loading experienced by racehorses, this was combined with high-speed treadmill exercise to create a more realistic model of chronic repetitive stress injury. It is recognized that another potential control group would have included inducing BMLs without follow-up treadmill exercise; however, inclusion of this group was not considered critical at this stage of model development and will be pursued in later studies, as described in Chapter 6.

Beginning on day 14 postoperatively, horses were exercised on a treadmill using an exercise protocol that simulates racehorse training and has been shown to induce adaptive changes in the subchondral bone within 6 months, even in normal horses without disease.[12] Treadmill exercise took place 5 consecutive days a week. Horses were exercised on the high-speed treadmill as follows: 2-minute trot (16-19 km/h [10-12mph]), 3-minute gallop (32 km/h

[20mph]), and 2-minute trot. After 36 days of treadmill exercise, the gallop speed was incrementally increased by 0.5mph per week to a final speed of 41.6 km/h (26mph), which was continued throughout the remainder of the study. This adjustment was made to the original treadmill protocol as outlined by Kawcak et al. due to safety concerns and differing abilities of the horses used in the present research.

2.4.7 Study Termination

At the end of the 6-month study period, all 3 horses were humanely euthanized with an overdose of intravenous sodium pentobarbital. This was performed while horses were under general anesthesia, following completion of the 24-week MRI and CT. Immediately after euthanasia, forelimbs were harvested from each horse for post-mortem evaluation including gross evaluation and photography, microcomputed CT, and histology. This was done to compare the final lesions to postmortem results in the published literature, as well as to gain further knowledge on the architectural and functional changes that occurred as a result of lesion induction and 6-months of high-speed treadmill exercise.

2.5 Statistical Model Development

As previously mentioned, this experimental model involved biaxial, bilateral lesion induction in which BMLs were created in an identical manner in the medial and lateral distal MC3 condyles of the left and right forelimbs of 3 horses of similar age and breed, for a total of 4 lesions per horse. All horses were then subjected to the same housing, training conditions, and evaluation protocols throughout the duration of the study. Due to the exploratory nature of this pilot study, a limited sample size of 3 horses was used while still allowing for variance.

Descriptive data were recorded for all outcome parameters measured, with measures of central tendency and dispersion (mean/median and standard deviation/range) reported. Ordinal

variables (e.g., a grading scale from 0-3) were treated as continuous for the purposes of data analysis; this enabled more efficient statistical modeling given the limited sample size and facilitated clearer interpretation of differences across groups.[36,37] A control horse was not included in this study and can be considered a limitation. A specimen was obtained from a 2-year-old Quarter Horse racehorse without gross evidence of POD on postmortem examination as a control for the microCT data; however, as it was not subjected to the same exercise surface or regime, it cannot be considered a direct control and was used primarily to compare differences in bone architecture between study horses and a racehorse with evidence of mild, normal adaptive remodeling on CT imaging.

For this study, it was important to consider that the 12 created lesions could not be considered independent samples, requiring all analyses to include horse, limb, and/or condyle as a fixed effect. This was taken into account for the development of this statistical model. A brief description of each of the parameters measured in this study are provided below, with a more complete description of the scoring systems provided in the respective chapters 3-5.

The primary objectives of this exploratory study were to evaluate the clinical, macroscopic, and microscopic effects of the pin penetration model combined with 6-months of high-speed treadmill exercise, and to provide proof-of-concept that this model induced lesions consistent with maladaptive stress remodeling and the early stages of POD in horses. It was not the goal to prove efficacy compared to other techniques, or to use this model in order to evaluate the effectiveness of various treatments. As a result, a control population was not included. The data collected from this study will provide a foundation for future study in a larger population of horses, at which time control specimens will become critical.

Regarding the scoring used in this study, previously-published grading systems related to POD, subchondral bone injury, and maladaptive stress remodeling in horses were used in order to measure how this experimental model compared to real-life disease. Upon reviewing the results, grading systems were then modified as needed to develop a grading system more specific to this model that could be utilized in future studies. These changes are specifically designated in the relevant chapters.

Data analysis was performed using R Studio (version 2024.12.1.56).

2.5.1 Variables Measured Over Time

For outcome parameters measured over multiple timepoints – lameness data, synovial fluid analysis, and diagnostic imaging variables as described in the study timeline – statistical analysis was performed to assess how each of the outcome parameters measured changed over time within and between condyles, limbs, and/or horses. The baseline samples for each horse were used as controls.

An analysis of variance (ANOVA) was conducted to evaluate the effects of time, condyle, limb, and horse on each of the outcome parameters measured in this study. In addition to the main effects, selected two-way interactions were also assessed to explore potential effect modification. Statistical significance was determined for both the main and interaction effects with a *P*-value < 0.05 being the criterion for statistical significance. Interaction terms were included to assess whether the relationship between one predictor and the outcome differed depending on another predictor. For each significant effect and interaction identified with the ANOVA ($p < 0.05$), a post-hoc Tukey-adjusted pairwise comparison of means was performed using the expected marginal means (emmeans) function in R Studio to look for significant differences between time points, condyles, limb, and/or horses. For the pairwise comparison of

means, a *P*-value ≥ 0.05 but ≤ 0.10 was considered to have marginal significance and a *P*-value > 0.10 was not statistically significant.

2.5.2 Variables Measured at a Single Time Point

Post-mortem analysis – gross examination, microcomputed tomography (microCT), and histopathology – could not be performed until the 24-week time point. For the outcome parameters measured from the gross examination, statistical analysis was performed to assess how each parameter measured compared between condyles, limbs, and horses.

For histological evaluation, an additional fixed variable was included – slice location. Slices were obtained from 4 locations within each condyle in the transverse plane: 1) proximal tract (PT), which was sectioned through the proximal half of the pin tract, 2) proximal distant (PD), which was sectioned from a site at least 5mm proximal to the pin tract, 3) distal tract (DT), which was sectioned through the distal half of the pin tract, and 4) distal distant (DD), which was sectioned from a site at least 5mm distal to the pin tract. For all scoring systems and data collected, the goal for analysis was to assess whether there were significant differences between each of the slice locations overall, as well as within and between condyles, limbs, and horses.

For microCT evaluation, rather than slice location as an additional variable, the additional variable for microCT analysis included nine volumes of interest (VOI) that were analyzed per condyle: 1) tip of the tract, 2) abaxial subchondral bone plate, 3) axial subchondral bone plate, 4) proximal subchondral bone plate, 5) distal subchondral bone plate, 6) abaxial mid-tract, 7) axial mid-tract, 8) proximal mid-tract, and 9) distal mid-tract. For all scoring systems and data collected, the goal for analysis was to assess whether there were significant differences between each of the VOIs overall, as well as within and between condyles, limbs, and horses.

An analysis of variance (ANOVA) was conducted to evaluate the effects of slice location or VOI (for histopathology or microCT, respectively), condyle, limb, and horse on each of the outcome parameters measured in this study. In addition to the main effects, selected two-way interactions were also assessed to explore potential effect modification. Statistical significance was determined for both the main and interaction effects with a *P*-value < 0.05 being the criterion for statistical significance. Interaction terms were included to assess whether the relationship between one predictor and the outcome differed depending on another predictor. For each significant effect and interaction identified with the ANOVA ($p < 0.05$), a post-hoc Tukey-adjusted pairwise comparison of means was performed using the expected marginal means (emmeans) function in R Studio to look for significant differences between slice location, condyles, limb, and/or horses. For the pairwise comparison of means, a *P*-value ≥ 0.05 but ≤ 0.10 was considered to have marginal significance and a *P*-value > 0.10 was not statistically significant.

2.6 Figures

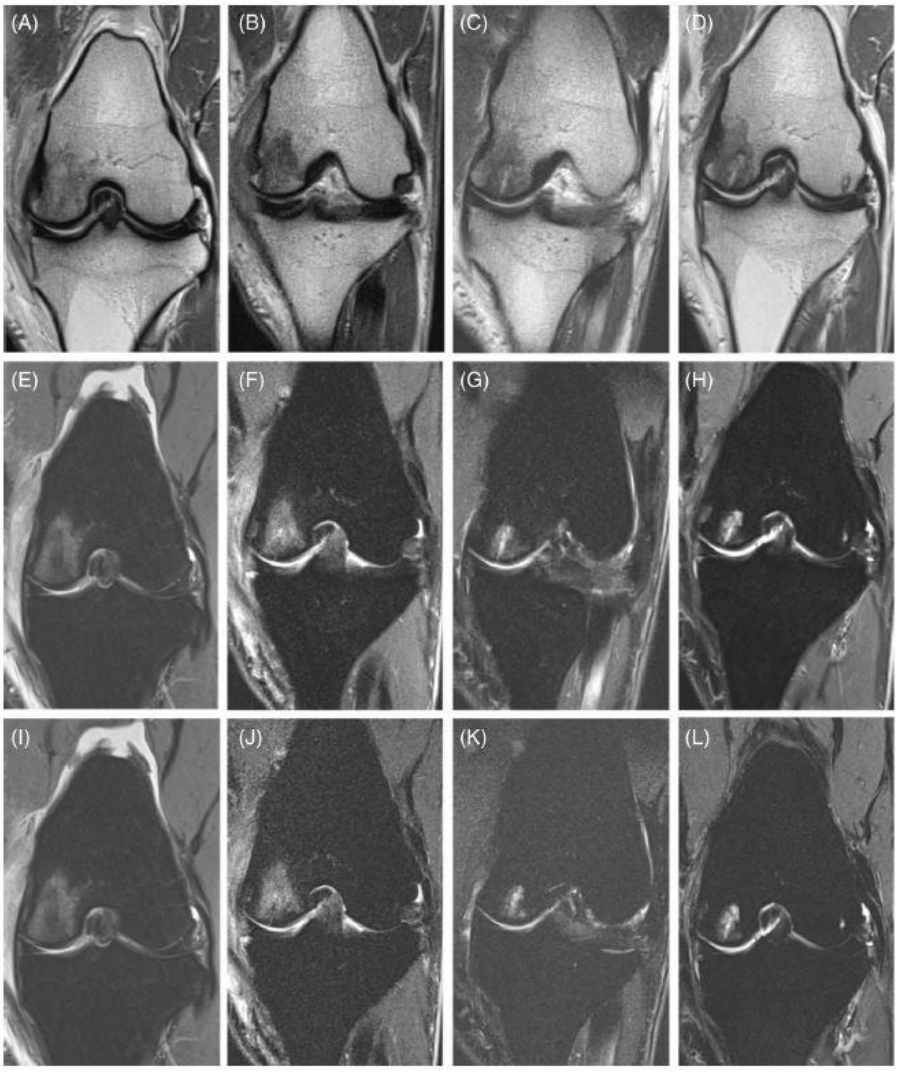

Figure 2.1 – Serial dorsal plane images of an experimentally-induced bone marrow lesion (BML) in a single animal from various sequences on magnetic resonance imaging (MRI). (A–D) Dixon in phase sequence images; (E–H) Dixon water only sequence images; (I–L) proton density fat saturation (PDFS) sequence images. Each column represents a different imaging timepoint. From the left, images in the first column are at 2 weeks post-BML induction; second column at 4 weeks; third column at 8 weeks; and fourth column at 12 weeks. This BML was induced by advancing a 1.1 mm Steinmann pin from the articular surface of the medial femoral condyle to a depth of 8 mm, through the articular and calcified cartilage, subchondral bone plate and into trabecular bone. A linear hyperintensity persists in the original region of the pin tract, extending beyond the 8 mm drilling depth. *With permission based on the Creative Commons License for the Open Access article Stewart HL, Easley JT, Selberg KT, et al. Experimental models of bone marrow lesions in ovine femoral condyles. Vet Surg. 2023;52:284-298*.

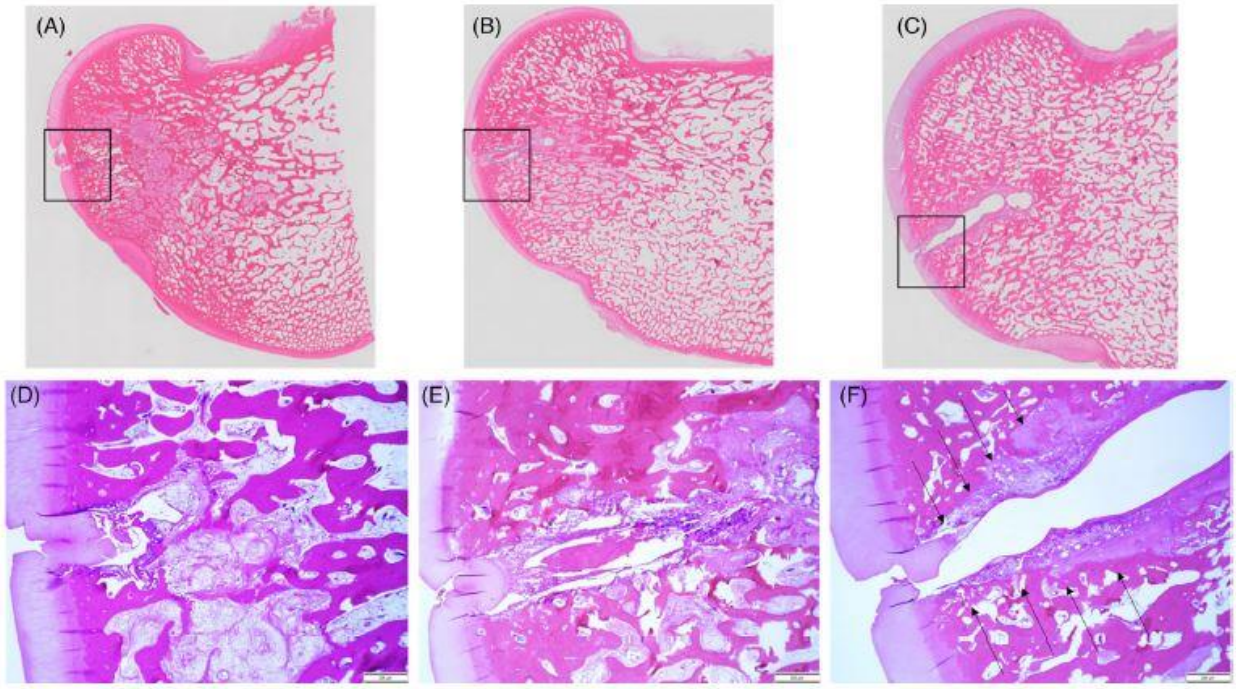

Figure 2.2 – Histological sections with hematoxylin and eosin stain of the ovine medial condyle of the distal femur 4 weeks (A, D), 8 weeks (B, E), or 12 weeks (C, F) after experimental-induction of bone marrow lesions (BMLs). The tract of the pin used for BML induction is visible in all images. Initially, the BML is characterized by a local hemorrhage and a high level of inflammatory cellular infiltrate. By 12 weeks, dense fibrous repair tissue is present along the periphery of the pin tract, in addition to structural remodeling within the adjacent bone (black arrows). The black boxes in the upper images identify regions of interest shown in the lower images at higher magnification; bar (lower images) = 200 µm. *With permission based on the Creative Commons License for the Open Access article Stewart HL, Easley JT, Selberg KT, et al. Experimental models of bone marrow lesions in ovine femoral condyles. Vet Surg. 2023;52:284-298*.

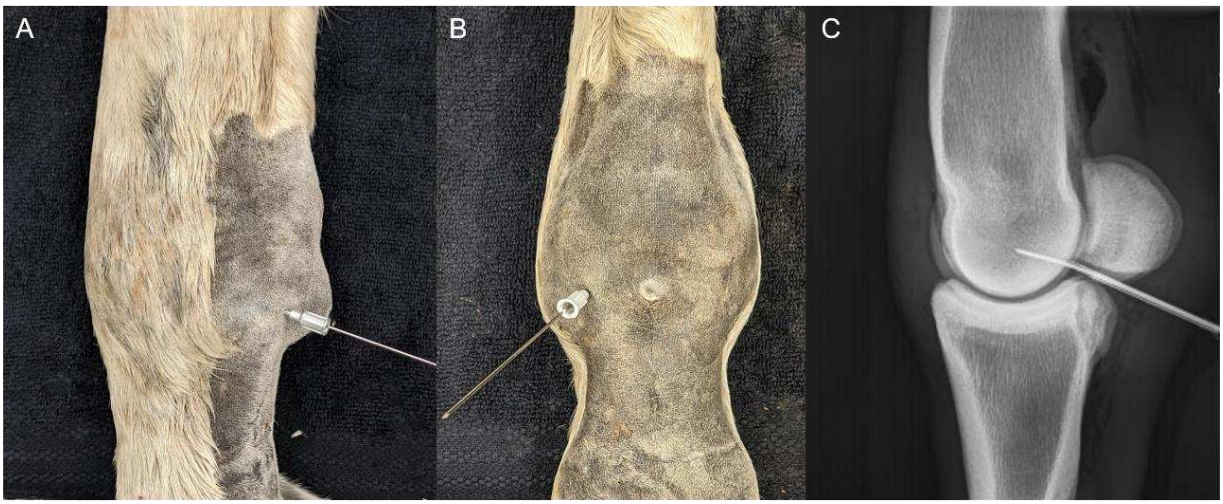

Figure 2.3 – Images of the medial (A) and plantar (B) aspect of the metatarsophalangeal (hind fetlock) joint of a cadaver limb used in the preliminary work for this research. A 14-gauge, 1.5-inch needle was advanced under ultrasound-guidance to the mid-plantarodistal aspect of the third metatarsal condyle, after which a 1.1 mm Steinmann was placed through the needle (A, B). C) A lateromedial radiograph following advancement of the pin to a depth of 8 mm.

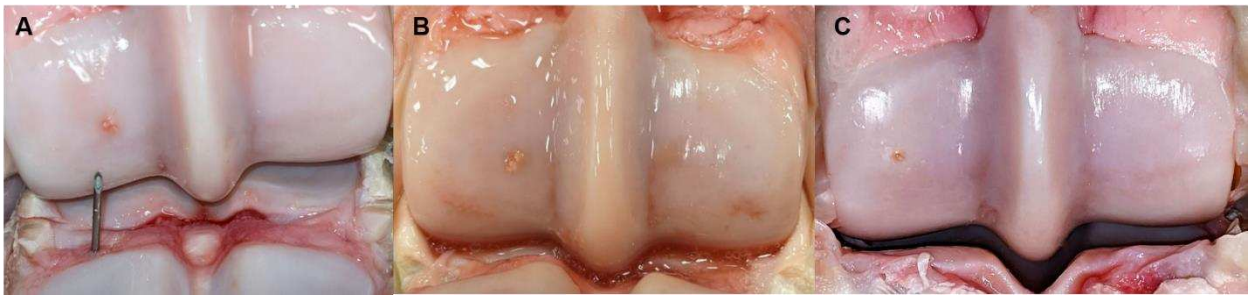

Figure 2.4 – Gross photographs of the point of pin entry in the plantarodistal surface of the medial third metatarsal condyle of three equine cadaver limbs used in the preliminary work. The path of the needle and pin distal to the medial proximal sesamoid bone is represented by an 18-gauge spinal needle in image A.

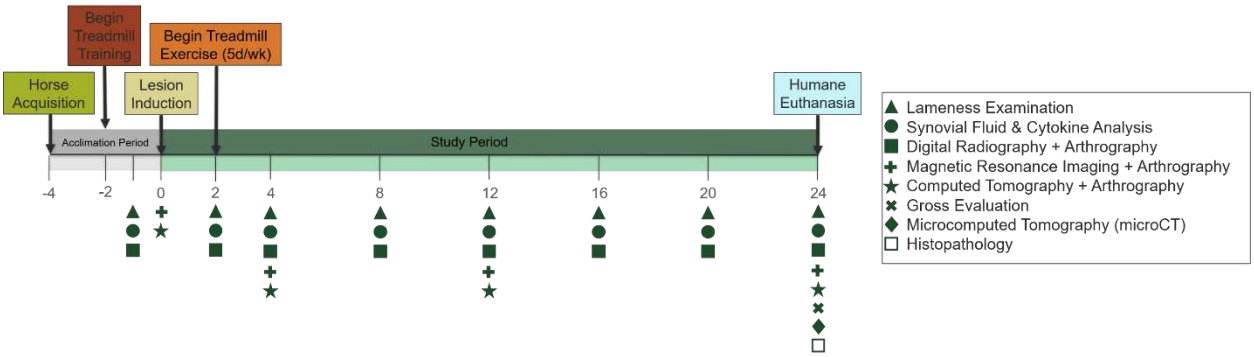

Figure 2.5 – Schematic of the study timeline. Each timepoint is shown as the number of weeks post-operatively, relative to lesion induction. Symbols represent the procedures performed at each timepoint, with a key provided on the right side of this figure.

2.7 References

1. Davis A, Fan X, Shen L, Robinson P, Riggs C. Improved radiological diagnosis of palmar osteochondral disease in the Thoroughbred racehorse. *Equine Vet J*. 2017;49:454-460.

2. Ramzan PH. Mind the gaps: The science of POD and the racehorse fetlock. *Equine Vet J*. 2021;53:217-220.

3. Reed S, Jackson B, McIlwraith C, et al. Descriptive epidemiology of joint injuries in Thoroughbred racehorses in training. *Equine Vet J*. 2012;44:13-19.

4. Rickey EJ, Cruz A, Trout D, McEwen B, Hurtig M. Evaluation of experimental impact injury for inducing post-traumatic osteoarthritis in the metacarpophalangeal joints of horses. *Am J Vet Res*. 2012;73(10):1540-1552.

5. Rice H, Brokken M, Hostnik E, Bertone A. Evaluation of a novel bone substitute injection technique for potential treatment of impact injury to the equine palmar metacarpal condyle. *Vet Comp Orthop Traumatol*. 2019;32(6):447-453.

6. Nixon A. Palmar/plantar metacarpal/metatarsal fragmentation. In: Auer J, Stick J, Kummerle J, Prange T, eds. *Equine Surgery*. 5th ed. St. Louis, Missouri: Elsevier, Inc.; 2019:1601-1603.

7. McIlwraith CW, Frisbie DD, Kawcak CE. The horse as a model of naturally occurring osteoarthritis. *Bone Joint Res*. 2012;1(11):297-309. doi:10.1302/2046-3758.111.2000132

8. McIlwraith C, Fortier L, Frisbie D, Nixon A. Equine models of articular cartilage repair. *Cartilage*. 2011;2:317-326.

9. Moran C, Ramesh A, Brama P, O'Byrne J, O'Brien F, Levingstone T. The benefits and limitations of animal models for translational research in cartilage repair. *J Exp Orthop*. 2016;3:1.

10. Roemer F, Neogi T, Nevitt M, et al. Subchondral bone marrow lesions are highly associated with, and predict subchondral bone attrition longitudinally: the MOST study. *Osteoarthr Cartil*. 2010;18(1):47-53.

11. Stewart HL, Kawcak CE. The importance of subchondral bone in the pathophysiology of osteoarthritis. *Front Vet Sci*. 2018;5:178. doi:10.3389/fvets.2018.00178

12. Kawcak C, McIlwraith C, Norrdin R, Park R, Steyn P. Clinical effects of exercise on subchondral bone of carpal and metacarpophalangeal joints in horses. *Am J Vet Res*. 2000;61(10):1252-1258.

13. Stewart HL, Easley JT, Selberg KT, et al. Experimental models of bone marrow lesions in ovine femoral condyles. *Vet Surg*. 2023;52:284-298.

14. Olive J, Mair TS, Charles B. Use of standing low-field magnetic resonance imaging to

diagnose middle phalanx bone marrow lesions in horses. *Equine Vet Educ*. 2009;21(3):116-123. doi:10.2746/095777309X383612

15. Biggi M, Zani DD, De Zani D, Di Giancamillo M. Magnetic resonance imaging findings of bone marrow lesions in the equine distal tarsus. *Equine Vet Educ*. 2012;24(5):236-241. doi:10.1111/j.2042-3292.2011.00288.x

16. Barrett MF, Selberg KT, Johnson SA, Hersman J, Frisbie DD. High field magnetic resonance imaging contributes to diagnosis of equine distal tarsus and proximal metatarsus lesions: 103 horses. *Vet Radiol Ultrasound*. 2018;59(5):587-596. doi:10.1111/vru.12659

17. Powell S. Low-field standing magnetic resonance imaging findings of the metacarpo/metatarsophalangeal joint of racing Thoroughbreds with lameness localized to the region: A retrospective study of 131 horses. *Equine Vet J*. 2012;44:169-177.

18. Nugent G, Law A, Wong E, et al. Site- and exercise-related variation in structure and function of cartilage from equine distal metacarpal condyle. *Osteoarthr Cartil*. 2004;12:826-833.

19. American Association of Equine Practitioners. Definition and classification of lameness. In: *Veterinarian's Guide to Equestrian Competition Official Duties*. Lexington, KY: American Association of Equine Practitioners; 2020:8.

20. Kawcak C, McIlwraith C, Norrdin R, Park R, Steyn P. Clinical effects of exercise on subchondral bone of carpal and metacarpophalangeal joints in horses. *Am J Vet Res*. 2000;61(10):1252-1258.

21. Kawcak C, McIlwraith C, Firth E. Effects of early exercise on metacarpophalangeal joints in horses. *Am J Vet Res*. 2010;71(4):405-411.

22. Frisbie D, Al-Sobayil F, Billinghurst R, Kawcak C, McIlwraith C. Changes in synovial fluid and serum biomarkers with exercise and early osteoarthritis in horses. *Osteoarthr Cartil*. 2008;16:1196-1204.

23. Norrdin R, Kawcak C, Capwell B, McIlwraith C. Subchondral bone failure in an equine model of overload arthrosis. *Bone*. 1998;22:133-139.

24. Pinchbeck G, Clegg P, Boyde A, Barr E, Riggs C. Horse-, training- and race-level risk factors for palmar/plantar osteochondral disease in the racing Thoroughbred. *Equine Vet J*. 2013;45:582-586.

25. Barr E, Pinchbeck G, Clegg P, Boyde A, Riggs C. Post mortem evaluation of palmar osteochondral disease (traumatic osteochondrosis) of the metacarpo/metatarsophalangeal joint in Thoroughbred racehorses. *Equine Vet J*. 2009;41:366-371.

26. Pinchbeck G, Clegg P, Boyde A, Riggs C. Pathological and clinical features associated with palmar/plantar osteochondral disease of the metacarpo/metatarsophalangeal joint in

Thoroughbred racehorses. *Equine Vet J*. 2013;45:587-592.

27. Bani Hassan E, Mirams M, Ghasem-Zadeh A, Mackie E, Whitton RC. Role of subchondral bone remodelling in collapse of the articular surface of Thoroughbred racehorses with palmar osteochondral disease. *Equine Vet J*. 2016;48:228-233.

28. Hagen J, Kojah K, Geiger M. Correlations between the equine metacarpophalangeal joint angulation and toe conformation in statics. *Open Vet J*. 2018;8(1):96-103.

29. Weller R, Pfau T, Verheyen K, May S, Wilson A. The effect of conformation on orthopaedic health and performance in a cohort of National Hunt racehorses: preliminary results. *Equine Vet J*. 2006;38(7):622-627.

30. Anderson T, McIlwraith C, Douay P. The role of conformation in musculoskeletal problems in the racing Thoroughbred. *Equine Vet J*. 2004;36(7):571-575.

31. CREVIER-DENOIX N, ROOSEN C, DARDILLAT C, et al. Effects of heel and toe elevation upon the digital joint angles in the standing horse. *Equine Vet J*. 2001;33(S33):74-78. doi:10.1111/j.2042-3306.2001.tb05364.x

32. Tracey A, McClure SR. Retrospective analysis of distal limb conformation and lameness in mature horses after desmotomy of the accessory ligament of the deep digital flexor tendon for management of a flexural deformity. *Equine Vet Educ*. 2018;30(1):53-56. doi:10.1111/eve.12768

33. Pool R, Meagher D. Pathologic findings and pathogenesis and racetrack injuries. *Vet Clin North Am - Equine Pract*. 1990;6(1):1-30.

34. Tull T, Bramlage L. Racing prognosis after cumulative stress-induced injury of the distal portion of the third metacarpal and third metatarsal bones in Thoroughbred racehorses: 55 cases (2000-2009). *J Am Vet Med Assoc*. 2011;238:1316-1322.

35. Bani Hassan E, Mirams M, Mackie E, Whitton RC. Prevalence of subchondral bone pathological changes in the distal metacarpi/metatarsi of racing Thoroughbred horses. *Aust Vet J*. 2017;95:362-369.

36. Robitzsch A. Why ordinal variables can (almost) always be treated as continuous variables: Clarifying assumptions of robust continuous and ordinal factor analysis estimation methods. *Front Educ*. 2020;5:589965.

37. Norman G. Likert scales, levels of measurement and the “laws” of statistics. *Adv Health Sci Educ Theory Pract*. 2010;15(5):625-632.

CHAPTER 3:

CLINICAL OUTCOMES FOLLOWING EXPERIMENTAL INDUCTION OF BONE MARROW LESIONS IN EQUINE METACARPOPHALANGEAL JOINTS

3.1 Introduction

The clinical impact of varying grades of palmar osteochondral disease (POD) on performance is still not fully understood. POD typically causes as a variable, performance-limiting lameness secondary to pain associated with chronic subchondral bone disease in the distal third metacarpal/metatarsal (MC3/MT3) condyles. POD is commonly a bilateral and, in many cases, quadrilateral disease, which makes it difficult to identify an overt lameness, especially in the early stages of disease. Lameness may be acute and severe after training or racing and improve with rest, or it may be intermittent and associated more with poor performance, potentially lingering for weeks to months.[1] As stated in Chapter 1, the degree of lameness is typically mild to moderate in the early stages (grade 2 out of 5 on the American Association of Equine Practitioners lameness scale[2]), with only 60% of horses being positive to flexion of the fetlock joint.[3] Furthermore, being a primary disease of the subchondral bone, there may be minimal localizing clinical signs in the fetlock joint such as joint effusion or swelling and pain to palpation.[1,4,5] Due to the lack of articular cartilage involvement in the earlier stages of disease, joint effusion may not even develop until significant damage to the articular cartilage occurs.[1,5–7] It has also been reported that some horses with POD may plateau or even demonstrate continual improvement in clinical signs without treatment and whilst continuing with race training.[8]

While not commonly performed as a diagnostic test for POD, synovial fluid analysis and cytology is routinely performed to evaluate the joint environment in various inflammatory states. Normal synovial fluid has less than 500 to 1,000 cells/uL, a total protein less than 2 to 2.5 g/dL, less than 10% neutrophils, and greater than 90% mononuclear cells.[9,10] Inflammation of the joint, or synovitis, is typically characterized by an increase in the total nucleated cell count and protein concentration.[11] In mild synovitis cases, or in cases of osteoarthritis, synovial fluid parameters may remain within reference ranges with just a slight shift in the ratio of neutrophils and mononuclear cells, or mild elevation in total protein.[10] Alternatively, it has also been reported for degenerative arthropathies to have total nucleated cell counts as high as 5,000 cells/uL with unremarkable differentials, with the latter starting to shift with progressive inflammation.[12]

Synovial fluid parameters have been shown to increase within 2 weeks of surgical induction of osteoarthritis, with a return to reference interval parameters for horses undergoing exercise alone.[13] Acute intra-articular fracture in the horse has been shown to increase synovial fluid parameters above values considered diagnostic even for septic arthritis,[14] suggesting that more significant trauma involving the underlying bone can be a significant contributor to synovial inflammation. Given the ease of acquiring synovial fluid at the time of contrast injection for radiographic arthrography as performed in this study, synovial fluid analysis and cytology were performed to evaluate the inflammatory effects of this experimental model.

The objective of this chapter was to longitudinally describe parameters that could be evaluated antemortem, without the need for general anesthesia, to determine their utility in monitoring disease progression using this experimental model. While this would also include certain forms of diagnostic imaging, such as digital radiography, standing computed tomography,

and standing magnetic resonance imaging, the diagnostic imaging findings for this study will be described separately in Chapter 4.

3.2 Materials and Methods

The horses and surgical protocol used in this pilot study, as well as data analysis, were as described in Chapter 2. Briefly, bone marrow lesions (BML) were induced in the medial and lateral MC3 condyles of both forelimbs in three healthy, 2- to 3-year-old horses. This was performed by drilling a 1.1 mm Steinmann pin to a depth of 8 mm in the palmarodistal aspect of each condyle. Horses were then subjected to high-speed treadmill exercise for 24 weeks, beginning two weeks after lesion induction.

3.2.1 Lameness Evaluation

Lameness evaluations were performed by the same investigator (LES) at baseline, then at weeks 2, 4, 8, 12, 16, 20, and 24 weeks post-operatively with lameness scores in each forelimb recorded and compared to baseline. A semi-objective grading scale, similar to that used by the American Association of Equine Practitioners (AAEP)[2] but altered to include more descriptive degrees of lameness,[15] was used to grade lameness at a trot. Briefly, grade 0 indicated no perceptible lameness under any circumstances; grade 1 indicated a slight, inconsistent lameness at the trot without head or neck movement; grade 2 indicated a mild inconsistent lameness in a straight line with inconsistent head and neck movement, or consistently apparent under certain circumstances; grade 3 indicated a moderate consistent lameness observable at a trot under all circumstances with consistent head and neck movement; grade 4 indicated lameness was obvious at a walk; and grade 5 indicated minimal weight-bearing while in motion and/or at a rest.

The response to distal limb flexion was evaluated and subjectively graded as none or a slight, mild, moderate, or severe worsening of lameness following flexion of each fetlock (scale

0-4). During flexion testing, range of motion through each metacarpophalangeal joint was also subjectively graded on a scale of 0-3. Grade 0 was asymptomatic with an absence of pain; grade 1 indicated mild pain and a mildly decreased range of motion; grade 2 indicated moderate pain that caused the horse to withdraw the limb with a moderate decrease in range of motion; and grade 3 indicated severe pain that caused the horse to withdraw the limb and attempt to escape from the handler, with a severe decrease in range of motion. Lastly, effusion associated with each metacarpophalangeal joint was subjectively graded as none, slight, mild, moderate or severe (scale 0-4). A composite score for each forelimb was then calculated (limb symptomatic grade) as the sum of the scores for each of the 4 lameness categories above, giving a total score out of 16.

Additionally, a 'whole horse clinical' scoring system was created with two grading categories – whole horse lameness score and whole horse symptomatic score. The whole horse lameness score was calculated as the sum of the lameness scores for each limb (left forelimb + right forelimb) for each horse at each time point, giving a total horse lameness score out of 10. The whole horse symptomatic grade was calculated as the sum of the composite limb symptomatic grade described above for each horse at each time point, giving a total horse symptomatic score out of 32. These two composite scores were included to provide a better description of the severity of clinical signs – lameness alone and all four parameters combined – for each individual horse.

3.2.2 Synovial Fluid Analysis

Synovial fluid aspiration of the left and right metacarpophalangeal joints was performed by a single investigator (LES) using standard aseptic technique at baseline and at weeks 2, 4, 8, 12, 16, 20, and 24 post-operatively. This was performed using a standard, palmarolateral

approach with the limb non-weight bearing and held in flexion. Synovial fluid aspiration was performed following the lameness examinations and pre-contrast radiographs, immediately prior to the injection of contrast for arthrography as described in Chapter 4. Maximal synovial fluid aspiration was performed in each joint, with a goal of 1.0mL per joint. Fresh synovial fluid (250-500uL) was placed into a 1 mL EDTA tube and submitted for immediate synovial fluid analysis. The remaining fluid from each sample was placed into an EDTA tube and processed for future use that is beyond the scope of this chapter (see Chapter 6). Synovial fluid analysis included the total nucleated cell count (# cells/uL), total red blood cells (# cells x 10^6/uL), total protein (g/dL), and a leukocyte differential including both the percentage and absolute cells/uL for neutrophils, large and small mononuclear cells, eosinophils, basophils, and mitotic figures. The glycosaminoglycan (GAG) quality in the background of each slide was also graded on a scale from 0-2 as adequate, slightly disrupted, or disrupted. Briefly, adequate corresponded to a smooth, even GAG layer without clefts or defects, slightly disrupted meant that a few defects or clefts were noted and disrupted corresponded to a broken or inconsistent GAG layer. The synovial fluid analysis and cytologic evaluation were performed by the same board-certified veterinary clinical pathologist for all samples (ARM).

3.3 Results

Surgery was successfully completed in all three horses. No complications related to surgery or any post-operative procedures occurred and all horses remained healthy throughout the duration of the study. No obvious lameness was observed during the two-week stall rest period, nor was there any evidence of heat, pain to palpation, or edema associated with the surgical sites. Increased lameness (grade 3 out of 5) was observed at the trot on the treadmill in all three horses within the first week of treadmill exercise. This began as lameness only observed

upon returning to the trot following the gallop phase and progressed to lameness at the trot before galloping by day 3. When this occurred, a single dose of phenylbutazone (4.4 mg/kg bwt IV) was administered and the horse was only exercised at a trot the next one to two days. This appeared to resolve the initial lameness and allowed horses to complete the study without further complications. Furthermore, lameness on the treadmill appeared increased, subjectively, compared to that observed during lameness examinations on a hard surface.

3.3.1 Lameness Evaluation

Grades for the described outcome parameters recorded for each horse, including the within horse means, are provided in Table 3.1. Graphs showing the results of the lameness examination over time, shown as the mean (range) for each horse and the overall mean, are provided in Figure 3.1. Results from the whole horse clinical scoring system, including the whole horse lameness grade and the whole horse symptomatic grade, are shown in Table 3.2 and Figure 3.3. Overall, experimental induction of BMLs in the palmarodistal MC3 condyles, combined with high-speed treadmill exercise, resulted in a variable, bilateral forelimb lameness that waxed and waned throughout the study period but was significantly increased compared to baseline. There were significant interactions between certain variables – primarily between horse and limb, in which differences only existed between limbs for certain horses or vice versa – for the outcome parameters measured ($p < 0.05$); however, this was outside the scope of the preliminary pilot study and future correlation analysis is required to determine the potential cause of these interactions, as there did not appear to be any obvious patterns associated with these interactions.

Lameness Grade (0-5) & Whole Horse Lameness Grade (0-10)

Overall, the lameness grade at weeks 2 ($p = 0.0161$), 8 ($p = 0.0370$), 16 ($p = 0.0161$), and 24 ($p = 0.0370$) were significantly increased compared to baseline (Figure 3.1 and 3.2). There was also a marginal increase in lameness at week 4 compared to baseline ($p = 0.0832$). There were no significant differences in lameness grade between horses ($p = 0.3532$) or between limbs ($p = 0.8205$).

When examining the whole horse lameness score (Figure 3.3), which was the sum of lameness scores for the left and right forelimbs for each horse, lameness was significantly worse at weeks 2 ($p = 0.0097$), 8 ($p = 0.0237$), 16 ($p = 0.0097$), and 24 ($p = 0.0237$) compared to baseline, and marginally worse at week 4 compared to baseline ($p = 0.0570$). There were no significant differences in lameness between individual horses ($p = 0.3091$) for the whole horse lameness score.

Flexion Grade (0-4)

The response to flexion was significantly greater, i.e. lameness was worse following flexion of the fetlock, at weeks 4 ($p = 0.0100$), 12 ($p = 0.0045$), 16 ($p = 0.0490$), and 20 ($p = 0.0222$) compared to baseline (Figure 3.1 and 3.2), with no significant differences in flexion between any of the other time comparisons ($p > 0.10$). There were no significant differences in the response to flexion among horses ($p = 0.5439$) or between limbs ($p = 0.2056$), overall.

Effusion Grade (0-4)

Effusion of the metacarpophalangeal joint was significantly worse at all post-operative time points compared to baseline (Figure 3.1 and 3.2; $p < 0.0001$), and at week 4 compared to week 20 ($p = 0.0298$). Effusion was also worse in horse #2 ($p = 0.0010$) compared to the other

two horses (Figure 3.2; $p = 0.0010$). There were no significant differences in effusion between limbs based on the analysis of variance (ANOVA) testing ($p = 0.0769$).

There was significant variation in the differences among horses based on the specific time point (Figure 3.2; $p < 0.0001$); no significant differences were present, however, by week 24 ($p > 0.10$). Two weeks postoperatively, horse #1 had significantly less effusion compared to both horse #2 ($p = 0.0037$) and horse #3 ($p = 0.0003$). By week 4, effusion in horse #3 had significantly improved and was better compared to both horse #1 ($p = 0.0474$) and horse #2 ($p = 0.0037$). Effusion grade generally remained highest in horse #2 and lowest in horse #3 for the remainder of the study, with the level of significance between the three horses varying depending on the individual time point. In horse #1, joint effusion was increased at weeks 4, 8, 12, 16, and 24 compared to baseline ($p < 0.003$), and at week 4 compared to weeks 2 and 20 ($p = 0.0228$). In horse #2, joint effusion was increased at all time points compared to baseline ($p < 0.003$), with no significant differences between the postoperative time points ($p > 0.10$). In horse #3, joint effusion was increased at all time points except week 16 compared to baseline ($p < 0.003$), peaking at week 2 compared to all postoperative time points ($p < 0.05$) except week 24.

Range of Motion Grade (0-3)

Overall, there was a greater reduction in range of motion and an increase in pain response in left forelimbs compared to right forelimbs ($p = 0.0002$). The reduction in fetlock range of motion was observed later in the post-operative period, with a significant reduction in range of motion observed at weeks 8 ($p = 0.0036$), 12 ($p = 0.0006$), 16 ($p = 0.0215$), and 20 ($p = 0.0006$) compared to baseline and to weeks 2 and 4 (Figure 3.1 and 3.2). There were no significant differences in range of motion between weeks 0, 2, and 4 ($p > 0.10$). Range of motion was not significantly different from baseline by week 24 ($p = 0.1239$). There were no significant

differences in range of motion between horses ($p = 0.0824$); however, a reduction in range of motion appeared to peak earlier for horse #2 (week 12) compared to horses #1 and #3 (week 20).

Limb Symptomatic Grade (0-16)

The limb symptomatic grade, for which each horse's scores for the four lameness parameters were summed together for each limb, was significantly higher at all time points compared to baseline (Figure 3.1 and 3.2; $p < 0.0001$), with no significant differences between any of the postoperative time points ($p > 0.10$). There were no significant differences in the limb symptomatic grade among horses ($p = 0.3639$) or between limbs ($p = 0.2134$).

Whole Horse Symptomatic Grade (0-32)

For the whole horse symptomatic grade, for which the limb symptomatic grades were summed for each horse, horses were more symptomatic at all time points compared to baseline (Figure 3.3; $p < 0.004$). There were no significant differences in grade between individual horses ($p = 0.6091$).

3.3.2 Synovial Fluid Analysis

Results of leukocyte differential and total protein from the synovial fluid analysis for each horse, including the within horse means, are provided in Table 3.3. Graphs showing the results of the same synovial fluid analysis parameters over time, shown as the mean (range) for each horse and the overall mean, are provided in Figures 3.4 and 3.5. Graphs comparing the leukocyte differentials for each horse over time, reported as the mean (range) percentage of the total nucleated cell count compromised of each cell type, are provided in Figure 3.6.

On cytologic evaluation, varying numbers of vacuolated large mononuclear cells were present at all time points in all horses throughout this study. Granulated lymphocytes were

present at weeks 4, 12 and 24 in horse #1, weeks 0, 2, 8, 20 and 24 in horse #2, and at all time points in horse #3.

Total Nucleated Cell Count (cells/uL)

Overall, synovial fluid total nucleated cell counts fell within or just above the reference range of 1,000 cells/uL. There was a significant difference in total nucleated cell count among horses (Figure 3.4; $p = 0.0486$), but not between limbs or over time, with no significant interactions ($p > 0.05$). The total nucleated cell count was marginally higher, overall, in horse #3 compared to horse #1 ($p = 0.0933$) and horse #2 ($p = 0.0645$). There were no significant differences in total nucleated cell count between horse #1 and horse #2 ($p = 0.9768$). Subjectively, horse #3 had a higher total nucleated cell count at baseline in the right metacarpophalangeal joint (3,000 cells/uL) compared to horses #1 (1,100-1,200 cells/uL) and #2 (200-400 cells/uL), with only 13% neutrophils. There was no lameness, positive response to flexion, or joint effusion associated with the elevated cell count in this forelimb, and the cause of this elevated total nucleated cell count was unknown. This may have contributed to the lack of difference in total nucleated cell count between baseline and the post-operative time points, overall. Despite the lack of statistical significance ($p > 0.10$), the total nucleated cell count did appear to increase in horse #3 from week 4 to week 16, after which it returned to the reference range by week 24. The total nucleated cell count in horse #2 changed minimally from baseline through week 16 but appeared to begin a gradual incline from week 16 to 24; however, there were no significant differences in total nucleated cell count between any time points for horse #2 ($p > 0.10$). The changes in cell count for horse #1 were also minimal, with no significant differences over time ($p > 0.10$), and the total nucleated cell counts remained under 1,000 cell/uL at every time point after baseline.

Red Blood Cell Count (cells/uL)

The synovial red blood cell count was not significantly influenced by horse ($p = 0.4515$), limb ($p = 0.9281$), or time point ($p = 0.4581$), or any of the interactions tested ($p > 0.05$).

Total Protein (g/dL)

Overall, the total protein in the synovial fluid fell at or below the reference limit of 2.5 g/dL, with a total protein above 2.5 g/dL in only 7 out of 48 total samples. The total protein was significantly higher at weeks 4 and 12 compared to week 2 and week 8 (Figure 3.4; $p < 0.05$). While only achieving marginal significance, the total protein was lower at week 24 compared to week 4 ($p = 0.0887$) and week 12 ($p = 0.0814$). There were no significant differences in the total protein between baseline and any of the postoperative time points in this study ($p > 0.10$).

There were no significant differences in synovial total protein among horses, overall ($p = 0.3156$); however, there was variation in the relationship between horses depending on the time postoperatively, and vice versa (Figure 3.4). At baseline, the total protein for horse #3 was significantly higher compared to horse #2 ($p = 0.0376$) with no differences between horse #1 and horses #2 or #3 ($p > 0.10$). At week 4, the total protein for horse #1 was significantly lower compared to both horse #2 ($p = 0.0005$) and horse #3 ($p = 0.0194$). While only marginally significant, the total protein was also lower in horse #1 compared to horse #3 ($p = 0.0831$) at week 12. There were no significant differences in total protein between horses at weeks 2, 8, 16, 20, or 24 ($p > 0.10$). While these differences existed, the amount of variation makes it difficult to draw any conclusions about differences between horses.

Subjectively, the total protein for horse #1 appeared to gradually increase throughout the study, peaking at week 20 prior to returning to normal by week 24; however, there were no significant differences between time points for horse #1 ($p > 0.10$) and all values were below the

reference limit of 2.5 g/dL. The other two horses had more variable patterns in total protein, peaking at week 4 and 12 but being relatively normal at all other time points. In horse #2, the total protein was significantly higher at week 4 compared to baseline and weeks 2, 8 (marginal; $p = 0.0759$), 16, and 20 ($p < 0.05$). In horse #3, there were no significant differences between baseline and any of the postoperative time points ($p > 0.10$). The synovial fluid total protein was marginally higher in this horse at week 4 compared to weeks 2 ($p = 0.0759$) and 8 ($p = 0.0653$), and at week 12 compared to week 16 ($p = 0.0880$), and significantly higher at week 12 compared to weeks 8 ($p = 0.0163$) and 24 ($p = 0.0482$).

Leukocyte Differential (%)

Overall, the percentage of neutrophils was greater than the reference limit of 10% in 24/48 of the synovial fluid samples. Synovial fluid contained a higher percentage of neutrophils at week 20 (Figure 3.5) compared to baseline ($p = 0.0357$) and weeks 2 ($p = 0.0045$), 4 ($p = 0.0015$) and 8 ($p = 0.0331$). The percentage of neutrophils was also higher at week 24 compared to weeks 2 ($p = 0.0402$) and 4 ($p = 0.0131$). There were no significant differences in the percentage of neutrophils in the synovial fluid at weeks 2, 4, 8, 12, 16, or 24 compared to baseline ($p > 0.10$).

Overall, there were no significant differences in the percentage of neutrophils among horses ($p = 0.0867$). While differences between horses were insignificant to marginal from baseline through week 16, there was a peak in the percentage of neutrophils in horse #3 at week 12 and horse #2 experienced a late rise in neutrophils by weeks 20 and 24. The percentage of neutrophils in the synovial fluid was significantly higher in horse #2 compared to horse #3 at week 20 ($p = 0.0194$) and compared to horses #1 and #3 by week 24 ($p < 0.003$).

There were no significant differences in the percentage of large mononuclear cells, small mononuclear cells, eosinophils, basophils, or mitotic figures in the synovial fluid between horses, limbs, or time points in this study ($p > 0.05$).

Leukocyte Differential (cells/uL)

Interestingly, when looking at the absolute cell counts, there were no significant effects of horse, limb, or time on the number (cells/uL) of neutrophils, large mononuclear cells, eosinophils, basophils, or mitotic figures in the synovial fluid ($p > 0.05$). Variation between individual horses, however, did have a significant effect on the number of small mononuclear cells in the synovial fluid (Figure 3.5; $p = 0.0018$). The number of small mononuclear cells per microliter of synovial fluid was significantly greater in horse #3 compared to both horse #1 ($p = 0.0329$) and horse #2 ($p = 0.0014$). The number of small mononuclear cells did not change significantly over time ($p = 0.5349$). Despite the lack of statistical significance, there appeared to be a spike in the number of large mononuclear cells per microliter of synovial fluid in horse #3 at week 16, something which did not occur in the other two horses. This was potentially a significant contributor to the peak in total nucleated cell count at week 16 in horse #3.

Glycosaminoglycan (GAG) Quality

There was more GAG disruption in synovial fluid samples from week 20 compared to weeks 2 and 8 ($p = 0.0408$), with a marginal increase in GAG disruption compared to weeks 4 and 24 ($p = 0.0904$). There were no other significant differences in GAG quality between the remaining time point comparisons, including when comparing each time point to baseline ($p > 0.10$). There were no significant differences in GAG quality between horses ($p = 0.7020$).

3.4 Discussion

These results provide proof of concept that the pin penetration model, followed by 6 months of high-speed treadmill exercise, produced clinically-detectable effects in each horse throughout the study period. Similar to POD, this model induced a dynamic, bilateral forelimb lameness that persisted, though to variable degrees. Furthermore, this corresponded to an increased response to flexion, increased joint effusion and a reduction in range of motion, with the latter proving to be a later development compared to the remaining parameters. Overall, the symptomatic grades increased following lesion induction and remained similarly greater throughout the study. Subchondral bone injury, including the presence of bone marrow lesions (BMLs), has been linked with the presence of pain in both horses and humans.[10,16,25–27,17–24] As will be demonstrated in the next chapter, this experimental model resulted in the consistent development of BMLs in all condyles that persisted throughout the 6-month study period. Similar to the early stages of clinical POD,[3] the degree of lameness induced by this experimental model was mild to moderate with an average lameness score of approximately 1 to 2 out of 5 throughout the study. Additionally, the general plateau in clinical signs seen here, despite continued training without treatment, has also been reported in some cases of POD.[8] In the experimental impact model published by Rickey et al.,[15] statistically similar lameness was observed (grade 3-3.5 out of 5) in both treated limbs and sham operated control limbs and persisted for a mean of 6 ± 6.5 weeks. It was suggested that the pain created with this technique was more likely caused by soft tissue damage at surgery rather than progression of disease.[15] While a sham-operated limb was not included in the present pilot study, the minimally-invasive nature of the technique makes it unlikely for lameness to have been caused by the surgical approach.

In contrast to early POD, however, localizing clinical signs including effusion and a positive response to flexion developed as early as 2-4 weeks, postoperatively. Being a primary disease of the subchondral bone, these localizing clinical signs typically do not occur until significant damage to the articular cartilage has occurred.[1,4–7] While the articular cartilage is devoid of innervation, the surrounding tissues such as the joint capsule, synovium, bone, tendons, and ligaments are rich in pain receptors and have all been identified as sources of pain in osteoarthritis, and can stimulate the release of pro-inflammatory cytokines into the joint.[10] One of the clinical signs observed in this study, joint effusion, is initiated by the inflammatory events within the joint and can be associated with discomfort due to an increase in synovial pressure. This results in abnormal usage of the joint and when allowed to continue without intervention, the inflammatory processes taking place lead to changes in the joint capsule and synovium that result in a reduction in joint range of motion.[10] The early development of these signs is suspected to be due to the nature of the model, in which a direct communication between the subchondral bone and the rest of the joint is created at the time of lesion induction, potentially resulting in the increased release of inflammatory mediators. While this communication was suspected to have been sealed early in the postoperative period based on diagnostic imaging, as will be described in Chapter 4, it is also possible that the combination of subchondral bone injury and focal articular cartilage healing resulted in the continuation of clinical signs. Since histopathology was not performed at all time points in this study, and without further analysis to determine the level of communication between the subchondral bone and the joint fluid at various stages, definitive conclusions cannot be made.

Arthrocentesis and synovial fluid analysis have been integral to the clinical evaluation of joint disorders in multiple species, especially in cases in which significant joint effusion is

present, as inflammatory, traumatic, and degenerative arthropathies can be reflected in changes in the synovial fluid. At the point of injury, chondrocytes and synoviocytes release cytokines, resulting in the vasodilation of capillaries underlying the synovial membrane, increased vascular permeability, and inevitably, the loss of fluid, protein, and inflammatory cells into the joint space.[28] The cellular composition of the joint fluid then helps to define the features of the occurring joint disease, such as non-inflammatory arthritis (degenerative joint diseases, joint trauma, hemarthrosis) versus infectious inflammatory disease versus noninfectious inflammatory disease (immune-mediated).[28] Despite altered regulation of several well-established markers of osteoarthritis, there is limited activation of pro-inflammatory and catabolic genes with POD, which suggests a distinct molecular phenotype compared to other similar diseases like post-traumatic osteoarthritis.[29]

In a study evaluating experimental impact injury for inducing post-traumatic osteoarthritis in the metacarpophangeal joint in horses, results of the synovial fluid analysis were within reference intervals for all horses at all time points over the 10-month study period, with no difference in synovial fluid variables between impact-injured and control joints.[15] These horses also exhibited a mild response to the procedure with a mild to moderate postoperative lameness that improved over time. Overall, the total nucleated cell counts in the present pilot study were near or below the upper limits of the reference interval (1,000 cells/uL), with the range of overall means across all horses being 467 to 1,117 cells/uL. The total nucleated cell counts also increased with continued exercise, exceeding the upper limit of normal at weeks 16 and 20 but then decreasing by week 24. Despite the focal trauma to the articular surface and corresponding communication into the subchondral and trabecular bones, this is a fairly mild inflammatory response. The ratio of cell types within the synovial fluid from each horse, and

thus the nature of the inflammatory response to this experimental model, was observed to be variable between horses; however, the differential appeared to contain primarily mononuclear cells at a majority of time points. Horse #3 had a marginally higher total nucleated cell count compared to the other two horses, and the mean cell count in this horse at baseline was increased in the right metacarpophalangeal joint with only 13% neutrophils: a minimal increase relative to the reference interval of less than 10% neutrophils. As mentioned above, there was no lameness, positive response to flexion, or joint effusion associated with the elevated cell count in this forelimb. It cannot be ruled out that this may have contributed to the lack of difference in total nucleated cell count between baseline and the post-operative time points, overall. The cause for this is unknown and given both the small sample size and variation between horses, no definitive conclusions can be made based on the current data.

As shown in Figure 3.6, the leukocyte differential was highly variable between individual horses. The percentage of neutrophils in horse #1 declined following lesion induction, then increased above the reference interval (10%) after the 4-week postoperative time point; however, there were no significant differences in the percentage of neutrophils between any time points. Horse #2 maintained an unremarkable leukocyte differential until week 16, after which there was a shift from a predominantly mononuclear to neutrophilic cell population at weeks 20 and 24, with the percentage of neutrophils being significantly greater at these two time points compared to all others. Lastly, horse #3 had a mild increase in the percentage of neutrophils at week 12, which was only marginally greater compared to weeks 2 and 24, but returned to below baseline by week 24.

Findings from this experimental model were consistent with a primarily mononuclear response, consisting of lymphocytes (small mononuclear cells) and large mononuclear cells;

however, synovial fluid analysis could also be considered within reference limits depending on the horse, limb, and postoperative time point. This is indicative of a non-inflammatory arthropathy, such as that from degenerative or traumatic joint diseases, that produces a mild nonsuppurative response often indistinguishable from normal synovial fluid.[30] Findings that help to distinguish the synovial fluid in this study from that of a healthy joint include: intermittent increase of synovial total protein; variable numbers of granulated lymphocytes; intermittent cytoplasmic vacuolization of large mononuclear cells, consistent with macrophage activation; and variable disruption of the glycosaminoglycan background layer.[30] Importantly, this study showed that lesion induction using the pin-penetration technique did not incite an abnormal or overtly pathologic response when measured as early as 2 weeks, postoperatively.

There are several limitations to this study, the most significant being the small sample size. Using the statistical model in this study, the high number of variables included in the model meant that a smaller change would result in a larger difference; however, it is difficult to otherwise identify significant differences between three horses. Despite this limitation, the primary objectives of this pilot study were to evaluate the ability to induce BMLs in the palmarodistal MC3 condyles of horses and measure the effects of lesion induction over time. This pilot study also lacked a control group in which lesions were induced but horses were maintained on box-stall rest, with another potential control group being one in which horses were exposed to the same high-speed treadmill protocol without lesion induction. This would allow investigators to better examine the individual contributions of exercise versus lesion induction to the clinical findings. Based on findings from Kawcak et al., in which a similar exercise protocol was used, four out of six exercised horses became lame approximately three months after beginning exercise.[31] Furthermore, these horses also exhibited a response to fetlock flexion and

joint effusion. Another significant limitation was the induction of lesions in both forelimbs and thus, the creation of a bilateral forelimb lameness which may have hindered the ability to accurately grade lameness in individual forelimbs. More objective modalities for measuring lameness could be considered in future studies.

One important consideration is that repeat arthrocentesis could affect outcomes of future lameness exams and synovial fluid analysis. In a study of four horses,[32] in which the left and right intercarpal joints were sampled as frequently as every 2 to 7-10 days with a final break for the last 30 days, all horses remained free from lameness throughout the study. This study showed an increase in macrophages and decrease in lymphocytes with frequent sampling over 2 weeks, but the values returned to normal when the 30-day break was provided. Additionally, cell counts were still within the normal reference ranges for healthy joint fluid. A study in dogs found that serial arthrocentesis at 3-week intervals was rarely associated with mild mononuclear inflammation, without neutrophil involvement, and this change was secondary to exercise.[33] It has also been reported in horses that cell counts tend to peak closer to 24 hours following arthrocentesis, returning to normal within another 24 hours.[34] Based on these findings, it is unlikely that monthly arthrocentesis performed in this study had an effect on lameness and synovial fluid parameters; however, the confounding effects of exercise cannot be ruled out. Induction of a chemical synovitis from intra-articular contrast is another consideration; however, all synovial fluid samples were acquired prior to contrast injection and if a chemical synovitis occurs, it usually resolves within three to seven days.[12,30] A further limitation of this study was that the fluid volume aspirated was not recorded for every horse at every time point; therefore, it is unknown whether the effusion in this study was truly an increase in synovial fluid volume or if there was a component of synovial and joint capsule thickening. This could be measured in

future studies with a correlation analysis performed to determine whether the fluid volume aspirated was related to the severity of joint effusion on clinical examination.

Unfortunately, the correlation between clinical signs and disease severity is often poor in both humans and horses.[10] In all three horses, symptomatic grades were increased compared to baseline by 2 weeks postoperatively and remained elevated, without progression, throughout the 6-month study period. There were no obvious associations between the synovial fluid analysis parameters and the clinical exam findings; however, further analysis is required and likely in a larger sample size before any definitive conclusions can be made. Synovial fluid analysis is further complicated by the fact that degenerative processes affecting joints can have minimal to no inflammation reflected in the synovial fluid, with overlap between cell counts from normal and osteoarthritic joints.[12] This is why it is critical to pair synovial fluid analysis with clinical examination. Given the nature of the pin penetration model, combined with the resulting lesions identified on diagnostic imaging (Chapter 4), it was surprising that the inflammatory response was not more significant. Further analysis involving measurement of specific pro- and anti-inflammatory cytokines over time is required to gather more information regarding the joint environment induced by the model. This work is underway and will be examined further moving forward (see Chapter 6).

3.5 Figures

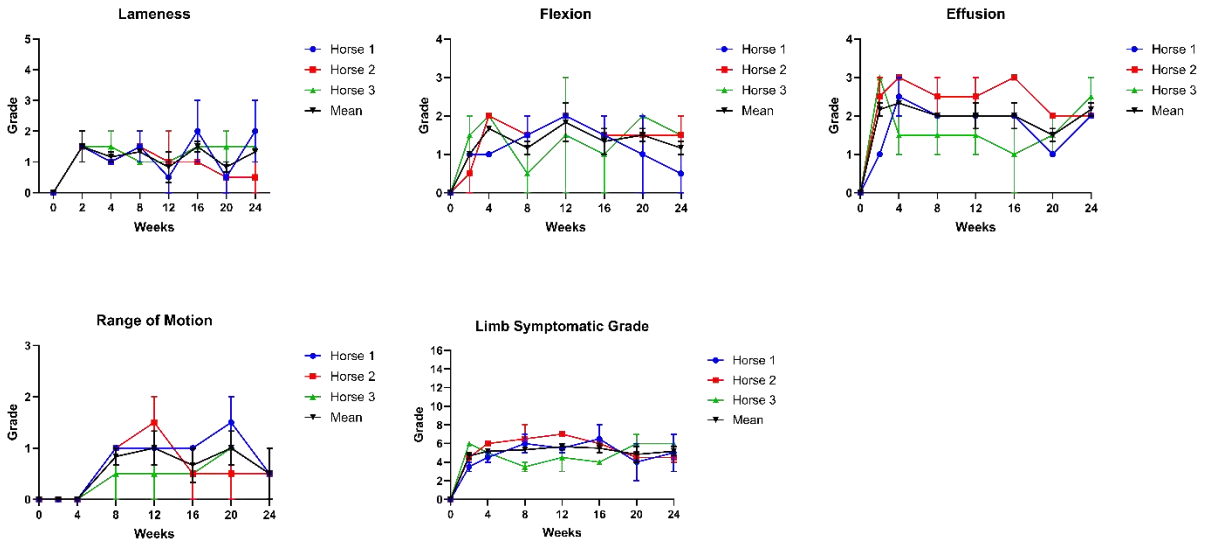

Figure 3.1 – Graphs showing the mean (range) grades for each horse over time for each of the outcome parameters evaluated, including the limb symptomatic grade (sum of grades of all four parameters for each limb). For each parameter, an overall mean score from all horses was also provided (black).

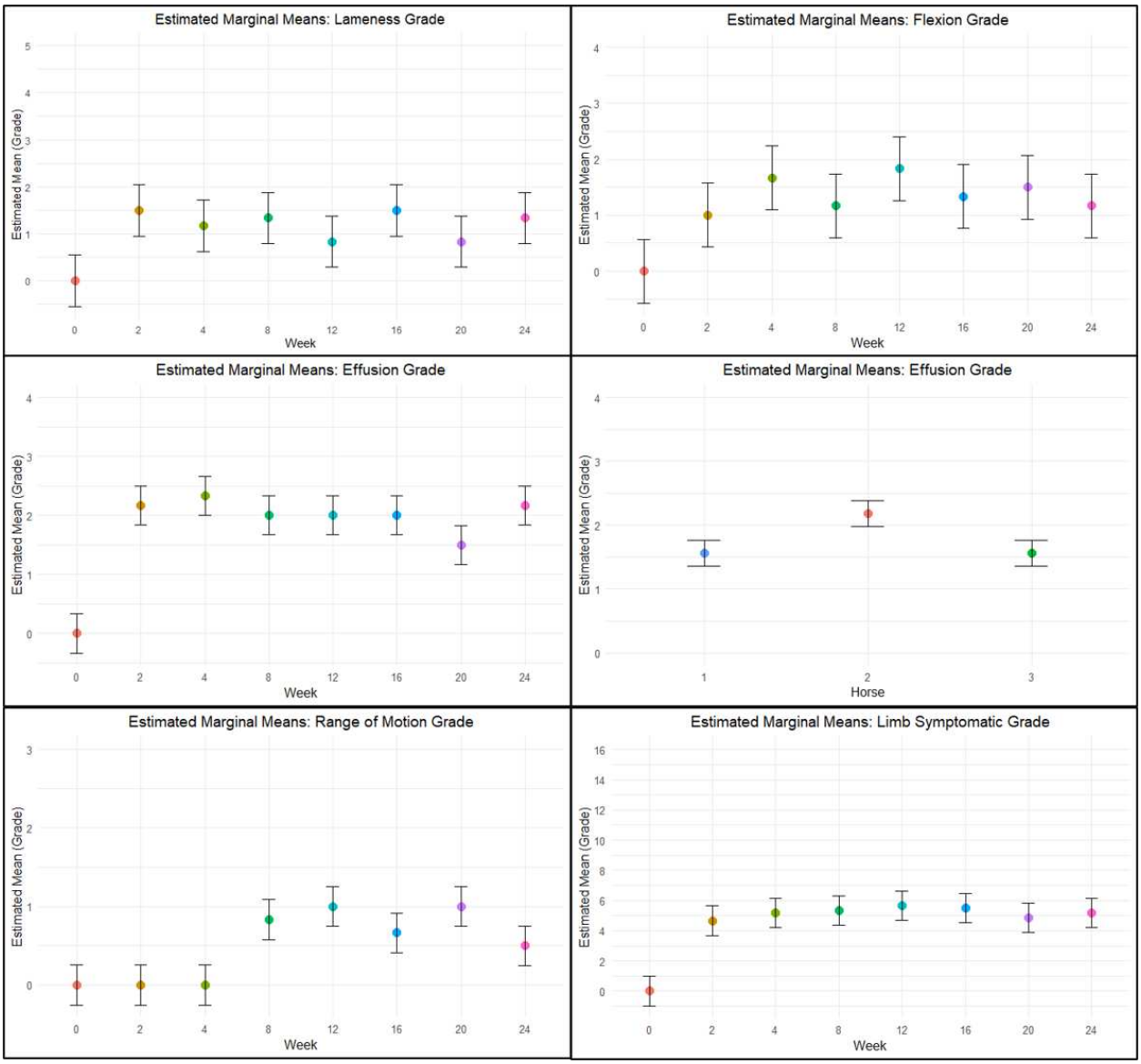

Figure 3.2 – Plots showing the estimated marginal means (95% CI) from the analysis of variance (ANOVA) and pairwise comparisons testing for each of the lameness examination parameters over time. Significant differences between horses were only detected for the grade of effusion (middle right image).

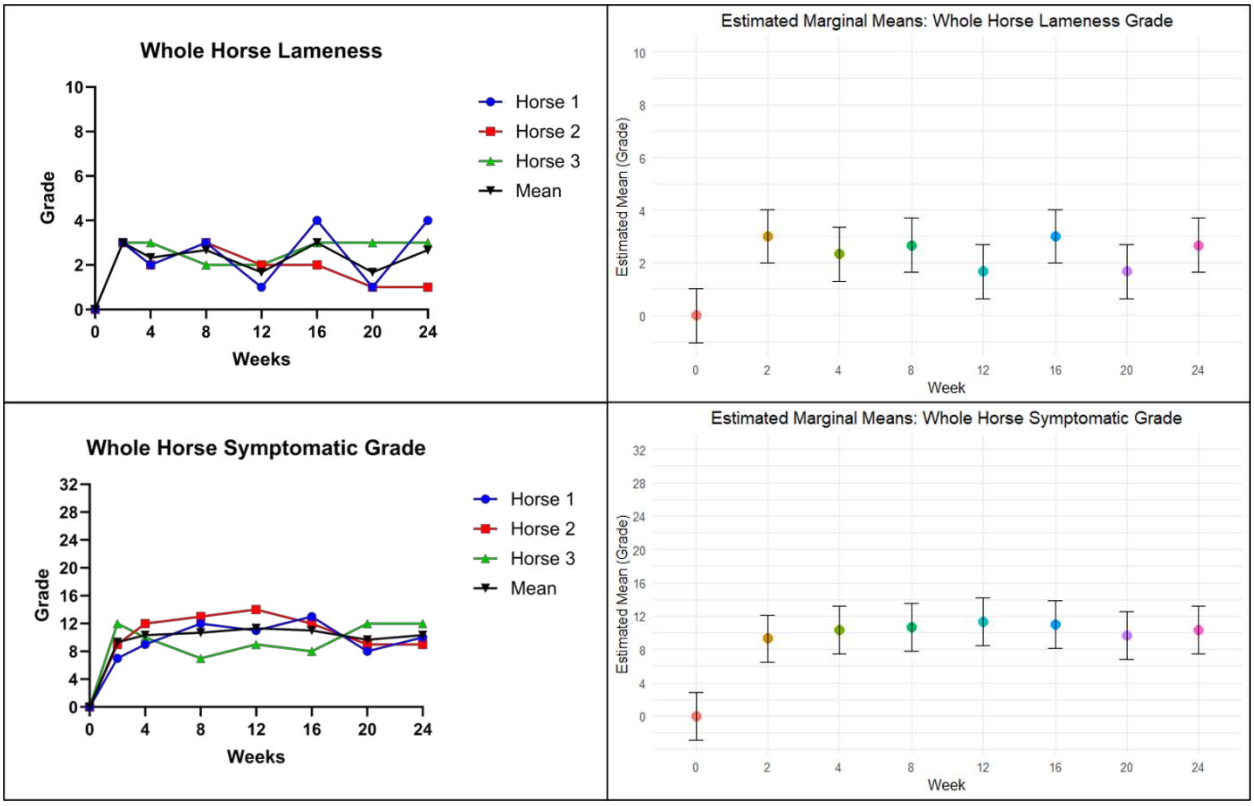

Figure 3.3 – *Left Images*: Graphs showing the mean grades for the whole horse lameness grade and whole horse symptomatic grades. For each parameter, an overall mean score from all horses was also provided (black). *Right Images*: Plots showing the estimated marginal means (95% CI) from the analysis of variance (ANOVA) and pairwise comparisons testing for the whole horse lameness and whole horse symptomatic grades over time.

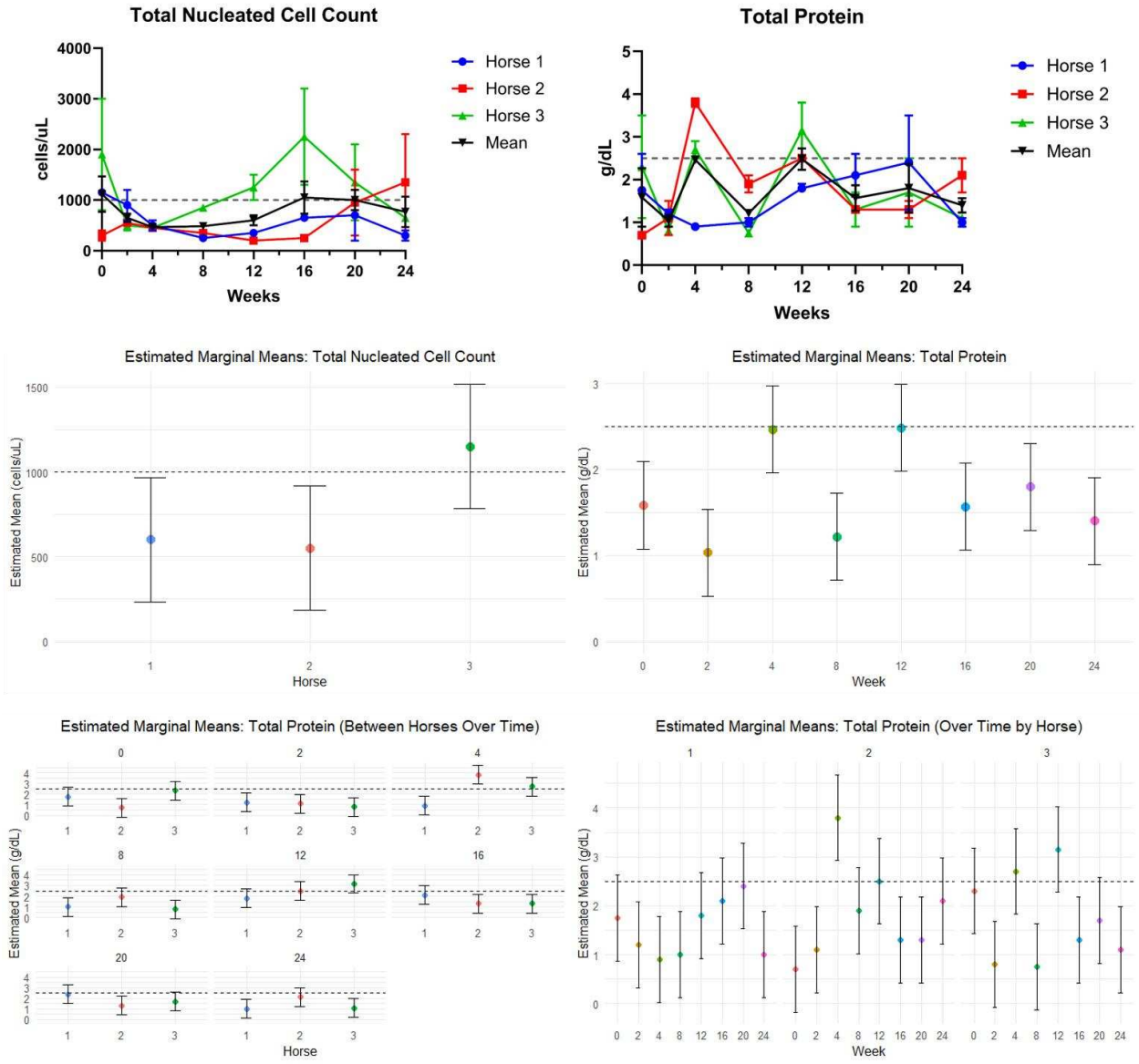

Figure 3.4 – *Top Row*: Graphs showing the mean (range) total nucleated cell count and total protein for each horse over time. For each parameter, an overall mean score from all horses was also provided (black). The horizontal dotted line in each graph represents the upper limit of the reference range for that parameter. *Bottom Two Rows*: Plots showing the estimated marginal means (95% CI) from the analysis of variance (ANOVA) and pairwise comparisons testing. Only horse and time had significant effects on the total nucleated cell count and total protein, respectively, with differences in total protein between horses varying depending on time and vice versa. There were no significant differences in total nucleated cell count over time, with minimal differences between horses. The horizontal dotted line in each plot represents the upper limit of the reference range for that parameter.

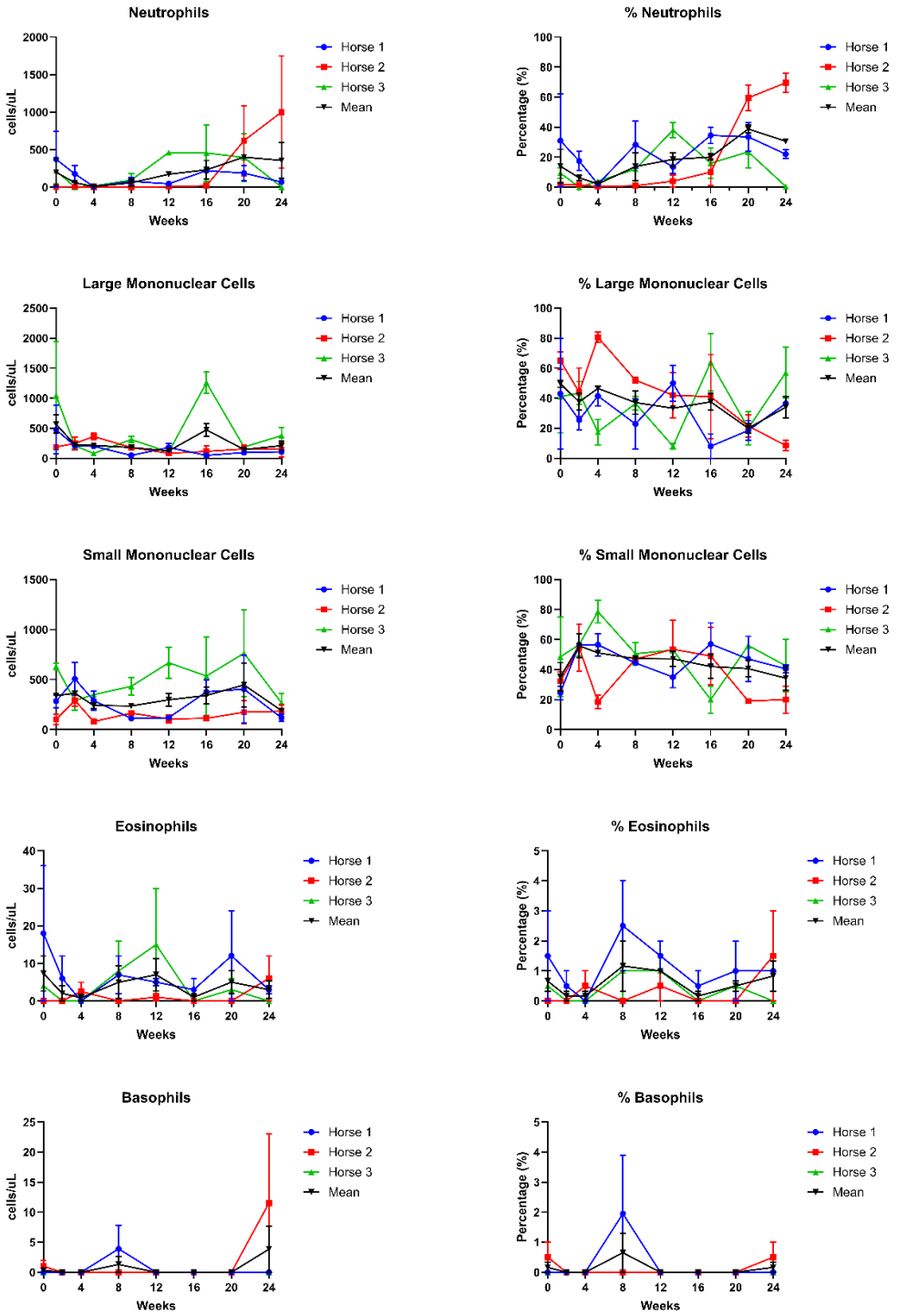

Figure 3.5 – Graphs showing the mean (range) cells/uL (left column) and percentage of the total nucleated cell count (right column) for each horse over time for each of the cell types included in the synovial fluid differential. For each parameter, an overall mean score from all horses was also provided (black).

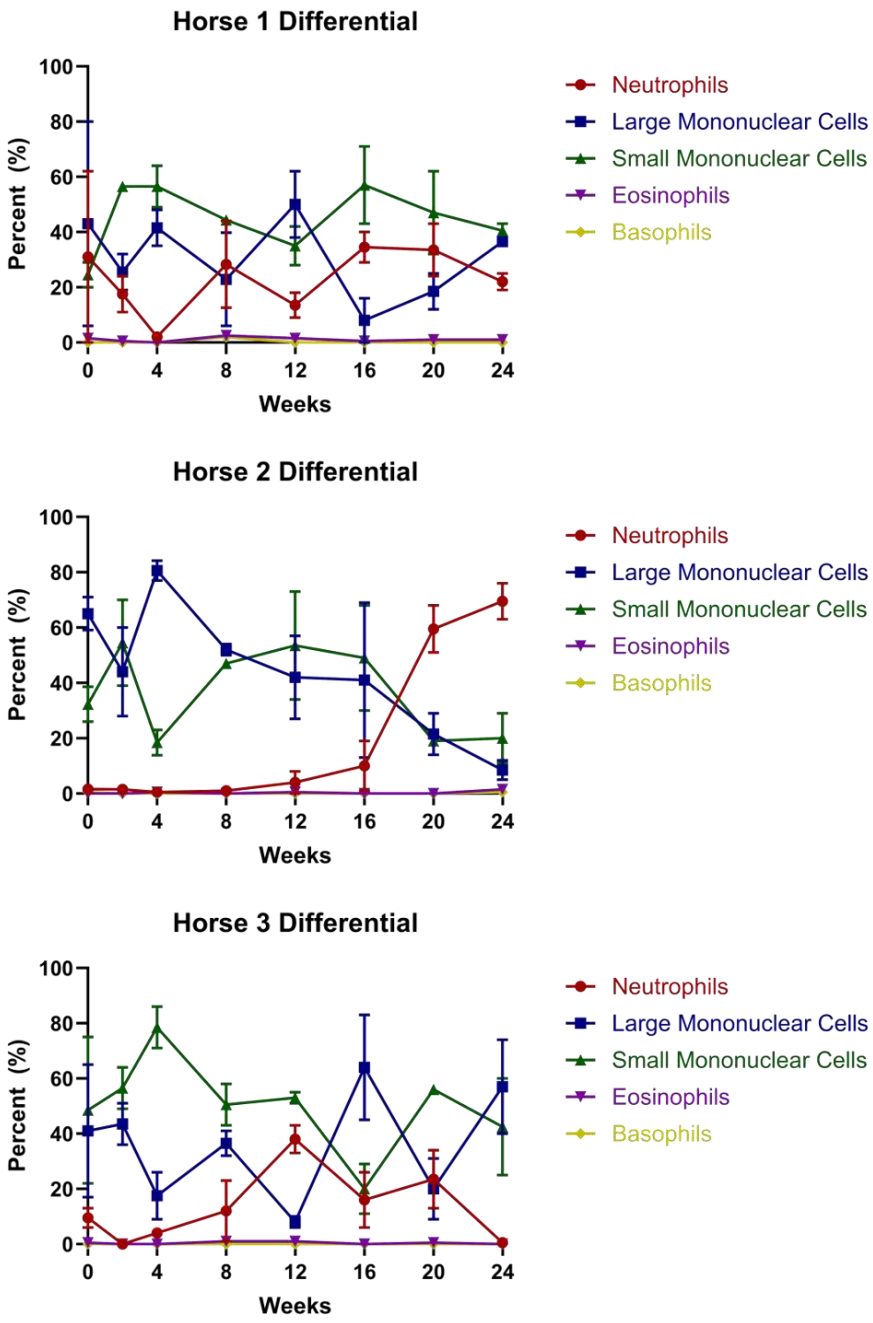

Figure 3.6 – Graphs showing the mean (range) percentage of the total nucleated cell count accounted for by each of five cell types for each horse over time. These graphs are provided to demonstrate the variations in the leukocyte differentials between the three horses.

3.6 Tables

Table 3.1 – Results of the lameness evaluation, including mean values for each horse at each time point. The grading scale for each parameter is provided alongside each subtitle within the table. *Left forelimb (LF), Right forelimb (RF).*

Week	Horse #1			Horse #2			Horse #3		
	LF	RF	Mean	LF	RF	Mean	LF	RF	Mean
Lameness (0-5)									
0	0	0	0	0	0	0	0	0	0
2	2	1	1.5	2	1	1.5	2	1	1.5
4	1	1	1	1	1	1	1	2	1.5
8	2	1	1.5	1	2	1.5	1	1	1
12	1	0	0.5	0	2	1	0	2	1
16	3	1	2	1	1	1	1	2	1.5
20	1	0	0.5	0	1	0.5	2	1	1.5
24	3	1	2	0	1	0.5	1	2	1.5
Flexion (0-4)									
0	0	0	0	0	0	0	0	0	0
2	1	1	1	1	0	0.5	1	2	1.5
4	1	1	1	2	2	2	2	2	2
8	2	1	1.5	1	2	1.5	0	1	0.5
12	2	2	2	2	2	2	0	3	1.5
16	2	1	1.5	1	2	1.5	0	2	1
20	2	0	1	1	2	1.5	2	2	2
24	1	0	0.5	1	2	1.5	1	2	1.5
Effusion (0-4)									
0	0	0	0	0	0	0	0	0	0
2	1	1	1	2	3	2.5	3	3	3
4	2	3	2.5	3	3	3	2	1	1.5
8	2	2	2	2	3	2.5	2	1	1.5
12	2	2	2	3	2	2.5	2	1	1.5
16	2	2	2	3	3	3	2	0	1
20	1	1	1	2	2	2	2	1	1.5
24	2	2	2	2	2	2	3	2	2.5
Range of Motion (0-3)									
0	0	0	0	0	0	0	0	0	0
2	0	0	0	0	0	0	0	0	0
4	0	0	0	0	0	0	0	0	0
8	1	1	1	1	1	1	1	0	0.5
12	1	1	1	2	1	1.5	1	0	0.5
16	1	1	1	1	0	0.5	1	0	0.5
20	2	1	1.5	1	0	0.5	1	1	1
24	1	0	0.5	1	0	0.5	1	0	0.5
Limb Symptomatic Grade (0-16)									
0	0	0	0	0	0	0	0	0	0
2	4	3	3.5	5	4	4.5	6	6	6
4	4	5	4.5	6	6	6	5	5	5
8	7	5	6	5	8	6.5	4	3	3.5
12	6	5	5.5	7	7	7	3	6	4.5
16	8	5	6.5	6	6	6	4	4	4
20	6	2	4	4	5	4.5	7	5	6
24	7	3	5	4	5	4.5	6	6	6

Table 3.2 – Results of the whole horse lameness scoring and whole horse symptomatic scoring systems, including mean values for each time point. The grading scale for each parameter is provided alongside each subtitle within the table.

Week	Horse #1	Horse #2	Horse #3	Mean
Whole Horse Lameness Grade (0-10)				
0	0	0	0	0
2	3	3	3	3
4	2	2	3	2.33
8	3	3	2	2.67
12	1	2	2	1.67
16	4	2	3	3
20	1	1	3	1.67
24	4	1	3	2.67
Whole Horse Symptomatic Grade (0-32)				
0	0	0	0	0
2	7	9	12	9.33
4	9	12	10	10.33
8	12	13	7	10.67
12	11	14	9	11.33
16	13	12	8	11
20	8	9	12	9.67
24	10	9	12	10.33

Table 3.3 – Results of the synovial fluid analysis, including the individual values from each metacarpophalangeal joint and a mean for each horse, for each time point throughout this study. The units reported in this table are provided alongside each subtitle within the table. Mitotic figures (1%) were only present in a single joint at baseline in horse #2 and horse #3; they are not shown in this table. *Left forelimb (LF), Right forelimb (RF).*

Week	Horse #1			Horse #2			Horse #3		
	LF	RF	Mean	LF	RF	Mean	LF	RF	Mean
Total Nucleated Cell Count (cells/uL)									
0	1100	1200	1150	400	200	300	800	3000	1900
2	600	1200	900	500	600	550	600	400	500
4	600	400	500	500	400	450	500	400	450
8	200	300	250	300	400	350	900	800	850
12	400	300	350	200	200	200	1500	1000	1250
16	600	700	650	300	200	250	3200	1300	2250
20	1200	200	700	300	1600	950	2100	600	1350
24	200	400	300	2300	400	1350	700	600	650
Total Protein (g/dL)									
0	0.9	2.6	1.75	0.7	0.7	0.7	1.1	3.5	2.3
2	1.3	1.1	1.2	1.5	0.7	1.1	0.7	0.9	0.8
4	0.9	0.9	0.9	3.7	3.9	3.8	2.9	2.5	2.7
8	0.9	1.1	1	2.1	1.7	1.9	0.7	0.8	0.75
12	1.9	1.7	1.8	2.5	2.5	2.5	3.8	2.5	3.15
16	1.6	2.6	2.1	1.3	1.3	1.3	0.9	1.7	1.3
20	3.5	1.3	2.4	1.1	1.5	1.3	2.5	0.9	1.7
24	1.1	0.9	1	2.5	1.7	2.1	1.1	1.1	1.1
Neutrophils (%)									
0	0	62	31	2.3	1	1.65	6	13	9.5
2	11	24	17.5	2	1	1.5	0	0	0
4	1	3	2	1	0	0.5	3	5	4
8	12.6	44	28.3	0	2	1	1	23	12
12	9	18	13.5	0	8	4	33	43	38
16	40	29	34.5	1	19	10	26	6	16
20	24	43	33.5	51	68	59.5	34	13	23.5
24	19	25	22	76	63	69.5	1	0	0.5
Large Mononuclear Cells (%)									
0	80	6	43	59.1	71	65.05	17	65	41
2	32	19	25.5	28	60	44	36	51	43.5
4	35	48	41.5	84.2	77	80.6	26	9	17.5
8	39.8	6	22.9	54	50	52	41	32	36.5
12	62	38	50	27	57	42	10	6	8
16	16	0	8	69	13	41	45	83	64
20	12	25	18.5	29	14	21.5	9	31	20
24	37	36	36.5	12	5	8.5	74	40	57
Small Mononuclear Cells (%)									
0	20	29	24.5	38.6	26	32.3	75	22	48.5
2	57	56	56.5	70	39	54.5	64	49	56.5
4	64	49	56.5	13.9	23	18.45	71	86	78.5
8	42.7	46	44.35	46	48	47	58	43	50.5
12	28	42	35	73	34	53.5	55	51	53
16	43	71	57	30	68	49	29	11	20
20	62	32	47	20	18	19	57	55	56
24	43	38	40.5	11	29	20	25	60	42.5

Eosinophils (%)									
0	0	3	1.5	0	0	0	1	0	0.5
2	0	1	0.5	0	0	0	0	0	0
4	0	0	0	1	0	0.5	0	0	0
8	1	4	2.5	0	0	0	0	2	1
12	1	2	1.5	0	1	0.5	2	0	1
16	1	0	0.5	0	0	0	0	0	0
20	2	0	1	0	0	0	0	1	0.5
24	1	1	1	0	3	1.5	0	0	0
Basophils (%)									
0	0	0	0	0	1	0.5	0	0	0
2	0	0	0	0	0	0	0	0	0
4	0	0	0	0	0	0	0	0	0
8	3.9	0	1.95	0	0	0	0	0	0
12	0	0	0	0	0	0	0	0	0
16	0	0	0	0	0	0	0	0	0
20	0	0	0	0	0	0	0	0	0
24	0	0	0	1	0	0.5	0	0	0
Glycosaminoglycan Quality (0 = adequate, 1 = slightly disrupted, 2 = disrupted)									
0	0	2	1	0	1	0.5	0	1	0.5
2	0	1	0.5	0	0	0	0	0	0
4	0	0	0	1	1	1	0	0	0
8	0	1	0.5	0	0	0	0	0	0
12	0	0	0	2	2	2	0	0	0
16	2	1	1.5	0	0	0	1	2	1.5
20	2	1	1.5	0	2	1	2	2	2
24	0	0	0	2	0	1	0	0	0

3.7 References

1. Davidson E, Ross M. Clinical recognition of stress-related bone injury in racehorses. *Clin Tech Equine Pract*. 2003;2(4):296-311.

2. American Association of Equine Practitioners. Definition and classification of lameness. In: *Veterinarian's Guide to Equestrian Competition Official Duties*. Lexington, KY: American Association of Equine Practitioners; 2020:8.

3. Tull T, Bramlage L. Racing prognosis after cumulative stress-induced injury of the distal portion of the third metacarpal and third metatarsal bones in Thoroughbred racehorses: 55 cases (2000-2009). *J Am Vet Med Assoc*. 2011;238:1316-1322.

4. Kawcak C, Barrett MF. Fetlock. In: McIlwraith C, Frisbie D, Kawcak C, van Weeren PR, eds. *Joint Disease in the Horse*. Second Edi. St. Louis, Missouri: Elsevier; 2016:302-317.

5. Richardson D, Dyson S. The Metacarpophalangeal Joint. In: Ross M, Dyson S, eds. *Diagnosis and Management of Lameness in the Horse*. St. Louis, Missouri: Elsevier Saunders; 2011:394-410.

6. Arthur R, Blea J, Ross M, Moloney P, Cheney M. The North American Thoroughbred. In: Ross M, Dyson S, eds. *Diagnosis and Management of Lameness in the Horse*. 2nd Ed. St. Louis, Missouri: Elsevier Saunders; 2011:977-993.

7. Pilsworth R. The European Thoroughbred. In: Ross M, Dyson S, eds. *Diagnosis and Management of Lameness in the Horse*. 2nd Ed. St. Louis, Missouri: Elsevier Saunders; 2011:994-1013.

8. Ramzan PH. Mind the gaps: The science of POD and the racehorse fetlock. *Equine Vet J*. 2021;53:217-220.

9. Steel C. Equine synovial fluid analysis. *Vet Clin North Am - Equine Pract*. 2008;24:437.

10. Frisbie D, Johnson S. Synovial Joint Biology and Pathobiology. In: Auer J, Stick J, Kummerle J, Prange T, eds. *Equine Surgery*. 5th ed. St. Louis, Missouri: Elsevier; 2019:1326-1348.

11. Wood R, Koenig J, Sharkey L, Seelig D, Radin M. Synovial Fluid Analysis of the Horse. In: *Veterinary Cytology*. John Wiley & Sons, Inc.; 2020:736-743. doi:https://doi.org/10.1002/9781119380559.ch55

12. Walton R. Fluid Analysis. In: Walton R, ed. *Equine Clinical Pathology*. John Wiley & Sons, Inc.; 2014:203-232.

13. Frisbie D, Al-Sobayil F, Billinghurst R, Kawcak C, McIlwraith C. Changes in synovial fluid and serum biomarkers with exercise and early osteoarthritis in horses. *Osteoarthr Cartil*. 2008;16:1196-1204.

14. Mason S, O'Neill H, Bladon B. Synovial fluid parameters following acute articular fracture in the horse. *Vet Surg*. 2025;54(4):751-756.

15. Rickey EJ, Cruz A, Trout D, McEwen B, Hurtig M. Evaluation of experimental impact injury for inducing post-traumatic osteoarthritis in the metacarpophalangeal joints of horses. *Am J Vet Res*. 2012;73(10):1540-1552.

16. Powell S. Low-field standing magnetic resonance imaging findings of the metacarpo/metatarsophalangeal joint of racing Thoroughbreds with lameness localized to the region: A retrospective study of 131 horses. *Equine Vet J*. 2012;44:169-177.

17. Saltzman BM, Riboh JC. Subchondral Bone and the Osteochondral Unit: Basic Science and Clinical Implications in Sports Medicine. *Sport Heal A Multidiscip Approach*. 2018;10(5):412-418. doi:10.1177/1941738118782453

18. Sharkey P, Cohen S, Leinberry C, Parvizi J. Subchondral bone marrow lesions associated with knee osteoarthritis. *Am J Orthop*. 2012;41(9):413-417.

19. Krebs N, Kehoe J, Van Wagner M, Rios-Bedoya C. The efficacy of subchondroplasty for the treatment of knee pain associated with bone marrow lesions. *Spartan Med Res J*. 2020;4(2). doi:10.51894/001c.11767

20. Powell S, Ramzan P, Head M, Shepherd M, Baldwin G, Steven W. Standing magnetic resonance imaging detection of bone marrow oedema-type signal pattern associated with subcarpal pain in 8 racehorses: a prospective study. *Equine Vet J*. 2010;42:10-17.

21. Dyson S, Murray R, Schramme M, Branch M. Magnetic resonance imaging of the equine foot: 15 horses. *Equine Vet J*. 2003;35:18-26.

22. Starr A, Wessely M, Albastaki U, Pierre-Jerome C, Kettner N. Bone marrow edema: pathophysiology, differential diagnosis, and imaging. *Acta radiol*. 2008;49(7):771-786.

23. King J, Zubrod C, Schneider R, Sampson S, Roberts G. MRI findings in 232 horses with lameness localized to the metacarpo(tarso)phalangeal region and without a radiographic diagnosis. *Vet Radiol Ultrasound*. 2013;54:36-47.

24. Gonzalez L, Schramme M, Robertson I, Thrall D, Redding R. MRI features of metacarpo(tarso)phalangeal region lameness in 40 horses. *Vet Radiol Ultrasound*. 2010;51:404-414.

25. Dyson S, Murray R. Osseous trauma in the fetlock region of mature sports horses. In: *Proceedings American Association of Equine Practitioners*. ; 2006:443-456.

26. Felson D, Chaisson C, Hill C, et al. The association of bone marrow lesions with pain in knee osteoarthritis. *Ann Intern Med*. 2001;134(7):541-549.

27. Guio C, Segard-Weisse E, Thomas-Cancian A, Schramme M. Bone marrow lesions of the distal condyles of the third metacarpal bone are common and not always related to

lameness in sports and pleasure horses. *Vet Radiol Ultrasound*. 2019;60(2):167-175.

28. MacWilliams P, Friedrichs K. Laboratory evaluation and interpretation of synovial fluid. *Vet Clin North Am Small Anim Pract*. 2003;33:153-178.

29. Turlo A, McDermott B, Barr E, et al. Gene expression analysis of subchondral bone, cartilage, and synovium in naturally occurring equine palmar/plantar osteochondral disease. *J Orthop Res*. 2021:1-9.

30. Conrado F, Beatty S. Fluid Analysis in the Equine Patient: Cerebrospinal, Synovial, and Peritoneal Fluids. *Vet Clin North Am Equine Pract*. 2021;36:e1-e28.

31. Kawcak C, McIlwraith C, Norrdin R, Park R, Steyn P. Clinical effects of exercise on subchondral bone of carpal and metacarpophalangeal joints in horses. *Am J Vet Res*. 2000;61(10):1252-1258.

32. Rinnovati R, Bonelli F, Tognetti R, et al. Effect of Repeated Arthrocentesis on Cytology of Synovial Fluid. *J Equine Vet Sci*. 2017;57:112-115.

33. Berg R, Sykes J, Kass P, Varnau W. Effect of Repeated Arthrocentesis on Cytology of Synovial Fluid in Dogs. *J Vet Intern Med*. 2009;23:814-817.

34. White K, Hodgson D, Hancock D, Parry B, Cordell C. Changes in equine carpal joint synovial fluid in response to the injection of two local anesthetic agents. *Cornell Vet*. 1989;79:25-38.

CHAPTER 4:

DIAGNOSTIC IMAGING FINDINGS FOLLOWING EXPERIMENTAL INDUCTION OF BONE MARROW LESIONS IN EQUINE METACARPOPHALANGEAL JOINTS

4.1 Introduction

Pain associated with subchondral bone disease in the distal condyles of the third metacarpal and metatarsal bones (MC3/MT3) is commonly recognized in most racehorses.[1,2] For palmar osteochondral disease (POD), definitive diagnosis of all but severe lesions is difficult without specialized advanced diagnostic imaging modalities, such as magnetic resonance imaging (MRI) or computed tomography (CT).[3] Digital radiography, while still the most common diagnostic technique used to evaluate the subchondral bone, often underestimates the amount of damage present and is inadequate for detecting subtle changes.[4,5] As previously mentioned, a reduction of at least 30% to 40% in mineral density is needed before a lesion becomes radiographically apparent.[6,7] Furthermore, the limited ability of radiographs to isolate the condyles without superimposition makes radiographs unreliable in the detection of POD, and a lack of findings does not rule out this disease process as a source of pain.[1,8] Despite this, given the ease of access to a majority of equine practitioners and the ease of acquisition, it is often the first-line diagnostic imaging modality for lameness localized to the fetlock.

Nuclear scintigraphy is a sensitive indicator of subchondral bone change but its poor specificity for describing fetlock pathology and discerning normal bone remodeling from damage makes it a less desirable option for monitoring lesions associated with POD.[4,9–12] Newer techniques such as magnetic resonance imaging (MRI) and computed tomography (CT) may better diagnose early and subtle joint lesions in horses prior to development of gross joint

damage.[4] MRI provides superior anatomic detail, demonstrating occult bone bruising, sclerosis and subchondral bone lesions before the loss of articular cartilage, and has been a valuable tool for monitoring POD and subchondral bone marrow lesions (BMLs) in both equine and humans.[3,13–19] Lastly, both fan-beam and cone-beam CT have been validated for detection of pathologic lesions in the fetlock joint of horses,[20–23] helping to identify subchondral bone pathology not detected on radiographs and characterize additional subchondral bone pathologies in cases with abnormalities identified on other imaging modalities.[21]

The objective of this chapter is to discuss the diagnostic imaging findings following experimental induction of BMLs in the palmarodistal MC3 condyles of three horses, using the study protocol and timeline described in Chapter 2, with a discussion of how the study findings compare to those in the published literature. It was hypothesized that this experimental model would consistently induce subchondral and trabecular bone changes similar to those seen in the early stages of POD and with repetitive stress injury. It was also hypothesized that digital radiography, MRI, and CT imaging would be suitable to monitor the initial host response to the pin penetration model, as well as to monitor how lesions changed over time with continued high-speed treadmill exercise throughout the course of this 6-month study.

4.2 Materials and Methods

The horses and study protocol used in this pilot study, including the timing of all diagnostic imaging modalities, were as described in Chapter 2. Briefly, BMLs were induced in the medial and lateral MC3 condyles of both forelimbs in three healthy, 2- to 3-year-old horses. This was performed by drilling a 1.1 mm Steinmann pin to a depth of 8 mm in the palmarodistal aspect of each condyle. Horses were then subjected to high-speed treadmill exercise for 24 weeks, beginning two weeks after lesion induction. All digital imaging was stored within the

picture archiving and communication system (PACS) at Colorado State University. Licensed imaging software (RadiAnt DICOM Viewer, version 2022.1.1 [64-bit]) was used for viewing and evaluating DICOM images.

4.2.1 Digital Radiography

Standard radiographic views were acquired of each metacarpophalangeal joint under standing sedation at baseline, at two- and four-weeks postoperatively, and then monthly thereafter. Standard radiographic images included the following views: lateromedial (LM), dorsal 15° proximal-palmarodistal (15° DP), 10° proximodistal 45° dorsomedial-palmarolateral oblique (10° DMPLO), 10° proximodistal 45° dorsolateral-palmaromedial oblique (10° DLPMO), flexed LM (FLM), and flexed dorsopalmar (FDP). An additional view, dorsal 125° distal-palmaroproximal (D125Di-PaPr or 125° DP), was also acquired to improve evaluation of the palmar aspect of the distal third metacarpal condyles.[24–26] The radiographs were taken immediately following serial lameness exams to correlate radiographic changes with each horse's degree of lameness at each point in time, as well as to avoid analgesic effects of the sedation from affecting the lameness parameters. Radiographs were also taken prior to synovial fluid aspiration to prevent the introduction of gas upon arthrocentesis from affecting the radiographic analysis.

Once all radiographic views were acquired, evaluation of the articular cartilage surface was also performed using positive-contrast arthrography, with the same radiographic views taken post-contrast. Following standard aseptic preparation and with the fetlock held in flexion, maximal aspiration of synovial fluid was performed and then each metacarpophalangeal joint was aseptically injected with a combination of 3.4 mL non-ionic iohexol (Omnipaque 350 mgI/mL) and 4.6 mL 0.9% sterile sodium chloride (8 mL total volume) via the lateral aspect of

the palmar joint pouch. This volume was chosen based on preliminary testing in cadaver limbs, achieving appropriate outline of the articular surface. The joint was then passively flexed and extended for a total of 30 repetitions prior to repeat radiographic evaluation. This was performed for one metacarpophalangeal joint at a time, with injection of the second fetlock not taking place until after post-contrast radiographs had been acquired of the first fetlock. A light bandage consisting of a sterile gauze sponge and adhesive tape (Elastikon) was applied to both fetlocks and maintained for 24 hours post-injection.

Radiographs were evaluated at the completion of the study by a boarded radiologist (KTS) and a boarded surgeon (LES) for changes over time that deviated from the baseline appearance for each horse. This included subjective changes in the appearance of the drill tracts (visibility and definition), condylar sclerosis (opacity, size, definition), subchondral bone injury (presence or absence of subchondral lysis or subchondral bone collapse), articular surface defects (based on contrast arthrography), and bony lysis. A subjective description of these changes was provided with comparison to other imaging modalities.

4.2.2 Magnetic Resonance Imaging (MRI) and Computed Tomography (CT)

MRI and CT were first performed of each metacarpophalangeal joint immediately prior to surgery, once the horse was anesthetized. Horses were positioned in right lateral recumbency for both imaging modalities. For MRI, fetlocks were scanned individually. For CT, fetlocks were scanned simultaneously. These images served as the baseline series for comparison throughout the study. Following surgery, each horse was anesthetized for repeat MRI and CT of the metacarpophalangeal joints at weeks 4, 12 and 24, postoperatively. Advanced diagnostic imaging was utilized to monitor the development and progression of the induced lesions in each horse over the 6-month period, following the induction of exercise.

MRI was performed of each front fetlock using a high-field magnet (3-Tesla; Siemens MAGNETOM Skyra, Siemens Medical Solutions USA, Inc., Malvern, PA, USA) with a bore diameter of 70cm. Sequences performed to detect changes in the surrounding bone and associated articular cartilage included T1-weighted gradient echo (GRE), T2*-weighted GRE, T2-weighted fast spin echo (FSE), T1-weighted VIBE, T2*-weighted dual echo steady state (DESS), short-tau inversion recovery (STIR), proton density (PD), T1-weighted SPACE, and intermediate weighted fat-suppressed sequences (Dixon technique). Relevant scan parameters are provided in Table 4.1. All sequences were performed exclusively in the sagittal plane with the exception of the PD (sagittal and transverse planes), STIR (transverse plane only), VIBE (dorsal plane only), and Dixon (sagittal and dorsal planes) techniques. Pixel spacing ranged from 0.2-0.6 mm.

CT was performed immediately following MRI using a conventional 64-slice helical fan-beam CT unit (Siemens Somatom Definition AS, Siemens Medical Solutions USA, Inc., Malvern, PA, USA). Images were acquired in the transverse plane relative to the joint surface. Relevant CT parameters included a 1.5 (thin) or 2 mm slice thickness, a 1 mm pitch, 270 mm field of view, and a 512 x 512 voxel matrix. Two sequential scans were performed at different energy levels: 80 kVp/50 mA (low energy) and 140 kVp/30 mA (high energy).

Following the conclusion of CT imaging, the lateral (uppermost limb) or medial (lowermost limb) aspect of each fetlock was aseptically prepared. With the fetlock held in flexion, each metacarpophalangeal joint was aseptically injected via the palmar joint pouch with a combination of 6 mL non-ionic iohexol (Omnipaque 350 mgI/mL), 8 mL 0.9% sterile sodium chloride, and 0.5 mL gadoterate meglumine (Clariscan 0.5 mmol/L), for a total volume of 14.5 mL per joint.[27] The joint was then passively flexed and extended for a total of 30 repetitions.

Immediately post-injection, CT then MRI were repeated as described above for post-contrast imaging.

At the end of the study, all images were evaluated by a board-certified radiologist (KTS) and a board-certified surgeon (LES). The initial scoring was performed by LES, with follow-up scoring and adjustments made by KTS to decide the final score. The development and progression of pathologic changes were described at each timepoint, including a subjective comparison of lesion characterization between modalities. MR images were evaluated for the presence of subchondral bone attrition, subchondral thickening, bone marrow lesions, changes in cartilage signal and morphology, and changes in trabecular bone signal and morphology. Lesions were scored as shown in Table 4.2, which was modified from a previously published grading scale[28] in order to better suit findings from this experimental model. If a specific sequence was not performed at a certain time point, the cell in the data sheet was left blank. Lastly, a total MRI score was calculated as the sum of each of the scores divided by the maximum possible score for that particular parameter, with a total possible score of 1. Due to technical error, the T1 GRE sequence was not acquired for horse #1 at week 4 or for the left forelimb of horse #3 at week 4; therefore, this was done to account for those parameters lacking specific data points, for which the total possible composite score would differ. Due to the information obtained from other sequences, the single omission of this sequence in these horses was not expected to have a significant effect on lesion interpretation or outcome, overall. The total MRI score was calculated to provide an overall score for the severity of pathologic changes identified on MRI.

For sequences in which a BML was present and the boundaries well-defined, maximum BML area (cm^2) was measured by a single investigator (LES) along with the condylar area on the respective slice. These measurements were used to calculate the maximum lesion area as a

percentage (%) of the condylar area occupied by a BML on the slice on which the lesion was largest. This was possible on the following sequences: T1 GRE, T2 FSE, T2* DESS, T1 SPACE, PD, STIR, and intermediate-weighted Dixon sequences.

CT images of each condyle were evaluated for changes in sclerosis, drill tract size, and articular cartilage morphology. Using three-dimensional multiplanar reconstruction, CT images were centered along the long axis of the pin tract in all three planes (sagittal, dorsal, transverse). In each of the three planes, the total area of sclerosis (cm^2) and the area of the pin tract (cm^2) were measured and recorded.

Data analysis was performed as described in Chapter 2, Section 2.5.

4.3 Results

4.3.1 Digital Radiography

The primary radiographic changes observed in this study related to sclerosis of the palmar condyles and alterations in the appearance of the pin tract, with changes lagging behind those observed on MRI and CT. Marginal remodeling of the proximal sesamoid bones, proximal phalanx, or third metacarpal bone was not observed, nor was there evidence of dorsal impact injury, narrowing of the joint space, fissure formation, or subchondral bone lysis within the distal condyles. Flattening of the palmar condyles was only seen in horse #1; however, this was also present at baseline and remained unchanged throughout the duration of this study. A representative composite of radiographic images depicting the changes seen for each horse in this study is provided in Figure 4.1.

Focal sclerosis of the palmar MC3 condyles, extending beyond any sclerosis present at baseline, became apparent at approximately week 4 in all horses on the LM radiographs, with increased definition of the area of sclerosis beginning at week 8. Additionally, changes in

sclerosis were more easily monitored using the LM projections in this study, potentially due to the added benefit of superimposition of the condyles. Overall, the pin tracts became visible on DP radiographs beginning at week 4, with increased and progressive remodeling and lysis associated with the pin tracts beginning at week 8 on both the LM and DP projections.

In horse #1, in which the pin tracts were inadvertently located more proximal in the condyle (Figure 4.2), the pin tracts were first visible on the DP radiographs at week 4, and on the LM radiographs at week 8. As the study progressed, the area of sclerosis on the LM radiographs first noticed at week 4 became more defined, remodeling from more diffuse to a focal area of palmar sclerosis, with increasing radiopacity most noticeable beginning at weeks 12-16 in the right forelimb and week 16 in the left forelimb. Subjectively, no differences were observed between medial and lateral condyles on DP images. Lastly, disruption of the subchondral bone plate from pin tract creation was present from week 4 through 12 and was no longer visible by week 16.

In horse #2, in which the pin tracts were placed more distal in the condyle (Figure 4.2), condylar sclerosis was more extensive at week 4; however, the appearance on DP radiographs was unchanged from week 2. The pin tract was slightly visible at week 2 in the right forelimb, with improved definition by week 4. After week 4, the pin tract became less visible on LM radiographs in the right forelimb, though they could still be seen on DP radiographs with increased radiolucency suggestive of lysis. In the left forelimb, the pin tracts could be identified on DP radiographs beginning at week 2. Increased lysis surrounding the medial pin tract was first observed at week 8, and for the lateral pin tract at weeks 16-20. Similar to the right forelimb, the pin tracts in the left forelimb were significantly less visible on the LM radiographs. Subchondral bone plate disruption was visible from weeks 2 through 8 and appeared resolved by week 12.

Lastly, as with horse #1, a more diffuse area of sclerosis was first observed at week 4, becoming more defined around week 12. No difference could be seen on DP radiographs between medial and lateral condyles regarding the pattern of sclerosis. Furthermore, the condylar sclerosis in horse #2 was subjectively more diffuse compared to that from horse #1 and extended further toward the dorsal surface of the condyle.

In horse #3, in which pin tract placement was more similar to horse #2 (Figure 4.2), diffuse sclerosis of the condyle was observed on LM radiographs at week 4 in both forelimbs, and at week 8-12 on DP radiographs. Increased radiopacity was seen beginning at week 12 with continued remodeling and increasing definition throughout the remainder of the study. The pin tracts were difficult to identify on the LM radiographs in the right forelimb but were first visible on DP radiographs at week 4. Widening of the pin tracts, with changes suggestive of bone lysis, began at week 8 and progressed throughout the study with changes being more apparent in the lateral condyle. In the left forelimb, the pin tracts were slightly apparent on LM radiographs at week 8 but more easily identifiable by week 12; however, they could be identified on DP radiographs beginning at week 2. Circumferential lysis associated with the pin tracts was observed on DP images beginning at week 8 and after week 12, appeared to remain consistent in appearance until week 24.

4.3.2 Magnetic Resonance Imaging (MRI)

BMLs were present in all condyles throughout the duration of the 24-week study. While the needle tracts through the palmar soft tissues, specifically the oblique sesamoidean ligaments, were still present on initial MRI images, assessed using the transverse PD sequence, evidence of the needle tracts could no longer be identified by week 24 in all horses. In horse #3, the area of the left medial oblique sesamoidean ligament was enlarged by 43.8% compared to the lateral

oblique sesamoid ligament, just distal to the proximal sesamoid bones, with a mildly abnormal architecture and increased fluid signal (Figure 4.3). These changes were first observed at week 12 and remained unchanged by week 24. No significant abnormalities were observed on gross examination; histology was not performed. No significant soft tissue injuries were observed in the other horses.

On Dixon out phase images, the pin tract in all horses appeared as a central region of iso- to hyperintensity, surrounded by a hypointense BML with a black rim relative to the surrounding trabecular bone. For T1 GRE, T2 FSE, Dixon in phase and PD images, the BML had a more intermediate to hypointense appearance relative to both the pin tract and the surrounding trabecular bone. For Dixon fat only images, the BMLs appeared as a homogenous region of hypointensity with minimal variation, with a less hypointense signal diffusing out from the primary lesion. The pin tracts were not distinguishable within this region of hypointensity. In contrast, on Dixon water only and STIR images, BMLs were diffusely hyperintense relative to the surrounding trabecular bone, with a more isointense signal within the subchondral bone at the entry of the hyperintense pin tract. On the T1 VIBE, T1 SPACE, and T2* DESS images, there was an intermediate to hypointense signal throughout the condyle, surrounding a hyperintense pin tract. This appeared to be more concentrated in the areas surrounding the pin tract, though the margins of the BML were less defined in the T1 VIBE images compared to the other sequences. Lastly, on the T2* GRE, the condyle was diffusely hypointense with an intermediate-signal pin tract and remained unchanged throughout the post-operative period.

Tissue remodeling was observed on MRI in this study with significant differences noticed in both fluid signal and sclerosis across time and between horses. Representative images of the changes in fluid and sclerosis over time are provided in Figure 4.4. These images were acquired

from the lateral MC3 condyle of the right forelimb in horse #2 and are representative of the general trends identified across all horses and time points. An additional finding observed on MRI in all horses was increased signal intensity near the tip of multiple pin tracts with subjective widening of the pin tract in this region by week 24, potentially suggestive of the development of resorptive or osseous cyst-like lesions in this location (Figure 4.5).

Bone Marrow Lesion Area (% Condyle Occupied by BML)

For each MRI sequence on which a BML was well-defined and the area could be easily measured, graphs showing the mean (range) percentage of the condylar area occupied by the BML on the slice it was largest, for each horse and overall, are provided in Figure 4.6.

On fluid-sensitive sequences (Dixon water, STIR), hyperintense fluid signaling was observed with the BML encompassing a greater percentage of the condyle at week 4 compared to baseline, week 12, and week 24 (Figure 4.6 and 4.7, $p < 0.0001$). The mean (SEM, range) percentage of the condyle occupied by the BML at each post-operative time point, averaged across all condyles from all three horses, was 50.84% (± 4.92%, 29.11-72.01%), 13.43% (± 0.59%, 8.04-16.58%), and 9.15% (± 1.73%, 6.11-11.66%), respectively, in Dixon water only images and 38.18% (± 4.98%, 26.60-56.53%), 3.74% (± 0.96%, 0.55-6.77%), and 2.82% (± 1.06%, 1.07-5.09%), respectively, in STIR images. There were no significant differences in the occupied percentage of the condyle between weeks 12 and 24 ($p > 0.10$); however, while the BML area at these two time points was still significantly larger compared to baseline on the Dixon water only sequence ($p < 0.05$), the occupied percentage of the condyle was not significantly different compared to baseline by weeks 12 and 24 on the STIR images ($p > 0.10$). Changes in the percentage of the condyle affected over time varied significantly based on variations in individual horses and condyles ($p < 0.05$); therefore, while there were no

differences in fluid signal on STIR images between baseline and weeks 12 and 24, focal areas of hyperintense fluid signal were still present at the tip of the pin tracts on multiple images similar to that seen on the Dixon water only images.

Bone sclerosis surrounding the pin tracts and across the palmarodistal condyles was another significant finding from this study. This was primarily evaluated based on T2 FSE, PD, and Dixon in phase images. For these sequences, the area of sclerosis encompassed a greater percentage of the condyle at weeks 4, 12, and 24 compared to baseline (Figure 4.6; $p < 0.0001$). The mean (SEM, range) percentage of the condyle occupied by the BML at each post-operative time point, averaged across all condyles from all three horses, was 24.40% (± 2.78%, 19.69-26.78%), 24.58% (± 2.25%, 18.64-30.61%) and 24.37% (± 3.41%, 16.30-30.29%), respectively, in T2 FSE images, 27.19% (± 2.65%, 24.55-29.37%), 25.69% (± 3.19%, 19.90-29.64%), and 25.02% (± 3.03%, 19.48-30.13%), respectively, in PD images, and 25.91% (± 2.21%, 23.29-29.22%), 24.97% (± 2.27%, 18.21-30.32%) and 23.01% (± 2.65%, 15.08-28.78%), respectively, in Dixon in phase images. Lesion area was not compared between these sequences, nor was a significant difference between these sequences expected. After week 4, the percentage of the condyle containing the BML remained relatively unchanged with no significant differences in the occupied percentage of the condyle between weeks 4, 12 and 24 ($p > 0.10$), overall, though it was marginally greater at week 4 compared to week 24 on Dixon in phase images ($p = 0.0686$).

For the T1 GRE images, the occupied percentage of the condyle was significantly greater at weeks 12 and 24 compared to baseline ($p < 0.0001$). Lesion area at week 4 could not be compared to other time points as this sequence was not performed in all three horses at this time point (not performed in horse #1 or in the left forelimb of horse #3). There was no difference in the percentage of the condyle occupied by the BML between weeks 12 and 24 ($p = 0.2282$). For

all remaining sequences (Dixon fat, Dixon out phase, T2* DESS, T1 SPACE), the percentage of the condyle occupied by a BML was significantly greater at weeks 4, 12, and 24 compared to baseline ($p < 0.0001$). In all but the T2* DESS, the BML also encompassed a greater percentage of the condyle at week 4 compared to both weeks 12 and 24 ($p < 0.05$), with no significant differences between these final two time points ($p > 0.10$). In T2* DESS images, the occupied percentage of the condyle remained unchanged between weeks 4 and 12 ($p = 0.9213$), after which it decreased by week 24 ($p < 0.05$).

In this experimental model, significant variation was also observed when comparing lesion area among horses. Some variation in the presence and significance of these differences was based on the individual time point for a majority of sequences ($p < 0.05$); however, as this is a preliminary pilot study, only the overall differences among horses while accounting for the other fixed variables will be reported here with significant interactions being examined in future studies. When evaluating changes in fluid signal, the occupied percentage of the condyle was significantly greater for horse #3 compared to horse #1 on both Dixon water and STIR images (Figures 4.6 and 4.7; $p < 0.05$). Any additional differences that existed between horses (horses #1 and #2 on Dixon water images, horses #2 and #3 on STIR images) were marginal (Figure 4.7; $0.05 > p < 0.10$). The largest difference in the occupied percentage of the condyle between horses was observed at 4 weeks post-operatively (Figure 4.7). In both fluid-sensitive sequences, the BML encompassed a greater percentage of the condyle in horse #3 compared to both horses #1 and #2 ($p < 0.001$) after 4 weeks. The occupied percentage of the condyle was also greater in horse #2 compared to horse #1 in Dixon water only images ($p = 0.0003$), though there were no significant differences between these two horses on STIR images ($p = 0.3797$) at week 4. No

significant differences were observed between horses on either sequence at week 12 or week 24 (Figure 4.7; $p > 0.10$).

On Dixon fat only, Dixon in phase, Dixon out phase, and T1 SPACE sequences (Figure 4.6), the percentage of the condyle occupied by the BML was significantly lower in horse #1 compared to both horse #2 and horse #3, and in horse #2 compared to horse #3 ($p< 0.05$), though the differences between horses #2 and #3 on the T1 SPACE images ($p = 0.0784$) and between horses #1 and #2 on the Dixon out phase images ($p = 0.0936$) were only marginal. On T2 FSE, T2* DESS, and PD sequences, the percentage of the condyle affected was still significantly lower in horse #1 compared to horses #2 and #3 ($p < 0.05$); however, there were no significant differences between horse #2 and horse #3 ($p > 0.10$). For the T1 GRE sequence, there was no difference in the occupied percentage of the condyle between horses #2 and #3, overall or at any post-operative time point ($p > 0.10$); however, these horses could not be compared to horse #1 as this sequence was not performed for horse #1 at all three time points (not performed at week 4). At weeks 12 and 24, the BML encompassed a smaller percentage of the condyle in horse #1 compared to horse #2 and horse #3 ($p < 0.05$).

Lastly, overall, the percentage of the condyle affected was significantly greater in right forelimbs compared to left forelimbs ($p < 0.05$) for all sequences. It was also larger in lateral condyles compared to medial condyles ($p < 0.05$), except for on the Dixon Water sequence where there was no significant effect of condyle ($p = 0.0898$).

MRI Grading System (Table 4.2)

Graphs showing the mean (range) score for each grading parameter, for each horse and overall, are provided in Figures 4.8 and 4.9.

Bone Marrow Lesion (BML) Score (% of Condyle Occupied; Graded 0-3)

As part of Table 4.2, a grade (0-3) was provided for each sequence based on the percentage of the condyle occupied by the BML. For each MRI sequence on which the BML area could be measured, as described previously, summary graphs of the mean (range) BML grades for each horse and overall are provided (Figure 4.8). The individual results for BML grade are not going to be described here for each sequence as the key differences were described above for the absolute percentages of occupied condylar area. The general trends observed for BML grade, both between time points and between horses, were consistent with those just described; however, due to the conversion from an absolute value to a grade (0-3), some differences observed were less dramatic. Briefly, the BML grade on fluid-sensitive sequences (Dixon water, STIR) was significantly higher at week 4 compared to baseline and compared to weeks 12 and 24 ($p < 0.0001$). While the BML grade was still higher at weeks 12 and 24 compared to baseline ($p < 0.0001$), there were no significant differences between these two time points ($p > 0.10$). There also were no significant differences, overall, between horses for these two sequences ($p > 0.10$). On those sequences that best identified areas of sclerosis (T2 FSE, Dison in phase, PD), BML grade was significantly higher at weeks 4, 12, and 24 compared to baseline ($p < 0.0001$) but not when compared to each other ($p = 1.00$).

Subchondral Bone Attrition (Graded 0-3)

The presence and severity of subchondral bone attrition was only affected by time ($p = 0.0010$) with no significant differences between horses, limbs, or condyles ($p > 0.05$). Subchondral bone attrition was not apparent in any horse until week 24 (Figure 4.9), at which point the attrition score was higher compared to baseline and to weeks 4 and 12 ($p = 0.0036$). There were no significant differences in score between baseline, week 4, and week 12 ($p =$

1.0000). Horse #1 developed evidence of subchondral bone attrition (grade 1) in a single condyle (left forelimb, medial condyle). Horse #2 developed evidence of subchondral bone attrition in the left lateral (grade 2) and right medial (grade 1) condyles. Lastly, horse #3 developed evidence of subchondral attrition in the left lateral condyle (grade 1) and both condyles in the right forelimb (grade 2). Examples of grade 1 and grade 2 subchondral bone attrition from this study are provided in Figure 4.10.

Subchondral Bone Changes (Graded 0-3)

Consistent with previous findings, subchondral bone changes were worse in right forelimbs compared to left forelimbs ($p = 0.0092$), though there were no differences between condyles ($p = 0.5748$). There also were no significant differences between horses, overall ($p = 0.7265$). Subchondral bone changes were worse at week 24 compared to baseline, week 4 and week 12 (Figure 4.9; $p < 0.0001$), with no differences in the extent of subchondral bone changes between the three earlier time points ($p > 0.10$). The highest grade of subchondral bone change assigned to any condyle was a grade 1, characterized by regions of subchondral bone plate sclerosis less than 1 cm^2 in area. No abnormalities suggestive of subchondral bone lysis were observed. In horse #1, this was first observed in the right forelimb condyles at week 12, progressing to all four condyles by week 24. In horse #2, changes were first observed in the right forelimb condyles at week 4; however, no gradable changes were present at week 12. Similar to horse #1, all four condyles had evidence of subchondral bone change (grade 1) at week 24. Lastly, in horse #3, subchondral bone changes were only observed in the right lateral condyle at week 12, with all four condyles affected at week 24. An example of the subchondral bone change observed in shown in Figure 4.11.

Trabecular Bone (Graded 0-4)

Changes to the trabecular bone were worse at weeks 4, 12, and 24 compared to baseline (Figure 4.9; $p < 0.0001$), with no significant differences between the post-operative time points ($p > 0.10$). When comparing individual horses, trabecular bone changes were more extensive in horse #3 compared to horses #1 and #2 ($p = 0.0008$), overall and at week 4. There were no significant differences in grade between horses #1 and #2 ($p = 1.00$), overall. There were no significant differences between horses at weeks 12 or 24 ($p > 0.10$). In horses #1 and #2, all condyles were scored as a grade 2 at all time points, characterized by generalized low signal intensity on intermediate-weighted sequences and high signal intensity on STIR sequences in < 50% of the region. All condyles except the left medial condyle were scored as a grade 3 at week 4 in horse #3, characterized by high signal intensity on STIR sequences in > 50% of the region. For weeks 12 and 24, all condyles were scored as a grade 2 in horse #3 with the exception of the right lateral condyle at both time points, which was scored as a grade 3 based on areas of low signal intensity extending further throughout the condyle from the primary lesion on multiple intermediate-weighted sequences.

Cartilage (Graded 0-3)

Overall, cartilage damage was worse in horse #3 compared to horse #2 ($p = 0.0450$) with no significant differences between horse #1 and horses #2 or #3 ($p > 0.10$). Compared to baseline, cartilage damage was worse at weeks 4, 12 and 24 (Figure 4.9; $p < 0.0001$), with no significant differences between any of the post-operative time points ($p > 0.10$). There were no differences between limbs or condyles ($p > 0.05$). In all three horses, condyles were scored as either a grade 1 or a grade 2 at all post-operative time points. Grade 1 was characterized by normal thickness to the articular cartilage but an abnormal signal on T1 VIBE images or mild

surface irregularities. Grade 2 condyles were characterized by either a partial thickness focal defect less than 5-mm-diameter with an abnormal signal and irregular surface. Examples of these changes are provided in Figure 4.12.

Cartilage Defects on Arthrography (Graded 0-3)

Compared to baseline, cartilage defects were worse at weeks 4, 12 and 24 (Figure 4.9; $p < 0.0001$), with no significant differences in cartilage defects between any of the post-operative time points ($p > 0.10$). Cartilage defects were less severe in horse #1 compared to horses #2 and #3 overall and at weeks 4 and 12 ($p = 0.0068$), but not at week 24 ($p = 1.0000$). There were no significant differences between horses #2 and #3 overall or at any time point ($p = 1.0000$). The highest-grade cartilage defect identified in this study was a grade 1 (Figure 4.12b), which was a partial thickness cartilage defect less than 5-mm-diameter that remained within the superficial half of the articular cartilage. No contrast was observed reaching or penetrating the subchondral bone plate in this study, with CT arthrography used to confirm both negative and positive findings. Scores were adjusted, as needed, based on the combination of MRI and CT arthrography.

Total MRI Score (out of 1)

The composite MRI score, for which a higher score represented larger lesions and more significant degeneration of the subchondral bone and articular cartilage, was calculated by dividing the total score across all evaluated parameters by the total score possible for that parameter. This was done to account for differences in the total possible score in horses or parameters with missing data, such as that related to the T1 GRE sequence. The total MRI score was higher at week 4 compared to baseline (Figure 4.9; $p < 0.0001$), as well as compared to weeks 12 ($p = 0.0002$) and 24 ($p = 0.0031$). While the total MRI score was still significantly

higher at weeks 12 and 24 compared to baseline ($p < 0.0001$), there were no significant differences in score between weeks 12 and 24 ($p = 0.6418$). The mean (SEM, range) total MRI score at each post-operative time point, averaged across all condyles from all three horses, was 0.49 (± 0.04, 0.40-0.58) at week 4, 0.40 (± 0.03, 0.35-0.45) at week 12, and 0.42 (± 0.03, 0.35-0.50) at week 24.

Overall, the total MRI score was higher for horse #3 compared to both horse #1 ($p < 0.0001$) and horse #2 ($p = 0.0187$), and for horse #2 compared to horse #1 ($p = 0.0012$). There were similar patterns across individual time points; however, by weeks 12 and 24 there was no longer a significant difference in total MRI score between horses #2 and #3 ($p > 0.10$). As described above for lesion area, the differences between individual horses were significantly influenced by variations between time, limbs, and condyles ($p < 0.05$); however, that is outside of the scope of this initial pilot study and will be examined in future work.

Abnormalities on MRI were also more severe in right forelimbs compared to left forelimbs ($p < 0.0001$), overall and at all post-operative time points ($p < 0.05$), and in lateral condyles compared to medial condyles ($p = 0.0123$).

4.3.3 Computed Tomography (CT)

Sclerotic lesions were successfully induced in all condyles using this experimental protocol. The mean (SEM, range) pin tract length, or penetration depth, measured on CT across all time points and condyles was 9.21 mm (± 0.28, 8.70-9.85 mm). The pin tracts appeared to be sealed with tissue by week 4, with no contrast ever observed within the pin tracts on CT arthrography. Representative images of changes seen on CT are provided in Figure 4.13, which can be compared to MRI images to see differences in lesion appearance. Of significance, unlike MRI, CT showed focal areas of hypoattenuation, suggestive of bone lysis or resorption, in

variable locations immediately adjacent to the pin tract in some condyles. CT also revealed changes in the area of the pin tract over time, with focal areas of widening near the tips of the pin tracts. This was consistent with the resorptive-type lesions seen near the tip of some pin tracts on MRI. In horse #1, this was first present at week 4, at the tip of the right medial and lateral pin tracts (Figure 4.13).

The total area of sclerosis and the area of the pin tracts (cm^2) were measured in three planes (sagittal, dorsal, transverse) on CT, with slices aligned with the long axis of the pin tract. Importantly, the planes are relative to the pin tract angle; therefore, the dorsal plane views were modified to be in the dorsal plane of the tract, not MC3, and the transverse measurement was taken on a transverse cross-section through the mid-length of the pin tract. An example of how the measurements were performed is shown in Figure 4.14. Graphs showing the mean (range) areas for all three planes, for each horse and overall, are provided in Figure 4.15. The mean (SEM, range) total area (cm^2) of sclerosis, averaged across all condyles from all three horses, at each time point was 2.20 (± 0.20, 1.70-2.51), 2.37 (± 0.16, 1.80-2.81), and 2.35 (± 0.17, 1.88-2.74), respectively, in the sagittal plane, 1.61 (± 0.11, 1.17-2.05), 1.76 (± 0.16, 1.37-2.26), and 1.62 (± 0.12, 1.52-1.80), respectively, in the dorsal plane, and 2.22 (± 0.07, 1.84-2.45), 2.43 (± 0.09, 2.23-2.71), and 2.06 (± 0.20, 1.78-2.24), respectively in the transverse plane. The mean (SEM, range) total area (cm^2) of the pin tracts, averaged across all condyles from all three horses, at weeks 4, 12 and 24 was 0.16 (± 0.02, 0.15-0.17), 0.17 (± 0.02, 0.14-0.20) and 0.20 (± 0.01, 0.18-0.21), respectively, in the sagittal plane, 0.12 (± 0.01, 0.10-0.14), 0.14 (± 0.01, 0.14-0.15) and 0.16 (± 0.01, 0.15-0.17), respectively, in the dorsal plane, and 0.03 (± 0.004, 0.03-0.04), 0.05 (± 0.004, 0.04-0.05), and 0.05 (± 0.005, 0.05-0.054), respectively, in the transverse plane.

Overall, there was an increase in sclerosis at week 4, 12, and 24 compared to baseline, similarly to that seen on MRI. In all three planes, the total area of sclerosis was significantly larger at weeks 4, 12, and 24 compared to baseline ($p < 0.0001$), with no significant differences between post-operative time points ($p > 0.10$). In the sagittal plane, the total area of sclerosis was smaller in horse #1 compared to horse #2 ($p = 0.0011$) and horse #3 ($p = 0.0001$), and not significantly different between horses #2 and #3 ($p = 0.6127$). This relationship did not change over time. In the dorsal plane, the total area of sclerosis was similarly smaller in horse #1 compared to horse #2 ($p = 0.0198$) and horse #3 ($p < 0.0001$), but the area in horse #2 was smaller compared to horse #3 ($p = 0.0001$). Additionally, as time progressed post-operatively, there was no longer a significant difference between horses #1 and #2 by week 12 ($p = 0.1051$), and there were no significant differences between any of the three horses by week 24 ($p > 0.10$). There were no significant differences in the total area of sclerosis between horses in the transverse plane ($p = 0.1100$) however, as this measurement was taken as a cross-section at the center of the pin tract length, it is possible that this lack of difference in sclerotic area was a result of the location and may have differed at different locations along the pin tract. Lastly, similar to those changes identified on MRI, the total area of sclerosis was larger in right forelimbs compared to left forelimb in both the sagittal and dorsal planes ($p < 0.05$), and in the lateral condyles compared to medial condyles in the dorsal plane only ($p = 0.0284$). These differences were not observed in the transverse plane.

The areas of the pin tracts were also significantly larger at weeks 4, 12 and 24 compared to baseline ($p < 0.0001$). While there were no significant differences in pin tract area after week 4 in the sagittal plane ($p > 0.10$), a gradual increase in pin tract area was observed over time in the dorsal and transverse planes. The pin tract area was significantly larger at week 24 compared to

week 4 ($p = 0.0174$) in the dorsal plane, and marginally larger at week 24 compared to week 4 ($p = 0.0771$) in the transverse plane. The area of the pin tract was not significantly different between weeks 4 and 12 or weeks 12 and 24 ($p > 0.10$) in either plane. There were no significant differences in pin tract area between horses in any of the three planes ($p > 0.10$).

4.4 Discussion

These results provide proof of concept that the pin penetration model – which involved using a 1.1mm Steinmann pin to create an osteochondral defect that extended approximately 8mm from the articular surface into the trabecular bone, followed by 6 months of high-speed treadmill exercise – consistently resulted in the development of BMLs in the MC3 condyles. These lesions were present throughout the course of this 6-month study. As reported by Stewart et al.,[29] the BMLs induced using this model changed over time, and modified the subchondral and trabecular bone without significant degeneration of the overlying articular cartilage, making this an appealing potential model for the study of repetitive stress injury and POD in horses. The dynamic nature of the lesions supports the need for serial imaging in order to determine the significance of BMLs on diagnostic imaging, as well as to develop an appropriate treatment plan. By using this model, treatment plans may be optimized to better promote healing while also studying individual risk factors that may result in lesion progression or regression. It also provides us with the opportunity to learn more about the duration and intensity of exercise required to result in lesion progression.

Overall, results from digital radiography revealed that, for this experimental model, while adaptive remodeling was still visible, it was unable to capture the breadth of changes to the lesion over time compared to more advanced modalities, with the most significant changes not becoming visible until on or after week 8. There was no evidence of subchondral bone collapse

or lysis beyond that created by the pin tract, or additional evidence of osteoarthritis within the metacarpophalangeal joints. The primary lesions observed were sclerosis throughout the condyle, which became more defined as the study progressed, with increased radiolucency associated with the pin tracts in some horses and condyles. As previously mentioned in Chapter 1, radiographic indicators of POD commonly include sclerosis, disruption of the outline of the subchondral bone, focal flattening of the palmar/plantarodistal condyles, and osteophytosis.[30] As the disease progresses, a central region of radiolucency within the area of sclerosis develops, potentially indicative of subchondral bone lysis and localized collapse of the articular cartilage.[8,30,31] Radiography is useful in the later stages of POD, but not for the early diagnosis.[30] The latter statement was consistent with the radiographic findings in this pilot study, as the changes were more representative of early disease states; however, if the pin tract is taken into account, radiographic evidence of bone lysis was observed following continued exercise after an osteochondral injury. When considering the effects of exercise alone, a prior study using a similar treadmill protocol found no radiographic lesions in the metacarpophalangeal joints.[32] In the model performed by Rickey et al., radiography did not consistently reveal injury progression throughout the study period, with no significant differences between impact-injured and control limbs within each horse.[33]

While digital radiography could be used to monitor changes in sclerosis, it was less sensitive to the degree of changes in the pin tract and the adjacent bone. MRI and CT were superior for monitoring lesion progression, with each modality providing complementary yet differing information about the changes occurring within the subchondral and trabecular bone. MRI is useful as it can demonstrate bone edema-like signal, shown as hyperintense signal on fluid-sensitive sequences, bone sclerosis (hypointense signal on relevant sequences), and

clinically or radiographically silent subchondral bone lesions before the obvious loss of articular cartilage. This was consistent with findings in this pilot study, in which the changes identified within the subchondral and trabecular bone were more significant and extensive compared to changes identified within the articular cartilage, further supporting its use for the study of POD. Aside from the articular cartilage defects observed at the level of the pin tract, there was no evidence of articular cartilage degeneration, characterized by surface irregularities or abnormal signal, on MRI at more distant locations. That being said, it is possible that the techniques used for MRI in this study may have affected the ability to diagnose more subtle cartilage lesions; therefore, the precise extent of articular cartilage damage cannot be fully deduced based on diagnostic imaging alone.

Changes identified on low-field MRI in association with POD include increased signal within the subchondral bone surrounded by an area of low signal on all sequences, a majority of which will have surrounding BMLs in the deeper trabecular bone.[3] Diffuse changes indicative of BML formation have been identified associated with the early stages of the disease prior to collapse of the articular surface. Similarly in this study, BML formation was observed by week 4 with more advanced changes in the subchondral bone plate not becoming apparent until week 24 in all cases. Fluid signal was present primarily at 4 weeks post-lesion induction, with a significant reduction by week 12. When examining the percentage of the condyle occupied by a BML, the fluid signal was not significantly different from baseline on STIR sequences at weeks 12 and 24; however, this was unlike that in the Dixon water only sequences. This difference between sequences is likely the result of the chemical composition of the fluid within these BMLs, with Dixon water images having improved fat suppression compared to STIR. Additionally, these differences over time were influenced by variation between individual horses,

limbs and condyles, with some condyles still exhibiting fluid signal on STIR sequences. This fluid signal was more focal compared to week 4, typically at the tip of the pin tracts. Further analysis of the cause of the significant interactions observed in this study will be required before being able to draw any significant conclusions. Simultaneously, hypointense signal on T2-weighted images, consistent with bone sclerosis, was significantly greater at week 4 compared to baseline; however, no changes in lesion area were detectable beyond week 4. Subjectively, the areas of sclerosis became more defined and more homogenously hyperintense with time.

These MRI findings are similar to findings from the initial application of the pin penetration model by Stewart et al. in ovine medial femoral condyles, in which the fluid signal decreased over time while the hypointense signal on Dixon in phase images remained relatively unchanged.[29] A benefit of this published study, in contrast to the present study, was the ability to correlate imaging findings with those from histopathology at earlier time points. Findings from that study revealed an initial accumulation of hemorrhage and edema within the marrow spaces, leading to the increased fluid signal volume. The decrease in fluid signal corresponded to a transition to more fibrotic, myxomatous tissue and sclerotic bone. Another shared observation was the development of a hyperintense, circular-to-ovoid pattern associated with the pin tract. The results by Stewart et al. showed that this corresponded to a coagulum of amorphous debris maturing into a necrotic sequestrum rather than resolving by week 12. It was suggested that this change, combined with increased sclerosis and fibrosis, could impair blood flow and subsequently increase intraosseous pressure, tissue hypoxia, and avascular necrosis.[29] As discussed in Chapter 1, these are all factors that in addition to chronic, abnormal mechanical stress, may play a role in the pathogenesis of POD and traumatic avascular necrosis.[34–37] POD begins with sclerosis of the subchondral bone of the palmar/plantar condyles in response to

repetitive loading, and is followed by thickening and sclerosis of the surrounding trabecular bone.[37–39] With continued racing, focal areas of sclerotic subchondral bone undergo ischemic necrosis.[37,40] These findings further support the potential for this experimental model to be utilized for the study of POD and repetitive stress injury. As opposed to necrosis occurring within the subchondral bone, the resorptive lesions in this study and the confirmed areas of necrosis published by Stewart et al. occurred further within the trabecular bone; in the present study, it was closer to the tip of the pin tract. Depth of osteochondral damage is an important factor in BML development, with damage needing to extend into the trabecular bone for BMLs to persist.[29] While a depth of approximately 8 mm was used in this study based on the previously published work, future studies refining this model for the study of POD, through all stages of disease, may include a reduced depth of penetration extending beyond but still remaining adjacent to the subchondral plate. This may allow for more of the remodeling to occur closer to the subchondral bone, as occurs in clinical disease. It would also be interesting to evaluate whether BMLs would persist following damage involving the subchondral bone plate but not trabecular bone if combined with high-speed treadmill exercise in horses.

When comparing the MRI results from this experimental model to other attempts at modeling injury to the palmarodistal MC3 condyles, direct comparisons are difficult due to differences between study protocols. In the impact model by Rice et al., MRI was performed immediately post-lesion induction without postoperative exercise. In 50% of control cases, in which an impact lesion was created without being followed by injection of the bone substitute material, a small region of cartilage disruption was visible on sagittal images in the location of lesion creation but was difficult to visually identify; however, there were no differences between pre- and post-procedure MRI images when evaluating the average grey scale within each

quintile.[41] In the impact model performed by Rickey et al., lesion induction was followed by lunging exercise rather than high-speed treadmill exercise.[33] Unfortunately, MRI and CT were not performed in this study and cannot be compared to the results of the present model. While MRI was not performed in the study by Kawcak et al. using a similar exercise protocol, results of nuclear scintigraphy and CT osteoabsorptiometry following 6 months of exercise revealed a significant increase in radiopharmaceutical uptake and a higher mean percentage of high-density bone in the MC3 condyles.[32] Due to the lack of specificity of nuclear scintigraphy, it is not possible to distinguish a normal bone response to exercise and a pathologic response. Based on the CT findings of this study, it cannot be ruled out that the exercise protocol used in the present experimental model contributed to the bone sclerosis identified on MRI. Lastly, the BML lesions and bone sclerosis were more severe in the present experimental model when compared to the dorsal fragmentation model for inducing fetlock osteoarthritis.[42]

As mentioned, MRI and CT provided complementary information in this study and will be used in combination for the future study of this experimental model. While CT has been shown to be more sensitive for diagnosing POD in horses and provide more information regarding alterations in bone density, MRI may be better able to detect changes associated with the pathological status or severity of POD.[4,23] CT imaging has been increasing in popularity in part for the superior level of trabecular bone detail and high spatial resolution, allowing a more comprehensive evaluation of stress remodeling within the subchondral bone.[8] Both fan-beam and cone-beam CT have been validated for detection of pathologic lesions in the fetlock joint of horses,[20–23] helping to characterize additional subchondral bone pathologies in cases with abnormalities identified on other imaging modalities.[21] In a study of 2-year-old Thoroughbred racehorses monitored over their first year of race training, a longitudinal change in subchondral

bone morphology was observed on CT imaging including a significant increase in subchondral bone sclerosis in the distal MC3/MT3 condyles and parasagittal grooves.[20] Increased mineralization of the subchondral bone in the distal MC3 condyles was also seen following 6 months of similar treadmill exercise.[32] This experimental model resulted in significant bone lesions with an increase in sclerosis at week 4, 12, and 24 compared to baseline. This pattern of sclerosis was consistent with that seen on applicable MRI sequences. In all three planes, the total area of sclerosis remained relatively unchanged from week 4 to week 24, though there was a gradual increase in the area of the pin tracts over this time period. Similarly to MRI, CT also revealed focal areas of widening near the tips of the pin tracts that corresponded to the focal areas of high signal intensity. Unlike MRI, CT showed focal areas of hypoattenuation, suggestive of bone lysis or resorption, in variable locations immediately adjacent to the pin tract in some condyles. CT arthrography was also better at detecting defects in the articular cartilage compared to arthrography on MRI, consistent with previous research.[43] This level of evidence of active remodeling in the subchondral and trabecular bone, while present on advanced diagnostic imaging, was not detectable using synovial fluid analysis as described in Chapter 3. Further reasoning behind this discrepancy will be discussed in Chapter 5.

One significant trend observed in this study was the relationship between individual horses. In general, the percentage of the condyle occupied by the BML, the total area of sclerosis, and the severity of imaging changes to the subchondral bone, trabecular bone and articular cartilage were less severe in horse #1 compared to the other two horses, and in horse #2 compared to horse #3; however, differences between horse #2 and horse #3 were less often or more variably significant. In horse #1, the pin tract was unintentionally located proximally within the condyles, closer to the level of the physis. For horses #2 and #3, the fetlock was

placed in a more hyperextended position during surgery, which allowed for pin tract placement to occur further distad in a more clinically-relevant location within the condyle. Due to the differences in applied forces in the palmarodistal condyle, it's possible that the reduced stress likely experienced by the pin tract location in horse #1 contributed to these differences in lesion progression. While, subjectively, the pin tracts in horse #3 were more distad compared to horse #2 and could explain the higher MRI score and larger lesions in horse #3, the similar distal location within the condyles could explain the reduced frequency in significant differences between these two horses compared to those with horse #1. Interestingly, there were no significant differences in pin tract area between horses in any of the three planes evaluated on CT which may indicate that the response to bone disruption is similar regardless of location. To determine the significance of pin tract location on the lesion outcome, further studies and comparisons are required.

BMLs consistently occupied a greater percentage of the condyles in the right forelimbs compared to left forelimbs, as well as in lateral condyles compared to medial condyles. The reason for this is unknown but could be influenced by factors such as the preferred lead of each horse during treadmill exercise, pin penetration depth, pin tract location and direction, or other factors not accounted for in this pilot study. Future work including correlation models will be required to learn more about many of these relationships; however, that was outside of the scope of this initial study.

Features of POD on MRI include focal subchondral bone hyperintensity in the palmar/plantar condylar region on T1-weighted, T2*-weighted, T2 FSE, and STIR sequences with surrounding hypointensity.[3,23,44,45] While areas of increased signal were less commonly observed within the subchondral bone in this study, outside of the pin tract, there were diffuse

sclerotic changes throughout the trabecular bone that were similar in appearance to that previously reported for POD.[3,46] Additional features include condylar flattening, irregularity in the outline of the subchondral bone, subchondral bone defects or collapse, and articular cartilage irregularity or disruption.[3,23] These findings were less significant in the present study, which could indicate either increased suitability for earlier stages of disease or the need to refine the approach in order to better balance changes between the subchondral and trabecular bone. While there are fewer studies monitoring the trends in BML progression on MRI in equine fetlock injury, CT studies have shown similar findings to those in this study. In a publication by Ciamillo et al., in which 19 two-year-old Thoroughbred racehorses were evaluated with standing CT over a period of 12 months, subchondral hyperdensity increased significantly in both condyles over time.[20] This study also showed that the odds of developing subchondral bone pathology increased significantly from 0 to 6 months but not from 6 to 12 months, suggesting that pathology accumulates more in the first 6 months of training; however, the volume of subchondral bone lesions within the palmar/plantar condyles was significantly greater at 12 months. For this model, the degree of pathology that would have developed beyond the 6-month duration is unknown. While this present study failed to show a significant difference beyond week 4 in bone sclerosis, it's possible that this would have been different in a larger sample of horses, or with the addition of more quantitative analysis techniques. Furthermore, there were subjective variations in the presence of hypodensities on CT imaging that were not accounted for in the evaluation of images in this present study.

This study provided proof of concept that BMLs can be consistently induced in the palmarodistal MC3 condyles in horses using this model, with the addition of high-speed treadmill to provide chronic, repetitive loading to the condyles, with trends in lesion progression

similar to that reported in the published literature. That being said, there are several limitations to this study that must be considered, the most obvious being the small sample size. Using the statistical model in this study, the high number of variables included in the model meant that a smaller change would result in a larger difference. This study also lacked a control group in which a lesion was induced and followed with strict box-stall rest, or conversely another control group exposed to high-speed treadmill exercise without lesion induction. BMLs in the study by Stewart et al. persisted throughout the 12-week study but those animals were allowed to move freely in a less confined space, which still allowed for a degree of mechanical loading beyond that experienced by horses on stall rest. The objective of this pilot study was to provide proof of concept for lesion induction, with further studies in a larger number of horses needed to evaluate causes of variation and make any conclusions regarding the reasons behind differences seen in this study. Similarly, pin tracts were also not placed in the exact same location and at the same angle within every condyle and the variability in lesions that may occur as a result of this is unknown.

Next, MRI must be interpreted with caution as signal changes may be non-specific, and areas of sclerosis may rather be representative of an increased volume of lower density bone.[47] Findings related to bone volume and bone density will be provided in the next chapter; however, as microcomputed tomography and histopathology were not performed until after termination of the study, information on lesion composition can only be provided for week 24 and not earlier time points. Furthermore, MRI was not initially performed until 4 weeks post-operatively; therefore, the true acute response to this model could not be evaluated, including when bone sclerosis first occurred. It is likely that BMLs would have been present by week 2 based on the previous work by Stewart et al., and based on reports in the current literature it's even possible

BMLs would be present sooner. Future work could include performing MRI and CT immediately following or within 24 hours of lesion induction. Another factor to consider would be the effects of pin drilling compared to an impact-based model such as a hammer drill. The act of drilling pins into the condyle likely induces more severe damage relative to the early stages of clinical disease.

The goal of this model is to be able to induce lesions without diffuse articular cartilage or extra-articular soft tissue damage serving as a catalyst for lesion development and progression, in order to study factors affecting progression and regression of lesions in a controlled manner. The diagnostic imaging findings reported here support continued work using this experimental model. Additionally, correlation statistics will be performed in future research to better examine the significance of the findings and variation observed in this study.

4.5 Figures

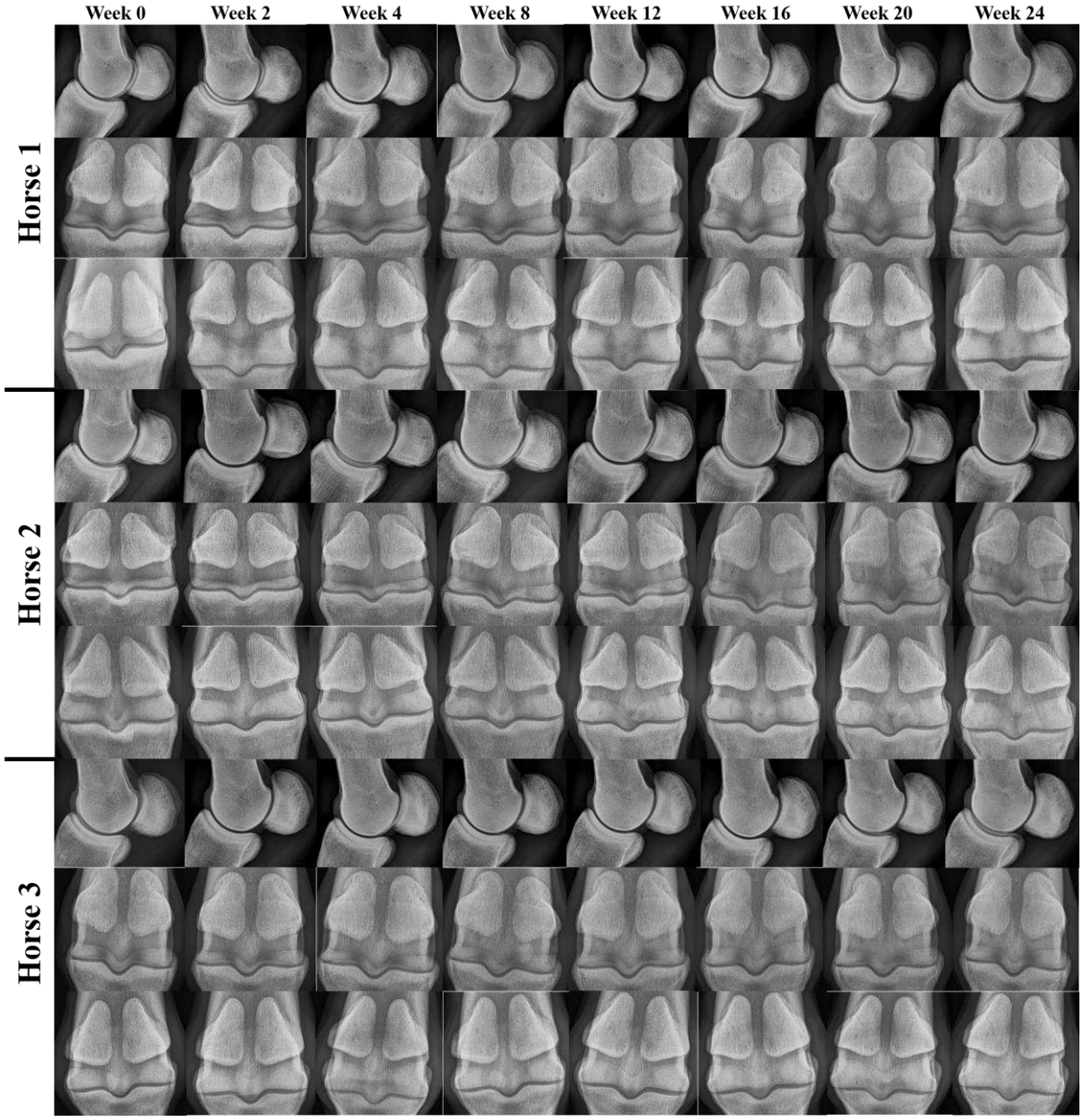

Figure 4.1 – Representative radiographic images for each horse taken at regular intervals over the course of this study. Within each horse, the top row contains lateromedial images, the second row contains dorsoproximal images, and the third row contains flexed dorsopalmar images.

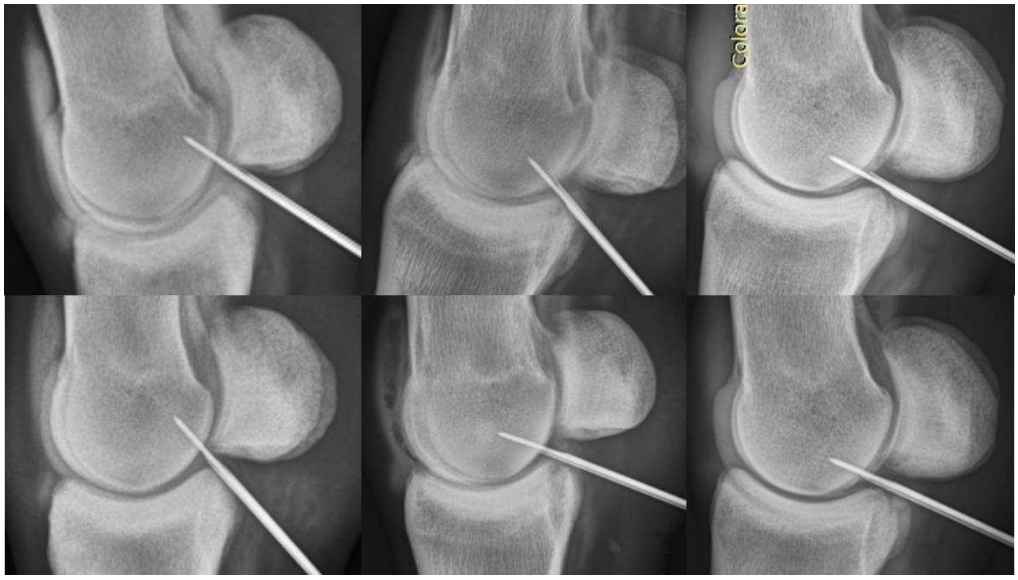

Figure 4.2 – Intraoperative radiographic images demonstrating the pin placement in the left (top row) and right (bottom row) third metacarpal bones (images representative of the pin location for both condyles) of horses 1 (left column), 2 (middle column), and 3 (right column). The pin was placed further distad within the condyles in the latter two horses by increasing the degree of fetlock extension.

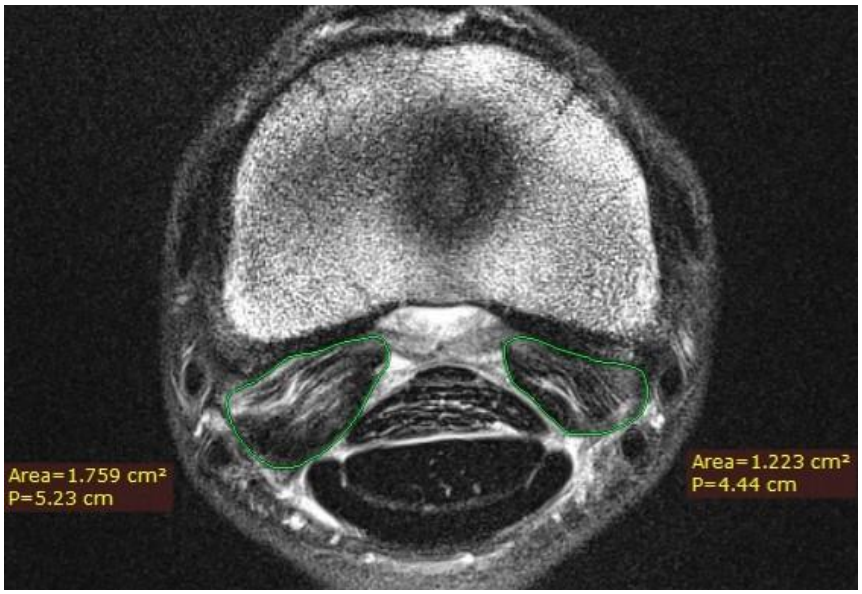

Figure 4.3 – Transverse proton density (PD) image from magnetic resonance imaging of the left forelimb from horse #3, just distal to the level of the proximal sesamoid bones, obtained 24 weeks post-experimental induction of bone marrow lesions in the third metacarpal condyles. The area of the medial oblique sesamoidean ligament (left) was enlarged by 43.8% compared to the lateral oblique sesamoid ligament (right), with a mildly abnormal architecture and increased fluid signal.

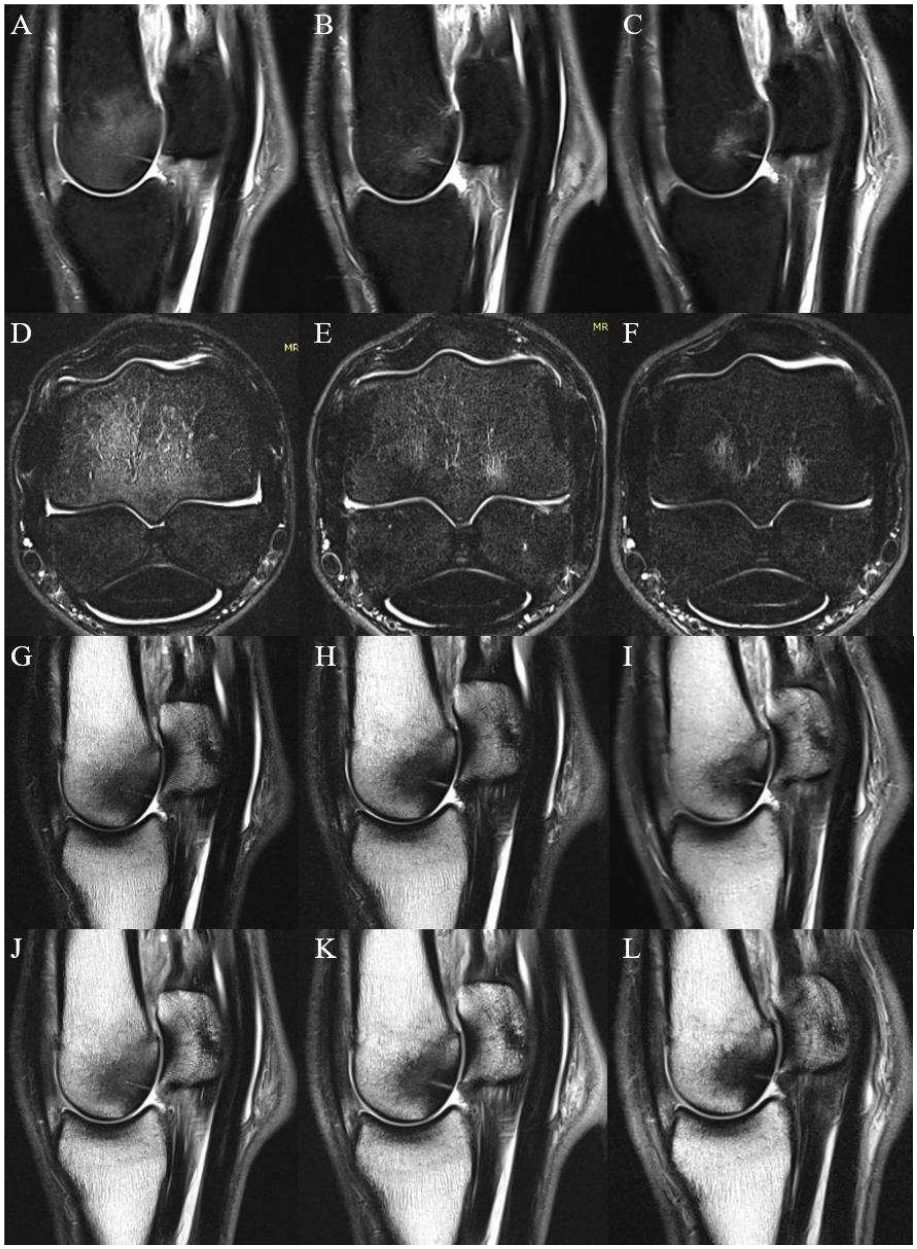

Figure 4.4 – Serial sagittal and transverse images of an experimentally-induced bone marrow lesion (BML), followed by 6-months of high-speed treadmill exercise, in a single horse (horse #2, right forelimb, lateral condyle) on magnetic resonance imaging (MRI) with various sequences shown to demonstrate changes in fluid signal and bone sclerosis throughout the course of this study. (A-C) Dixon water only images; (D-F) short tau inversion recovery (STIR) images; (G-I) T2-weighted fast spin echo (FSE) images; (J-L) proton density (PD) images. Images in the first column are 4 weeks post-lesion induction, images in the second column are 12 weeks post-lesion induction, and images in the third column are 24 weeks post-lesion induction. In the Dixon water and STIR images, fluid signal was significantly reduced by weeks 12 and 24, becoming more concentrated at the tip of the hyperintense pin tracts. The T2 FSE and PD images demonstrate the bone sclerosis surrounding the isointense pin tracts. While not significantly different in area, continued remodeling and increased definition in the region of bone sclerosis can be seen over time.

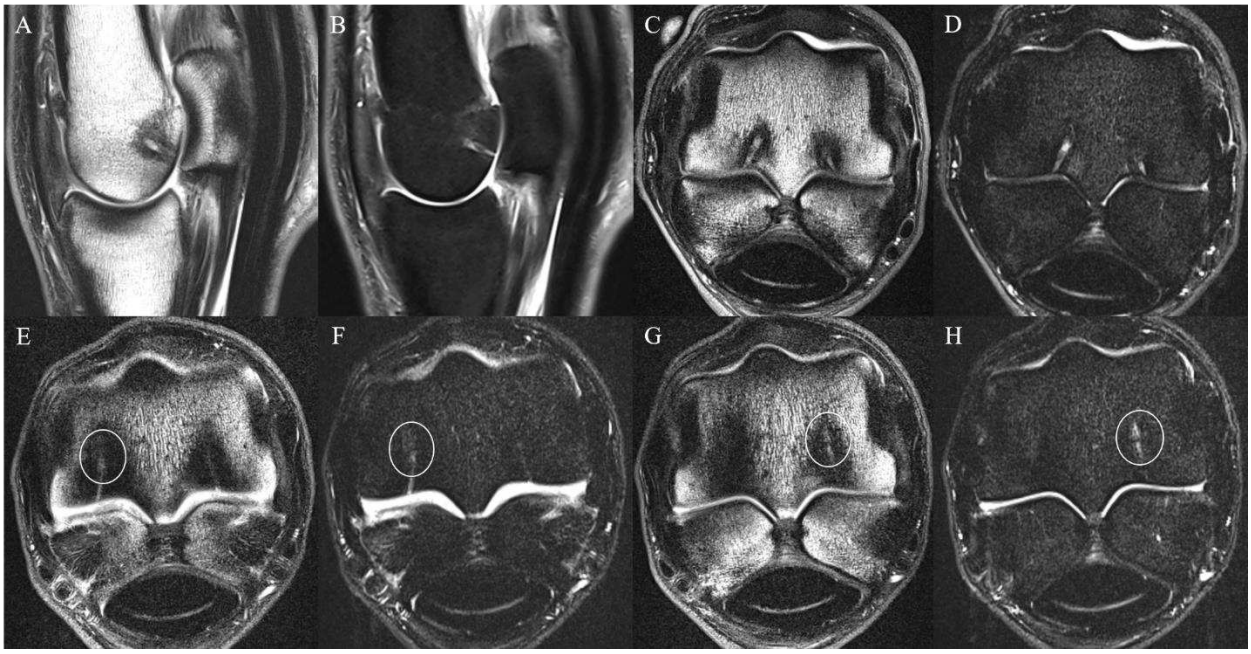

Figure 4.5 – Sagittal and transverse images of widening of the tip of the pin tract observed on magnetic resonance imaging at week 24 post-lesion induction. Lateral is to the left in all transverse images (C-H). (A-D) Images demonstrating widening of and increased signal intensity associated with the end of the right lateral pin tract in horse #1 on sagittal proton density (PD; A), sagittal Dixon water only (B), transverse PD (C), and transverse short tau inversion recovery (STIR, D) images. (E-H) Images from horse #3 demonstrating the presence of ovoid-shaped foci of increased signal intensity (circled) at the tips of the right lateral (E, F) and right medial (G, H) pin tracts on transverse PD (E, G) and STIR (F, H) images.

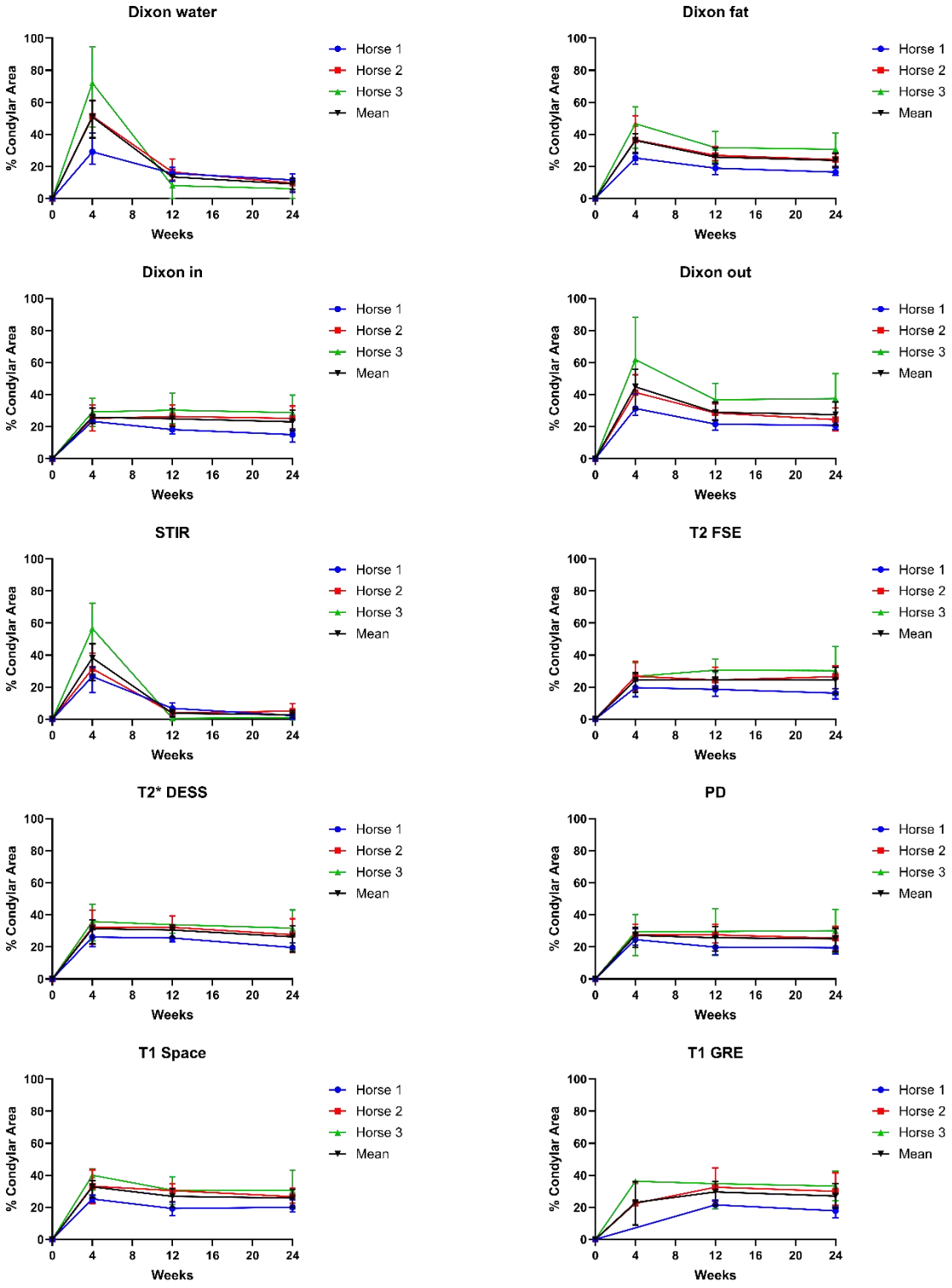

Figure 4.6 – Graphs showing the mean (range) maximum bone marrow lesion area – reported as the occupied percentage of the condylar area on the slice on which the lesion was largest – for each horse over time for all magnetic resonance imaging sequences on which this could be measured. For each sequence, an overall mean (range) from all horses was also provided (black).

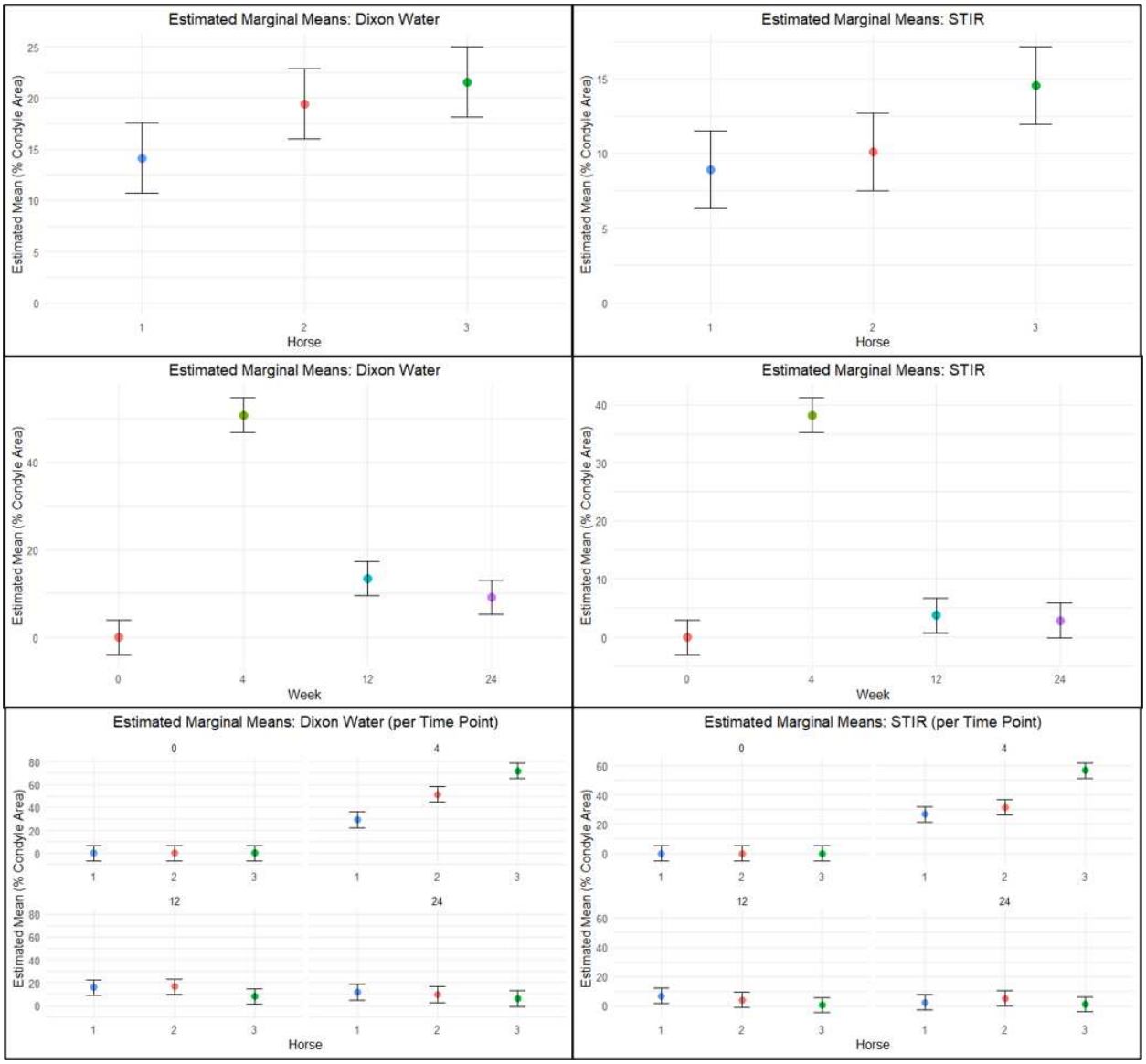

Figure 4.7 – Plots showing the estimated marginal means (95% CI) for the percentage of the condyle occupied by a bone marrow lesion (BML) on Dixon water only and short tau inversion recovery (STIR) magnetic resonance imaging (MRI) sequences. Plots in the first row show the comparison between horses, the second row shows the comparison between time points, and the third row shows the comparison between horses at each individual time point.

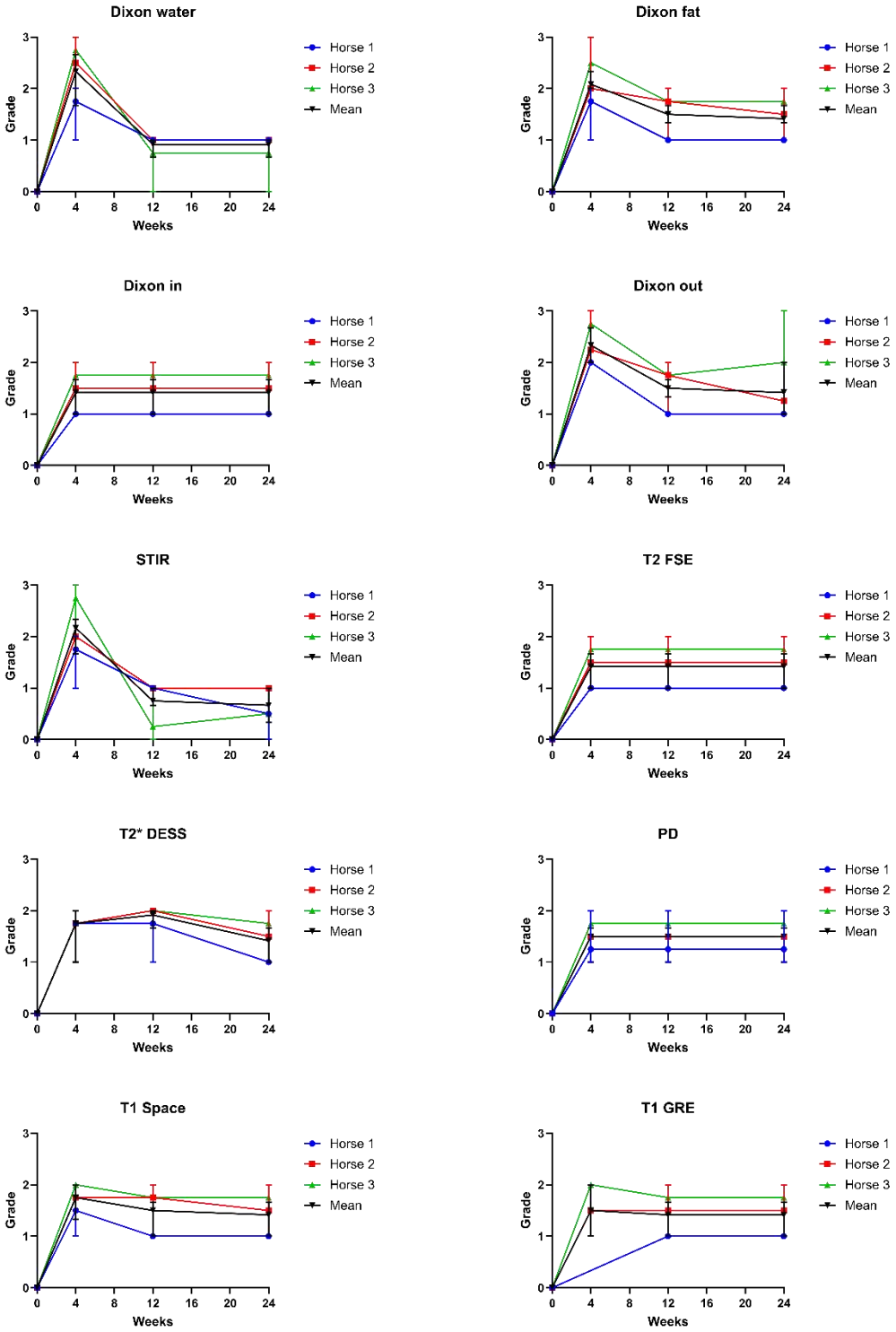

Figure 4.8 - Graphs showing the mean (range) bone marrow lesion (BML) grade – scored using Table 4.2 according to the percentage of the condylar area occupied by a BML on the slice on which the lesion was largest – for each horse over time for all magnetic resonance imaging sequences on which this could be measured. For each sequence, an overall mean (range) from all horses was also provided (black). The grading scale is provided on the y-axis.

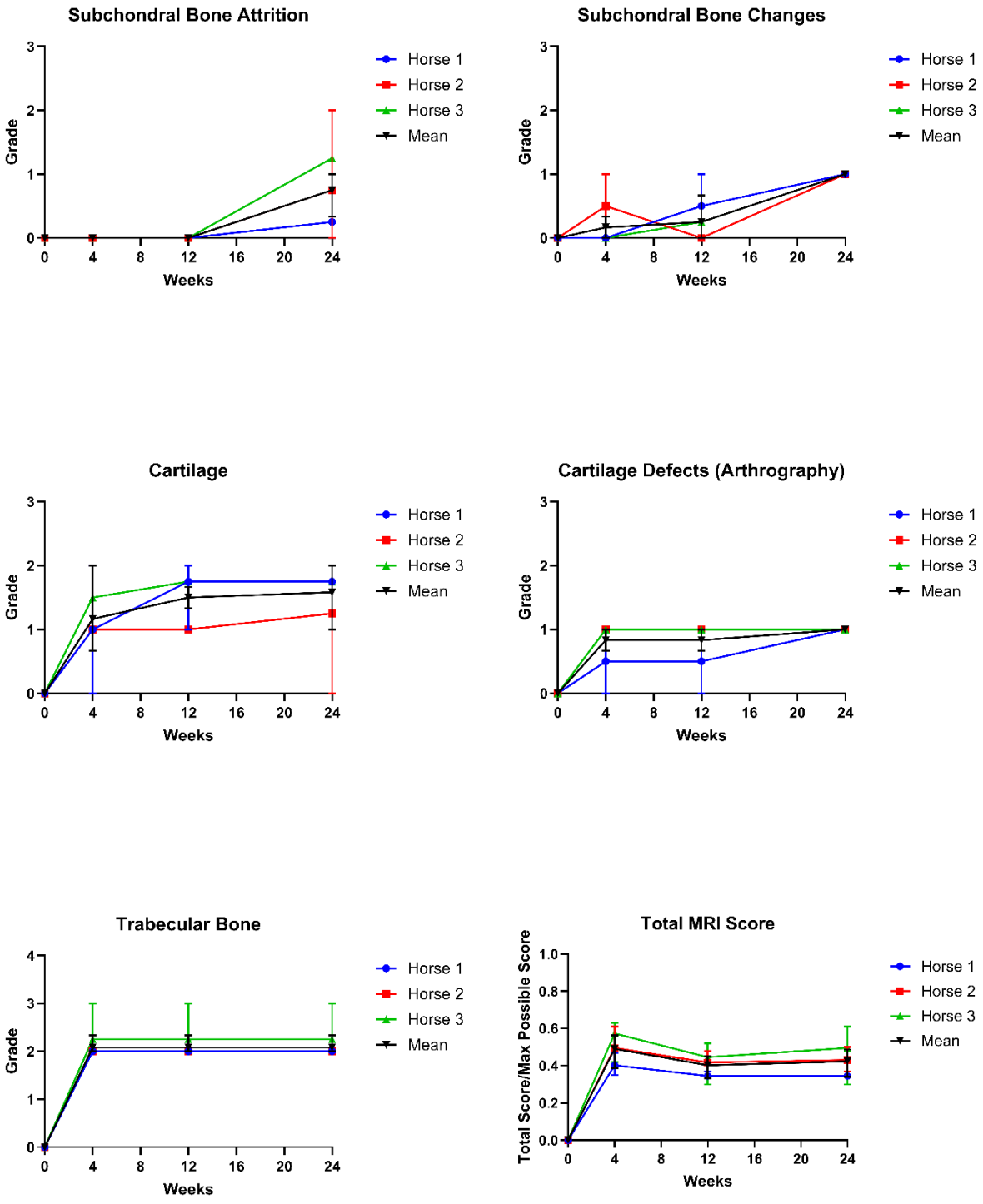

Figure 4.9 – Graphs showing the mean (range) scores for the remainder of the outcome parameters scored on magnetic resonance imaging (MRI) using Table 4.2, including the total MRI score, for each horse over time. An overall mean (range) from all horses was also provided (black). The grading scale for each parameter is provided on the y-axis.

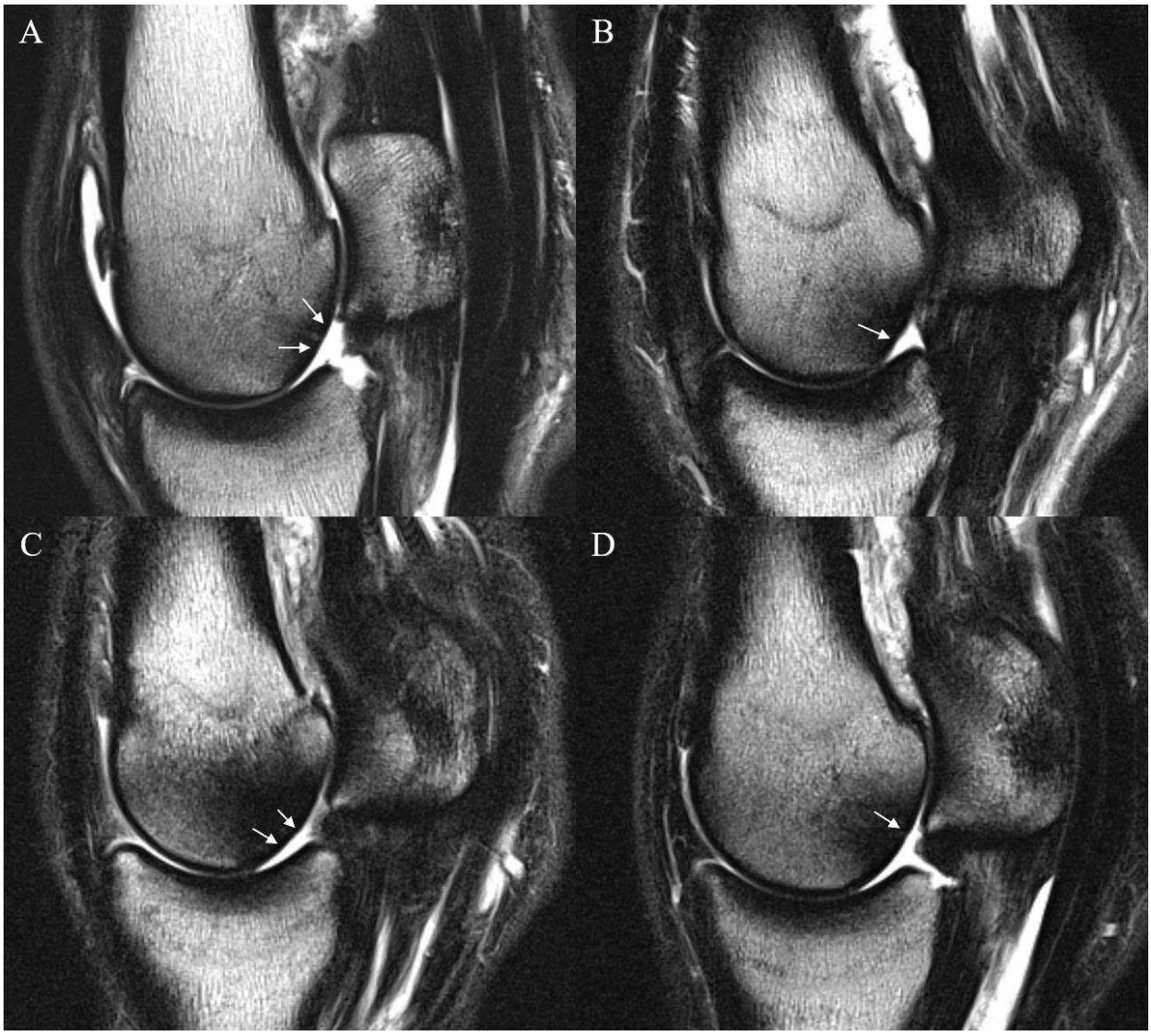

Figure 4.10 – Sagittal T2-weighted fast spin echo (FSE) images from magnetic resonance imaging of horse #2 (A,B) and horse #3 (C,D) at 24 weeks post-lesion induction, demonstrating the grades of subchondral bone attrition observed in this study. The two left images show grade 1 subchondral bone attrition, characterized by a focal flattening of the palmarodistal surface of the third metacarpal bone. The two right images show grade 2 subchondral bone attrition, characterized by a mild concavity within the palmarodistal surface of the third metacarpal bone.

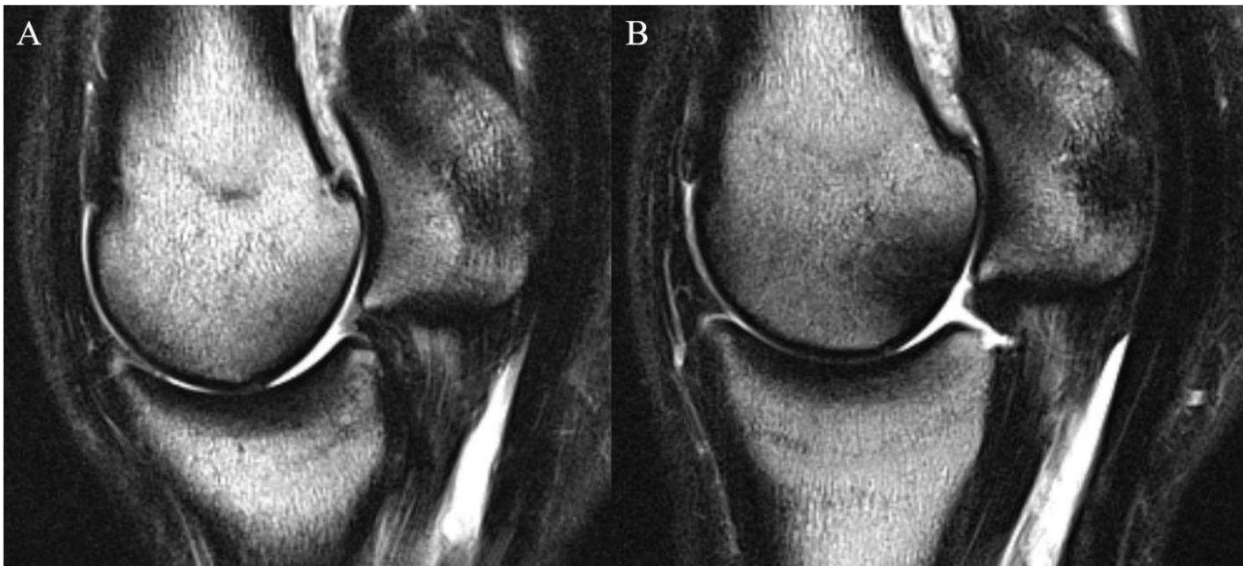

Figure 4.11 – Sagittal T2-weighted fast spin echo images from magnetic resonance imaging of horse #3 at baseline (A) and week 24 (B). Compared to the normal subchondral bone plate shown in image A, image B was scored as having grade 1 changes to the subchondral bone characterized by mild thickening of the subchondral bone plate in an area less than 1 cm^2, with moderate surrounding sclerosis.

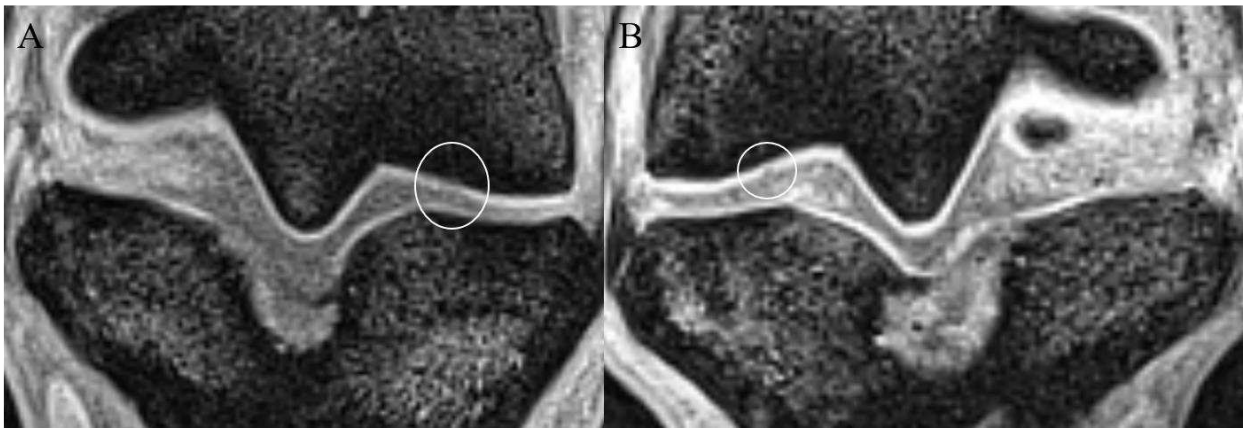

Figure 4.12 – Dorsal T1-weighted VIBE images from magnetic resonance imaging of horse #2 (A) and horse #3 (B) at 24 weeks post-lesion induction, demonstrating the grades of cartilage changes observed in this study. Image A shows grade 1 changes to the articular cartilage characterized by a focal area of abnormal signal with an irregular surface. Image B shows grade 2 changes to the articular cartilage characterized by a partial thickness articular cartilage defect < 5 mm diameter with an irregular surface. The latter was also scored as a grade 1 cartilage defect.

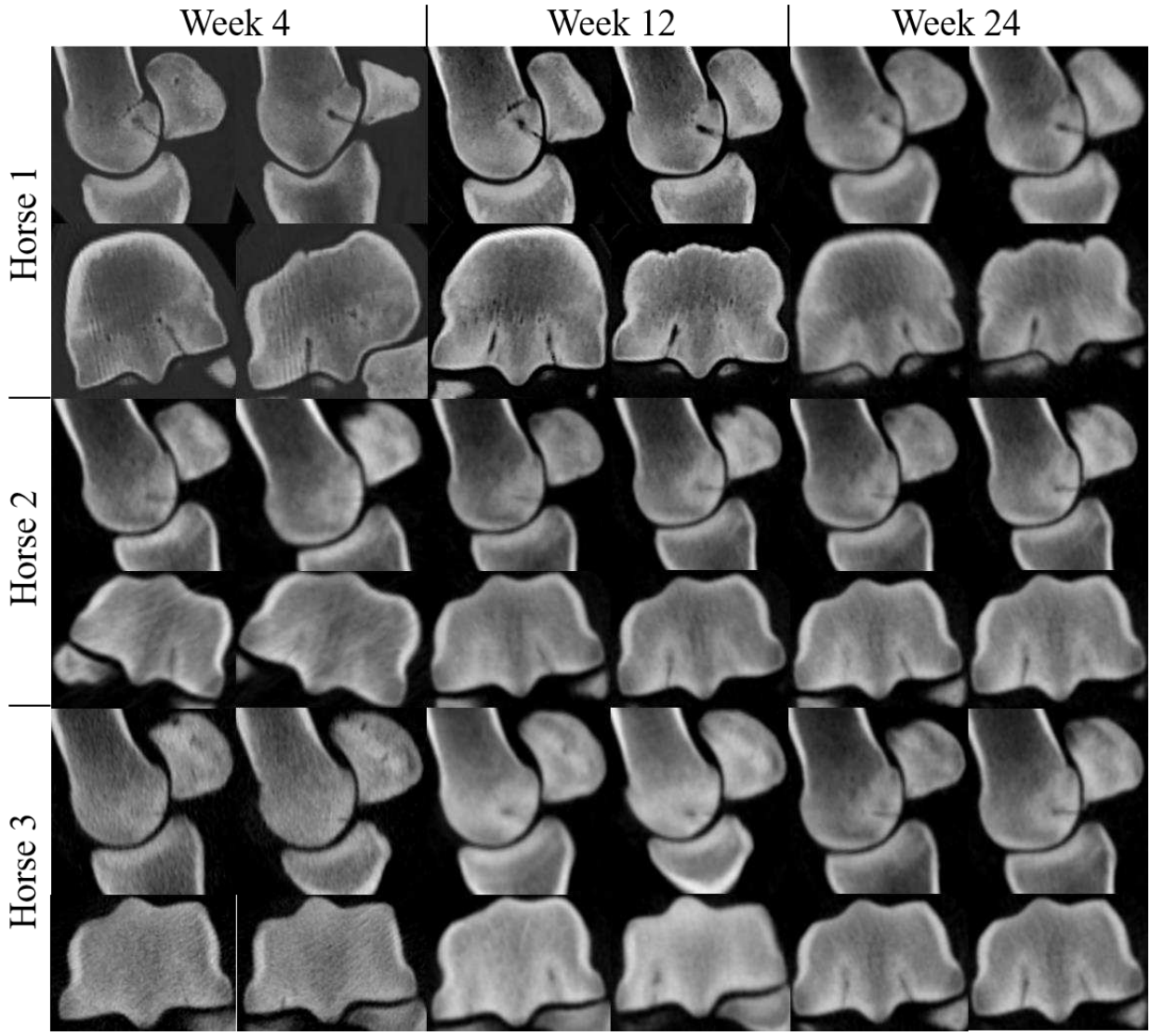

Figure 4.13 – Representative computed tomographic (CT) images of the right third metacarpal condyles for each horse over the course of this study. Within each horse, the left two images for each time point are of the right medial condyle/pin tract, and the right two images are of the right lateral condyle/pin tract. Lateral is to the left in all transverse CT images (representing the dorsal plane views of the pin tracts for the purposes of lesion measurement – see Figure 4.12).

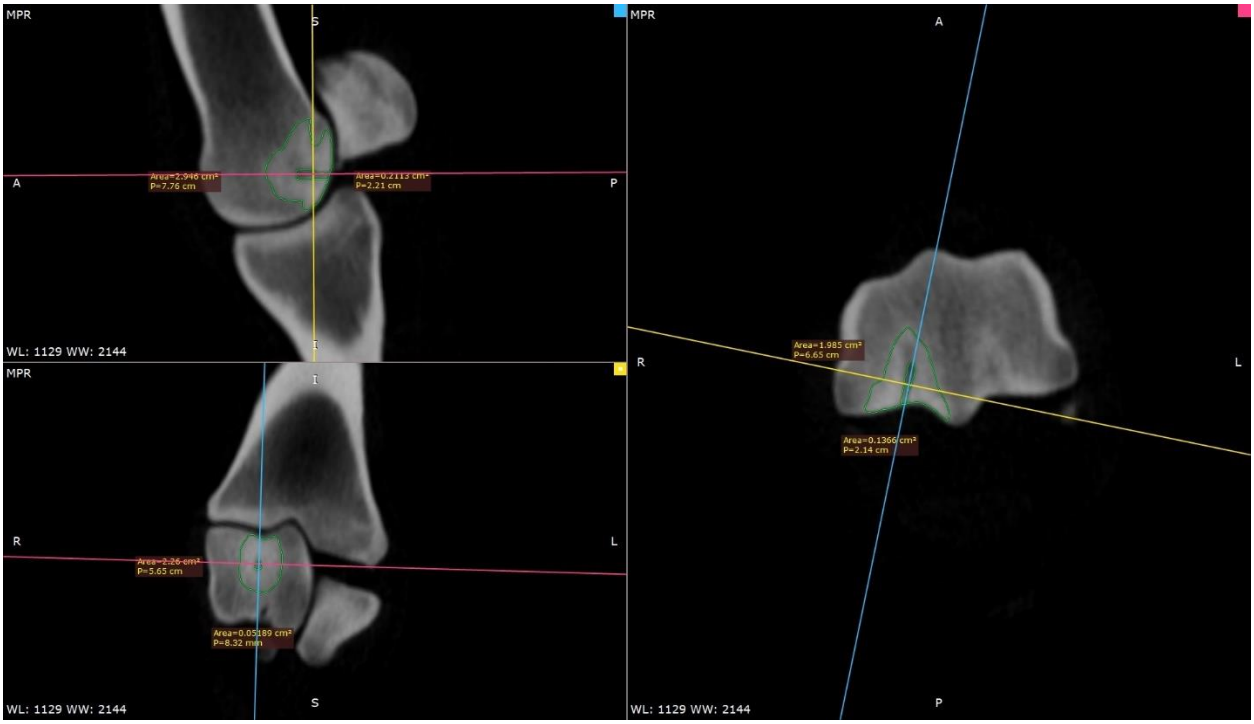

Figure 4.14 – Computed tomographic (CT) images of the right lateral condyle of horse #2 at week 24 post-lesion induction, showing how the total area of sclerosis and area of the pin tract was measured. The blue labeled image (upper left) and blue line represent the sagittal plane relative to the pin tract. The yellow labeled image (lower left) and yellow line represent the transverse plane relative to the pin tract. The pink labeled image (right) and pink line represent the dorsal plane relative to the pin tract.

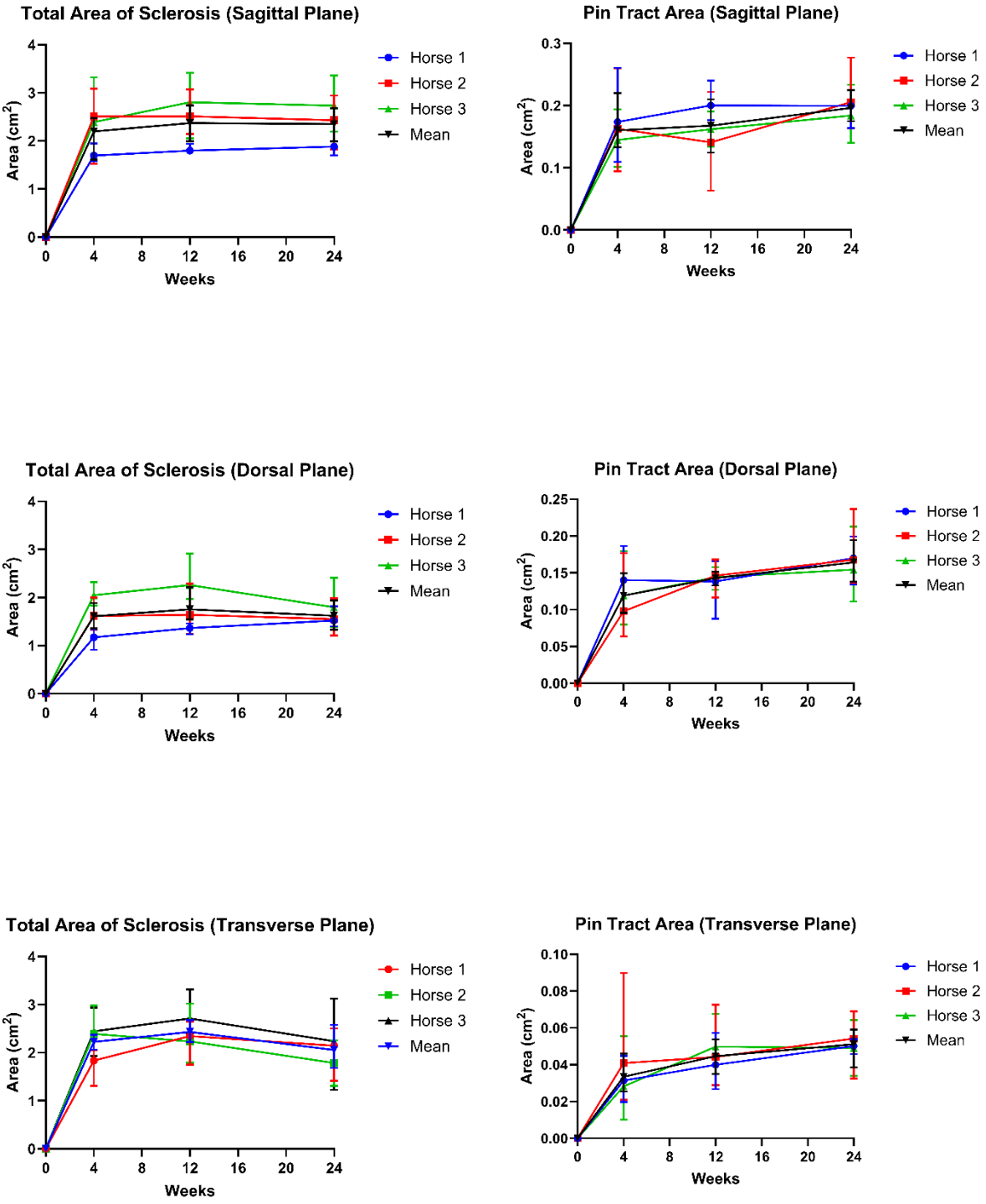

Figure 4.15 - Graphs showing the mean (range) area for regions of sclerosis and of the pin tracts for each horse over time, as measured on computed tomography (CT) in the sagittal, dorsal, and transverse planes. The CT was aligned and centered along the long axis of the pin tracts in all three planes. An overall mean (range) from all horses was also provided (black).

4.6 Tables

Table 4.1 – In order to monitor the development and progression/remodeling of the experimentally-induced bone marrow lesions induced over time, magnetic resonance imaging (MRI) was performed using a high-field magnet (3-Tesla) at baseline and weeks 4, 12, and 24 post-operatively. The MRI sequences used in this study are described below.

Sequence	Field of View (mm)	Matrix	Slice Thickness (mm)	TR	TE	Flip Angle
T1 GRE	150	320 x 182	3.0	471	4.6	83°
T2* GRE	150	256 x 233	3.0	32	17	8°
T2 FSE	150	512 x 512	3.0	4990	93	126°
T1 VIBE	150	320 x 320	0.5	11	4.9	10°
T2* DESS	180	320 x 320	0.6	13.4	5	25°
STIR	120	384 x 350	3.0	3180	44	121°
PD (sagittal)	150	512 x 512	3.0	3110	43	136°
PD (transverse)	120	512 x 512	3.0	2910	49	136°
T1 SPACE	150	256 x 256	0.6	700	15	120°
Intermediate-weighted Dixon	150	320 x 320	3.0	2500	40	150°

Abbreviations: DESS, dual echo steady state; FSE, fast spin echo; GRE, gradient echo; PD, proton density; SPACE, Sampling Perfection with Application optimized Contrast using different flip angle Evolution; STIR, short-tau inversion recovery; TE, time to echo; TR, repetition time; TSE, turbo spin echo; VIBE, volumetric interpolated breath-hold examination

Table 4.2 – Semi-quantitative scoring system used to grade changes in the cartilage, subchondral and trabecular bone of the third metacarpal (MC3) condyles on magnetic resonance imaging (MRI), modified from Table 1 by Smith et al.[28] to better suit the changes identified in this study.

Lesion	Score	Description
Bone marrow lesions*	0	None
	1	Lesion area <25% of condylar area
	2	Lesion area 25-50% of condylar area
	3	Lesion area > 50% of condylar area
Subchondral bone attrition	0	None (normal contour)
	1	Focal flattening of the palmarodistal surface of MC3
	2	Mild concavity within the palmarodistal surface of MC3
	3	Marked concavity within the palmarodistal surface of MC3
Subchondral bone changes	0	None
	1	Mild linear areas of subchondral bone lysis with mild surrounding sclerosis in <25% of condyle, or ≤ 1 cm^2 area of subchondral bone plate thickening
	2	Coalescing areas of lysis within the subchondral bone with moderate surrounding sclerosis in 25-50% of condyle, or > 1 cm^2 area of subchondral bone plate thickening
	3	Subchondral bone void with marked sclerosis in >50% of condyle
Cartilage	0	Normal cartilage thickness and uniform signal, smooth surface
	1	Normal thickness, ± abnormal signal on T1 VIBE or T2W images, ± surface irregularity
	2	Partial thickness focal defect < 5 mm diameter, abnormal signal, irregular surface
	3	Full thickness focal defect or a partial thickness focal defect > 5 mm diameter, ± high signal intensity extending into subchondral ± trabecular bone in FSE, T2* GRE, and/or STIR sequences

Cartilage defects (arthrography)	0	Intact cartilage surface with sharp line of contrast
	1	Partial thickness defect or focal cartilage depression < 5 mm diameter, focal concave deviation of contrast material or penetration of contrast within at least the superficial half of the cartilage thickness and not within the subchondral bone
	2	Partial thickness defect or focal cartilage depression > 5 mm diameter, focal concave deviation of contrast material or penetration of contrast within at least the superficial half of the cartilage thickness and not within the subchondral bone
	3	Full thickness defect with contrast reaching or penetrating the subchondral bone
Trabecular Bone	0	Normal regional variation in trabecular signal intensity for a given sequence, reflecting normal regional density. Small number of focal spots/lines of low signal intensity consistent with vessels within trabecular bone
	1	Generalized mild low signal intensity on the T1 GRE, T2 FSE and PD sequences (mild increase in TB density) but still with normal regional variation, or small (< 5 mm) osseous cyst-like lesions present with minimal change in surrounding bone density and no communication with the articular surface. ± diffuse area of mildly increased signal intensity in STIR images. Small number of focal spots/lines of low signal intensity consistent with trabecular bone vessels
	2	Loss of regional variation due to generalized low signal intensity on T1 GRE, T2 FSE and PD sequences (increased density) in < 50% region, or osseous cyst-like lesions > 5 mm surrounded by bone of low signal intensity (increased density) or areas (<50% region), or intermediate to high signal intensity in STIR images. More prominent focal lines of low signal intensity consistent with focal increased TB density
	3	Low signal intensity in > 50% of region on T1 GRE, T2 FSE and PD sequences (severe increased TB density) extending proximally to physis, or large osseous cyst-like lesions (> 5 mm) with direct articular communication, or area(s) of intermediate or high signal intensity over > 50% region in STIR images
	4	Fracture ± increased signal intensity within fracture plane in STIR, FSE and T2* images and low signal intensity in bone surrounding the fracture in T2* or PD images
Total MRI Grade	Out of 1	Sum of the scores for the above parameters, including the bone marrow lesion grades for each individual sequence on which it could be measured, divided by the total possible score**

**A separate grade for bone marrow lesions was given for each of the following MRI sequences to account for differences in lesion characteristics between sequences: Intermediate-weighted Dixon (water, fat, in, out), T2 FSE, T2* DESS, T1 GRE, PD, T1 SPACE, STIR*

*** The T1 GRE sequence was not acquired for horse #1 at week 4 or in the left forelimb of horse #3 at week 4; therefore, this was done to account for those parameters lacking specific data points, for which the total possible composite score would differ.*

4.7 References

1. Arthur R, Blea J, Ross M, Moloney P, Cheney M. The North American Thoroughbred. In: Ross M, Dyson S, eds. *Diagnosis and Management of Lameness in the Horse*. 2nd Ed. St. Louis, Missouri: Elsevier Saunders; 2011:977-993.

2. Pilsworth R. The European Thoroughbred. In: Ross M, Dyson S, eds. *Diagnosis and Management of Lameness in the Horse*. 2nd Ed. St. Louis, Missouri: Elsevier Saunders; 2011:994-1013.

3. Powell S. Low-field standing magnetic resonance imaging findings of the metacarpo/metatarsophalangeal joint of racing Thoroughbreds with lameness localized to the region: A retrospective study of 131 horses. *Equine Vet J*. 2012;44:169-177.

4. Kawcak C, McIlwraith C, Norrdin R, Park R, Steyn P. Clinical effects of exercise on subchondral bone of carpal and metacarpophalangeal joints in horses. *Am J Vet Res*. 2000;61(10):1252-1258.

5. McIlwraith C, Yovich J, Martin G. Arthroscopic surgery for the treatment of osteochondral chip fractures in the equine carpus. *J Am Vet Med Assoc*. 1987;191:531-540.

6. Harris W, Heaney R. Skeletal renewal and metabolic bone disease. *N Engl J Med*. 1969;280:193-202.

7. Greenfield G. Analytical approach to bone radiology. In: Greenfield G, ed. *Radiology of Bone Diseases*. Philadelphia, PA: JB Lippincott Co; 1986:7.

8. Kawcak C, Barrett MF. Fetlock. In: McIlwraith C, Frisbie D, Kawcak C, van Weeren PR, eds. *Joint Disease in the Horse*. Second Edi. St. Louis, Missouri: Elsevier; 2016:302-317.

9. Trope G, Anderson G, Whitton R. Patterns of scintigraphic uptake in the fetlock joint of Thoroughbred racehorses and the effect of increased radiopharmaceutical uptake in the distal metacarpal/tarsal condyle on performance. *Equine Vet J*. 2011;43(5):509-515.

10. Spriet M, Espinosa-Mur P, Cissell D, et al. 18F-sodium fluoride positron emission tomography of the racing Thoroughbred fetlock: validation and comparison with other imaging modalities in nine horses. *Equine Vet J*. 2019;51(3):375-383.

11. Kawcak C, McIlwraith C, Norrdin R, Park R, James S. The role of subchondral bone in joint disease: a review. *Equine Vet J*. 2001;33(2):120-126.

12. Davidson E, Ross M. Clinical recognition of stress-related bone injury in racehorses. *Clin Tech Equine Pract*. 2003;2(4):296-311.

13. Gonzalez L, Schramme M, Robertson I, Thrall D, Redding R. MRI features of metacarpo(tarso)phalangeal region lameness in 40 horses. *Vet Radiol Ultrasound*. 2010;51:404-414.

14. Tanamas SK, Wluka AE, Pelletier J-P, et al. Bone marrow lesions in people with knee osteoarthritis predict progression of disease and joint replacement: a longitudinal study. *Rheumatology*. 2010;49(12):2413-2419. doi:10.1093/rheumatology/keq286

15. Barrett MF, Selberg KT, Johnson SA, Hersman J, Frisbie DD. High field magnetic resonance imaging contributes to diagnosis of equine distal tarsus and proximal metatarsus lesions: 103 horses. *Vet Radiol Ultrasound*. 2018;59(5):587-596. doi:10.1111/vru.12659

16. Biggi M, Zani DD, De Zani D, Di Giancamillo M. Magnetic resonance imaging findings of bone marrow lesions in the equine distal tarsus. *Equine Vet Educ*. 2012;24(5):236-241. doi:10.1111/j.2042-3292.2011.00288.x

17. Wluka AE, Wang Y, Davies-Tuck M, English DR, Giles GG, Cicuttini FM. Bone marrow lesions predict progression of cartilage defects and loss of cartilage volume in healthy middle-aged adults without knee pain over 2 yrs. *Rheumatology*. 2008;47(9):1392-1396. doi:10.1093/rheumatology/ken237

18. Olive J, Mair TS, Charles B. Use of standing low-field magnetic resonance imaging to diagnose middle phalanx bone marrow lesions in horses. *Equine Vet Educ*. 2009;21(3):116-123. doi:10.2746/095777309X383612

19. Mitchell M, Kundal H, Steinberg M, Kressel H, Alavi A, Axel L. Avascular necrosis of the hip: comparison of MR, CT, and scintigraphy. *Am J Roentgenol*. 1986;147:67-71.

20. Ciamillo S, Wulster K, Gassert T, et al. Prospective, longitudinal assessment of subchondral bone morphology and pathology using standing, cone-beam computed tomography in fetlock joints of 2-year-old Thoroughbred racehorses in their first year of training. *Equine Vet J*. 2025;57:126-139.

21. Curtiss A, Ortved K, Dallap-Schaer B, et al. Validation of standing cone beam computed tomography for diagnosing subchondral fetlock pathology in the Thoroughbred racehorse. *Equine Vet J*. 2021;53:510-523.

22. Stewart H, Siewerdsen J, Nelson B, Kawcak C. Use of cone-beam computed tomorgraphy for advanced imaging of the equine patient. *Equine Vet J*. 2021;53:872-885.

23. Lin S-T, Bolas N, Peter V, et al. Comparison of cone-beam and fan-beam computed tomography and low-field magnetic resonance imaging for detection of palmar/plantar osteochondral disease in Thoroughbred horses. *Equine Vet J*. 2024;56:999-1007.

24. Hornof W, O'Brien T. Radiographic evaluation of the palmar aspect of the equine metacarpal condyles: a new projection. *Vet Radiol*. 1980;21(4):161-167.

25. Kawcak C, Bramlage L, Embertson R. Diagnosis and management of incomplete fracture of the distal palmar aspect of the third metacarpal bone in five horses. *J Am Vet Med Assoc*. 1995;206(3):335-337.

26. Hogan P. Nonstandard Radiographic Techniques for the Equine Practitioner. In: *Proceedings of the Annual Convention of the American Association of Equine Practitioners*. ; 1997:141-144.

27. Porter E, Winter M, Sheppard B, Berry C, Hernandez J. Correlation of articular cartilage thickness measurements made with magnetic resonance imaging, magnetic resonance arthrography, and computed tomographic arthrography with gross articular cartilage thickness in the equine metacarpophalangeal joint. *Vet Radiol Ultrasound*. 2016;57(5):515-525.

28. Smith M, Dyson S, Murray RC. Reliability of high- and low-field magnetic resonance imaging systems for detection of cartilage and bone lesions in the equine cadaver fetlock. *Equine Vet J*. 2012;44:684-691.

29. Stewart HL, Easley JT, Selberg KT, et al. Experimental models of bone marrow lesions in ovine femoral condyles. *Vet Surg*. 2023;52:284-298.

30. Davis A, Fan X, Shen L, Robinson P, Riggs C. Improved radiological diagnosis of palmar osteochondral disease in the Thoroughbred racehorse. *Equine Vet J*. 2017;49:454-460.

31. Norrdin R, Kawcak C, Capwell B, McIlwraith C. Subchondral bone failure in an equine model of overload arthrosis. *Bone*. 1998;22:133-139.

32. Kawcak C, McIlwraith C, Norrdin R, Park R, Steyn P. Clinical effects of exercise on subchondral bone of carpal and metacarpophalangeal joints in horses. *Am J Vet Res*. 2000;61(10):1252-1258.

33. Rickey EJ, Cruz A, Trout D, McEwen B, Hurtig M. Evaluation of experimental impact injury for inducing post-traumatic osteoarthritis in the metacarpophalangeal joints of horses. *Am J Vet Res*. 2012;73(10):1540-1552.

34. Wells M, Dunn J. Pathophysiology of Avascular Necrosis. *Hand Clin*. 2022;38:367-376.

35. Mont M, Cherian J, Sierra R, Jones L, Lieberman J. Nontraumatic Osteonecrosis of the Femoral Head: Where Do We Stand Today? *J Bone Jt Surgery-American Vol*. 2015;97-A(19):1604-1627.

36. Shah K, Racine J, Jones L, Aaron R. Pathophysiology and risk factors for osteonecrosis. *Curr Rev Musculoskelet Med*. 2015;8:201-209.

37. Pool R, Meagher D. Pathologic findings and pathogenesis and racetrack injuries. *Vet Clin North Am - Equine Pract*. 1990;6(1):1-30.

38. Bani Hassan E, Mirams M, Ghasem-Zadeh A, Mackie E, Whitton RC. Role of subchondral bone remodelling in collapse of the articular surface of Thoroughbred racehorses with palmar osteochondral disease. *Equine Vet J*. 2016;48:228-233.

39. Bani Hassan E, Mirams M, Mackie E, Whitton RC. Prevalence of subchondral bone

pathological changes in the distal metacarpi/metatarsi of racing Thoroughbred horses. *Aust Vet J*. 2017;95:362-369.

40. Nixon A. Palmar/plantar metacarpal/metatarsal fragmentation. In: Auer J, Stick J, Kummerle J, Prange T, eds. *Equine Surgery*. 5th ed. St. Louis, Missouri: Elsevier, Inc.; 2019:1601-1603.

41. Rice H, Brokken M, Hostnik E, Bertone A. Evaluation of a novel bone substitute injection technique for potential treatment of impact injury to the equine palmar metacarpal condyle. *Vet Comp Orthop Traumatol*. 2019;32(6):447-453.

42. Bertoni L, Jacquet-Guibon S, Branly T, et al. An experimentally induced osteoarthritis model in horses performed on both metacarpophalangeal and metatarsophalangeal joints: Technical, clinical, imaging, biochemical, macroscopic and microscopic characterization. *PLoS One*. 2020;15(6):e0235251.

43. Hontoir F, Nisolle J, Meurisse H, et al. A comparison of 3-T magnetic resonance imaging and computed tomography arthrography to identify structural cartilage defects of the fetlock joint in the horse. *Vet J*. 2014;199:115-122.

44. Tranquille C, Parkin T, Murray R. Magnetic resonance imaging detected adaptation and pathology in the distal condyles of the third metacarpus, associated with lateral condylar fracture in Thoroughbred racehorses. *Equine Vet J*. 2012;44:699-706.

45. Zubrod C, Schneider R, Tucker R, Gavin P, Ragle C, Farnsworth K. Use of magnetic resonance imaging for identifying subchondral bone damage in horses: 11 cases (1999–2003). *J Am Vet Med Assoc*. 2004;224:411-418.

46. Olive J, Serraud N, Vila T, Germain J-P. Metacarpophalangeal joint injury patterns on magnetic resonance imaging: A comparison in racing Standardbreds and Thoroughbreds. *Vet Radiol Ultrasound*. 2017;58:588-597.

47. Stewart H. Dissertation: Evaluation of bone marrow lesions as a manifestation of subchondral bone disease. 2021.

CHAPTER 5:

GROSS AND MICROSCOPIC CHANGES IN THE DISTAL THIRD METACARPAL CONDYLES FOLLOWING EXPERIMENTAL INDUCTION OF BONE MARROW LESIONS IN EQUINE METACARPOPHALANGEAL JOINTS

5.1 Introduction

Palmar osteochondral disease (POD) is a repetitive overload injury of the palmar distal third metacarpal and metatarsal condyles. It exhibits a wide spectrum of disease severity, from subtle alterations in bone remodeling to complete collapse of the articular surface.[1] In one study, 80% of racehorses had a POD lesion in at least one condyle on post-mortem exam, although this was likely an overrepresentation of the general population, and 14% were graded as severe.[2] In this study, lesions were more severe in the medial condyle in the forelimb and lateral condyle in the hind limb; however, there were no differences in severity between left and right limbs.[2] In Thoroughbred racehorses, POD has also shown to be associated with other pathologies of the MC3/MT3 condyles including wear lines, cartilage loss and ulceration (both on the condyles and the proximal sesamoid bones), marginal remodeling of the proximal sesamoid bones, dorsal impact injury, and linear fissures.[2,3] While advanced diagnostic imaging has been shown to be suitable for the detection and monitoring of POD lesions, it often underestimates the size of the lesions[4]; therefore, when developing an experimental model for the study of this disease, it is important that post-mortem evaluation be performed in order to determine the full extent of the changes that occur as a result of the model.

On gross examination, POD appears as small (2 to 4 mm), ovoid defects in the palmar articular surface of the condyles on either side of the mid-sagittal ridge (anywhere from 3 to

15mm medial or lateral), centered about 5-8 mm proximal and palmar to the transverse ridge.[5] Early lesions, prior to becoming symptomatic, are recognized as an ovoid, bluish discoloration or bruised area of an otherwise normal cartilage surface.[3,5,6] As the disease progresses, ulceration of the distopalmar/plantar aspect of the MC3/MT3 condyles develops to a varying degree, in some cases exposing irregular, discolored mineralized cartilage and subchondral bone.[7] The articular cartilage eventually collapses into an ovoid defect in the subchondral bone bordered by fissures; this stage is presumed to be when lesions become symptomatic.[3,5,6] In advanced cases, this collapsed piece of cartilage and underlying subchondral bone may be partially or completely displaced.[5]

In studies comparing Thoroughbred racehorses in training with non-athletic horses, clear differences have been noted in the osteochondral unit, including subchondral bone density, tidemarks in the calcified cartilage, and the thickness of the hyaline cartilage as a natural adaptation to exercise.[8] With continued exercise, these alterations can become pathologic, encompassing abnormalities such as bone necrosis, proteinaceous fluid accumulation, and cartilage infoldings into the subchondral bone.[9] Evaluation of metacarpal condyles from racehorses via electron microscopy has revealed increased lamellar bone, microcracks, and osteoclastic activity indicative of remodeling centered within the region of sclerosis, with microcracks being parallel to the surface and within 1 to 3 mm of the calcified cartilage.[10] These microcracks had a tendency to become enlarged, progressing to true microfractures with an increased amount of fragmentation and gaps and osteoclastic erosion indicative of active remodeling.[10] Additional microscopic findings include loss of mineralized cartilage and subchondral bone at varying depths at the site of macroscopic lesions, localized increases in underlying bone porosity with concentrated resorption spaces, and increased density of

subchondral bone underlying ulcerative cartilage lesions.[7] It has also been shown that as the cartilage thickness decreases with disease progression, the thickness and degree of disruption of the subchondral bone plate and the thickness of the calcified cartilage layer increase.[11]

The objective of this chapter was to describe the post-mortem changes identified in the study horses following experimental induction of bone marrow lesions (BMLs) and high-speed treadmill exercise, as described in Chapter 2, with a discussion of the similarities and differences between this model and what has been reported in the current literature. Furthermore, different focal regions were evaluated in this chapter relative to the pin tract. Trabecular morphometry analysis was performed at the abaxial, axial, proximal, and distal margins of the pin tract, both at the level of the subchondral bone plate and closer to the end of the tract in the trabecular bone. Histopathology was performed at locations adjacent to and distant from the pin tract. This was done to determine the extent of the resulting changes – focally associated with the pin tract as opposed to being more diffuse. Consideration of these different regions allowed for improved characterization of the extent of the effects of the pin penetration model, as well as comparison to morphometric gradients and histologic lesions reported in the published literature for clinical cases.

5.2 Materials and Methods

The study protocol and surgical technique used in this study were as described in the preceding chapters. Briefly, bone marrow lesions (BML) were induced in the medial and lateral MC3 condyles of both forelimbs in 3 horses by drilling a 1.1 mm Steinmann pin to a depth of 8 mm in each condyle. Horses were then subjected to high-speed treadmill exercise for 24 weeks. At the end of the 24-week study period, all 3 horses were humanely euthanized with an overdose of intravenous sodium pentobarbital. This was performed while horses were under general

anesthesia, following completion of the 24-week magnetic resonance imaging (MRI) and computed tomography (CT). Immediately after euthanasia, forelimbs were harvested from each horse for post-mortem evaluation. Data analysis was performed as described in Chapter 2, section 2.5.

5.2.1 Gross Examination

Each metacarpophalangeal joint (front fetlock) was completely disarticulated and the condyles were examined and photographed. Each individual condyle was graded according to two published scoring systems: a modification of the scoring system used by Pinchbeck et al. for POD and associated lesions (Table 5.1),[2] and the Osteoarthritis Research Society International (OARSI) scoring system for the assessment of equine articular tissues (Table 5.2).[12] In order to better capture the variability in gross lesion severity seen between the 3 horses, the scoring system by Pinchbeck et al. was updated to score cartilage loss on the transverse ridge, parasagittal groove, and central condylar region separately rather than in combination. A separate score for cartilage loss on the distal third metacarpal bone was then included as the sum of the scores from the 3 regions. For both grading tables, a total composite score for all grading parameters was also included.

Immediately following completion of the gross examination, the condyles and distal 1/4 of the diaphysis of the third metacarpal bones were removed *en bloc* and placed in 10% neutral buffered formalin at room temperature for 2 weeks. After 2 weeks, they were sectioned through the center in the sagittal plane and placed back in formalin for another week to complete tissue fixation, after which they were rinsed and transferred into a solution of phosphate buffered saline (1X PBS) for storage until decalcification. Additional tissues preserved for future use included the proximal phalanx, proximal sesamoid bones, and palmar soft tissues structures including the

oblique and straight distal sesamoidean ligaments, deep digital flexor tendon, and superficial digital flexor tendon.

5.2.2 Microcomputed Tomography

Microcomputed tomography was performed on each distal third metacarpal bone within the first week following euthanasia, submerged in 10% neutral buffered formalin. The right and left distal third metacarpal bones were obtained from a 2-year-old Quarter Horse racehorse filly, without gross evidence of POD on postmortem examination or evidence of maladaptive stress remodeling on CT, as a control for the microCT data. Specimens from this horse were processed in the same manner as those obtained from the study horses. As it was not subjected to the same exercise surface or regime, it cannot be considered a direct control and was used primarily to compare differences in bone architecture between study horses and a racehorse with evidence of mild, normal adaptive remodeling on CT imaging.

The specimens were scanned at a resolution of 37 μm (Scanco μCT 80, Scanco USA Inc. Wayne, PA.) with resultant DICOM images at an isotropic resolution of 37 μm. An upper limit of 1000 permilles (15,542 Hounsfield units [HU]) was set for all samples. The lower limit was determined subjectively by a single investigator (LES) for each horse using the segmentation tool, testing the thresholds at three separates sites in the same slice. The threshold at which the appearance of the segmentation overlay best matched the architecture of the trabecular bone, without over- or under-estimating the amount of bone present, was selected. The same threshold was used for all VOIs within the same horse, and all values within the threshold range were considered mineralized bone. The minimum density thresholds selected for each horse were as follows: Horse 1: 255 permilles (3,218 HU), Horse 2: 220 permilles (2,639 HU), Horse 3: 230 permilles (2,804 HU), Control: 245 permilles (3,052 HU). These thresholds were similar to and

within the range of the average densities previously reported for equine third metacarpal bones.[13,14]

Nine 3-mm-diameter cylindrical, contiguous, volumes of interest (VOI) were evaluated per condyle in this study, all immediately adjacent and relative to the pin tract margins (Figure 5.1), in order to gather a complete picture of the bone changes occurring around the pin tract: 1) tip of the tract (T), 2) abaxial subchondral bone plate (AbSCB), 3) axial subchondral bone plate (AxSCB), 4) proximal subchondral bone plate (PrSCB), 5) distal subchondral bone plate (DiSCB), 6) abaxial mid-tract (MidAb), 7) axial mid-tract (MidAx), 8) proximal mid-tract (MidPr), and 9) distal mid-tract (MidDi). VOIs located at the mid-tract level were centered on the slice that was halfway between the point of entry of the pin through the subchondral bone plate and the tip of the tract. Each bone sample was evaluated and viewed in the transverse plane for VOI creation. The goal was to have a cylindrical VOI that was 3 mm (or 81 slices [37 μm per slice]) in height; however, in more distally-located pin tracts, the number of slices in the VOI was reduced to ensure similar types of bone were being evaluated in all samples as there was less bone available to measure distal to these tracts (i.e. similar proportion of trabecular bone). The number of slices included in each VOI for each horse is provided in Table 5.3. For the abaxial, axial, and tip of tract VOIs, the cylinder was centered at the level of the pin tract and the VOI extended for an equal number of slices proximad and distad to this initial location (Figure 5.1). For the proximal and distal VOIs, both in the subchondral bone plate and at the center of the pin tract, the VOI extended proximad or distad, respectively, from the first slice on which there was not visible pin tract within the VOI (Figure 5.1). Furthermore, the VOIs in these regions were curved such that they followed the contour of the articular surface, keeping each slice of the VOI the same distance from the articular surface. For each study horse, the first slice from the distal

end of the sample that bone was first visible was noted, as were the relevant slice locations (range of slice numbers) for each VOI. From these data, the number of slices between the first visible bone at the distal end of the sample to the center or start of each VOI was calculated. This result was averaged between the 3 horses for each limb and VOI to determine the VOI slice locations for the control specimens in which there were no pin tracts to use for reference.

VOI selection and analysis were performed by a single investigator (LES). Quantitative measures of bone quality within each of the nine VOIs were performed using Scanco μCT 80 analyses software. Data analysis was performed as described in Chapter 2, section 2.5. The outcome parameters measured within the defined VOI, based on prior publications, included:[14–19]

1. *Bone volume fraction (BV/TV; %)*: The total volume of bone normalized to the entire volume of the VOI
2. *Bone Surface to Volume Ratio (BS/BV; 1/mm)*: The bone surface area per defined volume of bone
3. *Bone Mineral Density (BMD; mg HA/cm^3)*: The mean apparent density value for all tissue (TV) within the VOI
4. *Tissue Mineral Density (TMD; mg HA/cm^3)*: The mean material density value for bone tissue (BV) within the VOI
5. *Trabecular Thickness (Tb.Th; mm)*: The mean thickness of trabeculae
6. *Trabecular Spacing (Tb.Sp; mm)*: The mean space thickness or pore diameter between trabeculae
7. *Trabecular Number (Tb.N; 1/mm)*: The mean number of trabeculae

5.2.3 Histopathology

A previous study evaluating the reliability of MRI for detection of lesions within the metacarpophalangeal joint reported a moderate to high likelihood of false positive results for detection of SCB and cartilage lesions, respectively, compared with histopathology.[20] Thus, histopathology was performed on representative sections from each condyle, as described in Figure 5.2. To section each medial and lateral condyle, an Exact saw with a 350 μm blade was used to section the condyle transversely, centered within and parallel to the long axis of the pin tract. To do this, radiographic guidance was used to identify the trajectory of the pin tract on the halved bone specimens, with a line drawn that continued from the tip of the pin tract to the dorsal bone margin at the same angle. A radiopaque marker was applied to the dorsal condyle and the trajectory was confirmed radiographically. A laser mounted on the Exact saw was aligned between this dorsal marker and the entry site of the pin tract, resulting in a longitudinal cut along the center of the long axis of the pin tract. Two parallel cuts were made at 5 mm intervals proximal to this initial cut, creating the proximal tract block (PT) and the proximal distant block (PD). Two parallel cuts were also made at 5 mm intervals distal to the initial cut, creating the distal tract block (DT) and the distal distant block (DD).

Bone tissues were decalcified over 4 weeks in Nitr-Cal™ (Cancer Diagnostics) solution, which was exchanged at weekly intervals. Tissues were then processed using the automated Histocore processor (Leica Biosystems). Briefly, the tissues were dehydrated using a gradient of alcohol and xylene and suspended in warm paraffin. Tissues were embedded in paraffin and sectioned on a rotary microtome (Leica Biosystems) at a 5 μm thickness and placed on positively charged slides (Brain Research Laboratories). Sections were obtained through various depths from the distal surface of the PT and PD blocks (PT and PD slice locations; Figure 5.2), and

from the proximal surface of the DT and DD blocks (DT and DD slice locations; Figure 5.2). Selected slides were stained with hematoxylin and eosin (H&E) using the automated Histocore SPECTRA workstation (SelecTech Leica Biosystems), Masson Trichrome (Sigma Aldrich), and Toluidine Blue (Spectrum Chemicals). Digital images were obtained on the Evident VS200 and Orca Fusion BT (C15440) camera.

Sections were assessed by a board-certified pathologist trained in examining joint histology (MCH). Slides from each of the four sections from each condyle were graded according to multiple scoring systems. The overall appearance and changes to the subchondral bone were scored according to the system published by Aho et al. (Table 5.4),[11] as done in the study by Stewart et al.[17] Changes to the articular cartilage layer were scored using a modified scoring system (Table 5.5) combining those previously reported by McIlwraith et al.,[12] Little et al.,[21] and Pinilla et al.[9] Changes to the osteochondral unit were scored using Table VII by McIlwraith et al.[12] (Table 5.6). The calcified cartilage layer (Table 5.7) and the subchondral and trabecular bone layers (Table 5.8) were graded according to the scoring systems reported by Pinilla et al.[9] A subjective assessment was also performed of all tissues within each slide. Furthermore, histomorphometric measurements were performed on digital images of H&E-stained slides to quantify the percentage of bone tissue and fibrous tissue on the whole slide, outside the pin tract, and within the pin tract area using commercially available software. Images were imported into Visiopharm analytical software, version 2025.02.2.18022 x64, and processed through an artificial intelligence (AI) workflow. In brief, the workflow created regions of interest for the subchondral bone and areas directly related to the pin tracts while removing tissue processing artifacts. Quantitative assessment of bone and fibroplasia area was performed on whole tissue sections. All quantified assessments were validated by a board-certified veterinary

pathologist (MCH). Output parameters include total areas of bone and fibroplasia and percentages of bone and fibroplasia based on the area of the whole subchondral bone regions of interest (non-tract) or area of pin tract regions of interest (Figure 5.3). Articular cartilage was excluded from AI workflow analysis.

5.3 Results

5.3.1 Gross Examination

Overall, the gross changes identified were subjectively classified as mild to moderate, with variability among horses. Images of all gross specimens are provided in Figure 5.4, and a description of the significant findings is provided below for each component of the gross scoring systems. The pin track entry point itself was not considered when assigning a grade for each outcome parameter.

Pinchbeck et al. Scoring System (Table 5.1)

Overall, there were no significant differences in the severity of gross damage among horses ($p = 0.0825$), limbs ($p = 0.8954$), or condyles ($p = 0.6949$) when comparing the total composite score from Table 5.1. The mean (range) total composite score in this study was 7.08 (4-12) out of a total possible score of 26, consistent with mild to moderate gross changes, overall.

Variation among individual horses had a significant effect on the composite score for the severity of cartilage loss on the articular surface of the distal MC3 condyle (Figure 5.5; $p = 0.0312$). Overall, horse #3 had more significant cartilage loss compared to both horse #1 and horse #2 ($p = 0.0476$). There were no significant differences in cartilage loss on the distal third metacarpal bones between horse #1 and horse #2 ($p = 1.0000$). The mean (range) score for cartilage loss on the distal MC3 condyle was 1.92 (0-6) out of a total possible score of 9.

The results of the individual parameters scored using Table 5.1 are described below, with the individual grades for each condyle provided in Table 5.9a.

Palmar Osteochondral Disease (0-3)

The overall mean (range) POD score across all condyles in this study was mild at 1.17 (1-2) out of 3. There were no significant differences in the severity of POD among horses ($p = 0.0884$), limbs ($p = 0.1036$), or condyles ($p = 1.0000$). Each condyle was scored as a grade 1 out of 3 except for the medial and lateral condyles in the left forelimb of horse #3, which were scored as a grade 2 out of 5 (Figure 5.4, Table 5.9a). Grade 1 POD was characterized by the presence of discoloration of the subchondral bone visible through the articular cartilage, with no or minimal disruption of the articular cartilage layer. Mild to moderate disruption of the articular cartilage, in combination with discoloration of the subchondral bone, defined a grade 2.

Wear Lines (0-2)

There were no significant differences in the severity of wear lines on the metacarpophalangeal joint surfaces among horses ($p = 0.0884$), limbs ($p = 0.1036$), or condyles ($p = 1.0000$). Wear lines in the articular cartilage were classified as a grade 1 (partial-thickness) out of 2 for all condyles, except for in the left forelimb of horse #2 (grade 0; absent).

Cartilage Loss, Central Condyles (0-3)

The site of entry of the pin was visible in all condyles and appeared to be filled with tissue. In all condyles, a circumferential ring of what appeared to be thinning of the articular cartilage was present, surrounding the pin tract entry. Variations among individual horses had a significant effect on the amount of cartilage loss in the central condyles (Figure 5.6; $p = 0.0007$). Horse #1 had significantly less cartilage loss compared to both horse #2 ($p = 0.0062$) and horse

#3 ($p = 0.0006$). There was no difference in cartilage loss between horses #2 and #3 ($p = 0.1227$). Additionally, no significant differences were detected between limbs or condyles ($p > 0.10$).

Cartilage loss (Figure 5.6, Table 5.9a) was scored as a grade 0 in all condyles from horse #1, a grade 1 in all condyles from horse #2 and in the condyles of the right forelimb in horse #3 (partial-thickness loss characterized by cartilage fibrillation, erosion, or thinning), and a grade 2 in the condyles of the left forelimb in horse #3 (full-thickness cartilage loss, ulceration).

Cartilage Loss, Transverse Ridge (0-3)

Variations among individual horses had a significant effect on the amount of cartilage loss along the transverse ridge of the condyles (Figure 5.6; $p = 0.0148$). Horse #3 had significantly more cartilage loss compared to horse #2 ($p = 0.0131$), and marginally more cartilage loss compared to horse #1 ($p = 0.0754$). There was no difference in cartilage loss between horse #1 and horse #2 ($p = 0.4277$). Additionally, no significant differences were detected between limbs or condyles ($p = 1.0000$). Cartilage loss along the transverse ridge was scored as grade 0 in all condyles except the right forelimb of horse #1 (grade 1) and horse #3 (grade 1), and the left forelimb of horse #3 (grade 2), as shown in Figure 5.4 and Table 5.9a.

Cartilage Loss, Parasagittal Grooves (0-3)

There were no significant differences in the amount of cartilage loss within the parasagittal grooves of the distal condyles among horses ($p = 0.3080$), limbs ($p = 0.6682$), or condyles ($p = 0.2216$). Scoring was similarly aligned with that reported for the transverse ridge (Table 5.9a), with the exception of both medial condyles in horse #3 being scored as a grade 0. While there were no significant differences among horses, the marginal means plot is provided in Figure 5.6 for comparison to the two other regions on the condyle.

Linear Fissure Formation within the Parasagittal Grooves (0-3)

Variations between medial and lateral condyles had a significant effect on linear fissure formation within the parasagittal grooves ($p = 0.0479$). Compared to the medial condyle, fissure formation was more significant in the lateral condyle ($p = 0.0479$). There were no differences in fissure formation between horses ($p = 0.0565$) or limbs ($p = 0.4512$), overall, with a majority being classified as a faint groove with intact cartilage along its length.

Marginal Remodeling of the Proximal Sesamoid Bones (0-1)

There were no significant differences in the presence of marginal remodeling of the proximal sesamoid bones among horses ($p = 0.2419$), limbs ($p = 0.2275$), or condyles ($p = 0.2275$). Marginal remodeling was only present in the medial and lateral proximal sesamoid bones of the right forelimb in horse #2, and in both medial proximal sesamoid bones in horse #3 (Figure 5.4). While histopathology was not performed, this was characterized by the presence of osteophytes, not yet fully mineralized, on the axial basilar articular margin of the bone. As they did not appear to be fully mineralized on gross examination, this could explain why they went undetected on diagnostic imaging.

Dorsal Impact Injury (0-2)

There were significant differences among horses for the presence of dorsal impact injury ($p < 0.0001$). Both horse #1 and horse #2 had mild evidence of dorsal impact injury at the dorsoproximal margin of the distal third metacarpal condyles/dorsodistal third metacarpal bone (grade 1; Figure 5.4), characterized by mild synovial hyperplasia and thickening of the synovial pad. Subchondral bone bruising, visible through the articular cartilage, was also present in both horses. Horse #3 did not have evidence of dorsal impact injury.

Cartilage Loss, Proximal Sesamoid Bones (0-3)

There were no significant differences in the amount of cartilage loss on the proximal sesamoid bones among horses ($p = 0.0949$), limbs ($p = 0.6131$), or condyles ($p = 0.6131$). As shown in Table 5.9a and in Figure 5.4, the grade of cartilage loss on the proximal sesamoid bones varied from partial thickness erosions and fibrillation (grade 1) to focal areas of full-thickness cartilage ulceration. In all cases, this appeared to be located centrally along the articular surface of the proximal sesamoid bones, and it can't be ruled out that this abnormality was the result of articulation with the pin tract entry sites.

Tendon and Ligament Damage (0-3)

No evidence of overt damage to the tendons or ligaments associated with the metacarpophalangeal joints was detected on gross examination for any horse.

OARSI Scoring System (Table 5.2)

Overall, variations among individual horses had a marginal effect on the final OARSI score evaluating the degree of gross abnormalities on the distal third metacarpal condyles (Figure 5.7; $p = 0.0714$). The mean (range) total composite score using the OARSI scoring system in this study was 3.42 (2-6) out of a possible score of 9. Horse #3 had a marginally higher OARSI score, indicative of more severe damage, compared to both horse #1 ($p = 0.0785$) and horse #2 ($p = 0.0952$). There were no significant differences between horse #1 and horse #2 ($p = 0.8944$), or between limbs ($p = 0.1994$) or condyles ($p = 0.3745$). The results of the individual parameters graded using the OARSI scoring system in Table 5.2 are provided below, with the grades assigned to each condyle shown in Table 5.9b.

Wear Lines (0-3)

Variation among individual horses had a significant effect on the number of wear lines on the articular surface (Figure 5.7; $p = 0.0357$), which was not influenced by limb ($p = 0.2500$) or condyle ($p = 0.5000$). Overall, horse #3 had more significant wear lines compared to horse #2 ($p = 0.0327$), with no significant differences between horse #1 and the other two horses ($p = 0.1191$). This was in contrast with the analysis performed for wear lines based on the Pinchbeck et al. system, in which there were no significant differences among horses. The difference between these two scoring systems for this particular outcome parameter is that the OARSI system grades wear lines according to both thickness and number per joint surface. This likely contributed to the apparent differences in scoring between the two tables (Table 5.9). All condyles in horse #3, as well as the right lateral condyle in horse #1, were scored as a grade 2, characterized by 3-5 partial-thickness or 1-2 full-thickness wear lines per surface. The remaining condyles were scored as a grade 1, 1-2 partial-thickness wear lines per surface, except for the left forelimb condyles in horse #2 (grade 0).

Erosions (0-3)

There were no significant differences in the severity or presence of cartilage erosions among horses (Figure 5.7; $p = 0.1591$), limbs ($p = 0.5286$), or condyles ($p = 0.5286$). In comparison to the Pinchbeck et al. scale, the OARSI scoring system also accounted for differences in the size of any partial-thickness erosions or areas of cartilage thinning that were present. As shown in Table 5.9b and Figure 5.4, the erosion grade for a majority of condyles were either a grade 1, characterized by partial thickness erosions less than 5 mm in diameter, or a grade 2, characterized by partial thickness erosions greater than 5 mm in diameter. All condyles

in horse #1, except the right medial condyle (grade 1), received a grade of 0. The left lateral condyle in horse #3 was scored as a grade 3 (full-thickness).

Palmar Arthrosis (0-3)

There were no significant differences in the degree of palmar arthrosis among horses (Figure 5.7; $p = 0.4149$), limbs ($p = 0.3506$), or condyles ($p = 0.3506$). All condyles in this study were scored as a grade 1, characterized by a partial thickness cartilage or osteochondral erosions. While there were cartilage-specific erosions that exceeded 5 mm in diameter, they were not scored as a grade 2 for this outcome parameter as this parameter in the scoring system refers, more specifically, to erosions in the entire osteochondral unit rather than articular cartilage alone, and there were no focal areas of purple discoloration associated with the erosions in this study.

5.3.2 Microcomputed Tomography (microCT)

A composite of microCT images from each condyle is provided in Figure 5.8, demonstrating the breadth and severity of changes observed. Marked and extensive subchondral and trabecular bone sclerosis was apparent throughout the palmarodistal condyle in all study horses, with sclerosis extending to the level of the physis and/or to the dorsal condyle in some cases. Palmarodistal sclerosis was also present in all condyles of the control horse, though subjectively, it appeared to be more focal in comparison. Pin tracts appeared to contain debris in many condyles, with areas of subjectively reduced sclerosis near the tip of the pin tracts and along the pin tract margins. In horse #1, a focal lytic lesion was observed in the abaxial half of the medial condyle in the left forelimb (Figure 5.8). No lesions other than those associated with the pin tracts were observed in the remaining horses.

Values from the quantitative trabecular morphometry analysis are provided in Table 5.10, showing the values for each horse and for each VOI. While the analysis of variance (ANOVA)

testing showed significant variation in the relationships among horses depending on the limb, condyle, or VOI evaluated ($p < 0.05$), these interactions are outside the scope of this current study and will be examined in future work.

Bone Volume Fraction (BV/TV; %)

The overall mean bone volume fraction across all VOIs from all horses in this study was 87.57% (Table 5.10). For study horses, the mean (range) bone volume fraction across all VOIs was 88.20% (72.84-97.41%) compared to 85.68% (72.04-92.23%) for the control specimen. Overall, the % bone volume was higher in horse #3 (89.50%) compared to the control horse (Figure 5.9; $p = 0.0018$), with no other significant differences among horses ($p > 0.10$). The % bone volume was also higher in left forelimbs compared to right forelimbs ($p < 0.0001$), and in lateral condyles compared to medial condyles ($p < 0.0001$). While there were significant variations in the relationships among horses depending on the limb, condyle, or VOI ($p < 0.05$), these interactions are outside the scope of this current study and will be examined in future work.

The relationship between VOIs is shown in Figure 5.9. The % bone volume was significantly lower at the tip of the tract compared to all other VOI locations ($p < 0.05$). The % bone volume was higher in the abaxial subchondral bone plate VOI compared to all other locations ($p < 0.05$), except for the distal subchondral bone plate VOI ($p = 0.3739$). While the % bone volume was higher in the mid-axial location compared to the tip of the tract ($p = < 0.0001$), it was lower compared to all other locations ($p < 0.05$) except for the mid-distal and mid-proximal locations ($p > 0.10$). The % bone volume in the mid-proximal VOI was also lower compared to the other VOIs ($p < 0.05$) except for the tip of the tract (compared to which it was higher, $p < 0.0001$) and the mid-axial VOI ($p = 0.5835$). There were no significant differences among the distal, proximal, and axial subchondral bone VOIs ($p > 0.10$).

Bone Surface to Volume Ratio (BS/BV; 1/mm)

The overall mean bone surface to volume ratio across all VOIs from all horses in this study was 4.06 (Table 5.10). For study horses, the mean (range) bone surface to volume ratio across all VOIs was 3.87 (2.03-6.81) compared to 4.60 (3.15-7.14) for the control specimen. Overall, the BS/BV was higher in the control horse compared to horses #1 and #3 (Figure 5.9; $p < 0.05$) but not significantly different compared to horse #2 ($p = 0.2562$). The BS/BV was marginally higher in horse #2 compared to horse #1 ($p = 0.0986$). There were no significant differences in BS/BV between horse #3 and horses #1 and #2 ($p > 0.10$). The BS/BV was significantly higher in the right forelimb compared to left forelimbs ($p < 0.0001$), and in the medial condyle compared to the lateral condyle ($p = 0.0001$). While there were significant variations in the relationships among horses depending on the limb, condyle, or VOI ($p < 0.05$), these interactions are outside the scope of this current study and will be examined in future work.

The VOI with the highest BS/BV was the tip of the tract, which was significantly higher than all other VOIs (Figure 5.9; $p < 0.001$). The BS/BV in the mid-proximal and mid-axial VOIs was not significantly different from each other ($p = 0.8810$) but was significantly higher compared to all remaining VOIs ($p < 0.05$), though the difference between the mid-axial VOI and the axial subchondral bone was marginal ($p = 0.0669$). Lastly, the BS/BV in the axial subchondral bone plate and the mid-distal VOI was significantly higher compared to the abaxial subchondral bone plate ($p < 0.05$). There were no other significant differences between VOIs ($p > 0.10$).

Bone Mineral Density (BMD; mg HA/cm^3)

The overall mean BMD across all VOIs from all horses in this study was 663.29 (Table 5.10). For study horses, the mean (range) BMD across all VOIs was 659.30 (593.80-714.92)

compared to 675.26 (629.74-696.67) for the control specimen. Overall, the BMD was significantly higher in horse #1 compared to horse #2, horse #3, and the control horse (Figure 5.9; $p < 0.0001$). The next highest BMD was in the control horse, which was higher than both horse #2 and horse #3 ($p < 0.0001$). The BMD was also higher in horse #3 compared to horse #2 ($p < 0.0001$). The BMD was higher in left forelimbs compared to right forelimbs ($p < 0.0001$), and in lateral condyles compared to medial condyles ($p < 0.0001$). While there were significant variations in the relationships among horses depending on the limb, condyle, or VOI ($p < 0.0001$), these interactions are outside the scope of this current study and will be examined in future work.

The BMD was highest in the abaxial subchondral bone plate compared to other VOIs (Figure 5.9; $p < 0.05$) except for the mid-abaxial VOI ($p = 0.2151$), and lowest at the tip of the tract compared to other VOIs ($p < 0.05$). The VOI with the second lowest BMD was the mid-proximal VOI, which was lower than all remaining VOIs ($p < 0.05$) except for the mid-axial VOI ($p = 0.7465$). The BMD in the mid-abaxial VOI was significantly higher than the mid-axial VOI ($p = 0.0002$) and marginally higher compared to the axial subchondral bone plate ($p = 0.0735$). Lastly, the BMD in the distal subchondral bone plate was marginally higher compared to the mid-axial VOI ($p = 0.0751$).

Tissue Mineral Density (TMD; mg HA/cm^3)

The overall mean TMD across all VOIs from all horses in this study was 739.04 (Table 5.10). For study horses, the mean (range) TMD across all VOIs was 729.12 (712.73-745.66) compared to 768.81 (738.94-801.14) for the control specimen. Overall, the TMD was significantly higher in horse #1 compared to horse #2, horse #3, and the control horse (Figure 5.9; $p < 0.0001$). The next highest TMD was in the control horse, which was higher than both

horse #2 and horse #3 ($p < 0.0001$). The TMD was also higher in horse #3 compared to horse #2 ($p < 0.0001$). The TMD was higher in left forelimbs compared to right forelimbs ($p < 0.0001$), and in lateral condyles compared to medial condyles ($p < 0.0001$). While there were significant variations in the relationships among horses depending on the limb, condyle, or VOI ($p < 0.0001$), these interactions are outside the scope of this current study and will be examined in future work.

The TMD was highest at the tip of the tract compared to other VOIs (Figure 5.9; $p < 0.05$), except for the mid-abaxial, mid-axial and mid-proximal VOIs ($p > 0.10$), and lowest in the distal subchondral bone plate compared to other VOIs ($p < 0.05$) except the axial and proximal subchondral bone plates ($p > 0.10$). The VOIs with the second lowest TMD were the axial and proximal subchondral bone plates, which were not significantly different from each other ($p = 1.0000$) but were significantly lower compared to all remaining VOIs ($p > 0.10$). The exception was that the difference between the proximal subchondral bone plate and the mid-distal VOI was marginal ($p = 0.0631$) and there was no difference between the proximal subchondral bone plate and the abaxial subchondral bone plate ($p = 0.3028$). Lastly, the TMD in the mid-abaxial VOI was significantly higher compared to the abaxial subchondral bone plate ($p = 0.0021$) and the mid-distal VOI ($p = 0.0209$).

Trabecular Thickness (Tb.Th; mm)

The overall mean Th.Th across all VOIs from all horses in this study was 0.30 mm (Table 5.10). For study horses, the mean (range) Tb.Th across all VOIs was 0.33 mm (0.23-0.52 mm) compared to 0.23 mm (0.20-0.26 mm) for the control specimen. Overall, there was a gradual decrease in Tb.Th from horse #1 to the control. The trabeculae were significantly thinner in the control horse compared to all study horses (Figure 5.10; $p \leq 0.001$), in horse #3 compared to

horses #1 and #2 ($p \leq 0.0001$), and in horse #2 compared to horse #1 ($p < 0.0001$). The trabecular were also thinner in right forelimbs compared to left forelimbs ($p < 0.0001$), and in medial condyles compared to lateral condyles ($p < 0.0001$). While there were significant variations in the relationships among horses depending on the limb, condyle, or VOI ($p < 0.001$), these interactions are outside the scope of this current study and will be examined in future work.

The trabeculae were thicker in the abaxial subchondral bone plate compared to all other VOI locations (Figure 5.10; $p < 0.0001$). This was followed by the distal subchondral bone plate, which contained thicker trabecular compared to the remaining VOIs ($p < 0.05$) except for the mid-abaxial VOI and proximal subchondral bone plate ($p > 0.10$). The trabecular were thicker in the both the proximal subchondral bone plate and mid-abaxial VOI compared to the mid-axial and mid-proximal VOIs and the tip of the pin tract ($p < 0.05$). Trabeculae were also thicker in the axial subchondral bone and mid-distal VOIs compared to the tip of the pin tract ($p < 0.05$).

Trabecular Spacing (Tb.Sp; mm)

The overall mean Tb.Sp across all VOIs from all horses in this study was 0.10 mm (Table 5.10). For study horses, the mean (range) Tb.Sp across all VOIs was 0.10 mm (0.07-0.15 mm) compared to 0.09 mm (0.06-0.14 mm) for the control specimen. The Tb.Sp was significantly larger in horse #1 compared to horses #2 and #3, as well as the control horse (Figure 5.10; $p < 0.0001$). Tb.Sp was also larger in horse #2 compared to horse #3 ($p = 0.0001$), and marginally larger compared to the control ($p = 0.0923$). The Tb.Sp was marginally larger in the control horse compared to horse #3 ($p = 0.0937$). The relationship among horses was only affected by VOI ($p < 0.0001$) and this will be examined in future work. Tb.Sp was also larger in medial condyles compared to lateral condyles ($p = 0.0378$), with no significant relationship between trabecular spacing and limb ($p = 0.0715$).

Tb.Sp was significantly greater at the tip of the tract compared to all other VOIs (Figure 5.10; $p < 0.0001$). Aside from the tip of the pin tract, the Tb.Sp in the mid-proximal VOI was significantly greater compared to all remaining VOI locations ($p < 0.05$). Lastly, the Tb.Sp in the abaxial subchondral bone plate was significantly lower compared to the mid-abaxial, mid-axial, mid-distal and mid-proximal VOIs ($p < 0.05$), and marginally lower compared to the proximal ($p = 0.0653$) and distal ($p = 0.0847$) subchondral bone plate. There were no significant differences in Tb.Sp between the abaxial and axial subchondral bone plates ($p = 0.1108$).

Trabecular Number (Tb.N; 1/mm)

The overall mean Tb.N across all VOIs from all horses in this study was 4.90/mm (Table 5.10). For study horses, the mean (range) Tb.N across all VOIs was 4.65/mm (3.56-5.14/mm) compared to 5.64/mm (5.45-5.98/mm) for the control specimen. Overall, there was a gradual increase in Tb.N from horse #1 to the control. The Tb.N in the control horse was significantly higher compared to all study horses (Figure 5.10; $p < 0.001$), the Tb.N in horse #3 was significantly higher compared to horses #1 and #2 ($p < 0.0001$), and the Tb.N in horse #2 was significantly higher compared to horse #1 ($p < 0.0001$). The Tb.N was also higher in right forelimbs compared to left forelimbs ($p < 0.0001$), and in medial condyles compared to lateral condyles ($p < 0.0001$). While there were significant variations in the relationships among horses depending on the limb, condyle, or VOI ($p < 0.05$), these interactions are outside the scope of this current study and will be examined in future work.

The Tb.N was lowest in the abaxial subchondral bone plate compared to all other VOI locations (Figure 5.10; $p < 0.0001$). The next lowest Tb.N was in the distal subchondral bone plate, where it was significantly lower compared to the tip of the tract and the mid-axial VOI ($p < 0.05$), and marginally lower compared to the axial subchondral bone plate ($p = 0.0696$) but not

significantly different from the remaining VOIs ($p > 0.10$). The Tb.N in the mid-abaxial VOI was significantly lower compared to that in the mid-axial VOI and at the tip of the tract ($p < 0.05$). Lastly, the Tb.N in the proximal subchondral bone plate was significantly lower compared to the mid-axial VOI ($p = 0.0031$) and marginally lower compared to the tip of the tract ($p = 0.0667$). None of the remaining VOI comparisons were significant ($p > 0.10$).

5.3.3 Histopathology

The overall mean values for each of the outcome parameters graded using the various scoring systems (Tables 5.4-5.8), both for each individual horse and for each slice location, are included in Table 5.11. The overall means for the data measured using Visiopharm are also provided for each horse and slice location in Table 5.12. Changes similar to those identified in POD were present – albeit on a more focal scale due to the creation of the pin tract – including subchondral bone sclerosis, fibrosis, and articular surface collapse. Unsurprisingly, pathologic changes were more significant in the sections adjacent to and including the pin tract compared to more distant sections. In this section, the subjective descriptions of the four slice locations will be provided, followed by results from the individual scoring systems.

Proximal Tract (PT)

In sections cut from the proximal half of the pin tracts, there was a distinct tract characterized by cavitation, extensive myelofibrosis, abundant fibroplasia, scant to mild woven bone, and adjacent marked bony sclerosis. The tract and adjacent subchondral plate displayed marked sclerosis with separation of the medullary cavity from the articular cartilage. The adjacent medullary cavities were characterized by moderate myelofibrosis and cellular debris. There was regionally extensive thickening of the cancellous trabeculae with variable immature bone (woven bone) as appreciated on the Masson's histochemical stain. The surrounding articular

cartilage was characterized by mild to moderate fibrillation, degeneration (reduced toluidine blue stain uptake, chrondrone formation), and necrosis with chondrocyte loss within the superficial to intermediate zones of the cartilage layer. These changes were most severe in the regions overlying and immediately adjacent to the pin tract. There was also some variation between limbs and horses in the severity of the degenerative changes as characterized by decreased toluidine blue stain uptake and variable chondrocyte density variation. In the left lateral and right medial condyles of horse #2, the articular cartilage showed relatively mild pathology beyond the focal penetrating tract lesions, which was the reason for the high fibrillation and clefting scores. The calcified region in these samples was relatively intact with parallel tidemarks and no reduplication.

Distal Tract (DT)

In sections cut from the distal half of the pin tracts, there was similar pathology associated with the pin tract compared to the proximal half, with a subchondral cavity associated with myelofibrosis and adjacent subchondral bone sclerosis ranging from focal near the pin tract to more diffuse throughout the plate. Furthermore, there was less immature woven bone deposition throughout the tract and adjacent subchondral bone. Overall, the articular cartilage appeared better in many parameters compared to the proximal tract sections, with relatively little pathology within the calcified cartilage; although, pathology was worse for those samples containing better sections of cartilage directly associated with the pin tract. Other changes identified included variations in cartilage thickness, fibrillation, and some subchondral bone with islands of hyaline cartilage. Subjectively, the sample with the most severe pathology was the distal tract sample from the left lateral condyle of horse #2, containing subchondral bone plate

collapse, sclerosis and more significant articular cartilage pathology including necrosis, fibrillation and change to the calcified cartilage.

Proximal Distant (PD)

In samples taken at least 5 mm proximal to the pin tracts, the pathology in all parameters was, overall, less severe compared to the proximal pin tract sections. There were minimal to mild changes in the articular cartilage with tidemark duplication and scant degeneration and necrosis. There was a degree of subchondral plate and trabecular sclerosis that was more significant compared to changes in the articular cartilage, characterized by changes ranging from limited or mild to more diffuse subchondral plate sclerosis, thickening of the cancellous trabeculae deep to the subchondral bone, and variable amounts of medullary fibrosis and subchondral reorganization.

Distal Distant (DD)

In sections cut at least 5 mm distal to the pin tracts, the articular cartilage had relatively little pathology with minimal degeneration. This limited articular cartilage pathology was paired with more notable subchondral bone sclerosis and in one section, advancement of the subchondral bone into the mineralized cartilage. There was also thickening of cancellous trabeculae.

In the distal distant section of the right medial condyle from horse #1, there was more severe pathology compared to other distant sections. This was characterized by increased subchondral bone sclerosis and more progressed degeneration of the articular cartilage, with less uptake of the toluidine blue stain and duplicated tidemarks. In the distal distant section of the right lateral condyle from horse #1, there was increased subchondral plate sclerosis, which was more similar to the tract lesions in terms of the grading. In addition, there was mildly increased

articular cartilage degeneration with increased complex cluster formation (chondrone duplicates and rare triplicates), as well as slightly increased cartilaginous fibrillation.

Composite Scores

The only histological scoring system that did not have a composite score was that evaluating the overall appearance of and changes within the subchondral bone, Table 5.4, as it only gave a single score for the subchondral bone. For all remaining scoring systems, a composite score was calculated to better summarize the changes observed in this study. For ease of reporting, the composite results of Tables 5.5-5.8 are provided first, after which the results for the individual parameters in each table are provided. While a composite score was not provided for Table 5.4, the grades assigned using this table were included in the total histology score which was provided to represent the cumulative severity of pathologic changes identified on histology.

Composite Articular Cartilage Score (Table 5.5; 0-33)

Horses in this study had a mean composite articular cartilage score of 10.50 out of a total possible score of 33. Overall, slice location was the only variable that had a significant effect on the presence and severity of degenerative changes within the articular cartilage (Figure 5.11; $p < 0.0001$), which was not influenced by condyle, limb, or horse ($p > 0.05$). There were no significant differences in articular cartilage degeneration between condyles, limbs, or horses ($p > 0.05$). There were more severe degenerative changes in the articular cartilage in the DT and PT slice locations compared to the DD and PD slice locations ($p < 0.002$), with a combined average score of 13.71 compared to 7.29. There were no significant differences between the DD and PD locations or the DT and PT slice locations ($p > 0.10$).

Composite Osteochondral Score (Table 5.6; 0-10)

Slice location had a significant effect on the degree of osteochondral degeneration (Figure 5.11; $p < 0.0001$), the relationship between which was not influenced by condyle, limb, or horse ($p > 0.05$). Overall, there was increased evidence of osteochondral degeneration in the DT and PT slice locations compared to the DD and PD slice locations ($p \leq 0.0001$), with a combined average score of 4.63 compared to 1.71. There were no significant differences between the DD and PD locations or the DT and PT slice locations ($p > 0.10$).

Variations among individual horses also had a significant effect on the degree of osteochondral degeneration (Figure 5.11; $p = 0.0453$), the relationship between which was not influenced by condyle or limb ($p > 0.05$). There were no significant differences in the degree of osteochondral degeneration between condyles or limbs ($p > 0.05$). The average osteochondral score for horses in this study was mild at 3.17 out of a total possible score of 10. There was increased evidence of osteochondral degeneration in horse #3 compared to horse #1 ($p = 0.0359$), but no significant differences between horses #1 and #2, or horses #2 and #3 ($p > 0.10$).

Composite Calcified Cartilage Score (Table 5.7; 0-15)

Slice location had a significant effect on the severity of changes within the calcified cartilage layer (Figure 5.11; $p = 0.0004$), which was not influenced by condyle, limb, or horse ($p > 0.05$). Overall, there were increased degenerative changes within the calcified cartilage layer in the DT and PT slice locations compared to the DD and PD slice locations ($p < 0.05$), with a combined average score of 5.04 compared to 3.17. There were no significant differences between the DD and PD or DT and PT locations ($p > 0.10$).

Variation among individual horses also had a significant effect on the severity of changes within the calcified cartilage layer (Figure 5.11; $p = 0.0038$), which was not influenced by

condyle or limb ($p > 0.05$). There were no significant differences in the composite score between condyles or limbs ($p > 0.05$). The average composite score for calcified cartilage for horses in this study was 4.10 out of a total possible score of 15. There were increased degenerative changes within the calcified cartilage layer in horse #3 compared to horse #1 ($p = 0.0028$), with marginally increased degeneration compared to horse #2 ($p = 0.0871$). There was no difference in calcified cartilage degeneration between horse #1 and horse #2 ($p = 0.2943$).

Composite Subchondral and Trabecular Bone Score (Table 5.8; 0-24)

For horses in this study, the average composite score for subchondral and trabecular bone was 7.46 out of a total possible score of 24. Slice location was the only variable that had a significant effect on the severity of subchondral and trabecular bone remodeling (Figure 5.11; $p < 0.0001$), which was not influenced by condyle, limb, or horse ($p > 0.05$). There were no significant differences among horses, limbs, or condyles ($p > 0.05$). More evidence of maladaptive remodeling within the subchondral and trabecular bone was present in the DT and PT slice locations compared to the DD and PD slice locations ($p \leq 0.0001$), with a combined average score of 10.54 compared to 4.38. There were no differences in remodeling between the DD and PD or the DT and PT slice locations ($p > 0.10$).

Total Histology Score (sum of all scores from Tables 5.4-5.8; 0-85)

Slice location was the only variable that had a significant effect on the severity of histologic changes (Figure 5.12; $p < 0.0001$), overall, which was not influenced by condyle, limb, or horse ($p > 0.05$). For horses in this study, the average total histology score was only 19.46 out of a total possible score of 85. There were no significant differences among horses, limbs, or condyles ($p > 0.10$). Unsurprisingly, there were more severe histologic changes in the DT and PT slice locations compared to the DD and PD slice locations ($p \leq 0.0001$), with a

combined average score of 36.63 compared to 18.29. There were no differences in remodeling between the DD and PD or the DT and PT slice locations ($p > 0.10$). For each horse included in this study, a composite of the changes identified in those sections that received the highest (worst) and lowest (best) cumulative scores are provided in Figures 5.13-5.15.

Subchondral Bone Disease (Table 5.4; 0-3)

For horses in this study, the average subchondral bone score was 2.23 out of a total possible score of 3. Slice location had a significant effect on the severity of subchondral bone disease (Figure 5.16; $p < 0.0001$), the relationship between which was influenced by both limb ($p = 0.0002$) and horse ($p = 0.0407$); however, these interactions are beyond the scope of this pilot study. Overall, the DT and PT slice locations exhibited more severe subchondral bone changes than both DD ($p < 0.002$) and PD ($p < 0.0001$) locations, with a combined average score of 2.71 compared to 1.75. There were no significant differences between the DT and PT slice locations ($p = 0.9615$) or between the DD and PD slice locations ($p = 0.2386$). The subchondral bone disease score was also higher in lateral condyles compared to medial condyles ($p = 0.0247$). Overall, there were no significant differences among limbs or horses ($p > 0.10$).

Disease of the Articular Cartilage (Table 5.5)

Chondrocyte Necrosis (0-4)

Slice location was the only variable that had a significant effect on the degree of chondrocyte necrosis ($p < 0.0001$), which was influenced by both condyle ($p = 0.0389$) and horse ($p = 0.0175$); however, these interactions were beyond the scope of this pilot study. There were no significant differences in chondrocyte necrosis among condyles, limbs, or horses ($p > 0.10$). Overall, there was increased chondrocyte necrosis in the DT and PT slice locations compared to

the DD and PD slice locations ($p < 0.05$). There were no significant differences in chondrocyte necrosis between the DD and PD or the DT and PT slice locations ($p > 0.10$).

Cluster (Complex Chondrone) Formation (0-4)

There were no significant differences in chondrone formation among slice locations ($p = 0.0783$), condyles ($p = 0.3763$), limbs ($p = 0.1891$), or horses ($p = 0.5256$).

Fibrillation and Fissuring (0-4)

Slice location had a significant effect on the severity of articular cartilage fibrillation and fissuring ($p < 0.0001$), which was not influenced by condyle, limb, or horse ($p > 0.05$). Overall, the extent of fibrillation and fissuring was worse for the DT and PT slice locations compared to the DD and PD slice locations ($p < 0.05$). There were no significant differences between DD and PD locations or the DT and PT slice locations ($p > 0.10$).

Limb also had a significant influence on the severity of articular cartilage fibrillation and fissuring ($p = 0.0428$), the effect of which was not influenced by condyle or horse ($p > 0.05$). The extent of fibrillation and fissuring was worse in the right forelimb compared to the left forelimb ($p = 0.0428$). There were no differences in fibrillation among condyles or horses ($p > 0.05$).

Focal Cell Loss (0-4)

Slice location had a significant effect on the extent of focal cell loss within the articular cartilage ($p = 0.0024$), the effect of which was not influenced by condyle, limb, or horse ($p > 0.05$). Overall, there was more focal cell loss in the DT slice location compared to the DD location ($p = 0.0281$). Additionally, there was more focal cell loss in the PT slice location compared to both the DD ($p = 0.0049$) and PD ($p = 0.0281$) slice locations. There were no significant differences in cell loss between the DD and PD, DT and PD, or DT and PT locations ($p > 0.10$).

Toluidine Blue Stain Uptake (0-4)

Examples of differences in toluidine blue stain uptake are shown in the individual horse composites in Figures 5.13-5.15. Slice location had a significant effect on the quality of toluidine blue stain uptake ($p = 0.0116$), which was not influenced by condyle, limb, or horse ($p > 0.05$). Overall, there was less of a loss in staining characteristics for the PD slice location compared to the DT ($p = 0.0321$) and PT ($p = 0.0142$) slice locations. There were no significant differences in staining characteristics between the DD slice location and the DT, PD, or PT slice locations ($p > 0.10$), or between the DT and PT slice locations ($p > 0.10$).

Limb also had a significant effect on the quality of stain uptake ($p = 0.0463$), the relationship between which was not influenced by condyle or horse ($p > 0.05$); however, the pairwise comparison for limb revealed no significant difference in staining characteristics between the left and right forelimbs ($p > 0.10$).

Chondrocyte Density and Distribution (0-4)

Slice location had a significant effect on chondrocyte density ($p = 0.0023$), which was not significantly influenced by condyle, limb, or horse ($p > 0.05$). There were no significant differences in chondrocyte density among condyles, limbs, or horses ($p > 0.05$). Overall, the DT slice location had a greater decrease in chondrocyte density compared to the DD ($p = 0.0380$) and PD ($p = 0.0073$) slice locations. The PT slice location had a greater decrease in chondrocyte density compared to the PD slice location ($p = 0.0170$), with a marginally greater reduction in chondrocyte density compared to the DD slice location ($p = 0.0808$). There were no significant differences in chondrocyte density between the DD and PD slice locations or the DT and PT slice locations ($p > 0.10$).

Changes in the Tidemark, Calcified Cartilage, and Subchondral Bone (0-3)

Examples of the breadth of changes identified in the tidemark, calcified cartilage, and subchondral bone are shown in the individual horse composites in Figures 5.13-5.15. The variation among individual horses had a significant effect on the severity of changes in the tidemark, calcified cartilage, and subchondral bone ($p < 0.0001$), which was not significantly influenced by slice location, condyle, or limb ($p > 0.05$). There were no significant differences in the severity of these changes among slice locations, condyles, or limbs ($p > 0.10$). Overall, horse #3 had significantly more abnormalities in these regions compared to both horse #1 ($p < 0.0001$) and horse #2 ($p = 0.0066$). Horse #2 had significantly more abnormalities in these regions compared to horse #1 ($p = 0.0066$).

Irregularity of the Articular Cartilage Surface (0-3)

Slice location had a significant effect on the severity of irregularities in the articular surface ($p = 0.0010$), the effect of which was influenced by condyle ($p = 0.0116$); however, this interaction was beyond the scope of this study. Overall, there was more severe surface irregularity in the DT and PT slice locations compared to the DD and PD slice locations ($p < 0.05$). There were no significant differences in the severity of surface irregularities between the DD and PD or the DT and PT slice locations ($p > 0.10$).

Limb also had a significant effect on the severity of irregularities in the articular surface ($p = 0.0124$), which was not influenced by slice location, condyle, or horse ($p > 0.05$). There were more severe surface irregularities in the left forelimb compared to the right forelimb ($\hat{\beta} = 0.33$, $p = 0.0124$). There were no significant differences in surface irregularities among condyles or horses ($p > 0.05$).

Variation in Articular Cartilage Thickness (0-3)

The degree of variability in articular cartilage thickness was influenced by differences in slice location ($p = 0.04638$), which was not influenced by condyle, limb, or horse ($p > 0.05$). There were no significant differences in variability of the cartilage thickness among condyles, limbs, or horses ($p > 0.05$). There was increased variability in cartilage thickness in the DT slice location compared to the PD location ($p = 0.0421$). There were no significant differences in thickness variability between any of the other slice locations ($p > 0.10$).

Osteochondral Degeneration (Table 5.6)

Osteochondral Changes (0-4)

Slice location had a significant effect on the severity of changes within the osteochondral unit ($p < 0.0001$), the effect of which was influenced by horse ($p = 0.0022$); however, this interaction was beyond the scope of the present pilot study. There were no significant differences in osteochondral changes between condyles, limbs, or horses ($p > 0.05$), overall. Both the DT and PT slice locations had more severe osteochondral changes compared to the DD and PD slice locations ($p < 0.0001$). There were no significant differences between the DD and PD or between the DT and PT slice locations ($p > 0.10$).

Subchondral Bone Remodeling (0-3)

Slice location had a significant effect of the degree of maladaptive subchondral bone remodeling ($p = 0.0071$), the effect of which was not influenced by condyle, limb, or horse ($p > 0.05$). Overall, there was more severe subchondral bone remodeling in the PT slice location compared to the DD and PD slice locations ($p = 0.0145$). There were no significant differences in remodeling between the other slice location comparisons ($p > 0.10$).

Variation among individual horses also had a significant effect on the degree of maladaptive subchondral bone remodeling ($p = 0.0287$), which was not influenced by condyle or limb ($p > 0.05$). There were no significant differences in subchondral bone remodeling between condyles or limbs ($p > 0.05$). There was more maladaptive subchondral bone remodeling in horse #3 compared to horse #1 ($p = 0.0392$) and marginally more compared to horse #2 ($p = 0.0677$). There was no significant difference in remodeling between horse #1 and horse #2 ($p > 0.10$).

Osteochondral Splitting (0-3)

Slice location had a significant effect on the severity of osteochondral splitting ($p = 0.0001$), which was influenced by condyle ($p = 0.0462$); however, this interaction was beyond the scope of this pilot study. There were no significant differences in osteochondral splitting among condyles, limbs, or horses ($p > 0.05$). Overall, there was more severe osteochondral splitting in the DT and PT slice locations compared to the DD and PD slice locations ($p < 0.05$). There were no significant differences between the DD and PD locations and the DT and PT locations ($p > 0.10$).

Changes in the Calcified Cartilage (Table 5.7)

Clefts within the Calcified Cartilage (0-3)

A representative image of clefting is provided in Figure 5.17. Slice location had a significant effect on the presence of clefts within the calcified cartilage layer ($p = 0.0005$), which was not influenced by condyle, limb, or horse ($p > 0.05$). Overall, there was increased cleft formation in the DT and PT slice locations compared to the DD and PD slice locations ($p < 0.01$). There were no significant differences between the DD and PD or between the DT and PT slice locations ($p = 0.9783$).

Variations among individual horses also had a significant effect on the presence of clefts within the calcified cartilage layer ($p = 0.0359$), which was not influenced by condyle or limb ($p > 0.05$). There were no significant differences in cleft formation between condyles or limbs ($p > 0.05$). There was increased cleft formation in horse #3 compared to horse #1 ($p = 0.0296$), with no differences between horses #1 and #2 or horses #2 and #3 ($p > 0.10$).

Variations in Depth of the Calcified Cartilage (0-3)

Slice location had a significant effect on variability in the depth of the calcified cartilage ($p = 0.0059$), which was not influenced by condyle, limb, or horse ($p > 0.05$). There were no significant differences in depth variability among condyles, limbs, or horses ($p > 0.05$). There was increased variability in depth in the DT slice location compared to the PD slice location ($p = 0.0123$), with a marginal increase in variability compared to the DD slice location ($p = 0.0786$), and in the PT location compared to the PD location ($p = 0.0321$). There was no significant difference in depth variability for any of the other slice location comparisons ($p > 0.10$).

Tidemark Incongruency (0-3)

Variations among individual horses had a significant effect on the degree of tidemark incongruency ($p = 0.0073$), which was not influenced by slice location, condyle, or limb ($p > 0.05$). There were no significant differences in tidemark incongruency between slice locations, condyles, or limbs ($p > 0.05$). There were more significant incongruencies in horse #3 compared to horse #1 ($p = 0.0054$), with no differences observed between horses #1 and #2 or between horses #2 and #3 ($p > 0.10$). A representative image of changes identified in the tidemark is provided in Figure 5.18.

Vascular Incursions (0-3)

Slice location had a significant effect on the presence of vascular incursions at the interface between the subchondral bone and calcified cartilage ($p = 0.0117$), which was not influenced by condyle, limb or horse ($p > 0.05$). Overall, there was an increased number of vascular incursions in the PT slice location compared to the PD slice location ($p = 0.0065$). There were no significant differences among any of the other slice location comparisons ($p > 0.10$).

Variation among individual horses also had a significant effect on the presence of vascular incursions ($p = 0.0381$), which was not influenced by condyle or limb ($p > 0.05$). There were no differences in vascular incursions between condyles or limbs ($p > 0.05$). There were marginally increased vascular incursions in horse #3 compared to horses #1 and #2 ($p = 0.0644$), and no significant differences between horses #1 and #2 ($p = 1.00$).

Hyaline Cartilage Islands in the Subchondral Bone Plate (0-3)

There were no significant differences in the presence of hyaline cartilage islands in the subchondral bone plate among slice locations ($p = 0.4106$), condyles ($p = 0.3277$), limbs ($p = 0.3277$) or horses ($p = 0.3833$), or any of the tested interactions ($p > 0.05$).

Degenerative Changes in the Subchondral and Trabecular Bone (Table 5.8)

Sclerosis of the Subchondral Plate (0-3)

Slice location had a significant effect on the severity of sclerosis of the subchondral bone plate (Figure 5.19; $p = 0.0003$), which was influenced by limb ($p = 0.0347$); however, this interaction was beyond the scope of this pilot study. Overall, there was less severe sclerosis of the subchondral plate in the PD slice location compared to the DT ($p = 0.0032$) and PT ($p = 0.0003$) slice locations. There were no significant differences in sclerosis of the subchondral plate among the other slice location comparisons ($p > 0.10$).

Variations among individual horses also had a significant effect on the severity of sclerosis of the subchondral bone plate ($p = 0.0027$), which was also influenced by limb ($p = 0.0129$); again, this was outside the scope of this study. There were no significant differences in subchondral plate sclerosis between condyles or limbs ($p > 0.05$). There was more severe sclerosis of the subchondral bone plate in horse #1 compared to horse #2 ($p = 0.0429$) and horse #3 ($p = 0.0022$). There were no significant differences in subchondral plate sclerosis between horses #2 and #3 ($p = 0.4157$).

Subchondral Bone Collapse (0-3)

Slice location had a significant effect on the degree of subchondral bone collapse ($p < 0.0001$), which was not influenced by condyle, limb or horse ($p > 0.05$). There were no significant differences in subchondral bone collapse among condyles, limbs, or horses ($p > 0.05$). Overall, there was more significant subchondral bone collapse in the DT and PT slice locations compared to the DD and PD slice locations ($p < 0.0001$). There were no significant differences between the DD and PD or DT and PT slice locations ($p > 0.10$).

Obliteration of Cancellous Bone with Compact Bone (0-3)

Slice location had a significant effect on the degree of obliteration of cancellous bone with compact bone ($p = 0.0001$), which was affected by horse ($p = 0.0297$); however, this interaction was beyond the scope of this pilot study. There was less obliteration of the cancellous bone in the PD slice location compared to the DD ($p = 0.0223$), DT ($p = 0.0002$), and PT ($p = 0.0005$) slice locations, with no differences between the other slice location comparisons ($p > 0.10$).

Variation between the left and right forelimbs also had a significant effect on the degree of cancellous bone obliteration ($p = 0.0202$), with more cancellous bone obliteration in right

forelimbs compared to left forelimbs ($p = 0.0202$). There were no significant differences among condyles or horses ($p > 0.05$).

Replacement with Woven Bone (0-3)

Slice location had a significant effect on the deposition of woven bone (Figure 5.20; $p < 0.0001$), which was not influenced by condyle, limb, or horse ($p > 0.05$). There were no significant differences between condyles, limbs, or horses ($p > 0.05$). There was an increased deposition of woven bone in the DT and PT slice locations compared to the DD and PD slice locations ($p < 0.001$). There were no significant differences between the DD and PD or the DT and PT slice locations ($p > 0.10$).

Replacement with Lamellar Osteonal Bone (0-3)

There were no significant differences in lamellar osteonal bone deposition among slice locations ($p = 0.0719$), condyles ($p = 0.6274$), limbs ($p = 1.0000$) or horses ($p = 0.2995$), or between any of the tested interactions ($p > 0.05$).

Trabecular Thickening

Slice location had a significant effect on the degree of trabecular thickening (Figure 5.20; $p = 0.0066$), which was not influenced by condyle, limb, or horse ($p > 0.05$). There was more severe trabecular thickening in the PT slice location compared to the DD ($p = 0.0345$) and PD ($p = 0.0091$) slice locations. There were no significant differences for any of the remaining slice location comparisons ($p > 0.10$).

Microcracks in the Cancellous Bone

No microcracks were observed within the cancellous bone for any of the tested samples.

Presence of Howship's Lacunae

Slice location had a significant effect on the number of Howship's lacunae ($p < 0.0001$), which was influenced by limb ($p = 0.0198$); however, this interaction was beyond the scope of this pilot study. More lacunae were observed in the DT and PT slice locations compared to the DD and PD slice locations ($p = 0.0001$). There were no significant differences between the DD and PD or the DT and PT slice locations ($p > 0.10$).

Variations between the left and right forelimb also had a significant effect on the number of Howship's lacunae ($p = 0.0023$), which was not affected by condyle or horse ($p > 0.05$). More lacunae were present in right forelimbs compared to left forelimbs ($p = 0.0023$). Lastly, variations among individual horses had a significant effect on the number of Howship's lacunae ($p = 0.0431$), which was not influenced by any other interactions ($p > 0.05$). Pairwise comparisons revealed marginally more lacunae in horse #1 compared to horses #2 and #3 ($p = 0.0716$), but no differences in the presence of Howship's lacunae between horse #2 and #3 ($p = 1.0000$).

Histomorphometric Data (Visiopharm)

Figure 5.3 provides a representation of the distinction between bone sclerosis and fibrosis, as identified using Visiopharm analysis. Additional examples are also provided in the composite images for each individual horse (Figure 5.13-5.15). The overall means for the percent bone and fibrosis from the three regions analyzed – subchondral and trabecular bone outside of the pin tract (Figure 5.3, blue outline), the immediate pin tract region (Figure 5.3, red outline), and the whole tissue (Figure 5.3, blue and red outlines) – are provided for each slice location and horse in Table 5.12. Overall, the mean (range) percent bone was 66.56% (51.14-86.82%) in the non-tract region, 76.44% (54.04-95.10%) within and immediately around the pin tract, and

66.59% (51.13-86.81%) for the whole tissue section. The mean (range) percent fibrosis was 0.58% (0.03-1.92%) in the non-tract region, 8.89% (0.01-23.23%) within and immediately around the pin tract, and 1.01% (0.03-5.60%) for the whole tissue section. In general, a majority of the fibrosis was observed within the pin tract, itself, and this percentage would have likely been significantly higher had the bone immediately surrounding the pin tract not been included in this region of interest. When evaluating only the slice locations containing a pin tract (PT and DT), there was significantly more bone ($p = 0.0002$) and fibrosis ($p < 0.0001$) in the region of interest within and surrounding the pin tract (76.61% and 8.86%, respectively) compared to the rest of the specimen (non-tract; 66.98% and 0.52%, respectively).

Percent (%) Bone, Non-Tract

Overall, there were significant differences in the percent of bone outside the pin tract between condyles ($p = 0.0183$) and among horses (Figure 5.21; $p < 0.0001$), with the latter being significantly influenced by limb ($p = 0.0013$); however, this interaction was beyond the scope of this pilot study. There were no significant differences in the percentage of bone outside of the pin tract between slice locations or limbs ($p > 0.05$).

The percentage of bone outside of the pin tract was significantly greater in lateral condyles compared to medial condyles ($p = 0.0183$). The percentage of bone outside of the pin tract was also greater in horse #3 compared to both horse #1 ($p < 0.0001$) and horse #2 ($p = 0.0009$). There were no significant differences in the percentage of bone between horses #1 and #2 ($p = 0.2870$).

Percent (%) Bone, Tract

Overall, there were significant differences in the percent of bone within and immediately around the pin tract among horses (Figure 5.22; $p = 0.0477$), which was not influenced by slice

location, condyle, or limb ($p > 0.05$). There were no significant differences in the percentage of bone within and immediately around the pin tract between slice locations, condyles, or limbs ($p > 0.05$). The percentage of bone within the pin tract was significantly greater in horse #3 compared to horse #1 ($p = 0.0345$), but there were no significant differences between horses #1 and #2 ($p = 0.4664$) or between horses #2 and #3 ($p = 0.2352$).

Percent (%) Bone, Whole Slide

Variations between the medial and lateral condyles had a significant effect on the percentage of bone on the slide ($p = 0.0062$), which was not influenced by slice location, limb, or horse ($p > 0.05$). There were no significant differences in the percent bone on the slide among slice locations or limbs ($p > 0.05$). Pairwise comparison for condyle revealed a higher percent bone in samples taken from lateral condyles compared to medial condyles ($p = 0.0062$).

Variations among individual horses also had a significant effect on the percentage of bone on the slide (Figure 5.22; $p < 0.0001$), which was influenced by limb ($p = 0.0004$); however, this interaction was beyond the scope of this pilot study. Horse #3 had a higher percent bone per slide compared to both horse #1 ($p < 0.0001$) and horse #2 ($p = 0.0003$). There were no significant differences in the percent bone between horses #1 and #2 ($p = 0.2101$).

Percent (%) Fibrosis, Non-Tract

The only variable that had a significant effect on the percent fibrosis in tissue outside of the pin tract region was condyle ($p = 0.0186$), which was not influenced by slice location, limb, or horse ($p > 0.05$). Overall, the percentage of fibrosis outside the pin tract was greater in lateral condyles compared to medial condyles ($p = 0.0186$). There were no significant differences in the percent fibrosis outside the pin tract between slice locations, limbs, or horses ($p > 0.05$). For

comparison to the other histomorphometric parameters, the relationship among horses is shown in Figure 5.22.

Percent (%) Fibrosis, Tract

There were no significant differences in the percent fibrosis within and immediately around the pin tract among slice locations ($p = 0.5689$), condyles ($p = 0.3638$), limbs ($p = 0.8308$), or horses (Figure 5.22; $p = 0.0508$), or for any of the tested interactions ($p > 0.05$). Due to the marginal nature of the relationship between the percent fibrosis and horse, pairwise comparisons were performed and revealed significantly less fibrosis in and around the pin tracts of horse #3 compared to horse #1 ($p = 0.0476$). There were no significant differences between horse #2 and horses #1 and #3 ($p > 0.10$).

Percent (%) Fibrosis, Whole Slide

There were no significant differences in the overall percent fibrosis between slice locations ($p = 0.0652$), condyles ($p = 0.0746$), limbs ($p = 0.8912$), or horses (Figure 5.22; $p = 0.0949$), or for any of the tested interactions ($p > 0.05$).

5.4 Discussion

In combination with the two prior chapters, these results provide proof of concept that the pin penetration model – which involved using a 1.1mm Steinmann pin to create an osteochondral defect that extended approximately 8mm from the articular surface into the trabecular bone, followed by 6 months of high-speed treadmill exercise – consistently resulted in the development of BMLs in the MC3 condyles. While, histologically, there were changes to the articular surface, primarily associated with the area of the pin tract, the severity of subchondral and trabecular bone changes was greater compared to the articular cartilage. This could suggest that the articular cartilage damage was not the catalyst for progression of the subchondral bone changes. This

could provide further support for the use of this model to study repetitive stress injury in horses; however, this cannot be confirmed as histopathology was not performed prior to the end of this study.

Comparing the two gross scoring systems used,[2,12] the modified Pinchbeck et al. scoring system was considered more appropriate for this experimental model as it better captured the breadth of changes observed in this study. The OARSI scoring system was a macroscopic technique to describe gross changes associated with spontaneous osteoarthritis (OA) of the metacarpophalangeal joint. One benefit of the latter scoring system is the assessment of the severity of wear lines, the grades of which are based on both the depth and number of wear lines. Wear lines, or vertical clefts within the articular cartilage, have been observed in joints with mild OA and have been shown to reduce the mechanical integrity of the articular cartilage, with it being suggested that they are due to a weakening of the collagen matrix complex.[12,22,23] Additionally, palmar arthrosis, which represents a consistent, specific spectrum of molecular, cellular, and tissue-level changes for a specific disease process,[12,24–29] was scored separately from cartilage erosions elsewhere on the condyle. While this has advantages from the standpoint of clinical POD, the degree of changes depicted in the publication by McIlwraith et al. were not quite the same as those in the present pilot study.

Gross examination revealed changes to the articular surface that appeared similar to those previously reported in the palmarodistal MC3 condyles, but not advanced POD. In comparison to the research published by Stewart et al.,[17] changes were more severe as the articular surface was grossly normal in that study; however, those animals were not subjected to the same degree or duration of exercise. Similar to her study, the pin tract was also easily identified but appeared to be covered with fibrocartilage or other tissue. There were minimal differences among horses in

this study except for cartilage loss on the MC3 condyles. Overall and along the transverse ridge, gross cartilage loss was worse for horse #3 compared to the other two horses. When looking in the region of the central condyle, specifically, both horses #2 and #3 had more cartilage loss compared to horse #1. The reason for these differences is unknown and will be examined in future research (Chapter 6). Gross abnormalities were most consistent with other pathologies of the MC3 condyles shown to be associated with POD including wear lines, cartilage loss and ulceration (both on the condyles and the proximal sesamoid bones), marginal remodeling of the proximal sesamoid bones, dorsal impact injury, and linear fissures.[2,3] When considering the primary POD lesion, the findings from this study were most consistent with mild POD (grade 1), characterized by subchondral bone bruising and discoloration with minimal disruption of the overlying articular cartilage (disregarding the disruption caused by the pin).[2] In contrast, the apparent bruising appeared more diffuse in comparison to the published literature. It is unknown how long it would take for this model to result in collapse of the subchondral bone plate similar to that in clinical POD; however, the goal of this pilot study was to determine whether the pin penetration model, combined with treadmill exercise, would result in significant subchondral bone changes while minimizing diffuse cartilage damage. Focal areas of subchondral bone collapse and necrosis were still observed on histopathology, despite the differences in gross appearance. Furthermore, this could allow us to better study therapies and management protocols in the earlier stages of disease, in order to prevent advanced POD from occurring.

In the research performed by Stewart et al.,[17] the BMLs induced by the pin penetration technique alone modified the subchondral and trabecular bone without significant degeneration of the overlying articular cartilage. As just mentioned, it is possible that the inclusion of 6 months of strenuous exercise contributed significantly to the cartilage damage. Significantly

more gross damage – greater grades of cartilage erosion, wear lines, and palmar metacarpal arthroses – has been shown to occur following 6 months of high-speed treadmill exercise when compared to control horses.[28] This suggests that chronic stress and exercise, alone, can result in cartilage degeneration. Furthermore, it is known that when abnormal tissue characteristics are present within a joint, such as through the induction of BMLs, there is a significant effect on the dissipation of ground reaction forces that can disrupt strain distribution and alter the structure and composition of the osteochondral unit.[30–33] Unfortunately, since gross examination was not performed until 24 weeks after lesion induction and initiation of treadmill exercise, the timing of the development of articular cartilage damage relative to the progression of subchondral bone disease is unknown. What is known in the current pilot study is that the described model resulted in significant subchondral bone sclerosis. This sclerotic bone may contain poorer mineral quality and integrity,[34] thus reducing its ability to absorb energy and increasing the risk of abnormal shear forces and tensile failure in the articular cartilage.[35]

In a study of 2-year-old Thoroughbred racehorses monitored over their first year of race training, a longitudinal change in subchondral bone morphology was observed on CT imaging including a significant increase in subchondral bone sclerosis in the distal MC3/MT3 condyles and parasagittal grooves.[36] Subchondral bone has the capacity to acclimate to changing biomechanical stresses through repeated cycles of adaptive bone modeling and reparative bone remodeling. Repetitive, high-speed exercise impairs these normal repair processes, favoring net bone formation as osteoclastic resorption is inhibited.[34,37,38] Mild, subclinical damage that resolves without remodeling induces trabecular thickening and subchondral sclerosis, increasing the strength, stiffness, and fatigue life of the bone.[18,39,40] The presence of subchondral bone pathology also increased significantly over time in the palmar/plantar condyle. Compared to the

control specimen, trabecular morphometry analysis revealed that experimental induction of BMLs in the MC3 condyles, followed by 6 months of high-speed treadmill exercise, resulted in bone lesions with a lower number of thicker and generally less dense trabeculae. The bone volume fraction was also observed to be higher in study horses compared to the control, though only the relationship between horse #3 and the control was statistically significant. Similar to other reports in the published literature, the bone volume fraction, BMD, and TMD were observed to be higher in abaxial VOIs compared to axial VOIs, with varying levels of significance in the present study.[41,42] This trend has been demonstrated previously for joints that are not loaded in a uniform manner,[43] such as the metacarpophalangeal joint, and it has been proposed that this could be due to innate variation in subchondral bone density between individual horses.[41]

Direct comparisons of the trabecular morphometry parameters from microCT between the present study and the published literature are difficult to perform, especially when one considers the differences in sample size, horse population, and individual horse and training factors. For those VOIs that included the subchondral bone plate (AbSCB, AxSCB, PrSCB, DiSCB), the average bone volume fraction appeared similar to that reported for lateral MC3 condyles from trained 2-year-old racehorses, though the bone surface to volume ratio and TMD were subjectively lower compared to this prior report.[14] Similarly, for those VOIs further from the articular surface, the bone volume fraction was subjectively lower compared to trained 2-year-olds and appeared closer to the range of untrained 2-year-olds. Bone volume fraction in the subchondral bone plate was also similar to a study by Ayodele et al., with VOIs further from the articular surface appearing lower.[19] It could be that increased bone remodeling or lysis occurred closer to the end of the tract, thus affecting the gradient in parameter outcomes further from the

articular surface. The bone surface to volume ratio (BS/BV) appeared lower for the pin penetration model compared to that reported by Martig et al. for the trained racehorses,[14] but was more similar to that reported by Ayodele et al. with an older population of horses.[19] This could indicate reduced porosity of the subchondral bone as a result of the pin penetration model, with a similar relationship observed between the control and study specimens; however, larger sample sizes would be needed before definitive conclusions could be made. It must also be considered that the variability in pin tract location and thus, the location of the VOIs within the condyle of each horse, could also be affecting the ability to relate the findings from this experimental model to those from the published literature.

When examining the results from microCT for the various VOIs, several observations were made. Increased porosity was present at the tip of the tract, consistent with the focal areas of resorption observed using other modalities. Consistent with this, the bone volume fraction and BMD were lowest and the bone surface to volume ratio highest in this VOI. The referenced study by Martig et al. found that in horses in training, there was an increase in TMD and decrease in bone volume fraction in bone further from the articular surface, with an increase in porosity in horses with subchondral bone injury.[14] In the present pilot study, TMD was higher in VOIs further from the subchondral bone plate (non-SCB VOIs). Bone volume fraction was lower at the tip of the tract compared to other VOIs, followed by all mid-tract VOIs except midAb, consistent with these previous findings. It is possible that new bone production could be one of the factors affecting this relationship, with a higher volume of less mineralized bone closer to the articular surface. BMD, or bone mineral density, refers to the overall combined density of the bone within a mixed bone-soft tissue region, considering both the bone matrix and the mineral content within it, but does not give information about the material density of the bone itself.[44,45] TMD, or tissue

mineral density, on the other hand, specifically measures the density of the mineral content within a given volume of calcified bone tissue.[45] In contrast to the BMD, this gives us information about the material density of the bone itself, and ignores surrounding soft tissue. The mean density values in the present pilot study were subjectively lower when compared to other publications in which specimens were acquired from the MC3 condyles of Thoroughbred racehorses of variable ages and training, despite similarities in bone volume fraction and trabecular structure.[14,42] The reason for the density in the present study being lower is unknown. It is possible that, due to the presence of the pin tract and the resulting remodeling, that the bone analyzed in the present study was earlier in the mineralization process and thus, was less dense. Another consideration would be differences in scan and analysis parameters, as the BMD and TMD in the control horse were also subjectively lower compared to the referenced publications.[14,42]

Compared to the other two study horses and to the control, horse #1 exhibited the highest bone and tissue mineral density (BMD and TMD), trabecular thickness and trabecular spacing, and the lowest trabecular number. Overall, while horse #1 had the same volume of bone as other horses, the bone in this particular horse was thicker and denser. Trabecular thickness decreased and trabecular number increased from horse #1 to #2 to #3, with the control horse having a higher number of thinner trabeculae across VOIs compared to the study horses. Interestingly, the trend of significance for trabecular spacing among the study horses matched that of trabecular thickness, decreasing in a statistically significant manner from horse #1 to #2 to #3. The trabecular spacing in the control horse was similar or only marginally different compared to horses #2 and #3. Typically, as trabecular thickness decreases, trabecular spacing would be expected to increase. Due to the number of variables included in this model, the reason for the

lack of this inverse relationship is unknown. While it cannot be confirmed at this stage, it is possible that the observed differences in trabecular structure among study horses were the result of pin tract placement, or other factors not considered or evaluated in this study.

Overall, there were no significant differences in bone volume fraction between the study horses and the control, except for a higher % bone volume in horse #3 compared to the control. When examining the bone surface to volume ratio, which can be an indicator of the structural complexity and turnover of the bone,[46] there were no significant differences among study horses. The bone surface to volume ratio was higher in the control horse compared to horses #1 and #3, suggestive of increased bone turnover and structural complexity in this horse, consistent with the higher number of thinner trabeculae also observed in the control. As this horse was not subjected to the same exercise protocol, there are numerous factors that could be affecting bone turnover in this case including intensity and/or duration of exercise, and duration and/or timing of periods of rest, the latter not provided in this pilot study. The reparative actions of bone remodeling are accelerated during periods of rest, with a decrease in bone density of the MC3 diaphysis and an increase in porosity of the distal MC3 condyles during rest from training.[38,40,47,48] Unfortunately, the theory of potential rest from training, unlike the study horses, could be considered less likely based on that claim as the control horse actually had an increase in bone density relative to 2 of the 3 study horses. In the equine metacarpus, remodeling is reduced during periods of training and racing when microdamage is accumulating.[49] With the inhibition of this remodeling process, the dominant mechanism for maintaining the strength of and strains within the bone is adaptive bone modeling and the net formation of bone.[38,40] A decrease in loading will cause these layers to weaken through stimulation of bone resorption.[50] This is suggested to be the reason behind the high density and increased percent bone volume of the subchondral bone of the distal MC3/MT3

condyles in racehorses, with increased bone deposition within the marrow spaces and increased bone volume fraction of the distal subchondral trabecular bone.[34,38,40,51–53] In contrast, an increase in the porosity of the condylar subchondral bone is observed in horses rested from race training, reducing its ability to handle mechanical stress.[38,47,48] Despite exercise-induced reduction in subchondral remodeling, it has been shown that focal remodeling can still occur once failure develops in the subchondral bone. Whitton et al. demonstrated that fatigued subchondral bone in the MC3 condyles is focally remodeled in proportion to the modeling of the surrounding trabecular bone, with focal areas of porosity with an increased volume of surrounding trabecular bone observed at sites of fatigue failure.[54] This suggests that trabecular modeling allows the remodeling and repair of subchondral bone by focally unloading the damaged tissue. The bone damage associated with the creation of a 1.1 mm diameter pin tract, approximately 8 mm deep to the articular surface, could be viewed as an induced site of fatigue failure. It is possible that the surrounding bone remodeling resulted in the focal unloading of the pin tract area, resulting in the areas of bone resorption observed in this study.

Reported histological findings observed in horses with POD or other forms of maladaptive stress remodeling include thickening of the subchondral bone and underlying trabeculae, osteocyte necrosis that increases with advancing sclerosis, vascular channels with matrix debris beneath the articular cartilage, glycosaminoglycan loss, osteoclastic remodeling in and around zones of sclerosis, irregular microfracture development in the subchondral and trabecular bone, atypical subchondral bone matrix, fibroplasia within marrow spaces, superficial degeneration, fibrillation and erosion of the articular cartilage, chondrocyte loss, and collapse of the cartilage surface.[5,8,9,25,55,56] One study showed that in MC3 condyles from horses run on a

treadmill, changes were milder in comparison to the racehorse samples.[25] These findings are consistent with those identified in this pilot study, though the severity and frequency varied.

Histologically, there were extensive alterations to the subchondral bone surrounding the pin tract when compared to distant sites, consistent with findings by Stewart et al.[17] These changes included cavitation of the articular cartilage and subchondral bone plate, extensive myelofibrosis, cellular debris within the marrow spaces, fibroplasia within the pin tract, and adjacent marked bony sclerosis. Consistent with the trabecular morphometry analysis, there was regionally extensive thickening of the cancellous trabeculae with variable immature, and likely less dense, bone (woven bone). This increase in immature bone was only present adjacent to the pin tract and not in the distant sites, which is where VOIs for trabecular morphometry analysis were located. Furthermore, not only was the percentage of bone higher in this region of interest (within and immediately around the pin tract) on Visiopharm software analysis, but the percentage of fibrosis was also higher; however, the Visiopharm analysis included the pin tract in which a majority of the fibrotic change was located.

This level of evidence of active remodeling in the subchondral and trabecular bone, while present on advanced diagnostic imaging, microCT, and histopathology, was not detectable using synovial fluid analysis as described in Chapter 3. This may be due to the degree of changes in the articular cartilage being relatively mild compared to the severity of what appears to be a primary pathology of the subchondral and trabecular bone, though it could also be due to fluid sampling methods. As the pin tract entry point had evidence of complete tissue coverage on histopathology in many samples, it is possible that the reduced communication between the injured bone and the rest of the joint caused the synovial fluid analysis to not as accurately reflect the severity of the changes identified in this study.

While the changes to the subchondral and trabecular bone were more extensive, degenerative changes were also observed in the articular cartilage. The surrounding articular cartilage was characterized by mild to moderate fibrillation, degeneration (reduced toluidine blue stain uptake, chrondrone formation), and necrosis with chondrocyte loss within the superficial to intermediate zones of the cartilage layer. These changes were the most severe in the regions overlying and immediately adjacent to the pin tract. Unfortunately, due to the limited sample size, histology was not performed until the end of the 6-month study period, making it impossible to determine how much of the articular cartilage injury was a result of the act of pin penetration alone – in which the articular cartilage injury would be considered a catalyst for disease progression – or a result of high-speed treadmill exercise and bone remodeling. Stewart et al. reported no histological evidence of articular cartilage degeneration by 90 days post-lesion induction, with complete coverage of the pin tracts with fibrocartilage by 30 days. This could make the act of pin penetration alone less likely to be the catalyst for cartilage degeneration; however, differences in lesion location and load-bearing, species, and exercise between this study and the present pilot cannot be ignored. Future studies utilizing this model in a larger number of horses will need to include earlier histological sampling to evaluate this effect. In a group of 12 horses evaluated from birth to 18-months of age, in which 6 were raised on pasture and 6 were subjected to an additional training regimen, changes in cartilage biomechanical, structural, and biochemical properties consistent with early cartilage degeneration were present in this region of the metacarpophalangeal joint without detectable effects of exercise training.[57] It is possible that, due to the presence of focal bone damage, intense exercise had a more significant effect on the articular cartilage in this region. As previously mentioned, sclerotic bone may contain poorer mineral quality and integrity,[34] thus reducing its ability to absorb energy and

increasing the risk of abnormal shear forces and tensile failure in the articular cartilage.[35] There has also been shown to be a positive correlation between the number of race starts and the severity of articular cartilage scores.[9] The parasagittal area of the distal MC3 is also known to be a site with a higher prevalence of pathological change in both the bone and articular cartilage[57] and, given the more axial location of some of the pin tracts, this may have also contributed to the changes in this study.

As mentioned previously, direct comparison between this pilot study and other reports and models in the published literature is difficult due to differences in sample sizes and population, sampling methods, and study protocol. In the experimental model performed by Rice et al.,[58] horses were euthanized immediately after impact injury to the palmarodistal condyle via metacarpophalangeal joint arthrotomy, followed by extraarticular subchondral injection of a bone substitute material; therefore, results cannot be directly compared between this study and the present pilot study. On gross examination, the site of impact injury was visible following impact in all cases. Histological evaluation revealed evidence of hemorrhage within the marrow spaces as a result of the impact injury in all cases, with microfracture of the trabeculae in slices from 4 out of 6 horses. In the experimental impact injury model performed by Rickey et al.,[59] four impact lesions were created in a cloverleaf pattern on the palmarodistal aspect of one medial palmarometacarpal condyle via arthroscopic and fluoroscopic guidance, after which horses were exercised by lunging 5 days per week up to a maximum of 30 minutes per day until 6 months postoperatively.[59] Gross examination in this study revealed a wide variation in lesion placement, extent, and depth. MicroCT analysis revealed no significant difference in BMD and TMD between treatment and control limbs, both of which were highest at 1 month, decreased at 4 months, and increased again at 8-10 months postoperatively. There were no significant

differences in BV/TV in this study. Furthermore, there were no significant differences in the degree of articular cartilage disruption between treatment and control horses. While evidence of OA did develop in the study by Rickey et al. results suggested that cartilage injury, rather than subchondral bone injury, initiated OA.[59] In comparison, lesion location in the present pilot study appeared more consistent. While the pin tract location was more proximal in horse #1, all pin tracts were more consistently placed in horses #2 and #3 after adjusting the degree of fetlock extension intraoperatively. Further analysis will need to be performed in future studies to determine the effects of pin tract location, angle, and depth on the outcome parameters measured in this study. Additionally, the site of articular cartilage damage in the present pilot study was only 1.1 mm in diameter compared to 1 cm in the study by Rice et al. and 6.5mm (times 4 in a variable cloverleaf pattern) by Rickey et al.

In contrast to the diagnostic imaging findings in this study, there were no significant differences between limbs or condyles using the gross scoring systems or on histological analysis. This is consistent with other studies that showed no difference in prevalence or severity of POD between left and right limbs,[2,3,60] though one study did show histopathologic scoring to be worse in lateral condyles compared to medial condyles.[9] MicroCT analysis, however, revealed increased bone volume fraction, BMD, TMD, and trabecular thickness, and decreased bone surface to volume ratio and trabecular number in left forelimbs compared to right forelimbs and in lateral condyles compared to medial condyles. These changes correspond to an increased volume of thicker, more sclerotic or dense bone. The reason for this is unknown and could be examined in future work.

While this experimental model successfully induced changes in the subchondral and trabecular bone consistent with maladaptive stress remodeling, there are several limitations that

must be considered. As stated in previous chapters, the small sample size is a significant limitation. This study also lacked a direct control group in which a lesion was induced and followed with strict box-stall rest, or conversely another control group exposed to the same high-speed treadmill exercise without lesion induction. This would have allowed more specific evaluation of the effects of exercise or pin penetration alone on the articular cartilage and bone. Pin tracts were also not placed in the exact same location and at the same angle within every condyle and the variability in lesions that may occur as a result of this is unknown. Another significant limitation was that horses were not euthanized for postmortem evaluation until the end of the study period; therefore, the microscopic response and tissue composition at different stages of lesion progression could not be evaluated. Future studies in a larger number of horses, including those assigned as controls, with microscopic assessment at earlier stages would be beneficial.

One limitation with microCT analysis could be the need to individually assign density thresholds to each horse, as this could affect the resulting BMD and TMD. The greatest BMD and TMD were observed in horse #1, followed by the control, horse #2, and then horse #3. This was the same order as the bone density thresholds set for each horse and it cannot be ruled out that the lack of consistent thresholds had an effect on the resulting BMD and TMD for each specimen.[61] While it would have been ideal to select the same threshold for each horse, this would have resulted in a significant over- or under-estimation of mineralized bone in multiple samples. Furthermore, threshold selection was performed similarly by a single investigator for all specimens in an attempt to improve the ability to compare changes between horses. It is also possible that the pattern observed for BMD and TMD was the reason why the density thresholds had to be set as they were. One option to consider in future studies would be to maintain a

similar threshold for each horse but choose a control area within each sample not influenced by the model in which an average density from multiple VOIs could be used as a normalization factor. Inclusion of a standardized phantom could also be considered. That being stated, subjective selection based on segmentation has been reported previously,[14,19] and this method accounted for the natural variability in densities between horses. By using the segmentation tool and selecting density thresholds in the same manner among horses, thresholds were set that best matched the natural density of each horse; however, more objective measures may be considered in future work.

Lastly, histomorphometric analysis revealed no significant differences between slice locations, limbs, or condyles in percent bone or fibrosis in the three regions. One complicating factor could be that the percent bone and fibrosis within and immediately around the pin tracts was only analyzed for slice locations that contained the pin tract (PT, DT), and the other two regions of interest (non-tract, whole tissue) were analyzed in all slides without exclusion of what would have been the pin tract region of interest in the PD and DD slides for the percentages outside of the pin tract.

Overall, post-mortem analysis provided further proof of concept that this experimental model could produce advanced subchondral and trabecular bone lesions without more diffuse damage to the articular cartilage; however, without earlier histopathology, the progression of articular cartilage changes relative to the bone is unknown. These findings support continued work using this experimental model and given the degree of bone pathology, could be used as a potential model for the optimization of management and treatment strategies. Correlation statistics will be performed in future research to better examine the significance of the findings

and variation observed in this study, as well as to relate the post-mortem findings to those from clinical evaluation and diagnostic imaging at the same time point.

5.5 Figures

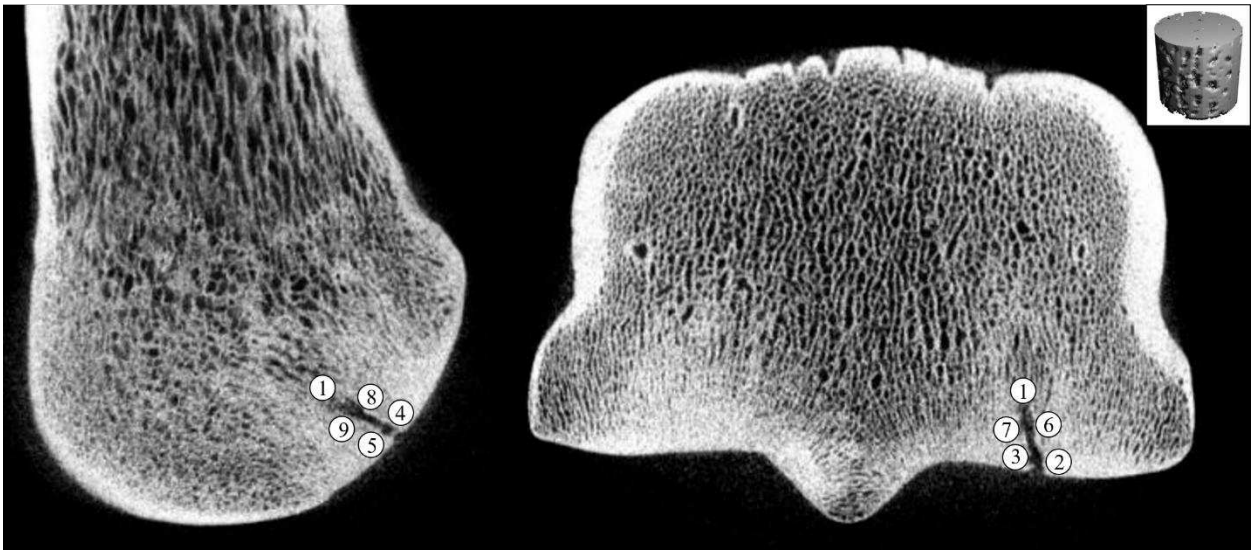

Figure 5.1 – Sagittal and transverse images from microcomputed tomography (microCT) showing the locations of the 9 volumes of interest (VOI) relative to the pin tract. Each cylindrical VOI (upper right corner) was 3 mm in diameter and 81 slices (3 mm) in height, with the latter adjusted as needed and described in Table 5.3. The 9 VOIs were as follows: 1) Tip of tract, 2) abaxial subchondral bone plate, 3) axial subchondral bone plate, 4) proximal subchondral bone plate, 5) distal subchondral bone plate, 6) abaxial mid-tract, 7) axial mid-tract, 8) proximal mid-tract, and 9) distal mid-tract.

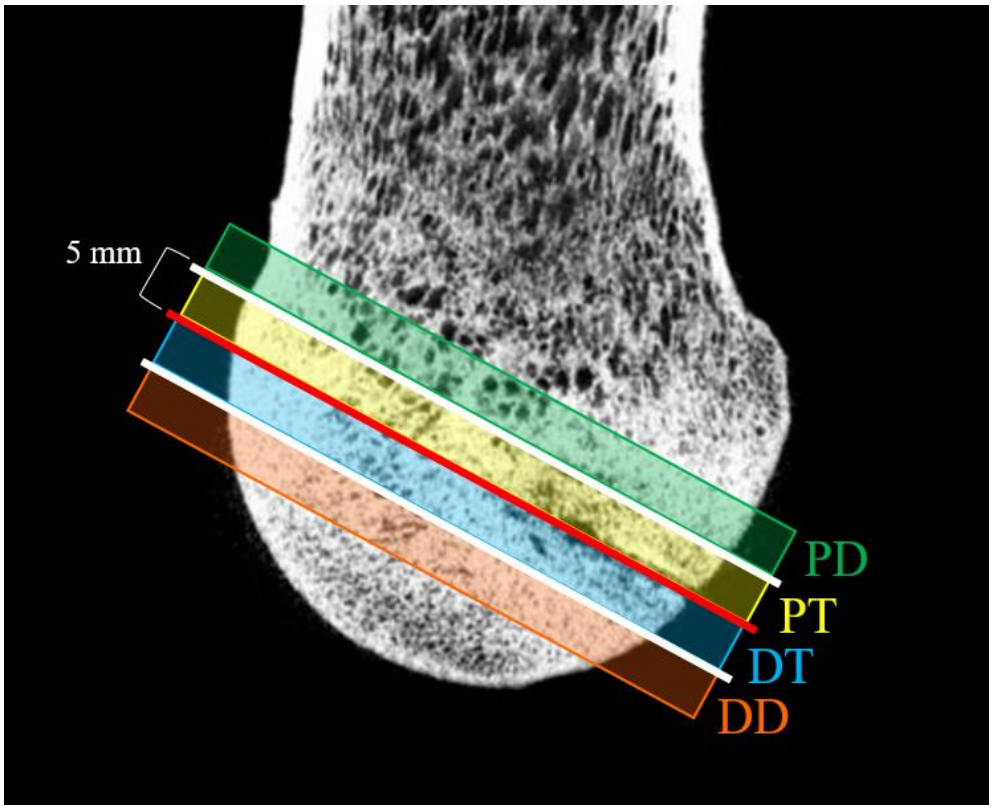

Figure 5.2 – Sagittal microCT image used to demonstrate sectioning of the bone specimens for histopathology. For each condyle, an initial cut (red line) was made using a mini Exakt saw along the center of the long axis of the pin tract. Two parallel cuts were made at 5 mm intervals proximal to this initial cut, creating the proximal tract block (PT) and the proximal distant block (PD). Two parallel cuts were also made at 5 mm intervals distal to the initial cut, creating the distal tract block (DT) and the distal distant block (DD). Each block was decalcified and embedded in paraffin. When sectioning each block, slides were obtained from the distal surface of the PT and proximal surface of the DT blocks (red line), and from the distal surface of the PD and proximal surface of the DD blocks (white lines).

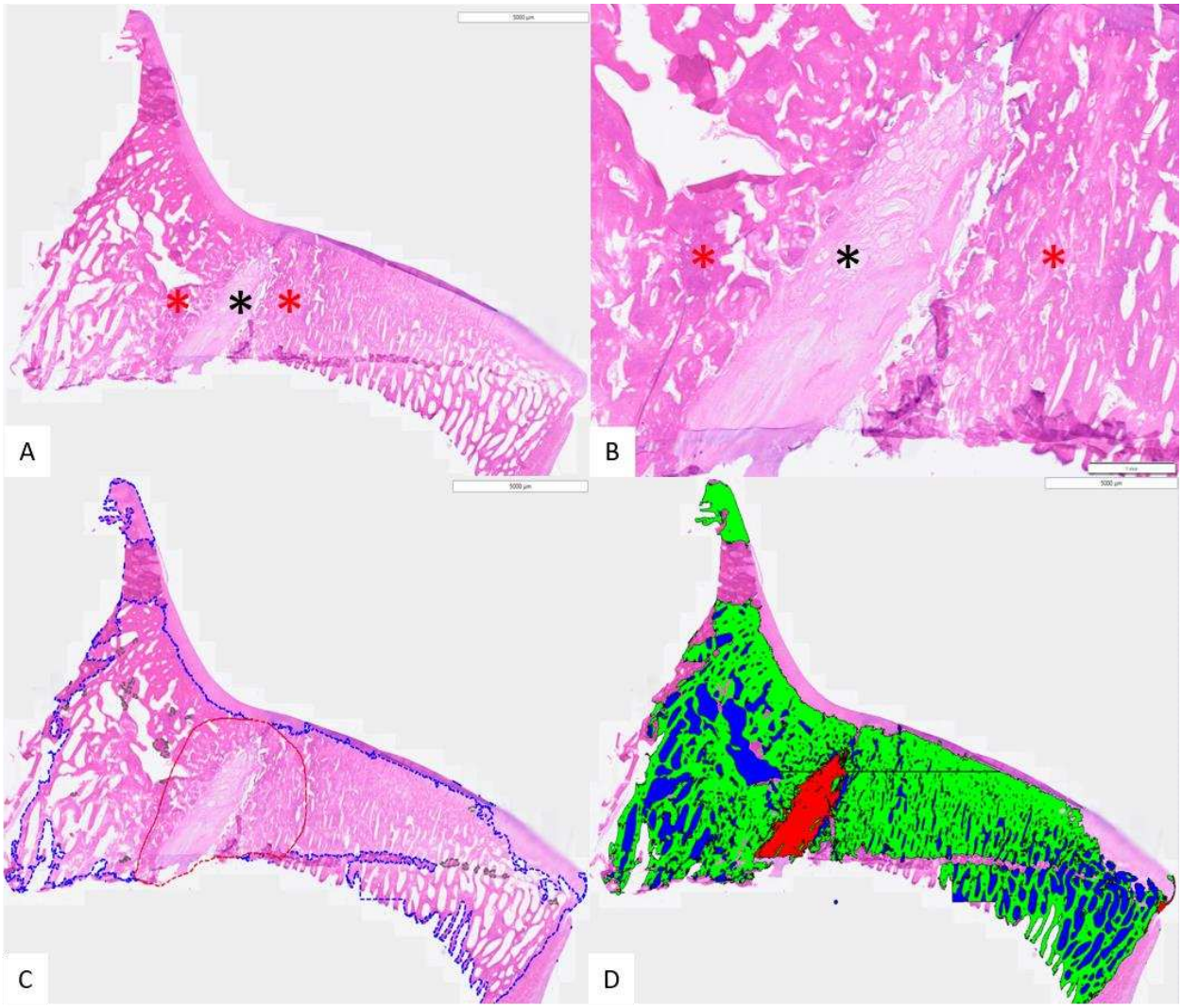

Figure 5.3 – Digital histologic images of the distal pin tract (DT) slice location from the left lateral third metacarpal condyle of horse #1, demonstrating the regions of interest and labeling of relevant changes for histomorphometric analysis using Visiopharm. A) Subgross H&E slide, with clear tract formation (black asterisk) and surrounding bony remodeling and sclerosis (red asterisk). B) Higher magnification H&E; The tract is filled with regions of fibroplasia and loss of bony architecture (black asterisk). The surrounding trabecular bone is markedly sclerotic (red asterisk). C) Subgross H&E image of Visiopharm analysis; Examined regions of interest included the subchondral bone outside of the area of the pin tract (blue dotted line), the region including and immediately surrounding the tract (red dotted line), and the whole tissue section. Regions of interest excluded tissue artifacts, such as tissue folding, to remove artifact bias. Articular cartilage was also excluded from Visiopharm software analysis. D) Subgross H&E image of Visiopharm analysis, showing labeling of the different tissue types; the percentage of bone and fibrosis were measured for each region of interest. The green annotation correlates with bone, blue annotation correlates with medullary cavity, and red annotation correlates with fibroplasia.

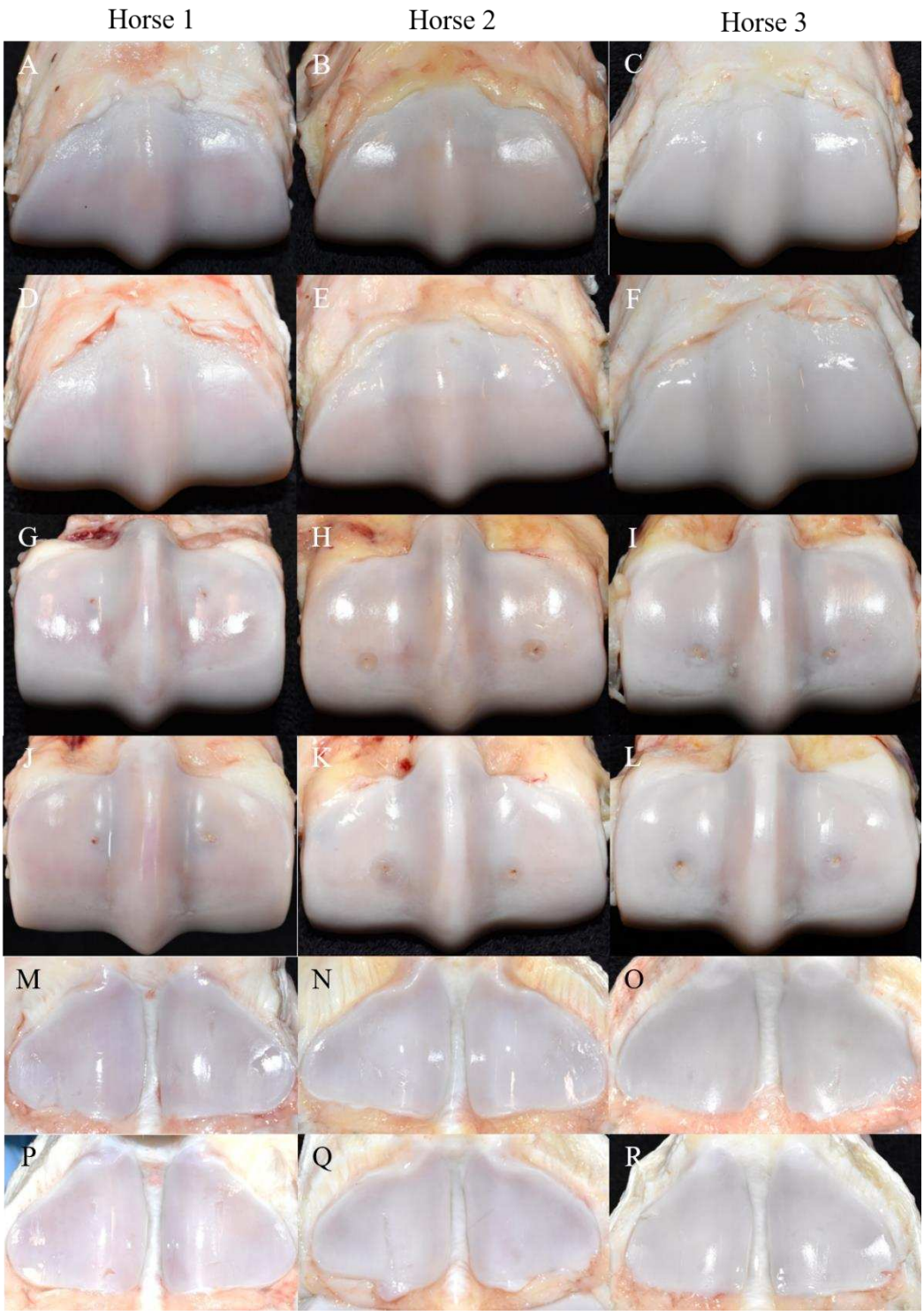

Figure 5.4 – Gross photographs of the dorsal third metacarpal condyles (A-F), palmar third metacarpal condyles (G-L), and proximal sesamoid bones (M-R) of each horse. For each group of six images, the left forelimb is shown in the top row (A-C, G-I, M-O) and the right forelimb is shown in the bottom row (D-F, J-L, P-R). Images are oriented so that lateral is to the left in all images, regardless of limb. The grades assigned to each condyle using the gross scoring systems from Table 5.1 and Table 5.2 are provided in Table 5.9.

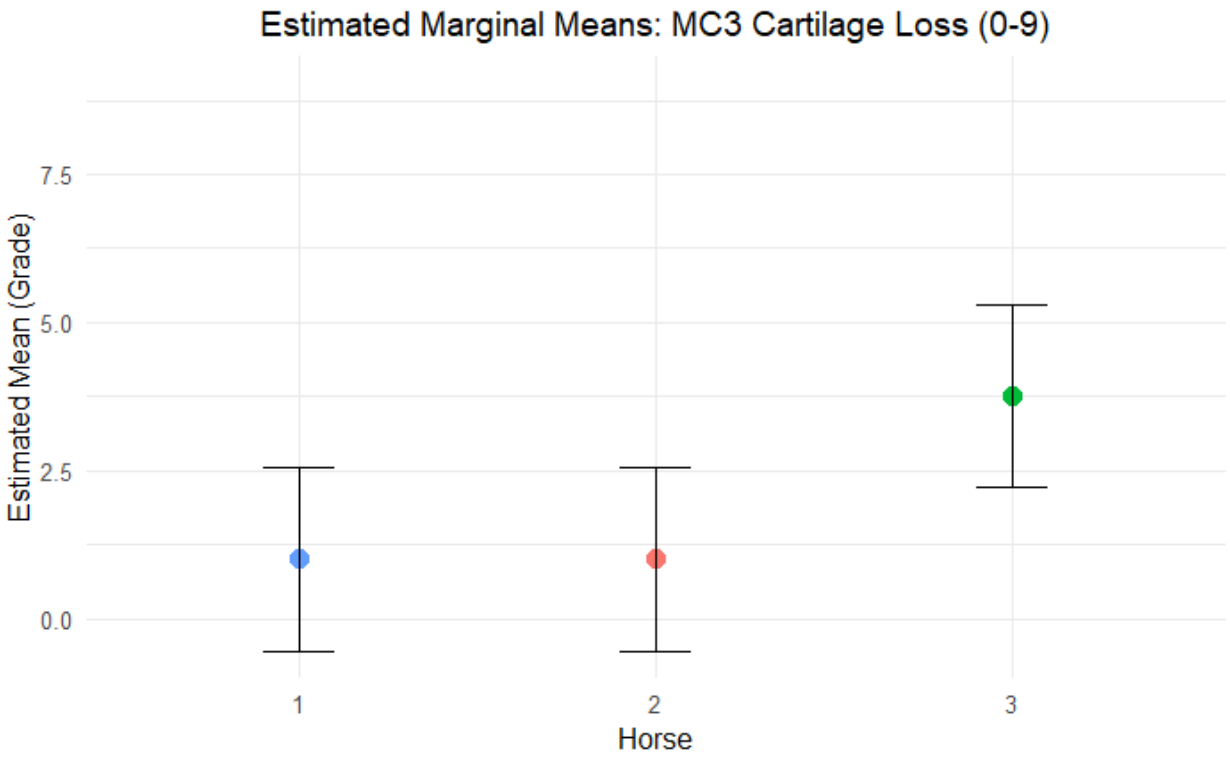

Figure 5.5 – Plot showing the estimated marginal mean (95% CI) grade for cartilage loss on the palmarodistal aspect of the third metacarpal condyle (MC3) for the three horses on gross examination, as described in Table 5.1. The total score for cartilage loss on the MC3 condyles was significantly higher in horse #3 compared to the other two horses ($p = 0.0476$).

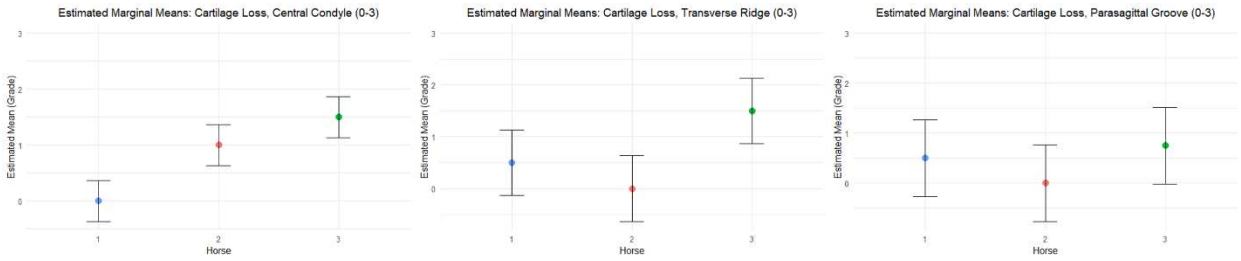

Figure 5.6 – Plots showing the estimated marginal mean (95% CI) grade for cartilage loss in each of the three main regions of the palmarodistal third metacarpal condyle (MC3) for the three horses, as described in Table 5.1. The mean grade in the central condyle was significantly lower in horse #1 compared to the other two horses ($p < 0.05$). In the transverse ridge, the grade was for horse #3 was significantly higher compared to horse #2 ($p = 0.0131$) and marginally higher compared to horse #1 ($p = 0.0754$). There were no significant differences in grade between horses in the parasagittal groove ($p > 0.10$).

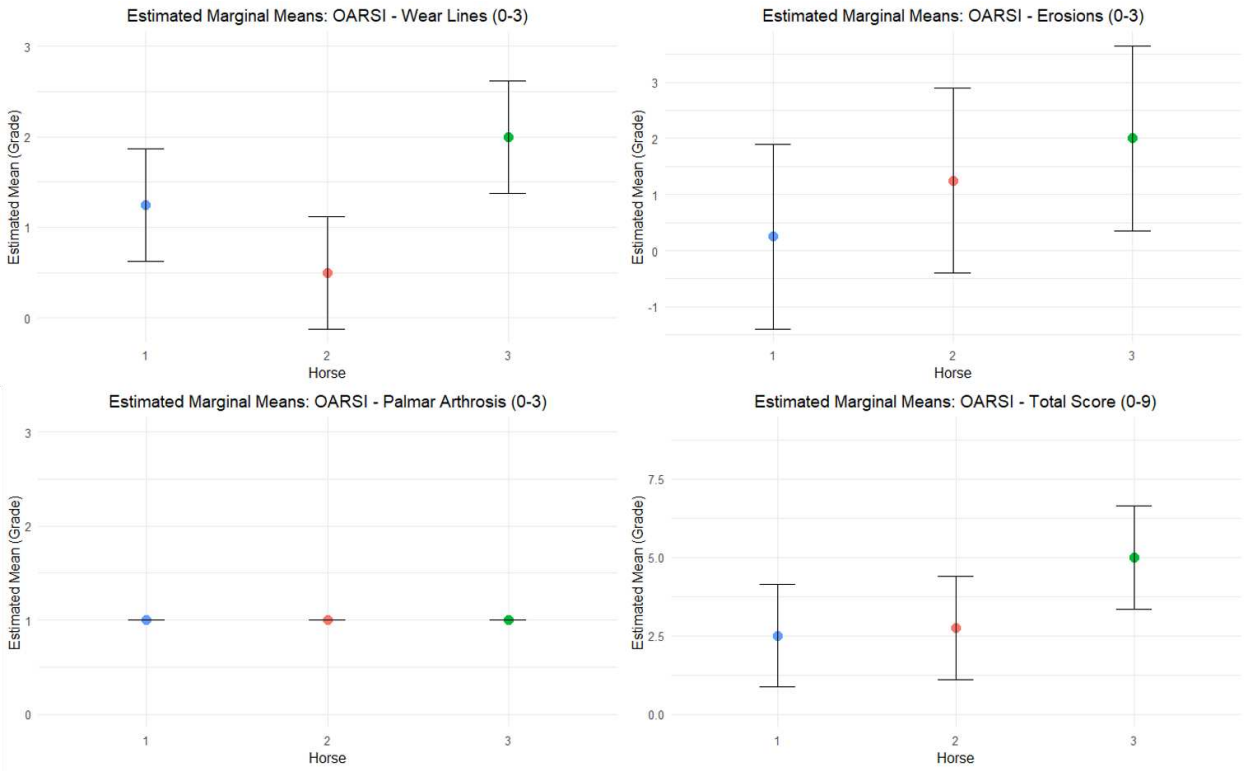

Figure 5.7 - Plots showing the estimated marginal mean (95% CI) grade for each horse from gross examination of the third metacarpal condyles for the outcome parameters included in the scoring system developed by the Osteoarthritis Research Society International (OARSI) for assessment of the palmar third metacarpal condyles in horses, as described in Table 5.2. The wear line grade for horse #3 was higher compared to horse #2 ($p = 0.0327$), with no other differences between horses. There were no significant differences between horses for the grade of erosions or palmar arthrosis ($p > 0.10$). A total composite score was also provided, for which the total score for horse #3 was marginally higher compared to horses #1 and #2.

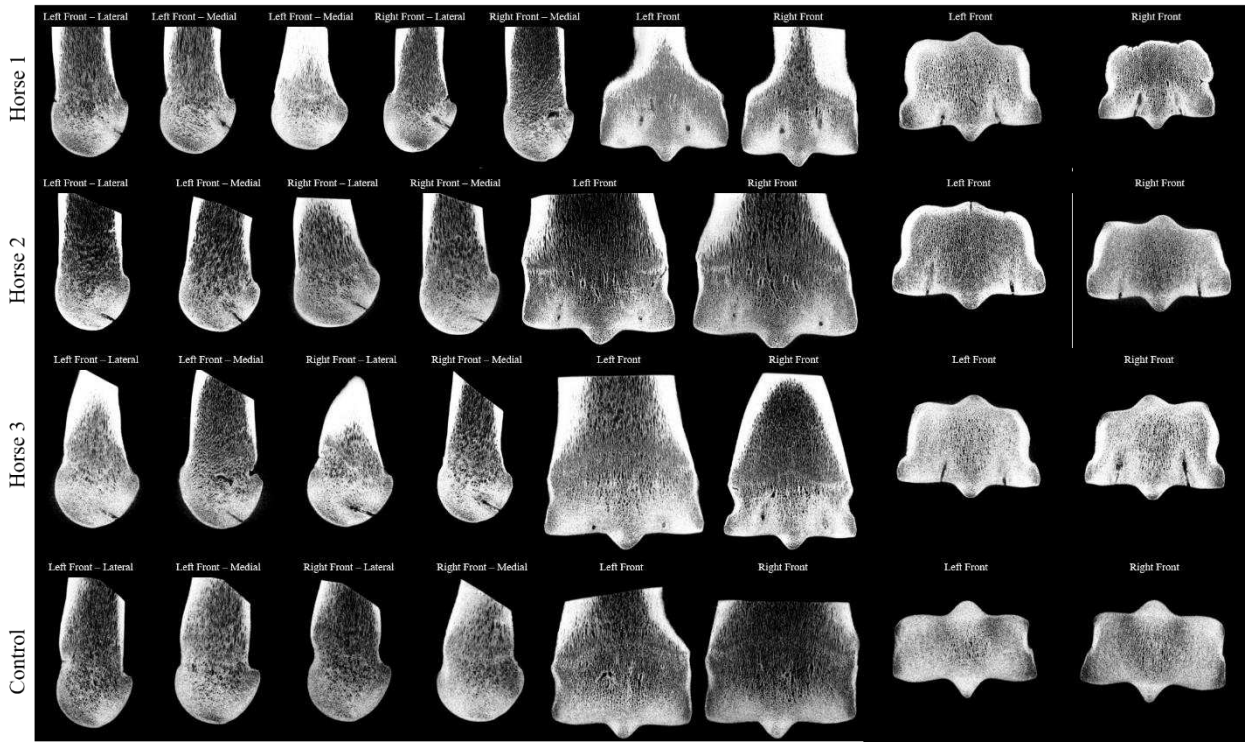

Figure 5.8 – Sagittal, dorsal, and transverse images of each horse acquired using microcomputed tomography (microCT) 24 weeks following experimental induction of bone marrow lesions and high-speed treadmill exercise. An addition sagittal image of the left front medial condyle is shown for horse #1, demonstrating an additional area of bone lysis located abaxial to the pin tract. This lesion was not present in the remaining horses. For all dorsal and transverse images, lateral is to the right in the left forelimb and to the left in the right forelimb.

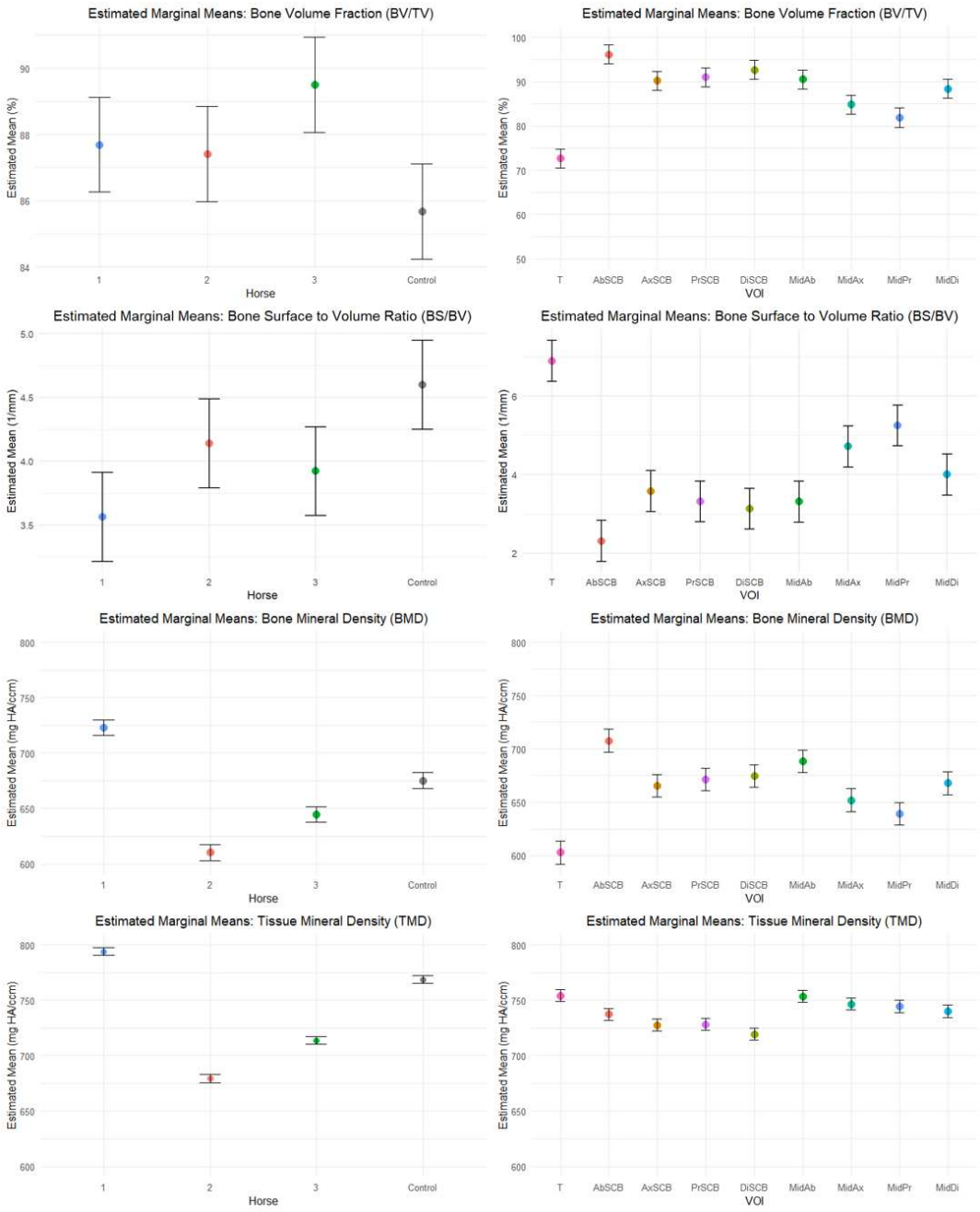

Figure 5.9 – Plots showing the estimated marginal means (95% CI) for bone volume fraction (BV/TV), bone surface to volume ratio (BS/BV), bone mineral density (BMD) and tissue mineral density (TMD) in the palmarodistal third metacarpal condyles of horses, measured using microcomputed tomography (microCT) 24 weeks following experimental induction of bone marrow lesions combined with high-speed treadmill exercise. Plots in the left column demonstrate differences between individual horses, while the right column shows the values for each volume of interest (VOI). The 9 VOIs analyzed in this study, relative to the pin tracts in the condyles, include the tip of the tract (T), abaxial subchondral bone plate (AbSCB), axial subchondral bone plate (AxSCB), proximal subchondral bone plate (PrSCB), distal subchondral bone plate (DiSCB), abaxial mid-tract (MidAb), axial mid-tract (MidAx), proximal mid-tract (MidPr), and distal mid-tract (MidDi).

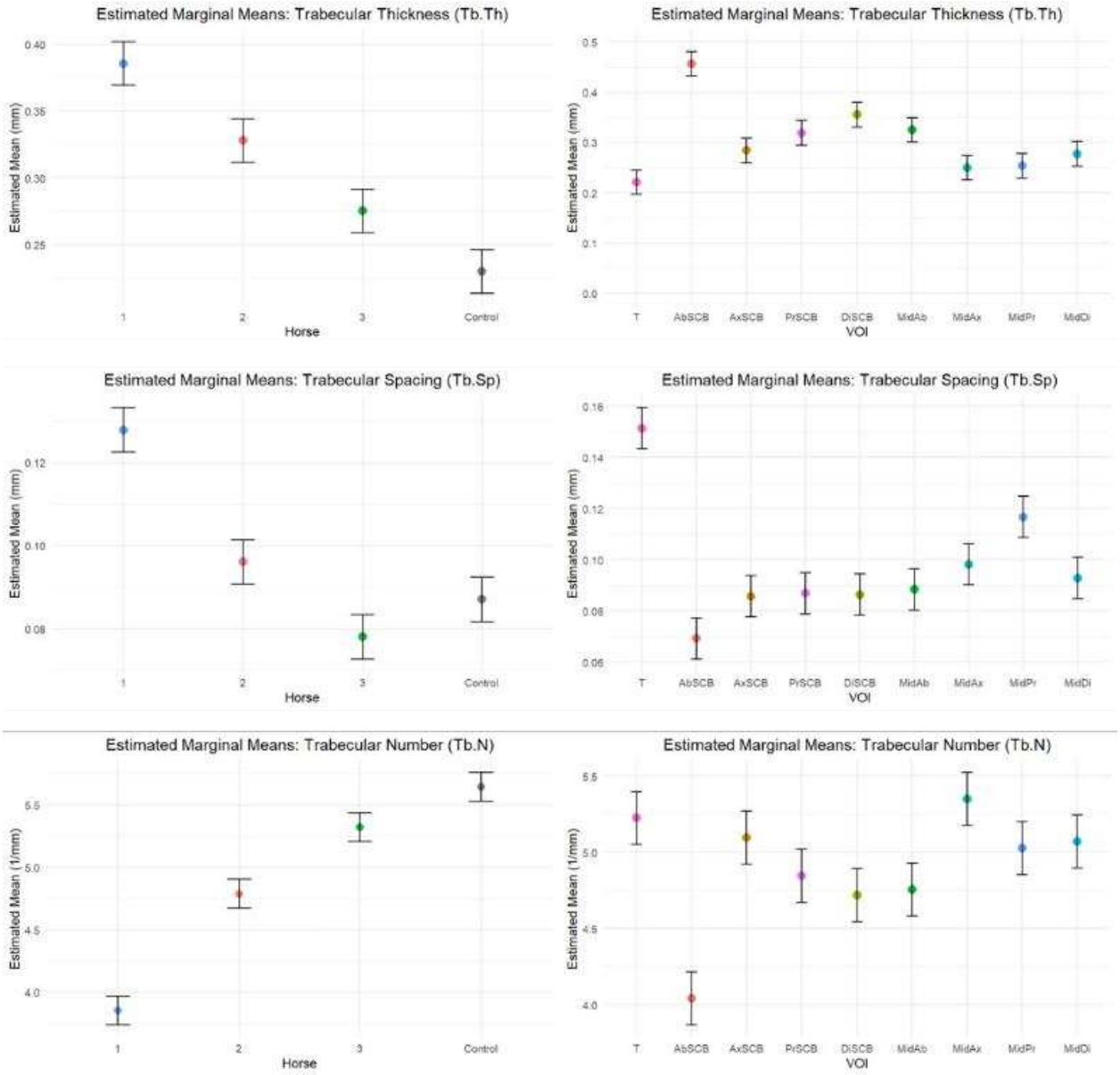

Figure 5.10 – Plots showing the estimated marginal means (95% CI) for trabecular thickness (Tb.Th), trabecular spacing (Tb.Sp), and trabecular number (Tb.N) in the palmarodistal third metacarpal condyles of horses, measured using microcomputed tomography (microCT) 24 weeks following experimental induction of bone marrow lesions combined with high-speed treadmill exercise. Plots in the left column demonstrate differences between individual horses, while the right column shows the values for each volume of interest (VOI). The 9 VOIs analyzed in this study, relative to the pin tracts in the condyles, include the tip of the tract (T), abaxial subchondral bone plate (AbSCB), axial subchondral bone plate (AxSCB), proximal subchondral bone plate (PrSCB), distal subchondral bone plate (DiSCB), abaxial mid-tract (MidAb), axial mid-tract (MidAx), proximal mid-tract (MidPr), and distal mid-tract (MidDi).

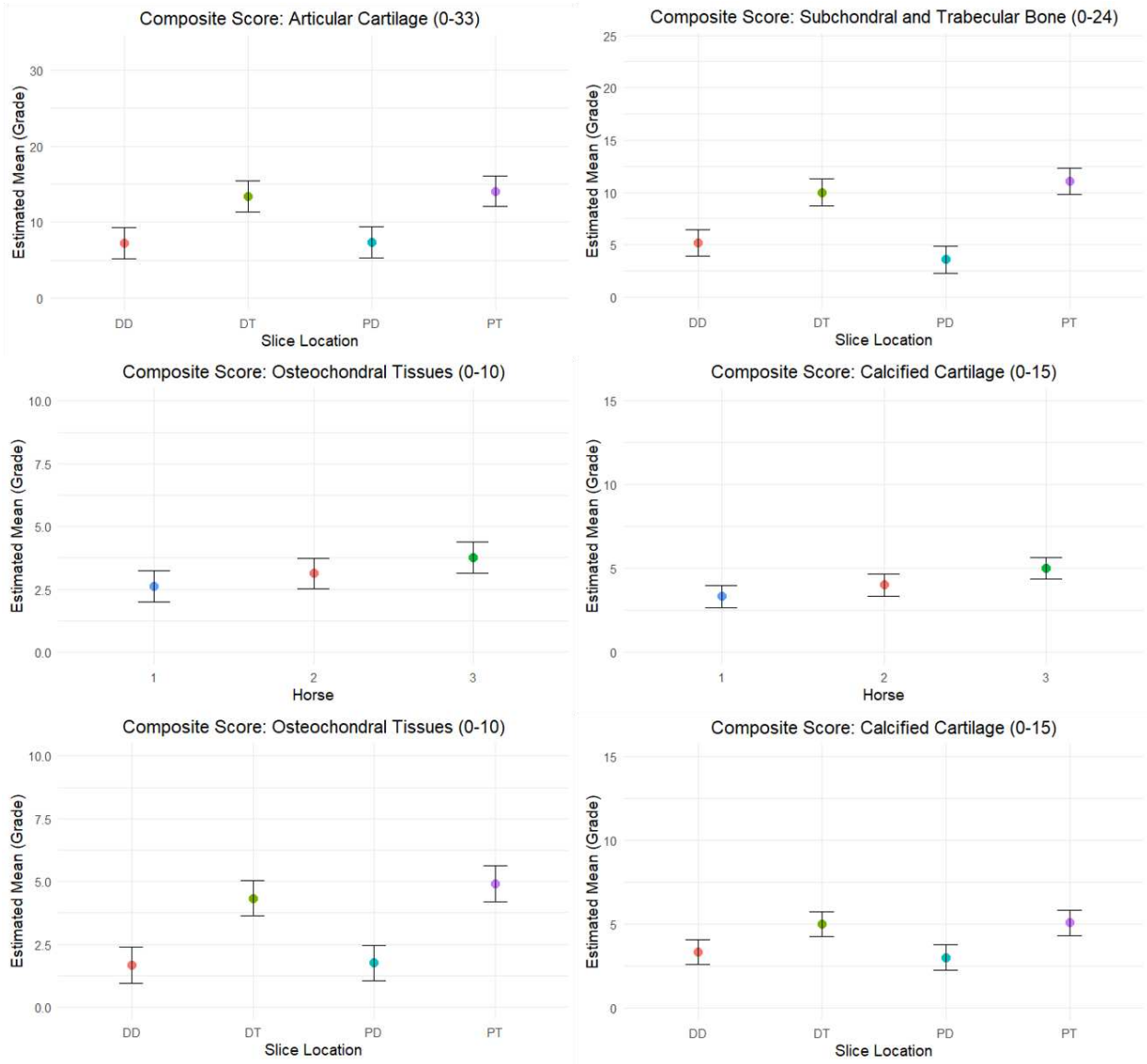

Figure 5.11 – Plots showing the estimated marginal means (95% CI) of significant variables for each of the composite histology scores. Histologic sections were analyzed from multiple locations within the palmarodistal third metacarpal condyles of three horses, 24 weeks following experimental induction of bone marrow lesions combined with high-speed treadmill exercise. Slice locations for histopathology included the proximal tract (PT), proximal distant to the tract (PD), distal tract (DT), and distal distant to the tract (DD). Distant sections were taken at least 5 mm from the tract sections. Slice location had a significant effect ($p < 0.05$) on all four composite scores, with changes in the DT and PT slice locations being more significant compared to the remaining slice locations. There were also significant differences between horses for the osteochondral and calcified cartilage composite scores. In both scoring systems, the score for horse #3 was significantly higher compared to horse #1 ($p < 0.05$), and there were no significant differences between horses #1 and #2 ($p > 0.10$). For changes in the osteochondral unit, there were no significant differences between horses #2 and #3 ($p = 0.3198$). For the calcified cartilage score, the score was also marginally higher in horse #3 compared to horse #2 ($p = 0.0871$).

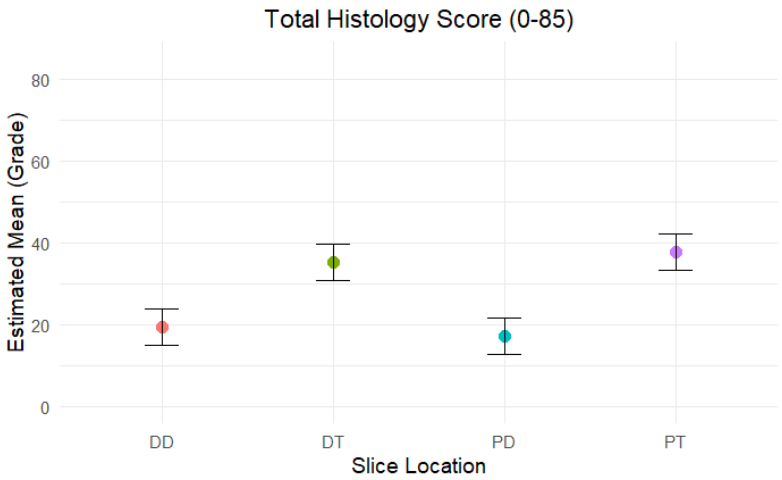

Figure 5.12 – Plot showing the estimated marginal mean (95% CI) for the total histologic score summating Tables 5.4-5.8. Histologic sections were analyzed from multiple locations within the palmarodistal third metacarpal condyles of three horses, 24 weeks following experimental induction of bone marrow lesions combined with high-speed treadmill exercise. Slice locations for histopathology included the proximal tract (PT), proximal distant to the tract (PD), distal tract (DT), and distal distant to the tract (DD). Distant sections were taken at least 5 mm from the tract sections. There were more severe histologic changes in the DT and PT slice locations compared to the DD ($p \leq 0.0001$) and PD ($p < 0.0001$) slice locations. There were no differences in the total histology score between the DD and PD or the DT and PT slice locations ($p > 0.10$).

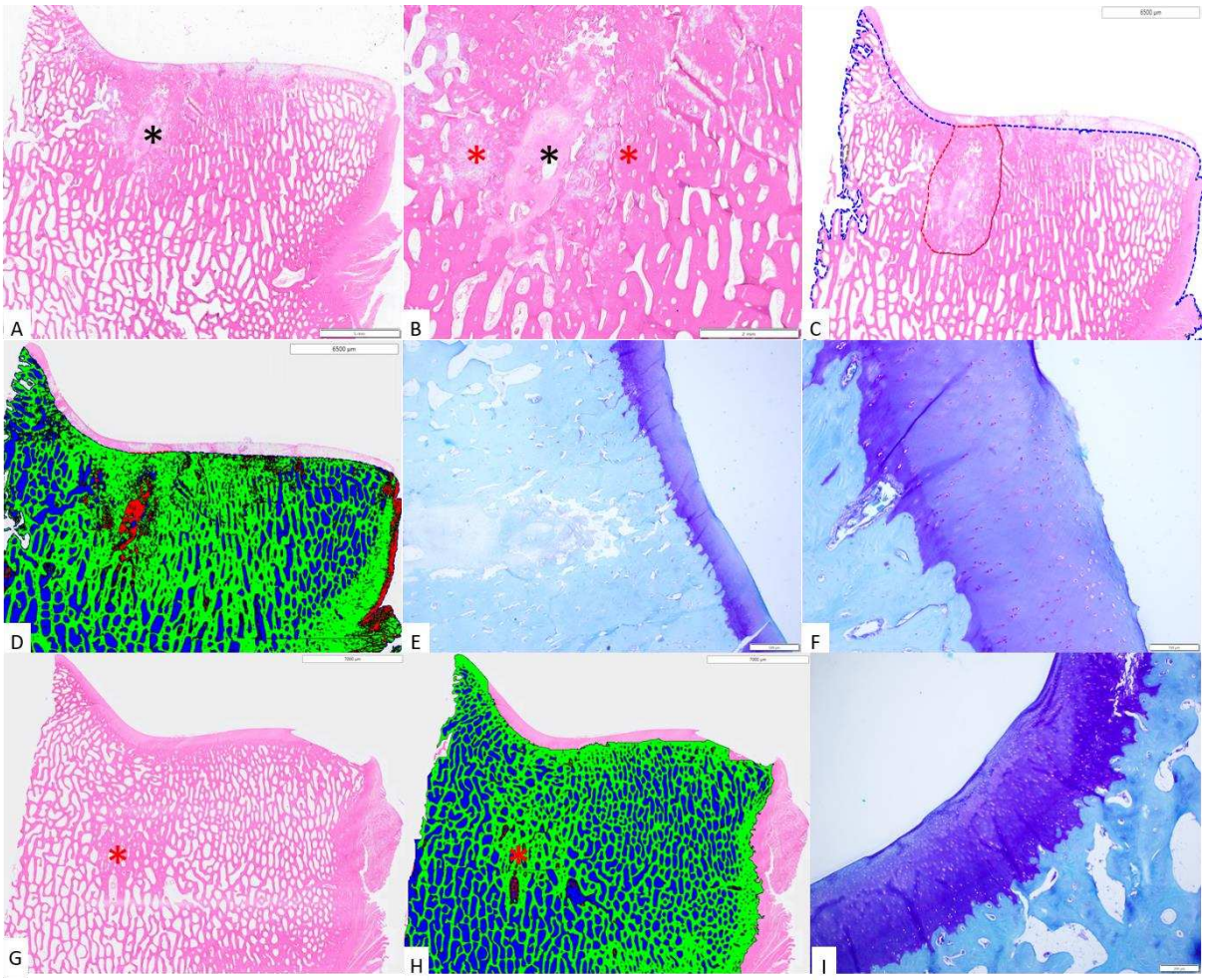

Figure 5.13 – Digital histology images of sections taken from the distal third metacarpal (MC3) condyles of horse #1, 6 months following experimental induction of bone marrow lesions and high-speed treadmill exercise. **A-F)** Section taken from the proximal half of the pin tract (PT) in the left medial MC3 condyle, which had the worst cumulative, semi-quantitative pathologic score (46/85) for this horse. **G-I)** Section taken at least 5mm proximal and distant to the pin tract (PD slice location) in the right lateral MC3 condyle, which had the lowest or best cumulative, semi-quantitative pathologic score (12/85) for this horse. A-B) Subgross and higher magnification H&E, with clear tract formation (black asterisk) and surrounding bony sclerosis (red asterisk). The tract is filled with regions of fibroplasia and loss of bony architecture. The surrounding trabecular bone is markedly sclerotic. C-D) Subgross H&E image from the Visiopharm analysis, showing the regions of interest and annotations representing bone (green), medullary cavity (blue), and fibrosis (red) for this slide as previously described in Figure 5.3. E-F) Subgross and higher magnification images showing toluidine blue staining of the articular surface directly overlying and adjacent to the pin tract. There is loss of tinctorial staining of the articular cartilage, indicating a loss of proteoglycan content, as well as superficial fibrillation. G) Subgross H&E image showing more subtle subchondral and trabecular sclerosis (red asterisk). H) Subgross H&E image from the Visiopharm analysis of subchondral bone, further highlighting subtle bony sclerosis (red asterisk). I) High magnification image of articular cartilage with toluidine blue staining, which demonstrates deep basophilic staining of the articular cartilage that correlates with appropriate proteoglycan content, and minimal subchondral plate remodeling.

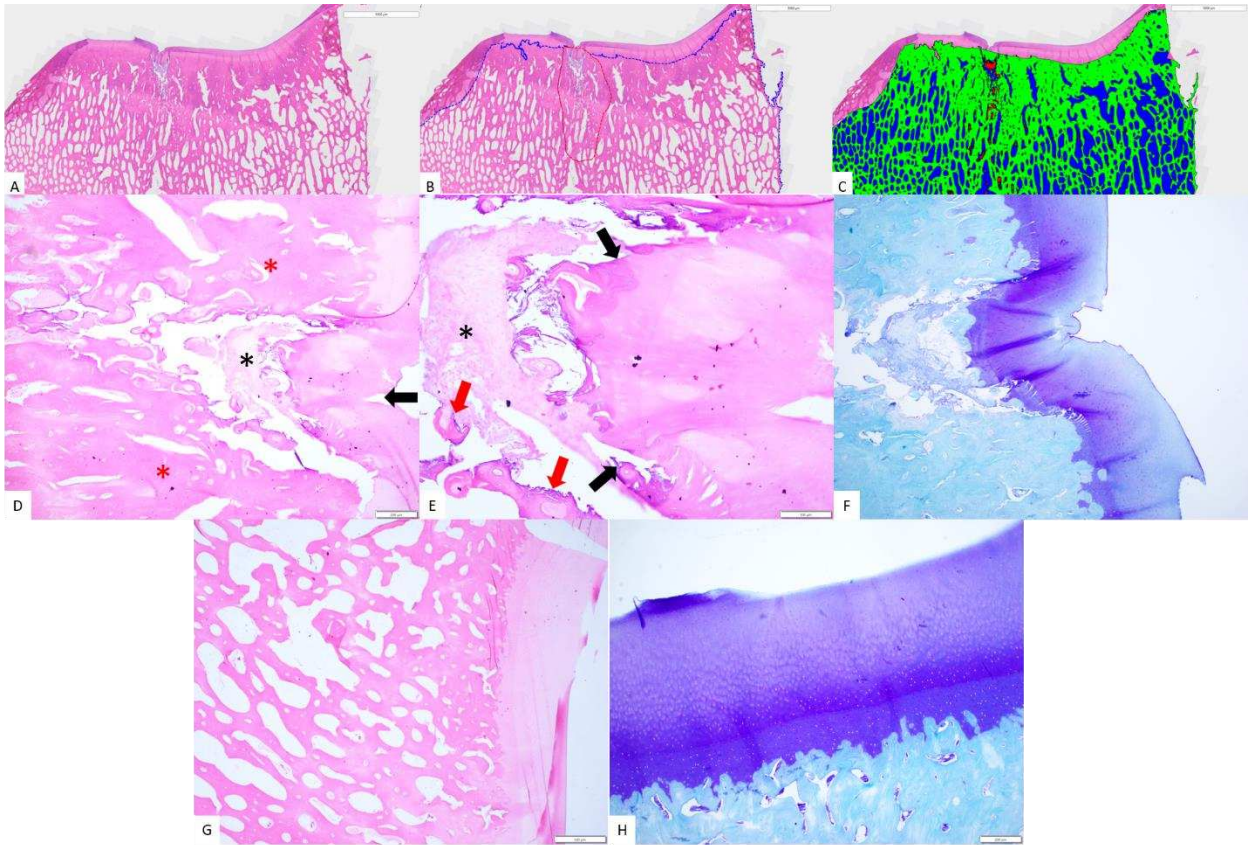

Figure 5.14 – Digital histology images of sections taken from the distal third metacarpal (MC3) condyles of horse #2, 6 months following experimental induction of bone marrow lesions and high-speed treadmill exercise. **A-F)** Section taken from the distal half of the pin tract (DT) in the left lateral MC3 condyle, which had the worst cumulative, semi-quantitative pathologic score (53/85) for this horse. **G-H)** Section taken at least 5mm distal and distant to the pin tract (DD slice location) in the left lateral MC3 condyle, which had the lowest or best cumulative, semi-quantitative pathologic score (10/85) for this horse. A) Subgross H&E-stained image that demonstrates the best sections of the pin tract with corresponding fibrosis and bony sclerosis (red asterisk). B-C) Subgross H&E image from the Visiopharm analysis, showing the regions of interest and annotations representing bone (green), medullary cavity (blue), and fibrosis (red) for this slide as previously described in Figure 5.3. D-E) High magnification H&E images demonstrating articular cartilage collapse and necrosis (black arrow), associated with fragmented necrotic bony spicules (red arrows) and fibrin (black asterisk). The surrounding bony architecture demonstrates sclerosis (red asterisk). F) Higher magnification toluidine blue image showing loss of tinctorial staining in the region of collapse and in the adjacent cartilage, indicating loss of normal proteoglycan content. G) Subgross H&E image showing minimal subchondral bone plate remodeling, articular cartilage degeneration, or trabecular bone sclerosis. There is a discernable tidemark, with minimal degenerative change. H) High magnification image of articular cartilage with toluidine blue staining, which demonstrates appropriate deep basophilic staining of the articular cartilage that correlates with appropriate proteoglycan content with a relatively uniform, visible tidemark (red arrow).

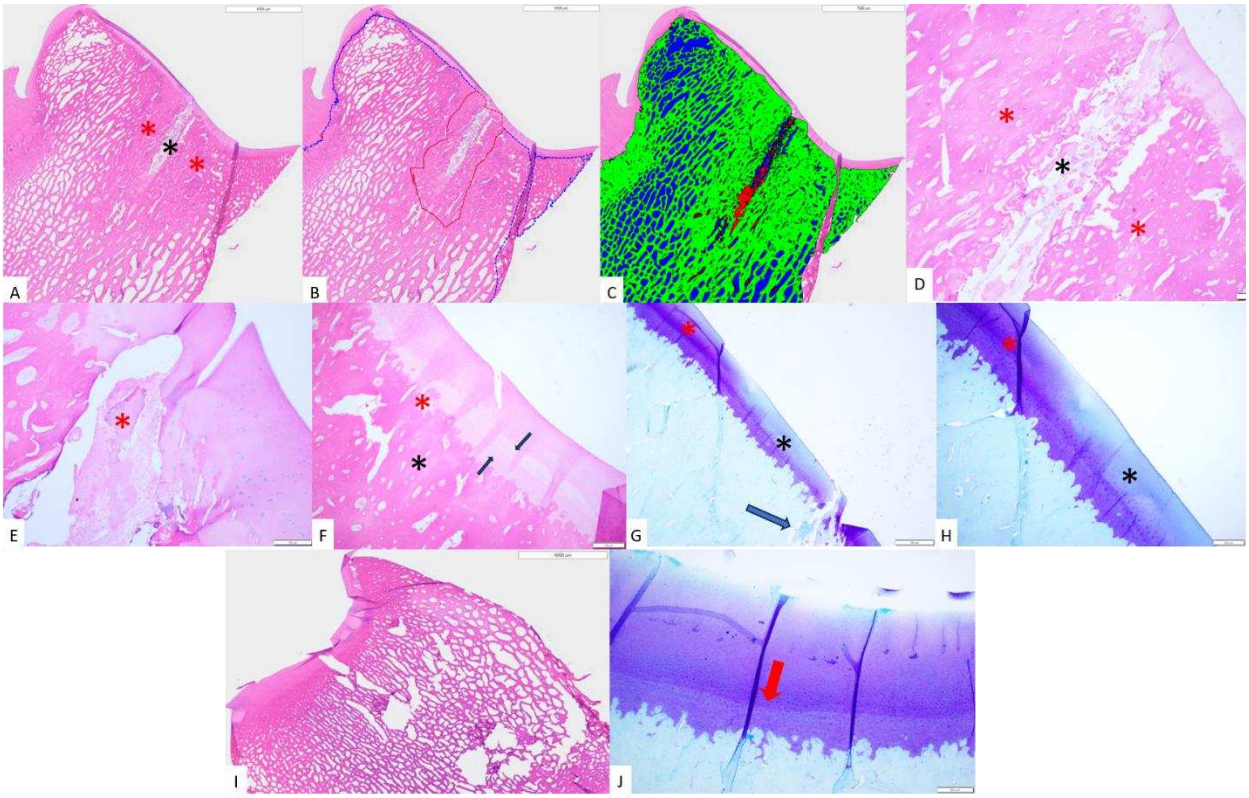

Figure 5.15 – Digital histology images of sections from the distal third metacarpal (MC3) condyles of horse #3, 6 months following induction of bone marrow lesions and high-speed treadmill exercise. **A-H)** Section from the proximal half of the pin tract (PT) in the right medial MC3 condyle, which had the worst cumulative, semi-quantitative pathologic score (49/85) for this horse. **I-J)** Section taken at least 5mm distal and distant to the pin tract (DD slice location) in the right medial MC3 condyle, which had the lowest or best cumulative score (16/85) for this horse. A) Subgross H&E image showing the best sections of the pin tract (black asterisk) with corresponding fibrosis and bony sclerosis (red asterisk). B-C) Subgross H&E images from the Visiopharm analysis, showing the regions of interest and annotations representing bone (green), medullary cavity (blue), and fibrosis (red) as previously described in Figure 5.3. D) Higher magnification H&E image with clear tract formation (black asterisk) and marked surrounding trabecular bone sclerosis (red asterisk). The tract is filled with regions of fibroplasia and loss of bony architecture. E) Articular cartilage overlying the tract bisects with regions of necrotic cartilage (red asterisk) surrounded by fibrin and fibroplasia. F) Sclerosis (black asterisk) and remodeling of the subchondral plate with bony advancement to the tidemark (red asterisk). There is variable loss of the tidemark with segmental tidemark duplication (arrows). G-H) Toluidine blue-stained images showing tinctorial staining variation from the peripheral articular cartilage (red asterisk) and that associated with the tract (black asterisk, arrow). Loss of staining profile indicates loss of proteoglycan content. I) Subgross H&E image showing minimal subchondral bone plate remodeling, articular cartilage degeneration, or trabecular bone sclerosis. J) High magnification image of articular cartilage with toluidine blue staining, which correlates with appropriate proteoglycan content with a relatively uniform, visible tidemark (red arrow).

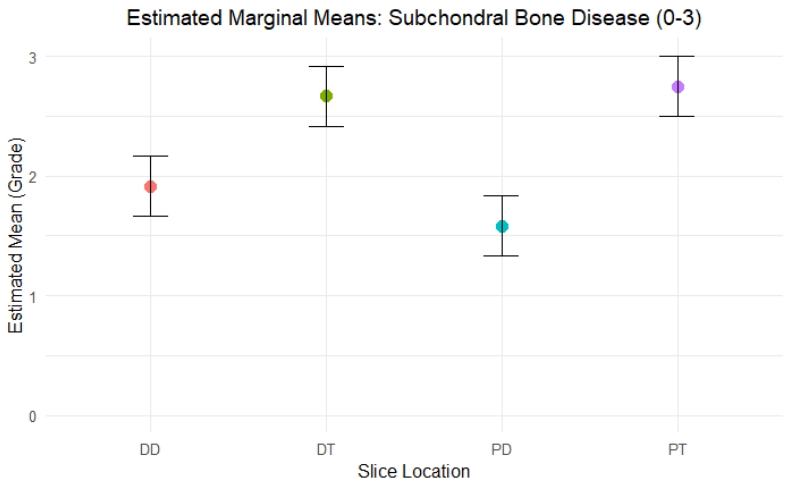

Figure 5.16 – Plot showing the estimated marginal mean (95% CI) for the subchondral bone disease grade, scored as described in Table 5.4. Histologic sections were analyzed from multiple locations within the palmarodistal third metacarpal condyles of three horses, 24 weeks following experimental induction of bone marrow lesions combined with high-speed treadmill exercise. Slice locations for histopathology included the proximal tract (PT), proximal distant to the tract (PD), distal tract (DT), and distal distant to the tract (DD). Distant sections were taken at least 5 mm from the tract sections. The score was significantly higher in the DT and PT slice locations compared to the DD and PD locations ($p < 0.002$). There were no significant differences in the subchondral bone score between the DD and PD or the DT and PT slice locations ($p > 0.10$).

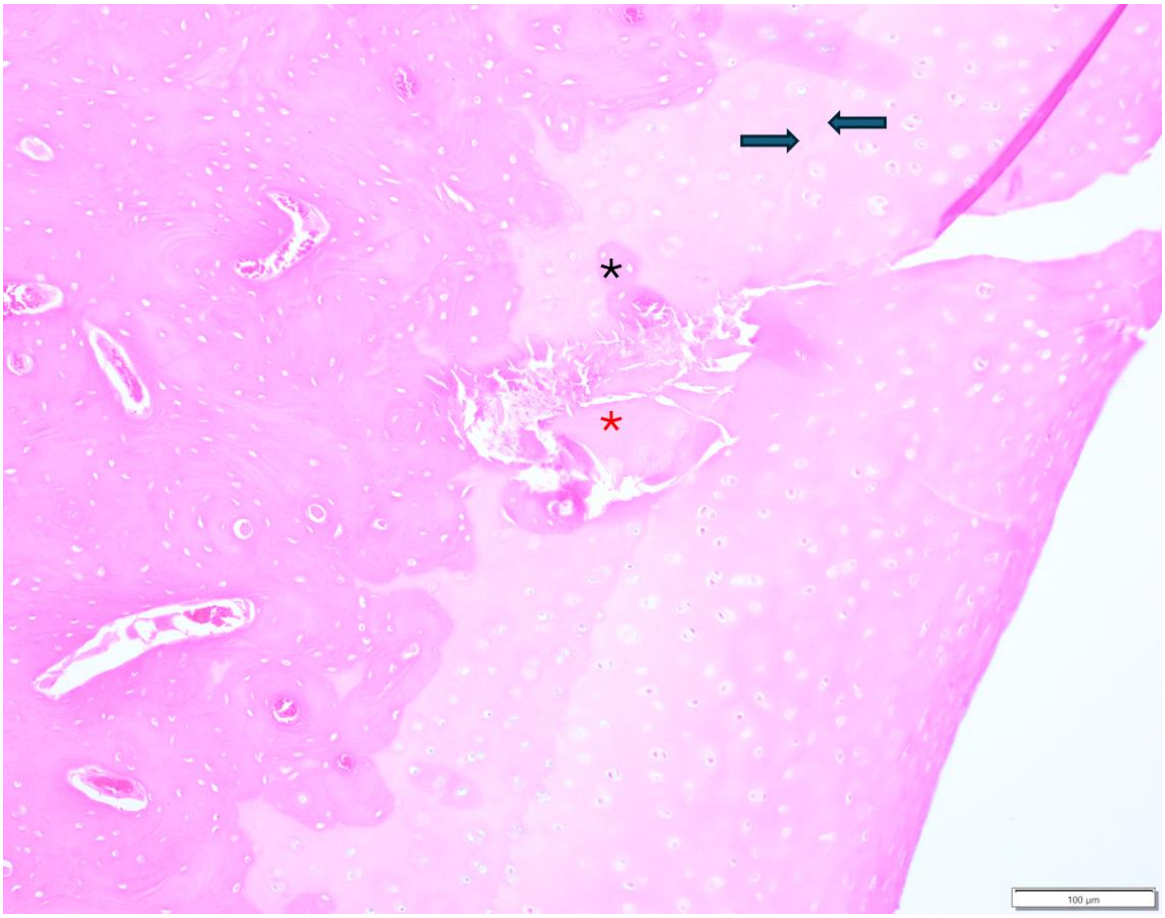

Figure 5.17 – Digital histology image (H&E) from the distal half of the pin tract (DT slice location) of the right lateral third metacarpal (MC3) condyle of horse #2, 6 months following induction of bone marrow lesions and high-speed treadmill exercise. There is a cleft extending from the articular surface to the zone of calcified cartilage, given a grade 2 for clefting out of 3. Within the zone of calcification, the cartilage is necrotic, fragmented and admixed with scant fibrin (red asterisk). There is subchondral plate remodeling with advancement of the bone towards the tidemark (black asterisk), as well as subtle tidemark duplication and incongruencies (grade 2 out of 3; arrows).

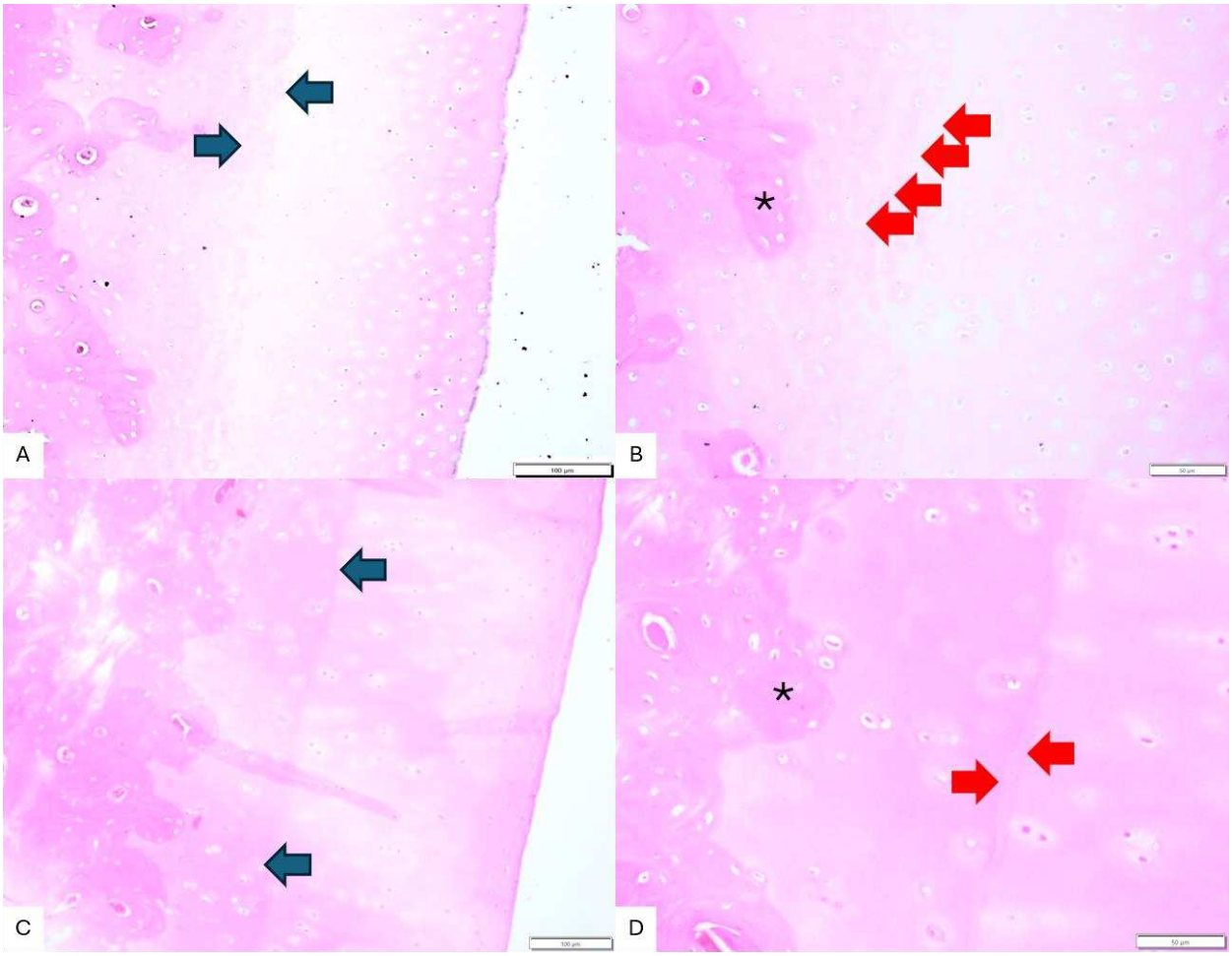

Figure 5.18 – Digital histology images (H&E) from a section taken from the distal half of the pin tract (DT slice location) of the left lateral third metacarpal (MC3) condyle (**A-B**) and a section taken at least 5mm proximal and distant to the pin tract (PD slice location) in the right medial MC3 condyle (**C-D**) of horse #2, 6 months following induction of bone marrow lesions and high-speed treadmill exercise. A-B) H&E image in which the tidemark is faintly observable to completely lost (blue arrows). The tidemarks lack the characteristic parallel nature and in regions demonstrate multiple duplications (red arrows). There is remodeling of the subchondral plate with advancement of bony spicules and neovascularization penetrating the poorly delineated deep tidemark (asterisk). This section was a grade 3 for tidemark incongruencies. C-D) H&E image in which the tidemark is discernable and is relatively parallel to the subchondral bone plate. There is segmental tidemark duplication (red arrows) with mild subchondral plate remodeling.

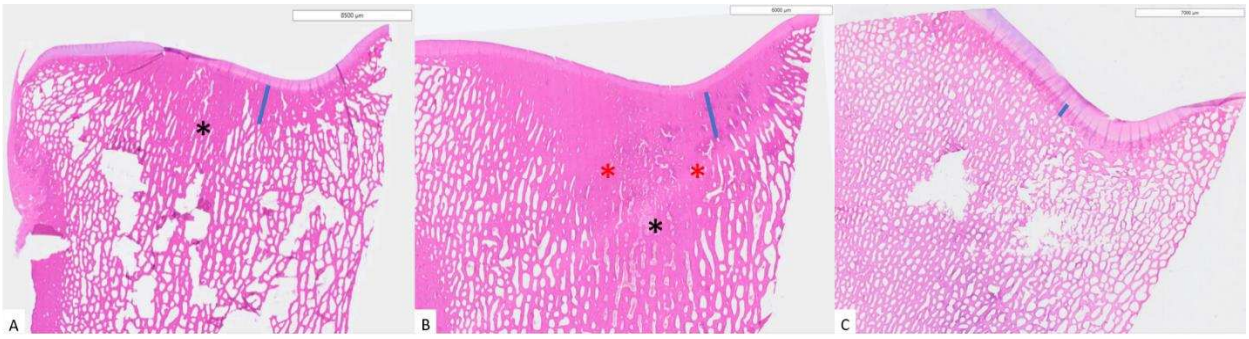

Figure 5.19 – Digital histology images (H&E) of sections taken from the distal half of the pin tract (DT slice location) of the left medial third metacarpal (MC3) condyle (**A**), from the distal half of the pin tract (DT) of the right lateral MC3 condyle (**B**), and at least 5mm distal and distant to the pin tract (DD slice location) in the left medial MC3 condyle (**C**) of horse #2, 6 months following induction of bone marrow lesions and high-speed treadmill exercise. A-B) Subgross H&E images showing marked sclerotic change of the subchondral bone plate (blue line) and trabecular bone (red asterisks), stemming from around the pin tracts (black asterisk). C) Minimal subchondral bone plate remodeling and sclerosis are seen in this distant section, with the blue line present for comparison to the other two sections which were taken from areas adjacent to the pin tracts.

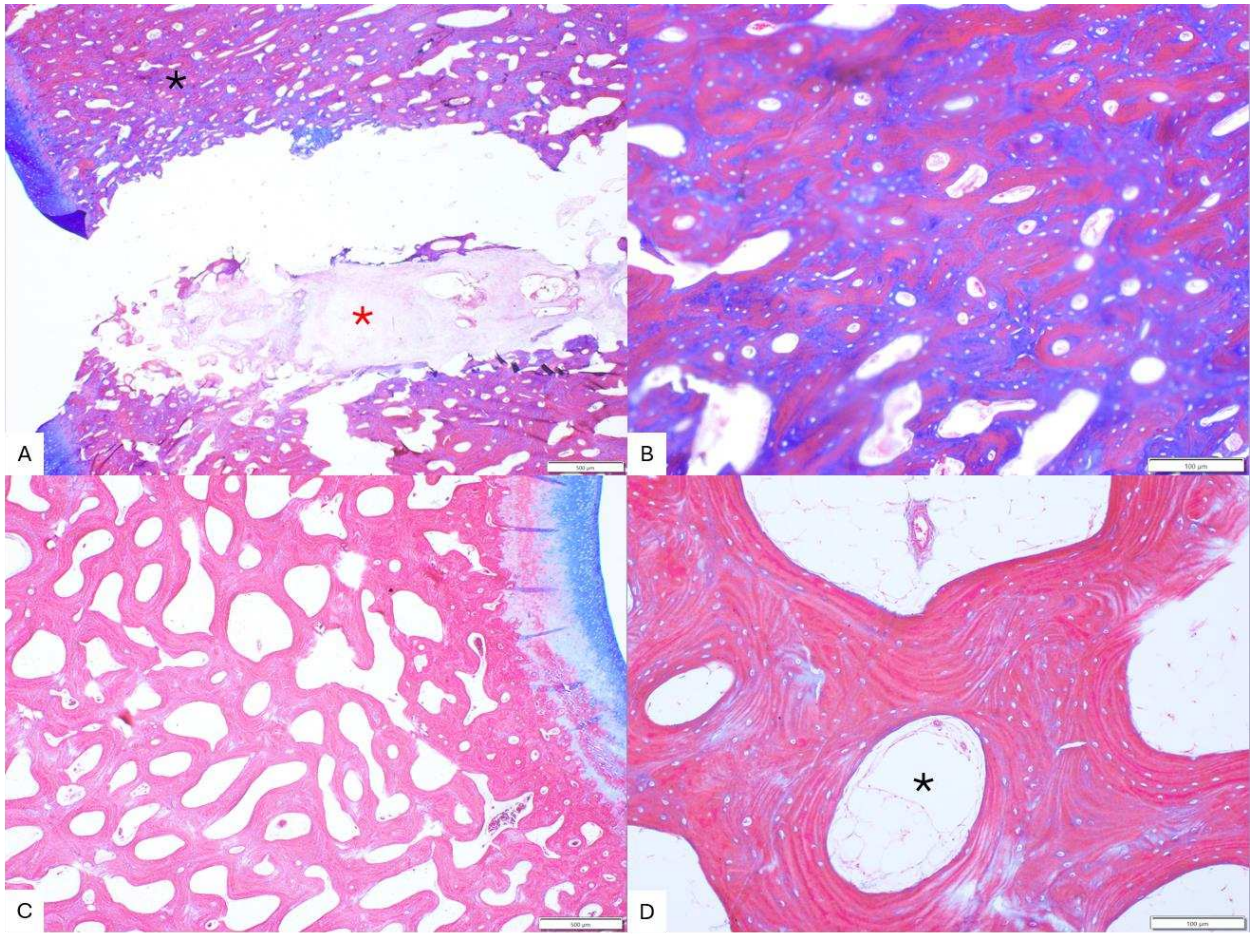

Figure 5.20 – Digital histology images (Masson's trichrome stain) taken from the proximal half of the pin tract (PT) of the left medial third metacarpal (MC3) condyle (**A-B**; grade 2/3 woven bone) and from at least 5mm proximal and distant to the pin tract (PD) of the right lateral MC3 condyle (**C-D**; grade 0/3 woven bone) of horse #1. A) Subgross image of the pin tract showing fibroplasia (red asterisk) and corresponding trabecular bony sclerosis (black asterisk). B) Higher magnification image showing a lack of medullary cavities with poorly formed bone. There is increased deposition of newly formed, non-mineralized bone (blue staining), indicating active boney remodeling and sclerosis. C) Subgross image in which no tract is present, with minimal to mild sclerosis of the subchondral plate and trabecular bone. D) Higher magnification image in which there are clear medullary spaces (black asterisk) with well-formed trabecular bone that is mineralized (red staining).

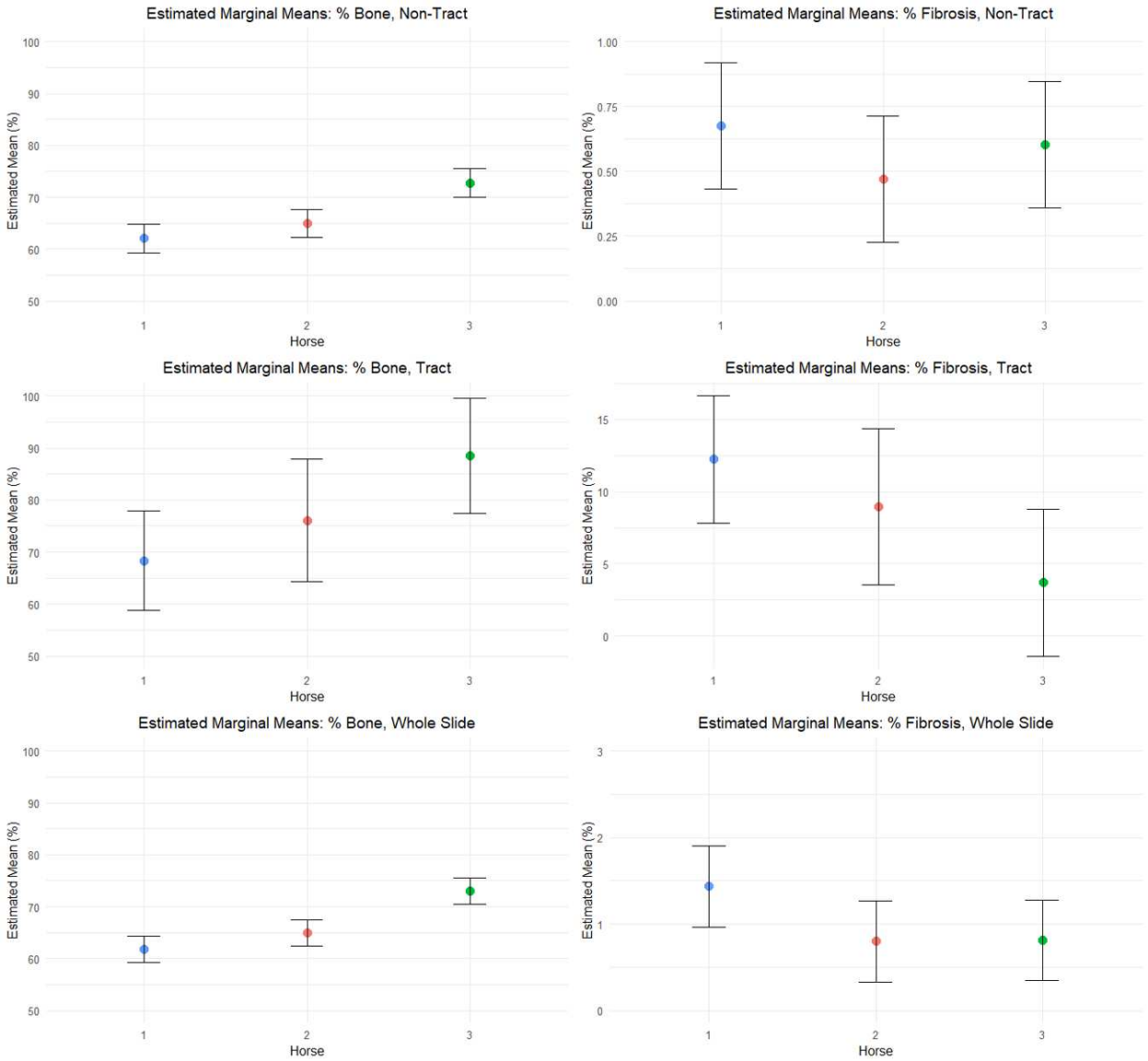

Figure 5.21 – Plots showing the estimated marginal means (95% CI) for the histomorphometric data obtained using Visiopharm, specifically, the comparisons between horses for the % bone and % fibrosis in the tissue outside the pin tract, the tissue within the pin tract, and the whole tissue specimen on each slide. The percentage of bone outside of the pin tract and across the whole slide were greater in horse #3 compared to horse #1 and horse #2 ($p < 0.001$). There were no significant differences in the percentage of bone between horses #1 and #2 ($p > 0.10$) for these two outcomes. The percentage of bone within the pin tract was significantly greater in horse #3 compared to horse #1 ($p = 0.0345$), but there were no significant differences between horses #1 and #2 ($p = 0.4664$) or between horses #2 and #3 ($p = 0.2352$). There were no significant differences in the percent fibrosis outside the pin tract, or overall, between horses ($p > 0.05$), but there was significantly more fibrosis in the pin tracts of horse #3 compared to horse #1 ($p = 0.0476$). There were no significant differences in the % fibrosis within the pin tracts between horse #2 and horses #1 and #3 ($p > 0.10$).

5.6 Tables

Table 5.1 – Modified scoring system of pathology of the distal third metacarpal (MC3) condyles and associated structures, adapted from Table 1 by Pinchbeck et al.[2] The original grading system was used to grade forelimb and hind limb POD lesions on postmortem examination of Thoroughbred racehorses, and has been adapted to better address the changes observed in this study following the experimental induction of bone marrow lesions combined with 6-months of high-speed treadmill exercise. The condyles of each forelimb were graded individually.

Feature	Score	Description
Palmar osteochondral disease	0	Normal
	1	Discoloration (bruising) of subchondral bone only; no or minimal disruption of overlying articular cartilage
	2	Discoloration (bruising), with mild to moderate disruption of articular cartilage
	3	Established palmar osteochondral disease lesions. Discoloration and disruption/collapse of articular surface
Wear lines (distal condyles, proximal sesamoid bones, and proximal phalanx)	0	Normal, i.e. wear lines absent
	1	Partial-thickness wear lines in cartilage
	2	Full-thickness wear lines in cartilage
Cartilage loss associated with MC3 (transverse ridge)	0	Normal
	1	Partial-thickness cartilage loss (fibrillation)
	2	Full-thickness cartilage loss (ulceration)
	3	Extensive full-thickness cartilage loss, with exposure of the subchondral bone
Cartilage loss associated with MC3 (parasagittal groove)	0	Normal
	1	Partial-thickness cartilage loss (fibrillation)
	2	Full-thickness cartilage loss (ulceration)
	3	Extensive full-thickness cartilage loss, with exposure of the subchondral bone
Cartilage loss associated with MC3 (central condylar region)	0	Normal
	1	Partial-thickness cartilage loss (fibrillation)
	2	Full-thickness cartilage loss (ulceration)
	3	Extensive full-thickness cartilage loss, with exposure of the subchondral bone
Linear fissures (within parasagittal grooves)	0	Normal
	1	Faint groove, with intact cartilage visible along length
	2	Well-defined groove, with partial thickness split in cartilage
	3	Well-defined groove, with full-thickness split in cartilage
Marginal remodeling of proximal sesamoid bones	0	Normal/marginal remodeling absent
	1	Marginal remodeling present
Dorsal impact injuries (dorsoproximal aspect of proximal phalanx against dorsodistal aspect of MC3)	0	Normal
	1	Mild (thickening/inflammation of synovial pad and mild scalloping of underlying MC3; mild erosion of dorsoproximal proximal phalanx)
	2	Severe (thickened, inflamed synovial pad and marked scalloping of MC3; full-thickness cartilage loss and/or chip fracture of dorsoproximal proximal phalanx)
Cartilage loss associated with proximal sesamoid bones	0	Normal
	1	Partial-thickness cartilage loss (fibrillation)
	2	Full-thickness cartilage loss (ulceration)
	3	Extensive full-thickness cartilage loss, with exposure of the subchondral bone
Tendon and ligament in gross sample	0	Normal
	1	Inflammation
	2	Grossly enlarged
	3	Ruptured
Total composite score	0-26	Sum of the scores for the above parameters
Cartilage loss associated with MC3 (total score)	0-9	Sum of the scores for rows 3-5 above grading cartilage loss associated only with MC3

Table 5.2 – Macroscopic OARSI scoring system to describe gross changes on the distal condyles of the third metacarpal bone of horses, adapted from Table III by McIlwraith et al[12] to also include a total composite score. The medial and lateral condyle of each forelimb was graded individually.

Lesion	Grade	Description
Wear lines	0	None
	1	1 or 2 partial-thickness wear lines per joint surface
	2	3-5 partial-thickness or 1-2 full-thickness wear lines per joint surface
	3	> 5 partial-thickness or > 2 full-thickness wear lines per joint surface
Erosions	0	None
	1	Partial-thickness erosion, < 5 mm in diameter
	2	Partial-thickness erosion, > 5 mm in diameter
	3	Full-thickness erosion
Palmar arthrosis (osteochondral lesions on the distal palmar aspect of the metacarpus)	0	None
	1	Partial-thickness erosion, < 5 mm in diameter
	2	Partial-thickness erosion, purple discoloration, > 5 mm in diameter
	3	Full-thickness erosion, purple discoloration, > 5 mm in diameter
Total composite score	0-9	Sum of the scores for the above parameters

Table 5.3 – The height, reported as the number of 37 um slices, of each 3-mm-diameter cylindrical volume of interest (VOI) analyzed on microcomputed tomography. The height had to be adjusted for some of the distal VOIs of the more distally-located pin tracts in horse #3 due to the amount of available bone. *Subchondral bone (SCB).*

Horse	Forelimb	Condyle	Volume of Interest Location								
			Tip of Tract	Abaxial SCB	Axial SCB	Proximal SCB	Distal SCB	Abaxial Mid-Tract	Axial Mid-Tract	Proximal Mid-Tract	Distal Mid-Tract
Horse #1	Left	Lateral	81	81	81	81	81	81	81	81	81
		Medial	81	81	81	81	81	81	81	81	81
	Right	Lateral	81	81	81	81	81	81	81	81	81
		Medial	81	81	81	81	81	81	81	81	81
Horse #2	Left	Lateral	81	81	81	81	81	81	81	81	81
		Medial	81	81	81	81	81	81	81	81	81
	Right	Lateral	81	81	81	81	81	81	81	81	81
		Medial	81	81	81	81	81	81	81	81	81
Horse #3	Left	Lateral	81	81	81	81	30	81	81	81	60
		Medial	81	81	81	81	21	81	81	81	50
	Right	Lateral	81	81	81	81	55	81	80	81	81
		Medial	81	81	81	81	81	81	81	81	81
Control	Left	Lateral	81	81	81	81	81	81	81	81	81
		Medial	81	81	81	81	81	81	81	81	81
	Right	Lateral	81	81	81	81	81	81	81	81	81
		Medial	81	81	81	81	81	81	81	81	81

Table 5.4 – Scoring system used to describe the overall appearance of the subchondral bone plate, as published by Aho et al,[11] with higher grades corresponding to more advanced subchondral bone changes.

Grade	Description
0	Normal or very early stage of osteoarthritis (OA). No evidence of subchondral bone sclerosis, thin subchondral bone plate and trabeculae. Articular cartilage is directly connected to bone marrow via open fenestrae in subchondral bone.
1	Some subchondral bone sclerosis and bone volume is increased. Thickened bone trabeculae can be seen. Cartilage contact with bone marrow persists.
2	A distinct increase in subchondral sclerosis and bone volume. Fibrillation can be seen in subchondral bone plate. No contact of bone marrow to articular cartilage can be identified.
3	Late-stage disease. Severe subchondral sclerosis and massively increased bone volume. Bone marrow distance from cartilage increases. Subchondral bone plate flattens.

Table 5.5 – Semi-objective microscopic grading rubric for articular cartilage adapted from the equine OARSI guidelines (Table V, McIlwraith et al.[12]). Additional parameters were selectively added to this table from those described by Little et al.[21] and Pinilla et al.[9] A total composite score was also added.

Parameter	Score	Description
Chondrocyte necrosis*	0	Normal section without necrosis
	1	No more than one necrotic cell located near the articular surface per 20x objective
	2	1-2 necrotic cells located near the articular surface per 20x objective
	3	2-3 necrotic cells located near the articular surface per 20x objective
	4	3-4 necrotic cells located near the articular surface per 20x objective
Cluster (complex chondrone) formation	0	No cluster formation throughout section
	1	Two chondrocytes (doublets) within same lacunae along superficial aspect of the articular cartilage section
	2	2-3 chondrocytes (doublets & triplets) within same lacunae along superficial aspect of the articular cartilage section
	3	3-4 chondrocytes within same lacunae along superficial aspect of the articular cartilage section
	4	Greater than 4 chondrocytes within same lacunae along superficial aspect of the articular cartilage section
Fibrillation/fissuring	0	No fibrillation/fissuring of the articular cartilage surface
	1	Fibrillation/fissuring of the articular cartilage restricted to surface and superficial zone
	2	Fissuring that extends into the middle zone
	3	Fissuring that extends to the level of the deep zone
	4	Fissuring that extends into the deep zone
Focal cell loss*	0	Normal cell population throughout the section
	1	A 10-20% area of acellularity per 20x field
	2	A 20-30% area of acellularity per 20x field
	3	A 40-50% area of acellularity per 20x field
	4	A greater than 50% area of acellularity per 20x field
Toluidine blue stain uptake	0	Normal staining
	1	Less than25% loss of staining characteristics
	2	25-50% loss of staining characteristics
	3	50-75% loss of staining characteristics
	4	Greater than 75% loss of staining characteristics
Chondrocyte density & distribution	0	Normal density with orderly distribution
	1	Areas of increased or mildly decreased chondrocytes
	2	Areas with a moderate decrease or variation in chondrocytes
	3	Areas with a severe decrease or variation in chondrocytes
	4	No cells
Tidemark/Calcified cartilage/Subchondral bone	0	Intact subchondral bone plate + single tidemark
	1	Intact subchondral bone plate + duplicated tidemark
	2	Blood vessels penetrate through subchondral bone plate to calcified cartilage
	3	Tidemark penetrated by blood vessels
Irregularity of articular surface	0	Normal
	1	Mild
	2	Moderate
	3	Severe
Articular cartilage thickness variation	0	Expected thickness for the area
	1	Mild variations
	2	Moderate variations
	3	Severe, extensive or focal variations (e.g. cartilage plugs)
Total composite score	0-33	Sum of the scores for the above parameters

*Chondrocyte necrosis is used to grade the presence of lacunae with necrotic nuclei still present compared to focal cell loss which is most likely an extension of the pathologic change but lacunae or nuclei are no longer present.

Table 5.6 – Microscopic scoring rubric for osteochondral sections modified from Table VII by McIlwraith et al.[12] to more better address osteochondral changes observed in this study associated with lesions created using the pin penetration model. A total composite score was also added.

Parameter	Score	Description
Osteochondral changes	0	No visible changes in cartilage or bone
	1	Minor disruption of subchondral bone matrix. Lesion occupies < 25% of histologic condylar surface and extends no more than 1-2mm deep to the normal chondrosseous junction. Occasional marrow spaces contain debris. Tidemark is reduplicated. No apparent superficial cartilage fibrillation.
	2	Moderate disruption of subchondral bone matrix. Areas of matrix are fragmented to comminuted and there is a moderate amount of debris within the marrow spaces. The tidemark is reduplicated and may be disrupted. Lesion occupies 25-50% of histologic condylar surface and extends approximately 2-4mm deep to the normal osteochondral junction. The cartilage overlying the lesion is thickened with superficial erosion and fibrillation. Reparative fibrocartilage may be apparent in the superficial cartilage layers.
	3	Lesion occupies >50% of histologic condylar surface and extends over 4mm deep to the normal osteochondral junction. Severe disruption of subchondral bone matrix with pale staining and abundant fibrin. The tidemark is reduplicated and often disrupted. Superficial thickening of cartilage and/or fibrocartilage present which may be completely detached from thickened deeper cartilage.
	4	Complete loss of osteochondral tissues.
Subchondral bone remodeling	0	No visible changes in cartilage or bone
	1	Advancement of the subchondral bone into the calcified cartilage layer with scalloped subchondral bone margins, but not crossing any tidemarks
	2	Subchondral bone advancement through the calcified cartilage layer, crossing one or more tidemarks but below the most superficial tidemark front
	3	Subchondral bone advancement through the calcified cartilage layer and disruption of the tidemark front
Osteochondral splitting	0	No visible changes in cartilage or bone
	1	Involve the tidemark and subchondral bone, but are simple, linear defects
	2	Have fragments and debris within the split and connections between splits
	3	Involve articular cartilage and displacement of calcified cartilage fragments into the underlying subchondral bone
Total composite score	0-10	Sum of the scores for the above parameters

Table 5.7 – Microscopic scoring rubric for changes in the calcified cartilage layer as published by Pinilla et al.[9] A total composite score was also added.

Parameter	Score	Description
Clefts	0	Absence of clefts
	1	Occasional focal clefts
	2	Moderate number of clefts
	3	Large number of clefts
Variations in depth	0	Expected variations in depth
	1	Minimal variation
	2	Moderate variation
	3	Severe variations
Tidemark incongruencies	0	Expected pattern of the tidemark
	1	Lack of parallelism
	2	Reduplication
	3	Absence
Vascular incursions at the subchondral bone-calcified cartilage interface	0	No incursion
	1	Occasional
	2	Moderate numbers
	3	Very frequent
Island of hyaline cartilage present in the subchondral bone plate	0	No islands
	1	Occasional, small islands
	2	Large single cartilage islands of calcified cartilage in the subchondral bone
	3	Numerous islands of calcified cartilage in the subchondral bone
Total composite score	0-15	Sum of the scores for the above parameters

Table 5.8 – Microscopic scoring rubric for changes in the subchondral and trabecular bone as published by Pinilla et al.[9] A total composite score was also added.

Parameter	Score	Description
Sclerosis of the subchondral plate and adjacent cancellous bone	0	No sclerosis
	1	Mild, focal sclerosis
	2	Moderate, focal to more extensive sclerosis
	3	Severe sclerosis, extending into non-weightbearing areas
Areas of subchondral bone collapse	0	No collapse
	1	Small, discrete areas of collapse
	2	Focal necrosis of the subchondral plate and minor hemorrhage
	3	Collapse of the subchondral plate with hemorrhage/haematoidin
Obliteration of cancellous areas with compact bone	0	Expected width of the cancellous areas
	1	Focal and minimal
	2	Moderate
	3	Marked and/or in areas that bear no weight
Replacement with woven bone	0	No presence of woven bone
	1	Occasional discrete areas of woven bone
	2	Moderate, focal to more extensive replacement with woven bone
	3	Marked replacement with woven bone
Replacement with osteonal bone	0	No lamellar bone deposit
	1	Minimal
	2	Moderate, focal to more extensive
	3	Marked deposition of lamellar bone
Increase in trabecular width with reduction of marrow spaces	0	No thickening of trabeculae
	1	Focal and minimal
	2	Moderate thickening
	3	Marked thickening and thickening in areas that bear no weight
Presence of microcracks in the cancellous bone	0	No microcracks
	1	Localized
	2	Moderate numbers
	3	Large numbers of microcracks in cancellous bone
Presence of Howship's lacunae with or without osteoclasts	0	No lacunae
	1	Discrete and few
	2	Multifocal
	3	Numerous resorption lacunae
Total Composite Score	0-24	Sum of the scores for the above parameters

Table 5.9 – Gross evaluation was performed of each third metacarpal condyle using two previously published grading scales for evaluation of palmar osteochondral disease (Pinchbeck et al.[2]; Table 5.1) and the palmarodistal third metacarpal condyles (McIlwraith et al.[12]; Table 5.2). A) Gross grades assigned to each third metacarpal condyle using the scoring system shown in Table 5.1. The originally published table was modified to grade cartilage loss on three regions of the palmar condyle separately, and to include both a composite score for this cartilage loss and a total score summed from all outcome parameters. B) Gross grades assigned to each third metacarpal condyle using the OARSI scoring system shown in Table 5.2. A total composite score for this table was also included.

A)

Horse	Limb	Condyle	POD (0-3)	Wear Lines (0-2)	Cartilage Loss, MC3			Linear Fissures (0-3)	PSB Remodeling (0-1)	DII (0-2)	Cartilage Loss, PSBs (0-3)	Tendon & Ligament (0-3)	Total Overall Score (0-26)	Total Score, MC3 Cartilage Loss (0-9)
					Condyle (0-3)	TR (0-3)	PSG (0-3)							
Horse 1	Left	Medial	1	1	0	0	0	1	0	1	2	0	6	0
		Lateral	1	1	0	0	0	1	0	1	1	0	5	0
	Right	Medial	1	1	0	1	1	1	0	1	2	0	8	2
		Lateral	1	1	0	1	1	1	0	1	2	0	8	2
Horse 2	Left	Medial	1	0	1	0	0	0	0	1	1	0	4	1
		Lateral	1	0	1	0	0	1	0	1	1	0	5	1
	Right	Medial	1	1	1	0	0	0	1	1	0	0	5	1
		Lateral	1	1	1	0	0	1	1	1	1	0	7	1
Horse 3	Left	Medial	2	1	2	2	0	1	1	0	2	0	11	4
		Lateral	2	1	2	2	2	2	0	0	1	0	12	6
	Right	Medial	1	1	1	1	0	1	1	0	1	0	7	2
		Lateral	1	1	1	1	1	1	0	0	1	0	7	3

Abbreviations: DII, dorsal impact injury; MC3; third metacarpal bone; POD, palmar osteochondral disease; PSB, proximal sesamoid bones; PSG, parasagittal grooves; TR, transverse ridge

B)

Horse	Limb	Condyle	Wear Lines (0-3)	Erosions (0-3)	Palmar Arthrosis (0-3)	Total Score (0-9)
Horse 1	Left	Medial	1	0	1	2
		Lateral	1	0	1	2
	Right	Medial	1	1	1	3
		Lateral	2	0	1	3
Horse 2	Left	Medial	0	1	1	2
		Lateral	0	1	1	2
	Right	Medial	1	1	1	3
		Lateral	1	2	1	4
Horse 3	Left	Medial	2	1	1	4
		Lateral	2	3	1	6
	Right	Medial	2	2	1	5
		Lateral	2	2	1	5

Table 5.10 – Overall mean value for each outcome parameter measured using microcomputed tomography (microCT), shown for each volume of interest and for each individual horse.

	BV/TV (%)	BS/BV (1/mm)	BMD (mgHA/cm^3)	TMD (mgHA/cm^3)	Tb.Th (mm)	Tb.Sp (mm)	Tb.N (1/mm)
Volume of Interest (VOI) – All Horses							
T	72.64	6.89	602.78	754.18	0.22	0.15	5.22
AbSCB	96.12	2.31	707.84	737.40	0.46	0.07	4.04
AxSCB	90.18	3.58	665.51	727.65	0.28	0.09	5.10
PrSCB	90.98	3.32	671.19	728.21	0.32	0.09	4.84
DiSCB	92.66	3.13	674.84	719.28	0.36	0.09	4.72
MidAb	90.49	3.31	688.44	753.53	0.33	0.09	4.75
MidAx	84.84	4.72	651.97	746.54	0.25	0.10	5.35
MidPr	81.87	5.25	639.16	744.50	0.25	0.12	5.02
MidDi	88.38	4.00	667.86	740.11	0.28	0.09	5.07
Mean	***87.57***	***4.06***	***663.29***	***739.04***	***0.30***	***0.10***	***4.90***
Volume of Interest (VOI) – Study Horses							
T	72.84	6.81	593.80	738.52	0.23	0.15	5.11
AbSCB	97.41	2.03	714.92	736.73	0.52	0.07	3.56
AxSCB	90.08	3.59	656.89	716.39	0.30	0.09	4.85
PrSCB	91.72	3.10	668.39	720.58	0.35	0.09	4.57
DiSCB	93.49	2.95	673.84	712.73	0.39	0.09	4.48
MidAb	92.44	2.82	691.88	745.66	0.36	0.09	4.50
MidAx	85.41	4.51	644.54	731.50	0.26	0.10	5.14
MidPr	82.31	5.05	631.15	731.85	0.27	0.12	4.84
MidDi	88.11	4.02	658.26	728.15	0.29	0.10	4.84
Mean	***88.20***	***3.87***	***659.30***	***729.12***	***0.33***	***0.10***	***4.65***
Volume of Interest (VOI) – Control Horse							
T	72.04	7.14	629.74	801.14	0.20	0.14	5.58
AbSCB	92.23	3.15	686.62	739.42	0.26	0.07	5.49
AxSCB	90.50	3.55	691.35	761.41	0.23	0.06	5.82
PrSCB	88.74	3.96	679.59	751.11	0.24	0.07	5.67
DiSCB	90.16	3.67	677.85	738.94	0.26	0.07	5.45
MidAb	84.64	4.78	678.12	777.16	0.23	0.09	5.51
MidAx	83.11	5.35	674.25	791.65	0.21	0.09	5.98
MidPr	80.53	5.86	663.18	782.43	0.21	0.11	5.57
MidDi	89.19	3.93	696.67	776.01	0.23	0.07	5.74
Mean	***85.68***	***4.60***	***675.26***	***768.81***	***0.23***	***0.09***	***5.64***
Horse							
Horse 1	87.69	3.56	723.10	794.15	0.39	0.13	3.85
Horse 2	87.41	4.14	610.19	679.37	0.33	0.10	4.79
Horse 3	89.50	3.92	644.60	713.85	0.28	0.08	5.32
Control	85.68	4.60	675.26	768.81	0.23	0.09	5.64

Abbreviations: AbSCB, abaxial subchondral bone; AxSCB, axial subchondral bone; BMD, bone mineral density; BS/BV, bone surface to volume ratio; BV/TV, bone volume fraction; DiSCB, distal subchondral bone; MidAb, abaxial mid-tract; MidAx, axial mid-tract; MidDi, distal mid-tract; MidPr, proximal mid-tract; PrSCB, proximal subchondral bone; T, tip of the tract; Tb.N, trabecular number; Tb.Sp, trabecular spacing; Tb.Th, trabecular thickness; TMD, tissue mineral density

Table 5.11 – Overall mean value for each outcome parameter measured using histopathology, shown for each individual horse and for each slice location (PT, PD, DT, DD).

	Horse 1	Horse 2	Horse 3	PT	PD	DT	DD
Subchondral Bone Disease (Table 5.4)							
Subchondral bone changes (0-3)	2.31	2.19	2.19	2.75	1.58	2.67	1.92
Articular Cartilage (Table 5.5)							
Chondrocyte necrosis (0-4)	0.75	0.81	1.0	1.33	0.58	1.17	0.33
Cluster (complex chondrone) formation (0-4)	1.44	1.19	1.38	1.5	1.08	1.67	1.08
Fibrillation/fissuring (0-4)	2.19	2.0	1.81	3.17	1.17	2.5	1.17
Focal cell loss (0-4)	1.19	1.19	1.13	1.58	0.92	1.42	0.75
Toluidine blue stain uptake (0-4)	1.38	1.67	1.29	1.75	1.0	1.67	1.33
Chondrocyte density & distribution (0-4)	1.0	0.81	0.75	1.17	0.42	1.25	0.58
Tidemark/calcified cartilage/subchondral bone (0-3)	0.94	1.63	2.31	1.92	1.50	1.67	1.42
Irregularity of articular surface (0-3)	0.75	0.69	0.81	1.0	0.42	1.08	0.50
Articular cartilage thickness variation (0-3)	0.56	0.50	0.63	0.67	0.25	0.92	0.42
Composite Score (0-33)	**10.19**	**10.38**	**10.94**	**14.08**	**7.33**	**13.33**	**7.25**
Osteochondral Unit (Table 5.6)							
Osteochondral changes (0-4)	1.19	1.50	1.31	2.0	0.67	2.0	0.67
Subchondral bone remodeling (0-3)	1.13	1.19	1.75	1.92	1.0	1.50	1.0
Osteochondral splitting (0-3)	0.31	0.44	0.69	1.0	0.08	0.83	0
Composite Score (0-10)	**2.63**	**3.13**	**3.75**	**4.92**	**1.75**	**4.33**	**1.67**
Calcified Cartilage (Table 5.7)							
Clefts (0-3)	0.19	0.38	0.69	0.83	0.08	0.75	0
Variations in depth (0-3)	0.75	0.75	0.81	1.0	0.42	1.08	0.58
Tidemark incongruencies (0-3)	1.31	1.75	2.06	1.75	1.67	1.83	1.58
Vascular incursions at subchondral bone-calcified cartilage interface (0-3)	1.06	1.06	1.44	1.5	0.83	1.25	1.17
Island of hyaline cartilage in subchondral bone plate (0-3)	0	0.06	0	0	0	0.08	0
Composite Score (0-15)	**3.31**	**4.0**	**5.0**	**5.08**	**3.0**	**5.0**	**3.33**
Subchondral and Trabecular Bone (Table 5.8)							
Sclerosis of subchondral plate and adjacent cancellous bone (0-3)	2.13	1.75	1.56	2.17	1.33	2.0	1.75
Areas of subchondral bone collapse (0-3)	1.0	0.94	0.88	1.83	0.08	1.75	0.08
Obliteration of cancellous areas with compact bone (0-3)	1.38	1.25	1.44	1.67	0.67	1.75	1.33
Replacement with woven bone (0-3)	0.63	0.38	0.63	1.25	0	0.92	0
Replacement with osteonal bone (0-3)	1.25	0.94	1.19	1.33	0.75	1.33	1.08
Increase in trabecular width with reduction of marrow spaces (0-3)	1.31	0.94	1.38	1.75	0.75	1.42	0.92
Presence of microcracks in the cancellous bone (0-3)	0	0	0	0	0	0	0
Presence of Howship's lacunae with or without osteoclasts (0-3)	0.69	0.38	0.38	1.08	0	0.83	0
Composite Score (0-24)	**8.38**	**6.56**	**7.44**	**11.08**	**3.58**	**10.0**	**5.17**
TOTAL HISTOLOGY SCORE (0-85)	26.81	26.25	29.31	37.92	17.25	35.33	19.33

Abbreviations: DD, distal distant; DT, distal tract; PD, proximal distant; PT, proximal tract

Table 5.12 – Histomorphometric data acquired from the Visiopharm analysis. The overall mean percent bone and percent fibrosis from three regions on each slide (outside of pin tract, within/around pin tract, whole tissue) are provided for each slice location and for each horse.

	% Bone, Non-Tract	% Fibrosis, Non-Tract	% Bone, Tract	% Fibrosis, Tract	% Bone, Whole Tissue	% Fibrosis, Whole Tissue
Slice Location						
Proximal tract	65.15	0.49	72.76	9.53	65.14	1.48
Proximal distant	66.03	0.68	N/A	N/A	65.85	0.68
Distal tract	68.81	0.54	80.47	8.19	69.12	1.28
Distal distant	66.27	0.61	N/A	N/A	66.25	0.61
Horse						
Horse 1	62.02	0.67	68.28	12.24	61.86	1.43
Horse 2	64.90	0.47	75.10	9.80	64.88	0.80
Horse 3	72.76	0.60	86.89	4.28	73.03	0.81

5.7 References

1. Ramzan PH. Mind the gaps: The science of POD and the racehorse fetlock. *Equine Vet J*. 2021;53:217-220.

2. Pinchbeck G, Clegg P, Boyde A, Riggs C. Pathological and clinical features associated with palmar/plantar osteochondral disease of the metacarpo/metatarsophalangeal joint in Thoroughbred racehorses. *Equine Vet J*. 2013;45:587-592.

3. Barr E, Pinchbeck G, Clegg P, Boyde A, Riggs C. Post mortem evaluation of palmar osteochondral disease (traumatic osteochondrosis) of the metacarpo/metatarsophalangeal joint in Thoroughbred racehorses. *Equine Vet J*. 2009;41:366-371.

4. Lin S-T, Bolas N, Peter V, et al. Comparison of cone-beam and fan-beam computed tomography and low-field magnetic resonance imaging for detection of palmar/plantar osteochondral disease in Thoroughbred horses. *Equine Vet J*. 2024;56:999-1007.

5. Pool R, Meagher D. Pathologic findings and pathogenesis and racetrack injuries. *Vet Clin North Am - Equine Pract*. 1990;6(1):1-30.

6. Riggs C. Osteochondral injury and joint disease in the athletic horse. *Equine Vet Educ*. 2006;18:100-112.

7. Riggs C, Whitehouse G, Boyde A. Pathology of the distal condyles of the third metacarpal and third metatarsal bones. *Equine Vet J*. 1999;31:140-148.

8. Muir P, Peterson A, Sample S, Scollay M, Markel M, Kalscheur V. Exercise-induced metacarpophalangeal joint adaptation in the Thoroughbred racehorse. *J Anat*. 2008;213:706-717.

9. Pinilla M, Tranquille C, Blunden A, Chang Y, Parkin T, Murray R. Histological Features of the Distal Third Metacarpal Bone in Thoroughbred Racehorses, With and Without Lateral Condylar Fractures. *J Comp Pathol*. 2017;157:1-10.

10. Norrdin R, Stover S. Subchondral bone failure in overload arthrosis: a scanning electron microscopic study in horses. *J Musculoskelet Neuronal Interact*. 2006;6(3):251-257.

11. Aho O-M, Finnila M, Thevenot J, Saarakkala S, Lehenkari P. Subchondral bone histology and grading in osteoarthritis. *PLoS One*. 2017;12(3):e0173726-e0173726.

12. McIlwraith C, Frisbie D, Kawcak C, Fuller C, Hurtig M, Cruz A. The OARSI histopathology initiative - recommendations for histological assessments of osteoarthritis in the horse. *Osteoarthr Cartil*. 2010;18:S93-S105.

13. Leahy P, Smith B, Easton K, et al. Correlation of mechanical properties within the equine third metacarpal with trabecular bending and multi-density micro-computed tomography data. *Bone*. 2010;46:1108-1113.

14. Martig A, Hitchens P, Stevenson M, Whitton R. Subchondral bone morphology in the metacarpus of racehorses in training changes with distance from the articular surface but not with age. *J Anat*. 2018;232:919-930.

15. Cox L, van Donkelaar C, van Rietbergen B, Emans P, Ito K. Alterations to the subchondral bone architecture during osteoarthritis: bone adaptation vs endochondral bone formation. *Osteoarthr Cartil*. 2013;21:331-338.

16. Pearce D, Hitchens P, Malekipour F, Ayodele B, Lee P, Whitton R. Biomechanical and microstructural properties of subchondral bone from three metacarpophalangeal joint sites in Thoroughbred racehorses. *Front Vet Sci*. 2022;9:923356-923356.

17. Stewart HL, Easley JT, Selberg KT, et al. Experimental models of bone marrow lesions in ovine femoral condyles. *Vet Surg*. 2023;52:284-298.

18. Martig S, Hitchens P, Lee P, Whitton R. The relationship between microstructure, stiffness and compressive fatigue life of equine subchondral bone. *J Mech Behav Biomed Mater*. 2020;101:103439.

19. Ayodele B, Malekipour F, Pagel C, Mackie E, Whitton R. Assessment of subchondral bone microdamage quantification using contrast-enhanced imaging techniques. *J Anat*. 2023;245:58-69.

20. Smith M, Dyson S, Murray RC. Reliability of high- and low-field magnetic resonance imaging systems for detection of cartilage and bone lesions in the equine cadaver fetlock. *Equine Vet J*. 2012;44:684-691.

21. Little C, Smith M, Cake M, Read R, Murphy M, Barry F. The OARSI histopathology initiative - recommendations for histological assessments of osteoarthritis in sheep and goats. *Osteoarthr Cartil*. 2010;18(3):S80-S92.

22. Mankin H, Dorfman H, Lippiello L, Zarins A. Biochemical and metabolic abnormalities in articular cartilage from osteoarthritic human hips. II. Correlation of morphology with biochemical and metabolic data. *J Bone Jt Surg*. 1971;53:523-537.

23. Bae W, Wong V, Hwang J, Antonacci J, Nugent-Derfus G, Blewis M. Wear-lines and split-lines of human patellar cartilage: relation to tensile biomechanical properties. *Osteoarthr Cartil*. 2008;16:841-845.

24. Kawcak C, McIlwraith C, Norrdin R, Park R, James S. The role of subchondral bone in joint disease: a review. *Equine Vet J*. 2001;33(2):120-126.

25. Norrdin R, Kawcak C, Capwell B, McIlwraith C. Subchondral bone failure in an equine model of overload arthrosis. *Bone*. 1998;22:133-139.

26. Dykgraaf S, Firth E, Rogers C, Kawcak C. Effects of exercise on chondrocyte viability and subchondral bone sclerosis in the distal third metacarpal and metatarsal bones of young horses. *Vet J*. 2008;178:53-61.

27. Easton K, Kawcak C. Evaluation of increased subchondral bone density in areas of contact in the metacarpophalangeal joint during joint loading in horses. *Am J Vet Res*. 2007;68(8):816-821.

28. Kawcak C, McIlwraith C, Norrdin R, Park R, Steyn P. Clinical effects of exercise on subchondral bone of carpal and metacarpophalangeal joints in horses. *Am J Vet Res*. 2000;61(10):1252-1258.

29. Norrdin R, Kawcak C, Capwell B, McIlwraith C. Calcified Cartilage Morphometry and Its Relation to Subchondral Bone Remodeling in Equine Arthrosis. *Bone*. 1999;24(2):109-114.

30. Berni M, Marchiori G, Massimiliano B, Gianluca G, Lopoma N. Biomechanics of the human osteochondral unit: A systematic review. *Materials (Basel)*. 2024;17(7):1698-.

31. Sanchez C, Pesesse L, Gabay O, et al. Regulation of Subchondral Bone Osteoblast Metabolism by Cyclic Compression. *Arthritis Rheum*. 2012;64(4):1193-1203.

32. Massicotte F, Aubry I, Martel-Pelletier J, Pelletier J, Fernandes J, Lajeunesse D. Abnormal Insulin-like Growth Factor 1 Signaling in Human Osteoarthritic Subchondral Bone Osteoblasts. *Arthritis Res Ther*. 2006;8(6):R177.

33. Zhang L, Wen C. Osteocyte Dysfunction in Joint Homeostasis and Osteoarthritis. *Int J Mol Sci*. 2021;22(12):6522.

34. Boyde A. The real response of bone to exercise. *J Anat*. 2003;203:173-189.

35. Radin E, Rose R. Role of subchondral bone in the initiation and progression of cartilage damage. *Clin Orthop Relat Res*. 1986;213:34-40.

36. Ciamillo S, Wulster K, Gassert T, et al. Prospective, longitudinal assessment of subchondral bone morphology and pathology using standing, cone-beam computed tomography in fetlock joints of 2-year-old Thoroughbred racehorses in their first year of training. *Equine Vet J*. 2025;57:126-139.

37. Janes J, Kennedy L, Garrett K, Engiles J. Common lesions of the distal end of the third metacarpal/metatarsal bone in racehorse catastrophic breakdown injuries. *J Vet Diagnostic Investig*. 2017;29(4):431-436.

38. Whitton R, Trope G, Ghasem-Zadeh A, et al. Third metacarpal condylar fatigue fractures in equine athletes occur within previously modelled subchondral bone. *Bone*. 2010;47(4):826-831.

39. Stover S. Skeletal Injuries in Equine Athletes - Pathogenesis and Training Concepts for Injury Prevention. In: *Proceedings of the 68th Annual Convention of the American Association of Equine Practitioners*. ; 2022:95-104.

40. Martig S, Chen W, Less P, Whitton RC. Bone fatigue and its implications for injuries in

racehorses. *Equine Vet J*. 2014;46:408-415.

41. Drum M, Les C, Park R, Norrdin R, McIlwraith C, Kawcak C. Correlation of quantitative computed tomographic subchondral bone density and ash density in horses. *Bone*. 2009;44(2):316-319.

42. Rubio-Martinez L, Cruz A, Gordon K, Hurtig M. Structural characterization of subchondral bone in the distal aspect of third metacarpal bones from Thoroughbred racehorses via micro–computed tomography. *Am J Vet Res*. 2008;69(11):1413-1422.

43. Muller-Gerbl M. The subchondral bone plate. *Adv Anat Embryol Cell Biol*. 1998;141:III-XI.

44. Haseltine K, Chukir T, Smith P, Jacob J, Bilezikian J, Farooki A. Bone Mineral Density: Clinical Relevance and Quantitative Assessment. *J Nucl Med*. 2021;62(4):446-454.

45. Bouxsein M, Boyd S, Christiansen B, Guldberg R, Jepsen K, Muller R. Guidelines for assessment of bone microstructure in rodents using micro-computed tomography. *J Bone Min Res*. 2010;25(7):1468-1486.

46. Sherry Liu X, Tseng W-J. MicroCT 101: How to get most out of your scans. 2019.

47. Firth E, Rogers C, van Weeren PR, et al. The effect of previous conditioning exercise on diaphyseal and metaphyseal bone to imposition and withdrawal of training in young Thoroughbred horses. *Vet J*. 2012;192:34-40.

48. Porr C, Kronfeld D, Lawrence L, Pleasant R, Harris P. Deconditioning reduces mineral content of the third metacarpal bone in horses. *J Anim Sci*. 1998;76:1875-1879.

49. Holmes J, Mirams M, Mackie E, Whitton R. Thoroughbred horses in race training have lower levels of subchondral bone remodelling in highly loaded regions of the distal metacarpus compared to horses resting from training. *Vet J*. 2014;202:443-447.

50. Rowe P, Koller A, Sharma S. Physiology, Bone Remodeling. In: *StatPearls [Internet]*. StatPearls. Treasure Island (FL): StatPearls Publishing; 2023.

51. Nunamaker D. Relationships of exercise regimen and racetrack surface to modeling/remodeling of the third metacarpal bone in two year old Thoroughbred racehorses. *Vet Comp Orthop Traumatol*. 2002;15:195-199.

52. Riggs C, Boyde A. Effect of exercise on bone density in distal regions of the equine third metacarpal bone in 2-year-old thoroughbreds. *Equine Vet J*. 1999;31(S30):555-560.

53. Boyde A, Riggs C, Firth E. Densification by infilling marrow space in response to exercise in thoroughbred horse distal cannon bone. *Bone*. 2001;28:S110-S110.

54. Whitton R, Mirams M, Mackie E, Anderson G, Seeman E. Exercise-induced inhibition of remodelling is focally offset with fatigue fracture in racehorses. *Osteoporos Int*.

2013;24:2043-2048.

55. Whitton R, Ayodele B, Hitchens P, Mackie E. Subchondral bone microdamage accumulation in distal metacarpus of Thoroughbred racehorses. *Equine Vet J*. 2018;50:766-773.

56. Drum M, Kawcak C, Norrdin R, Park R, McIlwraith C, Les C. Comparison of gross and histopathologic findings with quantitative computed tomographic bone density in the distal third metacarpal bone of racehorses. *Vet Radiol Ultrasound*. 2007;48(6):518-527.

57. Kawcak C, McIlwraith C, Firth E. Effects of early exercise on metacarpophalangeal joints in horses. *Am J Vet Res*. 2010;71(4):405-411.

58. Rice H, Brokken M, Hostnik E, Bertone A. Evaluation of a novel bone substitute injection technique for potential treatment of impact injury to the equine palmar metacarpal condyle. *Vet Comp Orthop Traumatol*. 2019;32(6):447-453.

59. Rickey EJ, Cruz A, Trout D, McEwen B, Hurtig M. Evaluation of experimental impact injury for inducing post-traumatic osteoarthritis in the metacarpophalangeal joints of horses. *Am J Vet Res*. 2012;73(10):1540-1552.

60. Reed S, Jackson B, McIlwraith C, et al. Descriptive epidemiology of joint injuries in Thoroughbred racehorses in training. *Equine Vet J*. 2012;44:13-19.

61. Buyuksungur A, Szabo B, Dobai A, Orhan K. The Effect of Micro-Computed Tomography Thresholding Methods on Bone Micromorphometric Analysis. *J Funct Biomater*. 2024;15(11):343.

CHAPTER 6:

CONCLUSIONS AND FUTURE DIRECTIONS

6.1 Summary & Conclusions

An overview of the equine metacarpophalangeal joint, the response of subchondral bone to exercise, and the pathophysiology behind repetitive stress injury are provided in Chapter 1. In addition, Chapter 1 also described the pathophysiology and significance of palmar osteochondral disease in horses. Palmar osteochondral disease (POD) is a chronic fatigue injury of the subchondral bone of the palmaro/plantarodistal third metacarpal/metatarsal (MC3/MT3) condyles that is highly prominent amongst the racehorse population. There is a wide spectrum of disease severity ranging from subtle alterations in bone remodeling to subchondral bone attrition and complete collapse of the articular surface. Subchondral bone marrow lesions (BMLs) have been shown to be predictive of subchondral attrition, and to precede and be associated with fatigue injury in the subchondral bone.[1–3] The development and progression of this disease tend to be unpredictable, with the time to lesion progression, the degree and timing of clinical effects, and the severity of the disease process varying between individual horses. A successful experimental model for inducing POD lesions does not yet exist and most involve the use of impact devices that injure articular cartilage.[4,5] Since there is little to no overlying cartilage damage in the early stages of POD,[6] an experimental technique that produces subchondral bone changes, in a minimally-invasive manner, without diffusely affecting cartilage at the time of lesion induction is critical. The development of an experimental model of POD, or repetitive stress injury in general, that would allow researchers to study the progression in a controlled, prospective manner would open the doors for future studies on variables that may affect an

individual horse's risk of injury, and facilitate development of an optimized treatment plan. A reliable, minimally-invasive pin penetration model was developed to induce BMLs in the femoral condyles of sheep[7] and rats with minimal damage to the articular cartilage and surrounding structures. As a novel extension of this work, the purpose of this pilot study was to provide *in vivo* proof of concept of this experimental model, combined with 6-months of high-speed treadmill exercise, in the distal MC3 condyles of horses. The central objective was to develop an experimental model of repetitive stress injury in horses that mimics the early stages of clinical disease. Chapter 2 focused on the preliminary work leading up to the present pilot study, as well as details surrounding study design and analysis.

The results of this preliminary pilot study confirmed that the pin penetration model – which involved using a 1.1 mm Steinmann pin to create an osteochondral defect that extended approximately 8mm from the articular surface into the trabecular bone – combined with 6 months of high-speed treadmill exercise, consistently resulted in the development of BMLs in the palmarodistal MC3 condyles of horses, which were present throughout the course of the study. Importantly, this study showed that lesion induction using this technique did not incite an overtly pathologic response when measured as early as 2 weeks postoperatively. Chapter 3 described the clinical effects of this experimental model including lameness evaluation and synovial fluid analysis. This was followed by Chapter 4, which described the appearance and progression of the induced BMLs on diagnostic imaging throughout the study period including digital radiography, magnetic resonance imaging (MRI), and computed tomography (CT). Lastly, at the end of the 6-month study period, post-mortem evaluation was performed including gross evaluation of the joint surface, microcomputed tomography (microCT) for trabecular

morphometry analysis of the bone surrounding the pin tracts, and histopathology of the regions adjacent to and distant from the pin tracts. These findings were discussed in Chapter 5.

Similar to POD, this model induced a dynamic, mild to moderate, bilateral forelimb lameness that persisted, though to variable degrees. This corresponded to an increased response to flexion, increased joint effusion and a reduction in range of motion, with the latter proving to be a later development compared to the remaining parameters. Additionally, the general plateau in clinical signs seen here, despite continued training without treatment, has also been reported in some cases of POD.[8] In contrast to early POD, localizing clinical signs including effusion and a positive response to flexion developed as early as 2-4 weeks, postoperatively. Being a primary disease of the subchondral bone, these localizing clinical signs typically do not occur until significant damage to the articular cartilage has occurred.[9–13] The early development of these signs is suspected to be due to the nature of the model, in which a direct communication between the subchondral bone and the rest of the joint is created at the time of lesion induction, potentially resulting in the increased release of inflammatory mediators. While this communication was suspected to have been sealed early in the postoperative period based on diagnostic imaging, it is also possible that the combination of subchondral bone injury and focal articular cartilage healing resulted in the continuation of clinical signs. Since histopathology was not performed at all time points in this study, and without further analysis to determine the level of communication between the subchondral bone and the joint fluid at various stages, definitive conclusions cannot be made. When evaluating the response using synovial fluid analysis, the total nucleated cell counts were near or below the upper limits of the reference interval (1,000 cells/uL), with the range of overall means across all horses being 467 to 1,117 cells/uL. The total protein in the synovial fluid also fell at or below the reference limit of 2.5 g/dL, with a total

protein above 2.5 g/dL in only 7 out of 48 total samples at weeks 4 and 12. Despite the focal trauma to the articular surface and corresponding communication into the subchondral and trabecular bones, the inflammatory response was fairly mild. Findings from this experimental model were consistent with a primarily mononuclear response, consisting of lymphocytes (small mononuclear cells) and large mononuclear cells; however, synovial fluid analysis could also be considered within reference limits depending on the horse, limb, and postoperative time point. This is indicative of a non-inflammatory arthropathy, such as that from degenerative or traumatic joint diseases, that produces a mild nonsuppurative response often indistinguishable from normal synovial fluid.[14] Findings that helped distinguish the synovial fluid in this study from that of a healthy joint included: intermittent increase of synovial total protein; variable numbers of granulated lymphocytes; intermittent cytoplasmic vacuolization of large mononuclear cells, consistent with macrophage activation; and variable disruption of the glycosaminoglycan background layer.[14] These results demonstrated why it is critical to pair synovial fluid analysis with clinical examination, as degenerative processes affecting joints can have minimal to no inflammation reflected in the synovial fluid, with overlap between cell counts from normal and osteoarthritic joints.[15] In all three horses, symptomatic grades were increased compared to baseline by 2 weeks postoperatively and remained elevated, without progression, throughout the 6-month study period. There were no obvious associations between the synovial fluid analysis parameters and the clinical exam findings; however, further analysis is required and likely in a larger sample size before any definitive conclusions can be made.

As reported by Stewart et al.,[7] the BMLs induced using this model changed over time, and modified the subchondral and trabecular bone without significant degeneration of the overlying articular cartilage as viewed on advanced diagnostic imaging. Magnetic resonance

imaging (MRI) and computed tomography (CT) were superior for monitoring lesion progression compared to digital radiography, with each modality providing complementary yet differing information about the changes occurring within the bone. MRI and CT demonstrated significant increases in bone sclerosis by 4 weeks post-operatively compared to baseline, with lesions persisting throughout the remainder of the study. BMLs at week 4 were characterized by significant hyperintense fluid signal on MRI (Dixon water only and STIR sequences), which was no longer significantly different from baseline by week 12. The total MRI score, characterizing the severity of degenerative and reactive changes on MRI, showed a similar response as lesion area; however, the score at week 4 was significantly higher compared to all other time points. Scoreable changes in the subchondral bone, specifically, developed later in the study period compared to that in the articular cartilage and subchondral bone, with most significant findings not showing until week 24. Unlike MRI, CT showed focal areas of hypoattenuation, suggestive of bone lysis or resorption, in variable locations immediately adjacent to and at the tip of the pin tract in some condyles. CT also revealed widening of the pin tract over time. Results from digital radiography revealed that, for this experimental model, while adaptive remodeling was still visible, it was unable to capture the breadth of changes to the lesion over time compared to more advanced modalities, with the most significant changes not becoming visible until on or after week 8. While digital radiography could be used to monitor changes in sclerosis, it was less sensitive to the degree of changes in the pin tract and the adjacent bone. Overall, the dynamic nature of the lesions supports the need for serial imaging in order to determine the significance of BMLs on diagnostic imaging, as well as to develop an appropriate treatment plan.

Gross abnormalities were most consistent with other pathologies of the MC3 condyles shown to be associated with POD including wear lines, subchondral bone bruising visible

through the articular cartilage, cartilage loss and ulceration (both on the condyles and the proximal sesamoid bones), marginal remodeling of the proximal sesamoid bones, dorsal impact injury, and linear fissures.[16,17] In support of the diagnostic imaging findings, microcomputed tomography (microCT) showed marked and extensive subchondral and trabecular bone sclerosis throughout the palmarodistal condyles in all horses, with sclerosis extending to the level of the physis and/or to the dorsal condyle in some cases. Similar to other reports in the published literature, the bone volume fraction, bone mineral density (BMD), and tissue mineral density (TMD) were observed to be higher in abaxial volumes of interest (VOIs) compared to axial VOIs, with varying levels of significance in the present study.[18,19] Increased porosity was present at the tip of the tract, consistent with the areas of resorption observed using other modalities. Consistent with this, the bone volume fraction and BMD were lowest and the bone surface to volume ratio highest in this VOI. Martig et al. found that in horses in training, there was an increase in TMD and decrease in bone volume fraction in bone further from the articular surface, with an increase in porosity in horses with subchondral bone injury.[20]

In the present pilot study, TMD was higher in VOIs further from the subchondral bone plate (non-SCB VOIs), while bone volume fraction and BMD were lower at the tip of the tract compared to other VOIs, followed by all mid-tract VOIs with variable significance, consistent with these previous findings. It is possible that new bone production could be one of the factors affecting this relationship, with a higher volume of less mineralized bone closer to the articular surface. The mean density values in the present pilot study were subjectively lower when compared to other publications in which specimens were acquired from the MC3 condyles of Thoroughbred racehorses of variable ages and training, despite similarities in bone volume fraction and trabecular structure.[19,20] It is possible that differences in scan and analysis

parameters may have played a role, as the BMD and TMD in the control horse were also subjectively lower compared to the referenced publications.[19,20] Compared to the control specimen, however, study horses had a lower number of thicker and generally less dense trabeculae. The bone volume fraction was also observed to be higher in study horses compared to the control, though only the relationship between horse #3 and the control was statistically significant. Another consideration could be that, due to the presence of the pin tract and the resulting remodeling, the bone analyzed in the present study was earlier in the mineralization process and thus, was less dense. This theory was supported by histopathology, which showed regionally extensive thickening of the cancellous trabeculae with variable immature, and likely less dense, woven bone in the region surrounding the pin tracts. This change was not identified in sections acquired from distant sites.

In the equine metacarpus, remodeling is reduced during periods of training and racing when microdamage is accumulating.[21] This is suggested to be the reason behind the high density and increased percent bone volume of the subchondral bone of the distal condyles in racehorses, with increased bone deposition within the marrow spaces and increased bone volume fraction.[22–27] A decrease in loading, such as with rest from training, will cause these layers to weaken through stimulation of bone resorption.[28] Despite exercise-induced reduction in subchondral remodeling, it has been shown that focal remodeling can still occur once failure develops in the subchondral bone. Whitton et al. demonstrated that fatigued subchondral bone in the MC3 condyles is focally remodeled in proportion to the modeling of the surrounding trabecular bone, with focal areas of porosity with an increased volume of surrounding trabecular bone observed at sites of fatigue failure.[29] This suggests that trabecular modeling allows the remodeling and repair of subchondral bone by focally unloading the damaged tissue. The bone damage associated with

the creation of a 1.1 mm diameter pin tract, approximately 8 mm deep to the articular surface, could be viewed as an induced site of fatigue failure. It is possible that the surrounding bone remodeling resulted in the focal unloading of the pin tract area, resulting in the areas of bone resorption observed in this study.

Histologically, BMLs – 24 weeks after induction – were characterized by extensive alterations to the subchondral and trabecular bone surrounding the pin tract when compared to distant sites, consistent with findings by Stewart et al.[7] These changes included cavitation of the articular cartilage and subchondral bone plate, extensive myelofibrosis, cellular debris within the marrow spaces, fibroplasia within the pin tract, and adjacent marked bony sclerosis. While the changes to the subchondral and trabecular bone were more extensive, degenerative changes were also observed in the articular cartilage. The surrounding articular cartilage was characterized by mild to moderate fibrillation, degeneration (reduced toluidine blue stain uptake, chrondrone formation), and necrosis with chondrocyte loss within the superficial to intermediate zones of the cartilage layer. These changes were the most severe in the regions overlying and immediately adjacent to the pin tract. Unfortunately, due to the limited sample size, histology was not performed until the end of the 6-month study period, making it impossible to determine how much of the articular cartilage injury was a result of the act of pin penetration alone – in which the articular cartilage injury would be considered a catalyst for disease progression – or a result of prolonged high-speed treadmill exercise and bone remodeling.

There were several limitations to the research presented in this dissertation. The most notable limitation was the small sample size. Using the statistical model in this study, the high number of variables included in the model meant that a smaller change would result in a larger difference; however, it is difficult to otherwise identify significant differences between three

horses. Despite this limitation, the primary objectives of this pilot study were to evaluate the ability to induce BMLs in the palmarodistal MC3 condyles of horses and measure the effects of lesion induction over time. This pilot study also lacked a control group in which lesions were induced but horses were maintained on box-stall rest, with another potential control group being one in which horses were exposed to the same high-speed treadmill protocol without lesion induction. This would allow investigators to better examine the individual contributions of exercise versus lesion induction to the clinical, diagnostic imaging, and post-mortem findings. Similarly, pin tracts were also not placed in the exact same location and at the same angle within every condyle and the variability in lesions that may occur as a result of this is unknown. Another limitation was the induction of lesions in both forelimbs and thus, the creation of a bilateral forelimb lameness which may have hindered the ability to accurately grade lameness in individual forelimbs. More objective modalities for measuring lameness could be considered in future studies. Furthermore, the synovial fluid volume aspirated was not recorded for every horse at every time point; therefore, it is unknown whether the effusion in this study was truly an increase in synovial fluid volume or if there was a component of synovial and joint capsule thickening. This could be measured in future studies with a correlation analysis performed to determine whether the fluid volume aspirated was related to the severity of joint effusion on clinical examination. Lastly, microCT and histopathology were not performed until the end of the study; therefore, information on lesion composition can only be provided for week 24 and not earlier time points.

In conclusion, the pin penetration model combined with high-speed treadmill exercise resulted in many gross and microscopic changes similar to that identified in POD and maladaptive stress remodeling; however, further research is needed to better compared the results

of this model to clinical disease and to optimize the technique for this purpose. Despite its limitations, this less-invasive model shows promise for its use to study the progression of maladaptive stress remodeling in equine fetlocks, including the evaluation of individual risk factors for injury progression and optimization of management and treatment strategies.

6.2 Significance of Work

The goal of the research presented in this dissertation was to provide in vivo proof of concept of a previously published pin penetration model, combined with high-speed treadmill exercise, in the distal MC3 condyles of horses, with the central objective being to develop an experimental model of repetitive stress injury in horses that mimics clinical disease. As discussed in Chapter 1, the cost of poor performance and injury has a large detrimental impact on sport horse industries. Racehorse injuries in particular have quite devastating effects, both on industry economics and the health of the athletes, contributing to the poor public perception and to increases in both racehorse death and jockey injury and death.[30,31] Economic wastage has been previously reported as $81 million per month nationally, based on a loss of 3% of horses from racing each month and median yearling auction price.[30] Furthermore, median financial return for yearling Thoroughbreds in training that lost 13 to 108 days of training was $23,000 less compared to those that only lost 1 to 11 days.[30,32] Of particular importance in the racehorse industry is POD. As previously mentioned, POD is a traumatic fatigue injury of the subchondral bone of the palmar metacarpal condyles of Thoroughbred racehorses.[6,8,17] Not only does it limit an equine athlete's potential, but it can also result in chronic pain and osteoarthritis secondary to a reduction in the structural ability of the subchondral bone to withstand high-intensity exercise.[33] Studies have reported 67-90% of racehorses exhibit POD lesions of some grade,[16,17,33]

with 14-30% having lesions of moderate or marked severity.[17,34] In addition to a wide spectrum of severity, progression of this disease tends to vary between individual horses.

The equine metacarpophalangeal (fetlock) joint is at the highest risk of repetitive stress injury in the racehorse,[27,35] with the initiation of disease focused primarily around derangements in the subchondral bone. Detection of subchondral bone disease is a clinical challenge, especially in the early stages where therapeutic intervention may be most beneficial.[16,36] We have developed a novel, minimally-invasive, experimental model of maladaptive stress remodeling in the equine fetlock that will allow us to study this disease in a controlled, prospective manner. This pilot work is significant because this model could allow us to carefully and quantitatively monitor the timeline of lesion progression and how it relates to articular surface collapse, helping determine the ideal timepoint for or duration of treatment and more closely investigate the pathologic mechanisms that will inform new therapeutic strategies. It will also allow us to better isolate and control for individual variables to determine to what extent they affect the likelihood of lesion progression or recurrence. The first step in this process is to take the data obtained from this pilot study and examine for potential cause-effect relationships between individual horse variables and the progression of BMLs, as well as examine the data further for potential correlations that may provide a better understanding of some of the reported findings. In doing so, we can progress towards building a more effective strategy to optimize our treatment protocols and improve the long-term outcome in these horses.

There are significant benefits to the pin penetration model compared to other currently-published models. First, this project is a novel extension of recently validated work in which a new, minimally-invasive, pin penetration technique has been used to consistently induce subchondral BMLs in sheep[7] and rats without negatively affecting the articular cartilage. This

technique was adapted for use in the equine metacarpophalangeal joint, successfully and reliably inducing BMLs similar to those of POD. A minimally-invasive technique that reliably produces subchondral bone changes without affecting the articular cartilage at the time of lesion induction is critical for modeling the early stages of POD. Early POD lesions often have little overlying cartilage damage with eventual subchondral bone resorption and displacement resulting in complete cartilage loss.[16,17,34,36] Ideally, progression of these lesions to articular surface collapse occurs with intense exercise and maladaptive subchondral bone remodeling, without articular lesions serving as a catalyst for progression. There is limited experimental research on POD and the few studies currently published use impact devices that diffusely injure the cartilage, resulting in clinical disease, cause significant soft tissue trauma, or cause focal osteoarthritis without progressing to POD.[4,5] In addition, it is unlikely that a single impact will result in the same degree of subchondral bone changes as chronic, repetitive loading. Access to the palmaro/plantarodistal condyles is limited by the small joint volume, thick periarticular soft tissues of the palmaro/plantarodistal aspect of the joint, limited access for arthroscopic evaluation of that area, and a curved condylar geometry which could create instability of the impactor device.[4] Other models published for the induction of OA in the equine fetlock joint include osteochondral chip fragmentation models in the proximodorsal proximal phalanx,[37–41] thus making them inappropriate for the study of subchondral bone injury. While the lack of earlier histopathologic evaluation prevents conclusions regarding the development of articular cartilage degeneration relative to that in the subchondral and trabecular bone, the discrepancy between the severe changes in the bone compared to the milder changes in the articular cartilage – combined with the results from Stewart et al. – would suggest that the primary pathology

induced by this model was related to the subchondral and trabecular bone, and that the articular cartilage pathology was secondary.

Despite the depth of clinical experience and research published on POD, there are still many fundamental gaps in our scientific knowledge. Advice on managing this disease is reliant upon anecdotal evidence and speculative claims. Through unlocking the complexities of disease staging and the influence of various risk factors, this model could help us solve some of the mysteries around the progression of POD. Additionally, POD is a fatigue injury that occurs at an articular site subjected to extreme loads. This equine model provides a natural model for acute onset, rapidly progressive subchondral bone injury in highly-loaded joints more relevant to injury in human athletes. The horse is considered one of the best and most challenging models for studying orthopedic ailments,[42–44] providing a naturally-occurring model of repetitive stress injury. There is a unique opportunity to not only utilize the data on repetitive stress injury and POD in equine athletes to help advance our knowledge on similar diseases in humans, such as subchondral bone attrition, subchondral bone injury in long distance athletes, and femoral head necrosis, but to also use the data in humans to help study potential treatment options for more advanced cases of equine disease. With the development of a prospective model of disease in equine, there is a greater chance of this testing being accomplished with the hope of preserving and improving the athletic careers of these animals.

6.3 Future Directions

The progression and recurrence of POD is difficult to predict. Results from a multilevel model by Pinchbeck et al.[17,45] showed evidence of varying predisposition to POD between individual horses, as well as environmental influences. Limited research has identified potential training- and race-associated risk factors for POD in racehorses; however, more work is needed

to understand an individual horse's risk for lesion progression, as well as how to optimize treatment. With the increasing interest in machine learning to identify and predict injury risk in human athletes, one future objective of this experimental model is to develop a predictive model of POD to help trainers and veterinarians optimize a horse's career while reducing its risk of injury. Before we can do this, we must first establish cause-effect relationships between individual horse variables and the progression of BMLs.

Three factors known to be influential on the progression and healing of musculoskeletal injuries are age, rest, and exercise – these are the factors that could be examined in future work. Despite 60-90 days of active rest being suitable for some horses to achieve soundness and/or lesion resolution, some have recurrence/progression of these lesions upon returning to work. Our ability to examine the effects of variable periods of rest on acute BMLs in a controlled, prospective manner could lead to future studies on the effects of different exercise intensities, durations, rest protocols, and surfaces. Continued, descriptive research aimed at identifying promising associations between individual horse variables and BML progression could be built upon for future causality and predictive research. Once the relation between individual horse variables and their effects on BML progression have been examined, we can continue with a step-wise approach toward developing a predictive model that could help trainers and veterinarians forecast the risk of BML progression in order to optimize training and treatment plans. Future studies using this model may also allow us to identify the ideal window in which to treat POD, prior to the occurrence of significant articular cartilage damage, as well as potential ways to modify training programs to reduce the likelihood of re-injury. Furthermore, human research has demonstrated the importance of subchondral bone in osteoarthritis.[46–49] This model and the data obtained from this pilot study will provide a foundation for the development of

treatment technologies targeting repair of the subchondral bone, as well as an evaluation of the effects on articular surface integrity and joint biomechanics. Prior to starting this work, further research is needed to better understand some of the outcomes in this pilot study. While not a goal of this dissertation, which simply evaluated the global effects of this model development, there were several variations and interactions among individual horses, limbs, condyles, and time points. Correlations could be examined in the future to determine the sources of these variations, as well as to establish connections between some of the findings from this study.

Another potential use for this model in future work includes studying the treatment of subchondral BMLs by directly addressing the injured bone using a minimally-invasive approach. As previously mentioned, derangements in the subchondral bone play a critical role in the initiation of osteochondral insufficiency, osteoarthritis progression, and the presence of pain.[3,47–51] BMLs have been strongly associated with the presence and severity of knee pain in humans,[52] and are predictive of subchondral attrition,[1] loss of cartilage volume,[53] and disease progression.[48] As a result, treatment strategies supporting both the subchondral bone and the articular cartilage have become increasingly important. A subset of the investigators involved in this experimental model have previously published pilot research evaluating the use of a modified subchondroplasty technique for the treatment of BMLs and osteochondral defects.[54] Subchondroplasty, a treatment for osteoarthritis-related BMLs in humans, has resulted in improved pain and function in patients with severe knee osteoarthritis.[50,55–59] By injecting a flowable, osteoconductive, calcium phosphate bone substitute material into the area of compromised subchondral bone, the overall goal is to support and repair the interface between the damaged subchondral bone and normal surrounding bone. It is possible that this technique could augment current therapies to allow better tissue integration and subchondral stability. With

the initial successes of using the subchondroplasty technique in humans, various biological materials are now being evaluated for their use in the treatment of subchondral bone injury. IntraOsseous BioPlasty (IOBP) is another minimally-invasive treatment method similar to subchondroplasty that directly targets bone marrow lesions to encourage physiologic bone remodeling. This technique involves the percutaneous injection of a demineralized bone matrix combined with a biologic material such as concentrated platelet-rich plasma or bone marrow aspirate concentrate. It has been used successfully for the treatment of bone marrow lesions[60] and subchondral cystic lesions[61–63] in humans. In theory, by improving the distribution and integration of a biologic therapeutic or injectable hydrogel through the subchondral bone, there would be improved dissipation of mechanical stresses over a larger surface area, in turn improving the functionality of the repair tissue. Additional work has been performed evaluating the injection characteristics of various injectates using the modified subchondroplasty approach described by Smanik et al., including a demineralized bone matrix, platelet rich plasma, and fibrin glue (unpublished data). The subchondroplasty technique was also applied successfully to the equine third metacarpal condyles immediately following impact injury in a preliminary study.[5] With the development of a model of BMLs in the equine metacarpophalangeal joint, subchondral injection of BMLs in this location could be further evaluated using a variety of injectates, such as biologics or bone substitute materials, to determine their effects on lesion progression and healing, and determine the ideal material for subchondral injection, helping to further optimize and provide additional treatment options to equine athletes.

Lastly, future directions using this experimental model also include further evaluation of some of the interactions and findings identified in this pilot study, helping to better characterize the effects of this model. One interesting finding was the relationship between the study horses,

with horses #2 and #3 generally having more similar results compared to horse #1. The pin tract in horse #1 was inadvertently placed further proximad in the condyles, with corrections in surgical technique thereafter resulting in those in horses #2 and #3 having a more similar distad location. In general, the percentage of the condyle occupied by the BML, the total area of sclerosis, and the severity of imaging changes to the subchondral bone, trabecular bone and articular cartilage were less severe in horse #1 compared to the other two horses, and in horse #2 compared to horse #3; however, differences between horse #2 and horse #3 were less often or more variably significant. Horse #1 also had significantly different microCT results compared to the other two horses. Due to the differences in applied forces in the palmarodistal condyle, it is possible that the pin tract location in horse #1 experienced reduced stress which contributed to these differences in lesion progression. Potential future work could include performing correlation analysis to determine whether the pin tract location in this study affected any of the outcomes reported, or performing future research in which the pin tract location is purposefully varied with the resulting effects analyzed. Another factor to consider would be the effects of pin drilling, as performed in this study, compared to an impact-based model such as a hammer drill or impact driver on lesion induction and progression. Depth of osteochondral damage is an important factor in BML development, with damage needing to extend into the trabecular bone for BMLs to persist.[7] While a depth of approximately 8 mm was used in this study based on the previously published work, future studies refining this model for the study of POD, through all stages of disease, may include a reduced depth of penetration extending beyond but still remaining adjacent to the subchondral plate. This may allow for more of the remodeling to occur closer to the subchondral bone, as occurs in clinical disease. It would also be interesting to

evaluate whether BMLs would persist following damage involving the subchondral bone plate but not trabecular bone if combined with high-speed treadmill exercise in horses.

Further use of correlation analysis for the present pilot study includes evaluating the relationships between all outcome variables reported in this study, as well as the interactions between variables. For lameness evaluations, there were significant interactions between certain variables – primarily between horse and limb, in which differences only existed between limbs for certain horses or vice versa – for the outcome parameters measured. The ratio of cell types within the synovial fluid from each horse, and thus the nature of the inflammatory response to this experimental model, was observed to be variable between horses; however, the differential appeared to contain primarily mononuclear cells at a majority of time points. When evaluated using advanced diagnostic imaging, significant variation was observed when comparing lesion area among horses, with some variation in the presence and significance of these differences based on the individual time point for a majority of sequences, and differences among horses for MRI grading were significantly influenced by variations between time, limbs, and condyles. Abnormalities on MRI were more severe in right forelimbs compared to left forelimbs, overall and at all post-operative time points, and in lateral condyles compared to medial condyles. BMLs also consistently occupied a greater percentage of the condyles in the right forelimbs compared to left forelimbs, as well as in lateral condyles compared to medial condyles. The reason for this is unknown but could be influenced by factors such as the preferred lead of each horse during treadmill exercise, pin penetration depth, pin tract location and direction, or other factors not accounted for in this pilot study.

Grossly, there were minimal differences between horses in this study except for cartilage loss on the MC3 condyles. Overall and along the transverse ridge, gross cartilage loss was worse

for horse #3 compared to the other two horses. When looking in the region of the central condyle, specifically, both horses #2 and #3 had more cartilage loss compared to horse #1. The reason for these differences is unknown. Results from the trabecular morphometry analysis also revealed significant variation in the relationships among horses depending on the limb, condyle, or VOI evaluated. In contrast to the diagnostic imaging findings in this study, there were no significant differences between limbs or condyles using the gross scoring systems or on histological analysis. This is consistent with other studies that showed no difference in prevalence or severity of POD between left and right limbs,[16,17,64] though one study did show histopathologic scoring to be worse in lateral condyles compared to medial condyles.[65] MicroCT analysis, however, revealed increased bone volume fraction, BMD, TMD, and trabecular thickness, and decreased bone surface to volume ratio and trabecular number in left forelimbs compared to right forelimbs and in lateral condyles compared to medial condyles. These changes correspond to an increased volume of thicker, more sclerotic or dense bone. The reason for this is unknown. Correlation analysis of all variables and outcomes included in this study could be performed to help determine the reasons behind some of the relationships just described, at least as it pertains to this pilot study and experimental model. Future work could also include performing MRI and CT immediately following or within 24 hours of lesion induction or including additional diagnostics such as positron emission tomography (PET) to monitor the metabolic activity of the lesions throughout the study. Importantly, in a larger study, it would be beneficial to perform histopathology and microCT at similar time points to diagnostic imaging and clinical evaluation as this could provide more information regarding lesion composition and how it relates to clinical exam findings throughout various stages of disease.

Supplemental analyses are underway to increase the breadth of data obtained from this pilot study. Despite altered regulation of several well-established markers of osteoarthritis, there is limited activation of pro-inflammatory and catabolic genes with POD, which suggests a distinct molecular phenotype compared to other similar diseases like post-traumatic osteoarthritis.[66] Further analysis involving measurement of specific pro- and anti-inflammatory cytokines over time is required to gather more information regarding the joint environment induced by the model. At the time of synovial fluid aspiration through this pilot study, the remaining synovial fluid was processed and saved for cytokine analysis. The methods, preliminary results, and future directions from this analysis are provided in Appendix A. Gene expression analysis using Nanostring technology was also performed on a small subset of samples as part of a larger body of work, with the methods and results provided in Appendix B.

The results of this dissertation provide proof of concept of the potential of this experimental model to serve as the foundation for a variety of future, prospective research on repetitive stress injury in equine athletes. By using this model, treatment plans may be optimized to better promote healing while also studying individual risk factors that may result in lesion progression or regression. It also provides us with the opportunity to learn more about the duration and intensity of exercise required to result in lesion progression.

6.4 References

1. Roemer F, Neogi T, Nevitt M, et al. Subchondral bone marrow lesions are highly associated with, and predict subchondral bone attrition longitudinally: the MOST study. *Osteoarthr Cartil*. 2010;18(1):47-53.

2. Kawcak C, McIlwraith C, Norrdin R, Park R, Steyn P. Clinical effects of exercise on subchondral bone of carpal and metacarpophalangeal joints in horses. *Am J Vet Res*. 2000;61(10):1252-1258.

3. Stewart HL, Kawcak CE. The importance of subchondral bone in the pathophysiology of osteoarthritis. *Front Vet Sci*. 2018;5:178. doi:10.3389/fvets.2018.00178

4. Rickey EJ, Cruz A, Trout D, McEwen B, Hurtig M. Evaluation of experimental impact injury for inducing post-traumatic osteoarthritis in the metacarpophalangeal joints of horses. *Am J Vet Res*. 2012;73(10):1540-1552.

5. Rice H, Brokken M, Hostnik E, Bertone A. Evaluation of a novel bone substitute injection technique for potential treatment of impact injury to the equine palmar metacarpal condyle. *Vet Comp Orthop Traumatol*. 2019;32(6):447-453.

6. Nixon A. Palmar/plantar metacarpal/metatarsal fragmentation. In: Auer J, Stick J, Kummerle J, Prange T, eds. *Equine Surgery*. 5th ed. St. Louis, Missouri: Elsevier, Inc.; 2019:1601-1603.

7. Stewart HL, Easley JT, Selberg KT, et al. Experimental models of bone marrow lesions in ovine femoral condyles. *Vet Surg*. 2023;52:284-298.

8. Ramzan PH. Mind the gaps: The science of POD and the racehorse fetlock. *Equine Vet J*. 2021;53:217-220.

9. Arthur R, Blea J, Ross M, Moloney P, Cheney M. The North American Thoroughbred. In: Ross M, Dyson S, eds. *Diagnosis and Management of Lameness in the Horse*. 2nd Ed. St. Louis, Missouri: Elsevier Saunders; 2011:977-993.

10. Davidson E, Ross M. Clinical recognition of stress-related bone injury in racehorses. *Clin Tech Equine Pract*. 2003;2(4):296-311.

11. Pilsworth R. The European Thoroughbred. In: Ross M, Dyson S, eds. *Diagnosis and Management of Lameness in the Horse*. 2nd Ed. St. Louis, Missouri: Elsevier Saunders; 2011:994-1013.

12. Richardson D, Dyson S. The Metacarpophalangeal Joint. In: Ross M, Dyson S, eds. *Diagnosis and Management of Lameness in the Horse*. St. Louis, Missouri: Elsevier Saunders; 2011:394-410.

13. Kawcak C, Barrett MF. Fetlock. In: McIlwraith C, Frisbie D, Kawcak C, van Weeren PR, eds. *Joint Disease in the Horse*. Second Edi. St. Louis, Missouri: Elsevier; 2016:302-317.

14. Conrado F, Beatty S. Fluid Analysis in the Equine Patient: Cerebrospinal, Synovial, and Peritoneal Fluids. *Vet Clin North Am Equine Pract*. 2021;36:e1-e28.

15. Walton R. Fluid Analysis. In: Walton R, ed. *Equine Clinical Pathology*. John Wiley & Sons, Inc.; 2014:203-232.

16. Barr E, Pinchbeck G, Clegg P, Boyde A, Riggs C. Post mortem evaluation of palmar osteochondral disease (traumatic osteochondrosis) of the metacarpo/metatarsophalangeal joint in Thoroughbred racehorses. *Equine Vet J*. 2009;41:366-371.

17. Pinchbeck G, Clegg P, Boyde A, Riggs C. Pathological and clinical features associated with palmar/plantar osteochondral disease of the metacarpo/metatarsophalangeal joint in Thoroughbred racehorses. *Equine Vet J*. 2013;45:587-592.

18. Drum M, Les C, Park R, Norrdin R, McIlwraith C, Kawcak C. Correlation of quantitative computed tomographic subchondral bone density and ash density in horses. *Bone*. 2009;44(2):316-319.

19. Rubio-Martinez L, Cruz A, Gordon K, Hurtig M. Structural characterization of subchondral bone in the distal aspect of third metacarpal bones from Thoroughbred racehorses via micro–computed tomography. *Am J Vet Res*. 2008;69(11):1413-1422.

20. Martig A, Hitchens P, Stevenson M, Whitton R. Subchondral bone morphology in the metacarpus of racehorses in training changes with distance from the articular surface but not with age. *J Anat*. 2018;232:919-930.

21. Holmes J, Mirams M, Mackie E, Whitton R. Thoroughbred horses in race training have lower levels of subchondral bone remodelling in highly loaded regions of the distal metacarpus compared to horses resting from training. *Vet J*. 2014;202:443-447.

22. Whitton R, Trope G, Ghasem-Zadeh A, et al. Third metacarpal condylar fatigue fractures in equine athletes occur within previously modelled subchondral bone. *Bone*. 2010;47(4):826-831.

23. Boyde A. The real response of bone to exercise. *J Anat*. 2003;203:173-189.

24. Nunamaker D. Relationships of exercise regimen and racetrack surface to modeling/remodeling of the third metacarpal bone in two year old Thoroughbred racehorses. *Vet Comp Orthop Traumatol*. 2002;15:195-199.

25. Riggs C, Boyde A. Effect of exercise on bone density in distal regions of the equine third metacarpal bone in 2-year-old thoroughbreds. *Equine Vet J*. 1999;31(S30):555-560.

26. Boyde A, Riggs C, Firth E. Densification by infilling marrow space in response to exercise in thoroughbred horse distal cannon bone. *Bone*. 2001;28:S110-S110.

27. Martig S, Chen W, Less P, Whitton RC. Bone fatigue and its implications for injuries in racehorses. *Equine Vet J*. 2014;46:408-415.

28. Rowe P, Koller A, Sharma S. Physiology, Bone Remodeling. In: *StatPearls [Internet]*. StatPearls. Treasure Island (FL): StatPearls Publishing; 2023.

29. Whitton R, Mirams M, Mackie E, Anderson G, Seeman E. Exercise-induced inhibition of remodelling is focally offset with fatigue fracture in racehorses. *Osteoporos Int*. 2013;24:2043-2048.

30. Stover S. Skeletal Injuries in Equine Athletes - Pathogenesis and Training Concepts for Injury Prevention. In: *Proceedings of the 68th Annual Convention of the American Association of Equine Practitioners*. ; 2022:95-104.

31. Rossdale P, Hopes R, Digby N, Offord K. Epidemiological study of wastage among racehorses 1982 and 1983. *Vet Rec*. 1985;116(3):66-69.

32. Hernandez J, Hawkins D. Training failure among yearling horses. *Am J Vet Res*. 2001;62:1418-1422.

33. Davis A, Fan X, Shen L, Robinson P, Riggs C. Improved radiological diagnosis of palmar osteochondral disease in the Thoroughbred racehorse. *Equine Vet J*. 2017;49:454-460.

34. Bani Hassan E, Mirams M, Mackie E, Whitton RC. Prevalence of subchondral bone pathological changes in the distal metacarpi/metatarsi of racing Thoroughbred horses. *Aust Vet J*. 2017;95:362-369.

35. McIlwraith C. Traumatic Arthritis and Posttraumatic Osteoarthritis in the Horse. In: McIlwraith C, Frisbie D, Kawcak C, van Weeren PR, eds. *Joint Disease in the Horse*. Second edi. St. Louis, Missouri: Elsevier; 2016:33-48.

36. Curtiss A, Ortved K, Dallap-Schaer B, et al. Validation of standing cone beam computed tomography for diagnosing subchondral fetlock pathology in the Thoroughbred racehorse. *Equine Vet J*. 2021;53:510-523.

37. Bertoni L, Jacquet-Guibon S, Branly T, et al. An experimentally induced osteoarthritis model in horses performed on both metacarpophalangeal and metatarsophalangeal joints: Technical, clinical, imaging, biochemical, macroscopic and microscopic characterization. *PLoS One*. 2020;15(6):e0235251.

38. Boyce M, Trumble T, Carlson C, Groschen D, Merritt K, Brown M. Non-terminal animal model of post-traumatic osteoarthritis induced by acute joint injury. *Osteoarthr Cartil*. 2013;21(5):746-755.

39. Kawcak C, McIlwraith C. Proximodorsal first phalanx osteochondral chip fragmentation in 336 horses. *Equine Vet J*. 1994;26:392-396.

40. Yovich J, McIlwraith C. Arthroscopic surgery for osteochondral fractures of the proximal phalanx of the metacarpophalangeal and metatarsophalangeal (fetlock) joints in horses. *J Am Vet Med Assoc*. 1986;188:273-279.

41. Broeckx S, Pille F, Buntinx S, et al. Evaluation of an osteochondral fragment–groove procedure for induction of metacarpophalangeal joint osteoarthritis in horses. *Am J Vet Res*. 2019;80(3):246-258.

42. McIlwraith C, Fortier L, Frisbie D, Nixon A. Equine models of articular cartilage repair. *Cartilage*. 2011;2:317-326.

43. McIlwraith CW, Frisbie DD, Kawcak CE. The horse as a model of naturally occurring osteoarthritis. *Bone Joint Res*. 2012;1(11):297-309. doi:10.1302/2046-3758.111.2000132

44. Moran C, Ramesh A, Brama P, O'Byrne J, O'Brien F, Levingstone T. The benefits and limitations of animal models for translational research in cartilage repair. *J Exp Orthop*. 2016;3:1.

45. Pinchbeck G, Clegg P, Boyde A, Barr E, Riggs C. Horse-, training- and race-level risk factors for palmar/plantar osteochondral disease in the racing Thoroughbred. *Equine Vet J*. 2013;45:582-586.

46. Hu W, Chen Y, Dou C, Dong S. Microenvironment in subchondral bone: predominant regulator for the treatment of osteoarthritis. *Ann Rheum Dis*. 2020;80(4):413-422. doi:10.1136/annrheumdis-2020-218089. Online ahead of print.

47. Sharkey P, Cohen S, Leinberry C, Parvizi J. Subchondral bone marrow lesions associated with knee osteoarthritis. *Am J Orthop*. 2012;41(9):413-417.

48. Tanamas SK, Wluka AE, Pelletier J-P, et al. Bone marrow lesions in people with knee osteoarthritis predict progression of disease and joint replacement: a longitudinal study. *Rheumatology*. 2010;49(12):2413-2419. doi:10.1093/rheumatology/keq286

49. Gomoll AH, Madry H, Knutsen G, et al. The subchondral bone in articular cartilage repair: current problems in the surgical management. *Knee Surgery, Sport Traumatol Arthrosc*. 2010;18(4):434-447. doi:10.1007/s00167-010-1072-x

50. Abrams G, Harris J, Cole B. Subchondral Bone Treatment. In: Cole B, Harris J, eds. *Biologic Knee Reconstruction: A Surgeon's Guide*. Thorofare, NJ: SLACK Incorporated; 2015:83-89.

51. Orth P, Madry H. Advancement of the subchondral bone plate in translational models of osteochondral repair: Implications for tissue engineering approaches. *Tissue Eng Part B Rev*. 2015;21(6):54-520.

52. Felson D, Chaisson C, Hill C, et al. The association of bone marrow lesions with pain in knee osteoarthritis. *Ann Intern Med*. 2001;134(7):541-549.

53. Wluka AE, Wang Y, Davies-Tuck M, English DR, Giles GG, Cicuttini FM. Bone marrow lesions predict progression of cartilage defects and loss of cartilage volume in healthy middle-aged adults without knee pain over 2 yrs. *Rheumatology*. 2008;47(9):1392-1396. doi:10.1093/rheumatology/ken237

54. Smanik L, Selberg K, Mason G, et al. Evaluation of a modified subchondroplasty technique in an equine full-thickness cartilage defect model: a pilot study. *Am J Vet Res*. 2023;84(4):1-10.

55. Cohen S, Sharkey P. Subchondroplasty for treating bone marrow lesions. *J Knee Surg*. 2016;29(7):555-563.

56. Byrd JM, Akhavan S, Frank DA. Mid-term outcomes of the Subchondroplasty procedure for patients with osteoarthritis and bone marrow edema [Abstract]. In: *The Orthopaedic Journal of Sports Medicine - AOSSM 2017 Annual Meeting*. Vol 6. ; 2017. doi:10.1177/2325967117S00291

57. Farr J, Cohen S. Subchondroplasty as an emerging treatment option for sports-related subchondral stress fractures. *ASPETAR Sport Med J*. July 2016:284-291.

58. Astur DC, de Freitas EV, Cabral PB, et al. Evaluation and management of subchondral calcium phosphate injection technique to treat bone marrow lesion. *Cartilage*. April 2018:194760351877024. doi:10.1177/1947603518770249

59. Hernigou P, Auregan JC, Dubory A, Flouzat-Lachaniette CH, Chevallier N, Rouard H. Subchondral stem cell therapy versus contralateral total knee arthroplasty for osteoarthritis following secondary osteonecrosis of the knee. *Int Orthop*. 2018;42(11):2563-2571. doi:10.1007/s00264-018-3916-9

60. Kasik C, Martinkovich S, Mosier B, Akhavan S. Short-term outcomes for the biologic treatment of bone marrow edema of the knee using bone marrow aspirate concentrate and injectable demineralized bone matrix. *Arthrosc Sport Med Rehabil*. 2019;1(1):e7-e14.

61. Alwood A, Giordano B. Arthroscopic bone and cartilage grafting of acetabular cysts with autologous tissue. *Arthrosc Tech*. 2021;10(2):e561-e567.

62. Elena N, Woodall B, Lee K, et al. Intraosseous bioplasty for a chondral cyst in the lateral tibial plateau. *Arthrosc Tech*. 2018;7(11):e1149-e1156.

63. Ankem H, Diulus S, Maldonado D, et al. Arthroscopic-assisted intraosseous bioplasty of the acetabulum. *Arthrosc Tech*. 2020;9(10):e1531-e1539.

64. Reed S, Jackson B, McIlwraith C, et al. Descriptive epidemiology of joint injuries in Thoroughbred racehorses in training. *Equine Vet J*. 2012;44:13-19.

65. Pinilla M, Tranquille C, Blunden A, Chang Y, Parkin T, Murray R. Histological Features of the Distal Third Metacarpal Bone in Thoroughbred Racehorses, With and Without Lateral Condylar Fractures. *J Comp Pathol*. 2017;157:1-10.

66. Turlo A, McDermott B, Barr E, et al. Gene expression analysis of subchondral bone, cartilage, and synovium in naturally occurring equine palmar/plantar osteochondral disease. *J Orthop Res*. 2021:1-9.

APPENDICES

Appendix A – Synovial Fluid Cytokine Analysis

Cytokine Quantification

As described in Chapter 3, synovial fluid was aspirated from both metacarpophalangeal joints in each horse at baseline and weeks 2, 4, 8, 12, 16, 20, and 24. After collection, synovial fluid not utilized for fluid analysis was placed into a 3 mL EDTA tube and then centrifuged at 3000rpm for 10 minutes at 20°C using the Allegra™ 6R Centrifuge (Beckman Coulter) to remove cellular debris. The supernatant was retained and fluid frozen in aliquots of 200uL at -80°C. Once all samples were obtained for evaluation, the samples were thawed and cytokine levels were measured. Fluorescent bead-based multiplex assay (Milliplex MAP Equine Cytokine/Chemokine Magnetic Beads Multiplex Assay, Millipore Sigma, Burlington, MA, 01803) was used to quantify the concentrations of 23 analytes [Eotaxin/CCL11, FGF-2, Fractalkine/CS3CL1, G-CSF, GM-CSF, GRO, IFN, IL-1α, IL-1β, IL-2, IL-4, IL-5, IL-6, IL-8/CXCL8, IL-10, IL-12 (p70), IL-13, IL-17a, IL-18, IP-10, MCP-1, RANTES/CCL5 and TNFα] in synovial fluid. ELISA immunoassays were used to measure the concentration of prostaglandin E2 (PGE-2 high sensitivity ELISA kit, Enzo Life Sciences, Inc. Farmingdale, NY 11735) and TGF-β (Human/Mouse/Rat/Porcine/Canine TGF-ß1 quantikine ELISA, R&D Systems, Inc. Minneapolis, MN 55413) in synovial fluid.

Preliminary Results

Cytokine concentrations were quantifiable within the detection limit of the assay for eight cytokines via multiplex immunoassay (FGF-2, G-CSF, Fractalkine, IL-6, IL-17a, IL-8, GRO, IL-10) and for both cytokines using ELISA (PGE-2, TGF-ß). Levels of the remaining cytokines

were either not quantifiable or they were below the detection limit of the multiplex assay. Additionally, several quantifiable cytokines were only within detectable limits for a few samples. Based on these findings, ELISA immunoassays will be used to better quantify the levels of the eight cytokines quantified via the multiplex immunoassay using remaining synovial fluid samples. Correlation analysis may then be performed to determine whether the results were associated with any of the other findings from this pilot study. These results will provide additional information regarding the effects of the experimental model on the synovial fluid environment and help guide cytokine analysis in future studies.

Appendix B – Nanostring

Gene expression analysis using Nanostring technology

Once all necessary sections were obtained for histopathology, select remaining paraffin blocks were utilized for gene expression analysis. Four groups were created for analysis: 1) control, 2) bone marrow edema, 3) sclerosis, and 4) lysis. Using results from diagnostic imaging and microCT, the three samples with the most significant lesions were assigned to the relevant groups. All chosen samples, incidentally, ended up being proximal tract specimens. Furthermore, two of the three samples in the sclerosis group were also in the lysis group. For the control group, a section from the medial condyle of the left third metatarsal bone of each of three control horses were used. The control horses were 2- to 3-year-old Quarter Horse mixed-breed geldings that had been treadmill exercised as part of a different study, chosen based on sample availability. Samples were collected and processed as previously described for the study horses. Formalin fixed paraffin embedded (FFPE) osteochondral lesions were cut from the blocks for RNA extraction. Total RNA was harvested from FFPE tissues using Qiagen RNeasy FFPE kit (Qiagen, Hilden, Germany; Catalogue ID: 73504) following the manufacturer's instructions. Samples

were analyzed via Nanostring (Nanostring Technologies Inc., Seattle, Washington, USA) gene expression using a custom-designed 200-gene equine immune panel. Genes included in the panel are listed in Supplemental Table B1. Gene selection to design the panel was based on previously performed bulk RNA sequencing of equine synovial and osteochondral tissues (data not shown) with previously demonstrated gene expression in the tissues of interest and recently reported for evaluation of equine synovial tissues.[1]

Before analysis by Nanostring, RNA quality and quantity were assessed by NanoDrop spectrophotometry, and integrity was evaluated by Agilent TapeStation. Samples where the proportion of RNA molecules > 200 nucleotides or larger exceeds 50% of total RNA were analyzed. Nanostring analysis was performed with the nCounter FLEX system at Colorado State University. Gene expression count data were analyzed via nSolver software v 4.0 (Nanostring Technologies Inc.).

Data Analysis

Analysis of targeted RNA transcript abundance and statistical significance was performed with the nCounter Analysis Flex software and with Partek Flow Genomics Analysis software v10.0 (Partek Inc, Chesterfield, Missouri, USA). Read counts were background corrected (negative controls) and normalized to housekeeping genes (GAPDH, B2M, G6PD, GATA3, GUSB, HPRT1). Principle component analysis (PCA) plots were generated and ANOVA for differential gene expression analysis performed with FDR step calculated for multiple test corrections.

Preliminary Results

Samples in the lysis and sclerosis groups were distinct from the controls and bone edema samples based on PCA. A description of all genes of interest detected in this analysis are

provided in Supplemental Table B2. Compared to the controls (n=3), samples in the lysis group (n=3) had 7 genes with significantly increased expression ($p \leq 0.05$). These included B2M, THBS4, LYZ, CD8A, CXCL6, IL33, and PLVAP, with the first two having the greatest fold change. Compared to the controls (n=3), samples in the sclerosis group (n=3) had 6 genes with significantly increased expression ($p \leq 0.05$). These included B2M, THBS4, CD8A, CXCL6, TBX21, and PLVAP, with the first two having the greatest fold change. This resulted in an overlap of 62.5% (5 of the 8 genes) of genes between the lysis and sclerosis groups. Gene expression between the bone marrow edema (n=3) and control (n=3) groups were not significantly different.

Overall, the transcript counts were very low, despite positive probe controls reading in the expected range. As the housekeeping genes were also low in expression, possible false negatives due to RNA degradation cannot be ruled out. Despite this, these preliminary results indicate that gene expression analysis may be valuable in future studies on maladaptive stress remodeling in horses. Based on these results, in order to identify differential gene expression between two groups, an estimated sample size of 47 specimens per group will be necessary to reject the null hypothesis that the population means of the two groups are equal with a probability (power) of 0.80.

References

1. Pezzanite L, Chow L, Engiles J, et al. Targeted transcriptomic analysis of synovial tissues from horses with septic arthritis treated with immune-activated mesenchymal stromal cells reveals induction of T-cell response pathways. *J Am Vet Med Assoc*. 2024;262(S1):S73-S82.

Supplemental Tables

Supplemental Table B1 – Equine Nanostring gene panel list

	Gene Name	Accession	Target Sequence
1	ACAN	XM_001917528.2	GGAGAGATTCATCTCGAGACCACTCCCTCTGGAGCAGAGGACCTTGGTGGACTTCCT TCTGGAGGAGAGATCCATCTCGAGCCCACTGCCTCTGGAGTAG
2	ACTB	NM_001081838.1	TGCTGTCCCTGTACGCCTCTGGCCGCACCACTGGCATCGTGATGGACTCCGGTGACGG GGTCACCCACACTGTGCCCATCTACGAGGGGTACGCCCTCCC
3	ADAMDEC1	XM_001491607.1	ATGTCACATGAGTTGGGTCATGTCCTTGGAATGCCTGATGTTCCCTATGACACCAAGTG TCCCTCTGGGAGTTGTGTGATGAATCAATATCTGAGTTCAA
4	ADAMTS5	XM_003364218.4	AAAGTCCGACAATTCAAAACCAAAGACCAGACTCGGTTCACTGCCTACTTAGCCCTT AAGAAGAAAAATGGTGAGTACCTTATCAATGGAAAGTACATGA
5	APOE	XM_005614763.3	GGATCCCTGAGGTCTATTCAGCTCCAGCGGACGCGAAGGACGCGCTTTCCCAGGACC GATTGACCAATCGCAGGCGGAAAAATGAAGGCTCTGTGGGCGG
6	ARG1	XM_001503285.3	AAGTCACTTCCACGGTGAACACAGCGGTGGCAGTAACCTTGGCTTGTTTTGGAGCTG CTCGGGAGGGTAATCATAAGACTATTGACTACCTTAGCCCGCT
7	B2M	NM_001082502.3	TCAGACCTGTCTTTCAGCAAGGACTGGTCTTTCTATCTTCTGGTCCATACTGACTTTAC TCCCAATGGTGTGGATGAGTATAGTTGCCGTGTACAGCACT
8	BAX	XM_014729717.1	GCGAGGTCTTTTTCCGAGTGGCAGCTGAGATGTTTTCCGACGGCAACTTCAACTGGG GCCGGGTTGTTGCCCTTTTCTACTTTGCCAGCAAATTGGTGCT
9	BGLAP	XM_008516800.1	TCCAGGCTGAGCAGAAGTGGCTCTCGGGTGTGGGATGGGGTTTTTCAGGCTGGATGT TCTGTCACTTGGAGGACAGGTCCCAAGGTTGTTGACACTGGGG
10	BMP2	XM_001493895.5	GGCCCACTTAGAGGAGAACCGAGGTGCCTCCAAGAGACACGTTAGGATTAGCAGGTC TTTGCACCAAGATGAGCATAGCTGGTCACAAATAAGGCCATTG
11	BMP4	NM_001163970.1	TCGGGCCAACACCGTGAGGAGTTTCCACCACGAAGAACATCTGGAGAGCATCCCAGG GACCAGCGAAAACTCTGCTTTTCGTTTCCTCTTTAACCTCAGC
12	CASP3	NM_001163961.1	CCGGCGAAGAAATTGTGGCATTGATGCGCAGTGTTTCTAAAGAAGATCATAGCAAAA GGAGCAGTTTTATTTGCGTGCTTCTAAGCCATGGTGAAGAAGG
13	CCL2	NM_001081931.2	GCCAGATGCAATTAATTCTCCAGTCACCTGCTGCTATACATTCACCGGTAAGAAGATCT CATCTCAGAGGCTGGGGAGCTATAAAAGAGTCACCAGCAGC
14	CCL25	XM_014741140.2	CCAACCCTTGTCTGTCCCTCGTGCAAATAGTTAGCTGAGGGAGTCACTGTTGCCTGCC TGGCTCTTTGACTTGGGTCCTCTTGTGTCCAGTCACCCAGGA
15	CCL5	NM_001081863.2	CCAAGAGTATTTCTACACCAGCAGCAAGTGCTCTATACCAGCAGTCGTCTTTGTCACC CGAAAGAAGCGCCAGGTGTGTGCCAATCCAGAGAAGAAATGG
16	CCL8	NM_001081864.1	GTAACGTTGTGAGGTCCTCCCATGGATCATCGGAGCAAAACACTTGTACGTTCTTAGG AAATCGGTGCTCCTGAAGTCAAATGCGTGCTATGGAGTGGTG
17	CCR2	NM_001097606.3	AGTTTTCTATGGGGAGACAGCAGACCGAGTGAGTTCAACATACACTCCTTCCACTGG GGAGCAGGAAGTCTCAGCTGGTTTGTAAGTGAGCAGCAGTTTG
18	CCR7	XM_001500181.4	TGCTACCTTGTCATCATACGCACGCTGCTCCAGGCACGCAACTTCGAACGCAACAAG GCCATCAAGGTGATCATCGCTGTGGTGGTGGTCTTCATTGCCT
19	CD14	NM_001081927.2	GCGCAGCTCCACAGTTTCTCGGCCCTCCACACCCTAGACCTGTCTGACAATCCTGGAC TGGGCGAGCGCGGACTGATTGCAGCTCTCTGTCCGCACAAGT
20	CD22	XM_001914991.4	TTTCGAGGTGGCTTGTGCCTTTTCAGCAGGCTGGCAGTTCTGATCTGCTCAGCTTGAG TCATTAGCATTTCCTGAGAGCTGGATCTAGCAGAAGCTGTGA
21	PDL1	XM_001492842.6	CTACTGCACTTTTCGGAGATCAGGTCTTGAGGAAAACAGTACAGCTGAGCTGGTCATC CCAGAACCACTTATAGTTCCGGCAAATAAGAGAACTCACTTG
22	CD34	XM_001491596.4	TGACCACGTGCTGCCTCCATCCCGGAGGTGCCATCTCTTACCTTCTACCCTTTCCCACT GCACACACCCTCCGAGGCCATTCCTGGGGCCCTGCACTGCA
23	CD3E	XM_003365338.4	ACTGTTCCAGAAAAACCCGCATCTGGACAGAAAAGATATGAAGTCTCCATCTCCGGA ACCACTGTAAAGCTGACATGCCCTGAGAATTTTGGAAACGAAT
24	CD4	XM_001497051.4	TCTTGGTGCTGGCTTTCCAGAAAGTCTCTCGCACAGTCTATGCGAAAGAGGGGACAC AGGCGGAGTTCTCCTTCCCGCTTACCTTCGCAGACGAAAACCT
25	CD55	XM_005609840.2	ATGTTCCACCCAGGCTGCCTTTTGCATCTCTCCAAAACCCTTATCGCAACCAGAATTAT TTCCCAGCGGGTTCCACTGTGGAATATGAGTGCCGAATGGG
26	CD5L	XM_005609987.3	CATCTGGCTGAGTCACGTGTCATGCTCAGGACAAGAAGTAAGCCTTCAGGATTGCCCT TCTGAGCCTTGGGGAATGAACAACTGCACCCACGATGAGGAC
27	CD68	NM_001099762.1	GAGCACTGTCTACCTGAACTATATCGCTGTGGAGTACAACGTGTCCTTCCCACAGGCA GCGCAGTGGACATTCTTGGTTCAGAATTCATCCCTTCGAGAT
28	CD86	XM_005601938.3	AGGACAAGGGCTTGTATCAATGTTACATCCATCATAAAGGGCCCAAAGGACTGGTTCC CGCCCACCAGATGAGTTCTGATCTATCAGTGCTTGCTAACTT
29	CD8A	XM_014731048.2	GCAAGGGTTACAGTACCGTTGTGCAAACATGCTGGGGTAAAGTGCGGGCAGGCCAGA GCTACCGCAAGCTGTGTTCTCAGAATCAGGCTGTTAGAGCTGG
30	CHRDL2	XM_001917318.1	GCAACGATGGGTCAAGTGAGATATCAACTGAAGAGGACTCCACGCAGTCACACCGTG GGGTGAGACATTCCCAGGATCCGTGTTCAGGGGACGGTGGGAG

31	CILP	XM_001498168.5	CCCATCAGGCTCACAATGCCCAAGACTCGCTTGAAGGCAGTCACCATCAATGCGGAG TTCAAGAGGGCAGAGACTCCATACATCGTGATGAACCCTGAGA
32	CNFN	XM_001501130.5	TGGCCTGCCCAATATAAGTAGCTCCTGGCCGAGACTGAGAACTCAGTGCCGGTGTCAC CCACATCTCTGTCTCCATCATCACCATCGCAGTCCTGCAGGT
33	COL11A1	XM_001918115.5	CAAGACATCGAGCATATGAAGTTTCCAATGGGTACTCAGACCAACCCAGCCCGAACTT GCAAAGACCTGCAACTAAGCCATCCTGATTTCCCAGATGGTG
34	COL14A1	NM_001163870.1	ACACAGACATTGAATTGAGGGGGCTGTTACCCAATACGGAATACACAGTTACGGTTTA TGCTATGTTTGGAGAAGAGGCCAGCGATCCTGTTACAGGACA
35	COL1A1	XM_001499586.3	CCCTGGCGAGCGTGGTGGACCTGGTGCCCGTGGCTTCCCTGGCGCAGATGGTGTTGC TGGTCCCAAGGGTCCCGCTGGTGAACGTGGTGCTCCTGGCCCT
36	COL1A2	XM_001492939.4	CTCCTGGACTGAGAGGAAGTCCTGGTTCTCGCGGTCTTCCTGGAGCTGACGGCAGAG CTGGTGTCATGGGCCCTGCTGGTAGTCGTGGTGCAAGTGGCCC
37	COL2A1	NM_001081764.1	AAGTGGGGCAAGACTACGATTGAGTACCGGTCACAGAAGACCTCGCGCCTGCCCATC ATTGACATTGCACCCATGGACATAGGAGGGCCTGAGCAGGAAT
38	COL3A1	XM_001917620.2	TCTGCCATCCTGAACTCAAAAGTGGAGAATATTGGGTTGATCCTAACCAAGGTTGCAA GCTGGATGCTATTAAAGTATTCTGTAATATGGAGACTGGGGA
39	COL5A1	XM_014736244.1	GAAATCGACACTCCCAAGGTGGAGCAAGTGCCCATCGTGGACATCATGTTCAATGAC TTCGGTGAAGCATCACAGAAATTCGGATTCGAAGTGGGGCCGG
40	COL9A1	XM_014734623.1	CAGGTAGAGCTCCAACAGACCAGCACATCAAGCAGGTTTGCATGAGAGTGATGCAAG AGCATCTTGCTGAGATGGCTGCTAGTCTCAAGCGTCCAGACTC
41	COMP	NM_001081856.1	GAGAAGCTGCGCTGCTCGGAGCGCCAGTGTCGCAAGGATAACTGCGTGACGGTACCC AACTCAGGACAGGAGGACGCGGATCGCGACGGCATCGGAGACG
42	CPXM1	XM_001497131.3	GGATGCTAGGCACCCTACCCGCTTCTCAGGCGTTATCACACAGGGCAGGAACTCTATC TGGAGGTACGACTGGGTCACATCATACAAGGTCCAGTTTAGC
43	CREBBP	XM_001499349.3	TGGCTCTACAATCGTAAGACGTCCCGGGTCTATAAGTTCTGCAGTAAACTCGCAGAGG TCTTTGAGCAAGAAATTGATCCTGTAATGCAGTCCCTTGGAT
44	CSF3R	XM_001499027.4	CCTTACCCACTACACCATCTTCTGGACCAATGCTCAGGACCAGTCCTTCTCCACTGTTC TGAATGCCTCCTCCCATGATTTTGTCCTCCATGGCCTGGAA
45	CST3	XM_023625992.1	CTCAGGAGACACACAGAGAAGGCTTCTCGGGTATTGTTTGTACAGCTAAGTGGCTCC AACTCACTTCTGTCTTCTGATTGCTTTCCAAATGCAGCAGTAC
46	CXCL10	NM_001114940.1	TATACTCTGCCTTATCTTTCTGACTCTGAGTGGAACTCAAGGAATACCTCTCTCTAGAA CTGCACGCTGTACCTGCATTAACATTAGTGATCGACCTATT
47	CXCL12	XM_001489644.5	CTTGCCGGTTCTTCGAGAGCCACGTTGCCAGAGCCAACATCAAACATCTTAAAATCCT CAACACTCCGAACTGTGCCCTTCAGATCGTGGCAAGGCTGAA
48	CXCL2	NM_001143955.1	TGCCAGTGCTTGCAGACCGTGCAGGGGATTCACTTCAAGAACATCCAGAGCGTGAAG GTGACGCCGGCGGGCTCCCACTGCGCCCAAACCGAAGTCATAG
49	CXCL6	NM_001081886.1	TGTCGCGGCCGCAGTGAGAGAACTGCGTTGCATGTGTTTAACCGTCACACCTGGGATT CATCCCAAAATGATCAGTAGTCTGCAAGTGTTCGCCGTGGGT
50	CXCL8	NM_001083951.2	CTTTCAATCCCAAACTGATCAAAGAAATGAGAGTGATTGAGAGTGGGCCACACTGCG AAAACTCAGAAATCATTGTAAAGCTCGTCAACGGAGCTGAGGT
51	DCN2	NM_001081925.2	AAAAATGCCCAAAACTCTTCAGGAGCTGCGTGTCCATGAGAACGAGATCACCAAAGT GCGAAAAGCGGTGTTCAATGGACTGAACCAGATGATAGTCGTA
52	DEFB1	XM_005606422.3	GGCCACAGGTCTGACCATTACATCTGTGCCAGGAGTGGCGGCACCTGTCACTTCTCCT CTTGCCCGCTCTTCACCAAGATTGAGGGCACTTGTTACGGCG
53	DPT	XM_001494376.3	GACTGTCTTGCACTCCACATACACAGTGTGCATGCTCACAGCCTGAAAAAGAGCCTG GTTCCTGGAGCACCTGTCATAGTCTTGCTGCTGCTTTTATTAC
54	DRA	NM_001284542.1	AGAATGTGGTGTGTGGCCTGGGCCTGGTTGTGGGTCTGGTAGGAATCATTGTTGGGAC CATCTTCATCATCAAGGGTGTGCGCAAAGGCAATGCTGTTGA
55	eCATH-1	NM_001081930.2	TTATCCAGAGACATCAGCAGATGATTCGTGACAAGAGTGAAGCAACTCGTCATGGTAT CAGGATTATTACTCGACCTAAGCTCCTTCTAGCATCCTAGGG
56	EGFL7	XM_001496705.4	CAGCTGGACCGCATCGACTCCCTGAGCGAGCAGATCTCCTTCCTGGAAGAGCAGCTG GGGTCTTGTTCCTGCAAGAAGGAGCTGTGACAGGCCGGACCAA
57	EGFR	XM_001497730.2	GAGAACCTGGAAATCATACGTGGCAGAACCAAGCAACATGGTCAGTTTTCTCTTGCG GTCGTCGGCCTGGACATTACATCTTTGGGATTACGCTCCCTCA
58	ELN	XM_014729930.1	TCCTGGGATTGGAGGCATCGCAGGGGTCGGGGCTCCAGCTGCTGCTGCAAAGGCGGC TGCTAAGGCAGCCAAATATGGAGCTGCTGGAGTTGGAGTCCCT
59	EPCAM	XM_001917795.4	GGTGTGTGAACACTGCCGGCGTCAGAAGAACTGATAAGGACTCTGAAATATCCTGCT TGGAACGAGTGAGGACCTACTGGATCATCATTGAACTAAAACA
60	ESPN	XM_014737583.1	AGACCAAGCAACCCGACTCGGGCATGTCCTCGCCCAATACCACCATGTCGGTCCAGC CACCGAACTTTGACCTCAGCTCGCCTACCAGCACCCTCTCCAA
61	FAP	XM_001494189.2	TAGTCATCGCCTTGGTGGATGGTCGAGGAACGGCTTTCCAAGGTGACAAACTCCTGTA CGCAGTGTATCGAAAGCTGGGTGTTTATGAAGTTGAGGACCA
62	CD23	NM_001081807.2	TCCCATTTAAAATGACAGCCCTGACTCCCAGTCCGTTTTACTCCTCTGTACTCTCCCAC CACGGCACCCTTCTCCTTCCGACAAGATGTGTAATTCACTG
63	FGF18	XM_005599689.1	CAGCAAGGAGTGTGTGTTCATTGAGAAGGTCCTGGAAAACAACTACACAGCCCTGAT GTCGGCCAAGTACTCCGGCTGGTACGTGGGCTTCACCAAGAAG
64	FGF7	NM_001163883.1	TCAAGTTGCACCAGGCAGACAACAGACATGGAATTCTTGTGTATCCAGCTGTTATCAA CAGAACAAAAGTCAAGTAGCAAACAGCATCGCAGCAACTGAG

65	FGFR1	XM_001492145.5	ATCTATTGCACGGGGGCCTTCCTCATCTCCTGCATGGTGGGCTCTGTCATCATCTACAA GATGAAGAGTGGCACCAAGAAGAGTGACTTCCACAGCCAGA
66	FLIT3LG	XM_023650139.1	TGGATGAGAAGGCTCAAGACTGTGGCTGGGTCCCAGATGCAAAACCTGCTGGAGGAT GTCAACACCGAGATACTCTTTGTCACCTTATGTGCCTTCCAGC
67	FN1	XM_023642281.1	CAATGCCAGGACTCGGAAACCCGAACGTTTTATCAGATTGGAGACTCCTGGGAGAAA TATGTGCATGGTGTCAGGTACCAGTGCTATTGCTATGGCCGTG
68	FoxP3	NM_001163272.1	GGCTCCTGAGAAGCAGCGGACACTCAACGAGATCTATCACTGGTTCACACGCATGTT CGCCTTCTTCAGAAACCACCCTGCCACCTGGAAGAATGCCATC
69	G6PD	XM_001492232.6	GACAACATCGCCTGTGTCATCCTCACTTTCAAGGAGCCCTTTGGCACTGAGGGCCGC GGGGGCTACTTCGATGAATTTGGGATCATCCGGGACGTGATGC
70	GAPDH	NM_001163856.1	GACCAGGTTGTCTCCTGCGATTTTAACAGTGACACCCACTCTTCCACCTTCGATGCTG GGGCTGGCATTGCCCTCAACGACCACTTTGTCAAGCTCATTT
71	GATA3	XM_023631902.1	TTGCAGGAGCAGAATCATGAAGCCGACAACCGATGGATATATGTTTTTGAAGGCAGAA AACAAAATGATGTTTGCCACTTTTGCAGAGGAGCTCACTGTG
72	HSP90B1	NM_001163873.1	TGGGTCCAGCAGAAAAGAGGCCGAATCTTCTCCGTTTGTTGAGCGACTTCTGAAAAA GGGCTACGAAGTGATTTATCTCACAGAACCTGTGGACGAATAC
73	GUSB	XM_001493514.2	GTGCGCAGGGACAAGAATCACCCAGCTGTCGTGATGTGGTCTGTGGCCAATGAGCCT GCTTCCTACCTGAAACCTGCTGGTTACTACTTCAAGACGCTGA
74	GZMA	XM_001494044.5	TCCCTAAAAAGGGGGATGACGTGAAACCAGGAACAGTGTGTCGAGTTGCAGGGTGG GGGAAGTATTCCAATAGGTCACCTGCATCTGATATCTTGAGAGA
75	GNZMB	NM_001081881.1	GGGGCCCACGACATCGAGAAGCAGGAGACAACCCAGCAGAATTTCTCTGTGAAAGC AGCCATCCCACACCCAGACTATAACCCTAAGAACTACTCCAACG
76	HCST	XM_001493266.5	CAGAAGCTTTGGTCATCCTGGGTCCTTCTCTCTCATACATACCCACATCCACTCCATCA GCAAGCTCTACTTCCAAAACCTTCCAGAATCTCCCTAGTGC
77	HGF	XM_014739139.2	AAAGCAAGAAAACGATGCCTCTGGTTCCCTTTCAATAGTATGTCAAGTGGAGTGAGA AAAGAGTTTGGCCATGAATTCGACCTCTATGAAAACAAAGACT
78	HIF1A	XM_014735822.1	CCTCAAAGTGCGAGCACGATTACAGTATTCCAGCCGACTCAAATGCAAGAACCTGCT CTTCCTACCGTCACTAACACTGCTGCCAATGATGAATTAAAAA
79	HPRT1	XM_014729196.1	GTGTCATTAGTGAAACTGGAAAAGAAAAATACAAAGCCTACGATGAGAATTCAGGTT GAGTTGAGAAACATCTGGAGTCTCATTGAAATCACCAGTGAAA
80	HTRA3	XM_005608928.2	CCAGCAACCCAGACCTTCCGACGGTCAGCAGTGGCATTTATGTGCAAGAGGTTGTTC CGAATTCACCTTCTCAGAGAGGGGGCATCCAAGATGGCGACAT
81	ICAM1	XM_014741568.2	GGGGTCAACTGGAAGACCTTCGAACTGAGTGATGTGCGAGAGGACATCTCTCCAATA TGCTACGCAAACTGTCCCAACCAGACGGAGTCTTCAGTGTCCA
82	ICOS	XM_001497868.6	AGTGTGCACGACCCTAATAGTGAATACATGTTCATGGCTGCGGTGAACACGGCTAAGA AGCCTAGACTCGCAGATGTGAGCCGTCATTTGGAACTCTCTG
83	IDO1	XM_014736538.2	GGAGGAACTACCTCACCCTTATGATGACTGGATTTCCATTGCTAAAAATCTGCCAGCA CTGATTGAGAAGGACCAGTTACGTGCAGAAGTTGAGAAGTTA
84	IFNA1	NM_001099441.1	TCGTCTGCTGCCTGGGACGAGAGCCTCCTAGACAAGCTCTACACTGGACTCTATCAGC AGCTGACTGAGCTGGAAGCCTGTCTGAGCCAGGAGGTGGGGG
85	IFNAR1	XM_001494639.5	GTGACCGGAAACCAACTCTCAAATGGTAGGGAGTTTTGTGGGAGTTTACCGGGAGCC TGACCTCTTTGCTTCTCTCAGTAAGTATCAAGAAGATTTTCGG
86	IFNb1	NM_001099440.1	TGCCCCGAGGACACAATGAACTTCCAGGTCCCTGAGGAGATTGAGCAAGCACAGCA GTTCCAGAAGGAGGATGCTGCATTGGTCATCTATGAGATGCTCC
87	IFNG	NM_001081949.1	CATGGACACCATCAAGGAGGACCTGTTCGTTAAGTTCTTTAACAGCAGCACCAGCAA GCTGGAAGACTTCCAAAAGCTGATTCAGATTCCGGTAAATGAT
88	IGF1	NM_001082498.2	CGCTCTTCAGTTCGTGTGTGGAGACAGGGGCTTTTATTTCAACAAGCCCACAGGGTAC GGCTCCAGCAGTCGGAGGGCGCCTCAGACAGGCATCGTGGAC
89	IGFBP4	XM_014736810.2	TTATTGACCACGTACTACATGCCACTTCTAGTTTTCAGCCCTGGGGCCTCTTATTCTGC CTTCCTCTGATTTAGGGATGTGGGGCCACCTCCTATAAGAT
90	IL10	NM_001082490.1	GCGGCGCTGTCATCGATTTCTGCCCTGTGAAAATAAGAGCAAGGCAGTGGAGCAGGT GAAGAGTGCCTTCAGTAAGCTCCAAGAGAAAGGTGTCTACAAA
91	IL12A	NM_001082511.2	GTTGATAGATCCTCAGAGGCAGATCTTTCTGGATGAGAACATGCTGACAGCCATTGAC AAGCTGATGCAGGCCCTGAACTTCAACAGTGAGACTGTGCCA
92	IL12RB2	XM_001499968.4	CAAACAAGACTGCTCGCGATGTTCCCGCTGCAACAAGTTAATCCTCTACAAGTTCGAC AGAAGAATCCATTTTCAGCAGGGTCGCTCCCTCAGTTCTCAA
93	IL13RA2	XM_001490946.5	GAAGTTCAAAGCTCGTGGGCAGAAGTTACTTATTGGACATCACTACAAGGAAATCTG GGAACTAAAATTCAGGATATGGACTGTATATATTACAACTGGC
94	IL17A	NM_001143792.1	GACAAGAACTTCCCTCAGAATGTGAAGATCAACCTAAACGTCCTTAACCGGAAAACG AATTCCAGAAGGGCCTCAGATTACCACAACCGCTCCACCTCCC
95	IL17B	XM_001503774.4	ACAAGAGGAGCCTGTCGCCCTGGGGCTACAGCATCAACCATGACCCCACCCGTGTCC CTGCGGACCTGCCGGAGGCGCGGTGCCTGTGTCTGGGCTGCGT
96	IL1B	NM_001317261.1	GACTCCGGGACATATACCATAAATCCCTGGTGCTGTCCGGTGCATGTGAGCTGCAGGC TGTCCACCTCAATGGAGAGAATACAAACCAACAAGTGGTGTT
97	IL1RA	NM_001082525.2	TCTACCTCCAGGAGGACCAGTAGAACTGCCCGTAGCTCCGCTTCCCCTATTCCCAGCA CGTCGATGACTCCAGAGACTGCCTCTCCACCCCAGGGTCTCC
98	IL2	NM_001085433.2	ACTCTTGGCTTGCATCGCACTAACTCTTGCAGTCCTTGCAAACAGTGCACCTACTTCA AGCTCTAAGAGGGAAACACAGCAACAACTGAAGCAATTACAG

99	IL21	XM_001503013.4	CCTCTCCCTGAAGGATGAATAAATAGGTAGCTTTACTGACAACCTGTTCACAGTCAAA CTGAAGTGAAAACTGAGACCAAGGTCTTGTTCTACTGGCACT
100	IL21R	XM_001496989.3	CTGAGGCCACAGAAAAGGCTGATCTCGGTGGACTCGAGAAGCGTCTCCCTCGTTCCC TTGGAGTTCCGCGGAGACTCGAGCTACGAGCTGCAGGTGCGGG
101	IL22	NM_001309428.1	TCAAAGCAATTGGGGAACTGAATTTGCTGTTTATGCGGCTGAAAAATGCCTGCATTGG ACCAGAGAAAAGCTGGAAAATGGATAACTAATCCTTCTTGCC
102	IL23R	XM_023641892.1	GTATTTCAAGTGAGATGTCAAGAAACGGGTAAAATTTACTGGCAGCCCTGGAGTCCAC CTTTTTTTCATAAAACACCTGATGCAGTTCCCCAGGTCACCC
103	IL2RA	NM_001111342.1	TGCGAGAAGGGCTTCCGCAGGATAAGCAAAGGGTCTCTCGCCATGGTTTGTAAAGGA AACTCGAGCCACTCTTTCTGGGAACAGACGTGTCACTGCGTCC
104	IL33	XM_001492329.5	AAAGGCACGCAGGTTGCCCATTCCAAAAGTGGAATAAAACACCAAGTTTGTTTATAG ATGCCGGAAACTTCAGATGCCTCTATGGCTAGGCAGGTAATAT
105	IL4	NM_001082519.1	CTGGTCTGCTTACTAGCATGTACCAGCAACTTCATCCAGGGATGCAAATACGACATCA CCTTACAAGAGATCATCAAAACGCTGAACAACCTCACAGATG
106	IL5	NM_001082499.1	TAGTGGCAGAGACCTTGACACTGCTCTCCACTCATCGAACTCTGCTGATAGGCGATGG GAACCTGATGATTCCTACTCCTGAACATAAAAATCACCAACT
107	IL6	NM_001082496.2	GAAAACAACCTGAATCTTCCAAAGATGGCAGAAAAAGACGGATGCTTCCAATCTGGG TTCAATCAGGAGACCTGCCTGATGAAAATCACCACTGGTCTTT
108	IL7	XM_001491850.6	GCCATAGCCCAGCTTTCGCCCTACACATTTGCGGCTTTCGTGGATACATTAGCAAGCG ATGCTTTTAGATCCCAGTCGCCTGGCTTTGCCAAGGCGGCTA
109	IRF3	XM_014729821.2	CCTGCCCGAATGTGGAACCCGCTGAAAACCCACTGAGGCAGCTGTTGGTGCCCGAGG ATGCGTGGGAGTTCGAGGTGACCGCCTTCTACCGGGGCCGACA
110	CD11a	XM_001496070.1	CCGGTCAAGTCCTGCACTGAGTTTTGGTTCCACTTCCCGGTGTGCATTCAGGACCTCA TCTCTCCCATCAATGTCTCCCTAAATTTCTCTCTCTGGGAGG
111	CD11c	NM_001114177.3	CGCCGATGTCTGCCTTCGTATTTATGAAAGTCCCAAGAACCGGCTGGGTGACCTCCAA AGCTCTGTGACCTTTGACCTGACCCTTGATCCTGGCCGCATG
112	CD18	NM_001301217.1	AATCCGAAGTACGAGGGAAAATGAGCACTCGCTGTGCAAATTTCACAACACTGAATG CAAAGCAGTACTTTTCCTAGTCACAGTAAGGTAGCTGTAGGGC
113	KRT4	NM_001346204.2	CTCTTTTTCTGGGGCTTCTCTTAGCAGTGTCACCTCAGTGCTGGGGTGTGGACTCTGC CCTCTTGGAGTTTGGTAGCTTCTTCTCGATTTGGGCTTGGTG
114	LAMA5	XM_001914998.2	GGGCCCTTCAGGACCATCCGAGATGCCTACCAGTTTGGGGGTCCTCTGCTCAGTTACC TGGAGTTTGCACACGTCCCGGCACCTCCCGGGGACTGGTCCC
115	LCN2	XM_005605819.2	GGTGACATTAAACGTTACTTTGGAGTGCAGAGCTATATCGTGCGCGTGGCGGACACCG ACTACAACCAGTTTGCCATCGTGTTCTTCAGGAAGGTTTACA
116	LGALS3	XM_005605195.2	GAAGCCCAATCCAAACAGGTTTGCTTTAAATTTCAACAGAGGGCATGATGTTGCCTTC CACTTTAACCCGCGCTTCAACGAGAACAACAGGAGAGTCATT
117	CD16	NM_001317252.1	ATTCTGAGTTCCACATTCCAAAAGCAAGACAAGAAGACAGTGGCTCCTACTTTTGCA GGGCGCTTATCGGGCCTAGTAGAAACGAGTCTTCAAAGGCTAT
118	C3	XM_023644588.1	GATACATCAAGAAATGATTGGTGGCTTCCGGAATGCGGAGGAGAAAGACGTGTCCCT CACAGCCTTTGTTCTCATCGCACTGCAGGAAGCTAAAGATATT
119	CLEC4A	XM_023644029.1	GGCACCCAGGTGAACCCAGTAATCCTAGTGAGCGTTGTGTTATCCTAAATTATGCATCA AAACAATGGGGCTGGAACGATGTCTATTGTCATGGAGCTCA
120	HAS1	XM_005596467.3	GCTGCAAGCGCCAGGTCGTGTACGCCGCCTTCAAGGCGCTGGGCGCCGCCTTTGGAG TGAGAAAAACTCCCAGGCATTTGGTAACCAGAGTACAGAAGTG
121	LUM	NM_001081780.2	AGATCCTGGGACCTCTATCCTACTCCAAGATCAAGCATTTGCGTTTGGATGGCAATCGC CTCACCCATACTAGTCTGCCACCTGATATGTATGAATGTCT
122	LYZ	XM_001494130.3	TGGCGTGGAGAAATCGTTGTCAGAACCACGACCTCACTCAGTATGTCAAGGGTTGCA GAGTGTAACTGAGGAGGTGTCCTTCTTCAGCTCATCTTGTCTT
123	MARCO	XM_005601449.3	AAGGTCAAAAAGGTGACTCCATGTTAGCGGTCAGGATCATTGGCTCTAGCAACCGAG GCCGGGCTGAAGTTTTCTATAACGGTTCCTGGGGAACAATCTG
124	MMP1	NM_001081847.2	GTTGCTGACAAGTACTGGAGGTACGATGAATATAAACGATCTATGGATGCAGGTTATCC CAAAATGATAGCAGATGACTTTCCTGGAATTGGCGACAAAG
125	MMP11	XM_001490252.2	CACCAGATGCATGCGACGTCTCCTTTGACGCGGTCTCCACCATCCGTGGCGAGCTCTT CTTCTTCAAGGCAGGCTTTGTGTGGCGGCTGCGTGGGGGCCG
126	MMP13	NM_001081804.1	AGACGTTAAAAAGATAAGTGCAGCTGTTCACTTTGAGGACACAGGGAAGACTCTCTT CTTCTCAGGAAACCAGGTCTGGAGGTATGATGATACTAACCGT
127	MMP2	XM_001493281.1	GGAGCACTCACAGGACCCTGGAGCCCTGATGGCGCCCATTTACACGTACACCAAGCA CTTCCGCCTGTCCCATGATGACATCAAGGGCATTCAAGAGCTC
128	MMP3	NM_001082495.2	AGCTCTGAAAATCTGGGAGGAGGTGACTCCACTTACATTCTCCAGGATTTATGAAGGA GAGGCTGACATAATGATCACTTTTGCAGTTCGAGAACATGGA
129	MMP9	NM_001111302.1	TTGGGTCCAGGGGAGGAGGTCTGCAACGTGGACATCTTCGATGCCATCGCGGAGATC GGGAATCATCTCCATTTCTTCAAGGACGGGAGGTACTGGCGAC
130	MRC1	XM_001497471.3	TGCCTTCATTTGCCAACGGCATAACAGCAGCATCAACGCCACGGCTATTCCTACCACG CCGTCCGTCCCAGGAGGTTGTAAGGAAGGTTGGAGTTTTTAC
131	CD20	NM_001309429.2	TGCTTGTATCCTCCACATCTCTCTCTGGTCTTTGCGTGGAGTGGCCAGCTCCCTCTCTC TCGTTCAGACAATTATAGCCACTTTAGCAGACTGTGTCCTC
132	MSR1	XM_001488563.5	CTATTCTGAATGAGGGCCCATTAGAGAAGTCAAGGTCTGCTGACTTATAGACCTAATAT GTCATATATCCAAGTGAGCTGCCAGAGTGGTTAGGGGATAA

133	MXRA5	XM_001500228.4	CTTTCTTGACTCGACCAACTCAAGTACCTGAGGTGAAGATTCCATACCAAGTGGAGAGTTTGCTGGTTCCCACGTCTTGGGTTGATAGCACAGTTGGCAC
134	MYH1	NM_001081759.1	GGAGCGAATTGAAGCCCAGAATAAGCCTTTCGATGCCAAGACATCAGTTTTTGTGGCTGACCCTAAGGAGTCCTTTGTGAAAGCAACAGTGCAGAGCAGG
135	CD56	XM_001501933.3	CCATCAGACACTATCTGGTCAAGTACCGAGCGCCGTCCTCCGAGTGGAAACCAGAGATCAGGCTTCCATCTGGCAGTGACCACGTCATGCTCAAGTCCCT
136	NKP46	NM_001256845.1	GCACTCACAAGACGGTTGAGTATCAGCTGCATTTCGAAGGACAACTTTCTGCTTCAGAGAGACCAAAAACACCTGGAATGATGAACAAAGTCAAGTTCCC
137	NLRP3	XM_014730834.1	CCTCAGATGCCACCTACTCTCCTCGGTTGGTGAACTGCTCTCTCACTTCCAGCTTTTGTCAGAGCCTCTTCTCAGCCCTGAGCACTAACTGGAGCCTCAC
138	NOD1	XM_001499566.3	TCGGAGGGGACCAGCCGTCCTATGAGTTTTTCCATCTCACCCTCCAGGCCTTCTTTACCGCTTTCTTCCTCGTGGTGGATGACAAGGTGGGCACCCGGGG
139	NOD2	XM_014738410.1	TGTAAGAAATTCATGTCCAAGCTGAGGACCACGGTATCTGCTCAGTCTCGCTTTCTGAACACCTATGATGGGGCAGAAAATCTTTGCCTGGAGGAAATAT
140	NOS2	NM_001081769.1	GGTATGCTGTGTTTGGCCTTGGCTCCAGCATGTACCCTCAGTTCTGTGCCTTCGCTCATGACATTGACCAGAAGTTGTCTCACCTGGGGGCCTCGCAGCT
141	NOTCH1	XM_001498582.2	GCAGTGCTGGAAGTATTTCAGCAACGGCCACTGCGACAGCCAGTGCAACTCGGCCGGCTGCCTCTTCGACGGCTTCGACTGCCAGCGCGCGGAGGGCCAG
142	NPDC1	XM_023629427.1	GTGACGGCCTCGCCCTCGTGCTGGTCGTGGTGTGCTCCGTGGCCGGCGCCGCCGCCTTCGCCGTGGCCGCTCTTTGCTGGTGCAGGCTGCAGCGGGACGC
143	NXT1	XM_005614879.2	GACTTGCCAGCCGTGCCCGACGAGGCCACCCGAAGCCAGACACGGTCCTTGTCGTCATCTGTGGGACCCGTGAAGTTCGAGGGCAACAAGCAGCGGGACT
144	OSM	XM_001495055.4	CCCCAAAGCCCGGGACTGGCTAACGGTGACAATGAACATCCGTGGGTTCCAGAACAACATCCACTGCCTGTCCCAGCTGCTTCGTGCCTCCTCGGAGACG
145	OSMR	XM_001496993.1	TTCTGGAAGCCGCTATCAAAATCGCATGCCAATGGGAAGATTCGATTCTATAATGTCATTGTCGAAAATCTAGACAAACCATCCGAATTAGAGCCCGTCC
146	PALMD	XM_001489422.4	ACAAGCTTCAGAGAGAAACTCTAAATCTCCCACAGAGTATCACGAGCCTGTATATGCCAATCCATTTTGCAGGCCTATTACTCCACAGAGAGAGAAGGTA
147	PCSK1N	XM_023633514.1	GCAGCTTTGCCCGCTAGCCCGAGCGCTGCGCATTTGCCAGCCAGTCCGCCCGTCCGGAGCCCGGCTCGCTGGGGCAGTATGGCGGGGTCGCCGCTGCTCC
148	PDGFRA	XM_001492277.5	ACTGCCTCTTGGCAGTGCTTTAGTAGCATCTCAGCGGTGTGTGAAGTTTGGAAGTAGACGGACAAGGAAATAATAGGCCGTGGAAGACGAACTTTGTATT
149	PI3	XM_001503186.5	ACCCTCTCTCACACTGCCCATTCTTCCTCTCGTTCAGGAAGCCCAAGCCCGGGGCTGCCGCCCTCAGTGACTTTCCAATAAAAGACTGCTTTGTGCTCCA
150	PIK3CA	XM_001494941.5	CTTGGTAAAAGATTGGCCTCCAATCAAACCTGAACAGGCTATGGAGCTTCTGGACTGCAATTACCCAGACCCTATGGTTCGCGGTTTTGCTGTTCGATGC
151	PLCG2	XM_001501998.6	ATACTTTCCGTCTAATTACGTCGAGGACATCTCAACAGCTGACGTGGAGGAGCTGGAAAAGCAGATTATTGAAGACAATCCCTTAGGGTCTCTCTGCAGA
152	PLVAP	XM_005604171.2	CCGCGCACCCTCGACATGGGCTACAGCCTGTACCATCCCATCAACCCGGAACTGGCGTCCATCCGGAGGACCTGCGACCACTTGCCCACCATCATGAGCA
153	POLR2A	XM_014728559.2	CATGGAGCAGATTGCTGAAAAGATCAATGCTGGTTTTGGCGATGACTTGAATTGCATCTTTAATGATGATAACGCAGAGAAGTTGGTGCTCCGTATCCGC
154	POSTN	XM_001495813.2	GTACCACATTTTAAATACTCTCCAGTGTTCTGAGGCTATCATGGGAGGAGCAGTCTTTGAGACTCTGGAAGGAAACACAATTGAGATAGGTTGTGATGGT
155	PRF1	XM_001502776.5	ACCTCCTCGGCAGCTGTGACCATGCTCCGAAGTCTGGCTCACATACGGTGATGTGCCCTCTGAACCACGGCCTCCTGAAATTCTCCTACCAAGCCAAGTG
156	lubricin	XM_023640721.1	ACCACCATGAAGCCTCCCACTACTCCCAAGAATCTTGCTGAATCAACTCCTGAGTTTCCTGCAGAACCCACACCAAAGGCTCTTGAAAACAGTCCCAAGG
157	PTGER4	XM_001499068.4	CCTGGCTTTTGAGCACTTTTCAAACGAGCAAGGTGATTCACATGGGTCCCGAGGTCTGAAGCACATCGGTTGCCACCTCGTTATGACACAGGATTTCCGT
158	PTGES2	XM_005605814.2	GCAAGTTCGGGGTCGTGGAGGGTGCTGTGGCCAAGTACATGGGTGCAGCTGCCATGTACCTCATCAGCAAGCGGCTCAAGAGCAGGCACCACCTCCAGGA
159	PTPRC	NM_001309162.1	ACGCAGCAGCTCCAGGCGAGGTCAGAAACCTAAGGGCTTCGCGGATTTCAGATAATACCATGCGCGTGACTTGTGATGCTCCTGTGGAGCGTAATGGCCC
160	RGS5	XM_001492029.5	CCAAAGATTAGGCCAGGTGATGGCCCATAACCAAAGTTTTTCTCCCTGGGTTTGATATGGTTTGGGGTTGGCGTCAGATTAGGATCTAAACTGGACTGGA
161	RPL30	XM_001491150.6	TCCACAGCTCTGCGCAGCAGAGTAACACAGCGCCTAGACGCCTAAGGCCGGCAGCCGGGCGAAGCGTTCGCCGCAACCGCCACTCTAACTAGCGGTATTT
162	RRM2	XM_001502334.3	TCCATATTCTGGCTCAAGAAACGAGGACTGATGCCCGGCCTCACATTTTCCAATGAACTTATTAGCAGAGATGAGGGTTTACACTGCGACTTTGCCTGCC
163	RTL5	XM_023634495.1	CTGCCGCCGCTGGAGCGGCCTGAGATAGAGCCCTTTTCAGGAGACCCAGTCTACCTGGCTGAGTTCCTCATGCAGCTAGAGACCTTCATAGCCGACCATG
164	S100A4	XM_001494605.6	GGAAAAGGACAGATGAAGCTGCATTCCAGAAGCTGATGAGCAACTTGGACAGCAACAAGGACAACGAGGTGGATTTCCAGGAGTACTGTGTCTTCCTGTC
165	S100A8	XM_001493589.4	TCAGGCGTGCATGTCCTCTGTCAATTCTGTTTCGGGGAGACCTGGTGGGGCAACTCCTTGGGCATCATGCTGACGGATCTGGAGAATGCTATCAACTCCC
166	S100A9	XM_001494378.5	ATTCAAACAGCTGGTTCAAAAAGAGCTGGCGAACTTCCTCAAGAGTAAGAAGAAGGATGAGAAAGCCATAAATCATATCATGGAGGACCTGGATACCAAT

167	SAMD14	XM_014741082.1	GCTCGCTTGAGTCATGGCTTCTTCAAAGCTCCGAGAACCCGCGGATGAAGTTTTCGACTTGGACTTGGCTGTGCCAGAGACCGTCAGACTGGACAGCAGT
168	SCGB1A1	NM_001081858.2	TTCAAGGCCTCTTCCTGGGCACACCTGCCAGTTTCGAGGCTGCAGTGGAACCCTTCAAACCTGATGCAGACATGAAAGCTGCGGCGACCCAGCTGAAGAC
169	SERPINF1	NM_001143954.1	AATAAGAACTTCAAGAGCGCTTCCCGAATCATCTTCGAGAAGAAGCTGCGCATCAAATCCAGCTTTGTTACACCACTGGAGAAGTCATATGGGACCAGGC
170	SMAD3	XM_001496822.3	TACATCGGAGGGGAGGTCTTCGCAGAGTGCCTCAGCGACAGCGCTATCTTCGTCCAGTCTCCCAACTGTAACCAGCGTTATGGCTGGCACCCGGCCACCG
171	ENSECAG00000039617	XM_023617169.1	AGAAAACCAAGGAGCAGGCATCACATCTGGGAGGAGCCGTGTTCTCTGGGGCTGGAAACATCGCGGCAGCCACGGGTCTCGTGAAGAGGGAGGAATTCCC
172	SOCS1	XM_005615004.1	TGTTGTAGCAGCTTAATTTAACTGTGTCTGGCGCCGGAACCTCCTACCTCTTCATGTTTACATATACCCACTTATCTTTGCACAAACCAGGGGTTGGGGG
173	SPARCL1	XM_001496019.4	GGAAAACCTGGCCTTGAATTTATCAGCAACCACGAGGAGATGGATAAAAAGACTGTTTCTGAGGCTTTGCTCGTAGATCCTACTGATGACGGTAACACCA
174	SPP1	XM_001496152.4	CAGAAGCAGAATCTCCTAGCACCACAGACCGTGTCCTCTGAAGAAACTGACAACCTCAAACAAGAGACCCTCCCAAGTCAGTCCAACGAAAGCCATGACC
175	SRPX	XM_001489643.3	GTGATAATTACGGAGCCACTTGTGAGTTCTCCTGCATCGGTGGCTACGAGCTACAGGGTAGCCCTGCTCGAGTATGTCAGTCCAACTTGGCTTGGTCTGG
176	STAT1	XM_001499369.6	GGGCTTCATGCATCTTATTAAAGGTAAAATTGAGAGACCCTCTCCACAGAGTGGGTTTGACAAACGAACAACATTCAGATACACCCACAACCTCAGGACT
177	STAT3	NM_001309512.1	ATCAGCTTAAAATTAAAGTGTGCATTGACAAAGACTCCGGGGACGTTGCAGCTCTCAGAGGATCCCGGAAATTTAACATTCTGGGCACAAACACAAAAGT
178	STAT6	XM_001488414.3	GAATCCGGGACCTTGCTCAGCTCAAAAACCTCTACCCTAAGAAACCCAAGGATGAGGCTTTCCGGAGTCACTACAAGCCTGAACAGATGGGTAAGGATGG
179	TANK	XM_001493298.5	TGGAAGCCCTTTCCTCATCAAGACAGTGACTTATCATCGGTACTCAGTGGCACGGGCGCAGAACTGCATATACCTCGAGTATGTGAATTCTGTCAAGCAG
180	TBX21	XM_005597928.1	CAGAGCCGGCCTGCATTACCTCCAAAACGCATGTCTTTACTTTCCAAGAAACCCAGTTTATTGCTGTGACTGCCTACCAGAATGCCGAGATTACTCAGCT
181	TERT	XM_003363842.3	ACCGTCTTCACAAACGTCTACCAGATATTCCTGCTTCAGGCCTACAGGTTCCATGCGTGTGTGCTCCAGCTTCCGTTTAATCAGCCAGTGAGGAACAACC
182	TGFb1	NM_001081849.1	CAGAGCTGCGCCTCCTAAGGCTCAAGTTAAGCGTGGAGCAGCATGTGGAGCTGTACCAGAAATACAGCAATAATTCCTGGCGCTACCTCAGTAACCGGCT
183	TGFB3	XM_001492687.6	GCGTGAATGGCTCTTGCGAAGAGAGTCCAACTTAGGTCTGGAAATCAGCATCCATTGTCCATGTCACACCTTTCAGCCCAATGGAGATATCCTGGAAAAC
184	TGFbR1	XM_014735926.1	TATGAAACACTTTGAATCCTTCAAACGTGCCGACATCTATGCAATGGGCTTAGTGTTCTGGGAAATAGCTCGACGATGCTCCGTTGGTGGAATTCATGAA
185	THBS4	XM_001503877.4	CCAATGCGCCGGTGTGATTCCAACCCATGTTTCCGTGGCGTCCGCTGTACCAACACCAGAGATGGCTTTCAGTGTGGGCCCTGTCCCGAGGGCTACACGG
186	TIMP1	NM_001082515.1	AGGTCGGAGAACCGCAGCGAGGAGTTTCTCATCGCCGGACAACTATTGGACGAGAAGCTGTACATCACCACCTGCAGTTTCGTGGCTCCCTGGAACAGTC
187	TIMP2	XM_001916682.2	TTCAAAGGACCTGACAAGGACATCGAGTTCATCTACACGGCTCCCTCCTCGGCCGTGTGCGGGGTCTCGCTGGACGTTGGAGGGAAGAAGGAGTACCTCA
188	TIMP3	NM_001081870.2	CAGCGCAAGGGGCTGAACTATCGGTATCACCTGGGTTGTAACTGCAAGATCAAATCCTGCTACTACCTGCCTTGCTACGTGACCTCCAAGAACGAGTGTC
189	TLR3	NM_001081798.1	TGACTAGCAACTCTTTTGCCTTGGTTCCAAGCCTTCAAAGACTGATGCTCCGAAGGGTGGCCCTTAAAAATGTGGACAGCTTCCCTCCACCTTTTCGCCC
190	TLR4	NM_001099769.2	ATCCAGGAAGGTTTCCACAAAAGCCGGAAAGTTATTGTCGTGGTGTCCCAGCACTTCATTCAGAGCCGATGGTGTATCTTTGAGTATGAGATTGCCCAGA
191	TLR9	NM_001081790.2	GGGAGACCTCTATCTCCGCTTCTTCCAAGGCCTGAGAAGCCTAATCCGGCTAGACCTGTCCCAGAATCGTCTGCATACCCTCCTGCCATGCACCCTGGGC
192	STING1	XM_005599365.3	GGATCCAAGTTTACAATCAGCTCCACAACAACGTACTATGCGGCGCAGGGAGCCATCGGCTGCACATCCTCTTCCCATTGGATTGTGGGGTGCCTGACGA
193	TNC	XM_001916622.4	GGCTGGGATGGCCTCAAACTCAACTGGACCGCAGCTGACCAGGCCTATGAGCTCTTTGTCATACAGGTGCAGGAGGTCAACAGGGTGGAGGCGGCTCAGA
194	TNF	NM_001081819.2	CGACTTTGCGGAGTCCGGGCAGGTCTACTTTGGGATCATTGCCCTGTGAGGGGGGTACGTCCGTCCTCGCCCACCTCAATCCCTTTATTATCTGCTCCTT
195	TSLP	NM_001164063.2	CGAGTTGTCTCACCGAAATCGAGCGCCTTACCTTCAAGTCCAGCCAATGCCTGTCACTCGCCAAGAAAATTGTAACAGCAACTAACGCTACGCTCAACAG
196	TSPAN15	XM_014733020.1	CATCTACTCCACAGTGTTTTGGCTGATTGGGGCCCTGGTCCTATCAGTGGGGATCTACGCAGAGGTCGAGCGGCAGAAATATAAAACCCTCGAAAGTGCC
197	UNC93A	XM_001499947.1	AAGCTTCTCAGAGATAAACGTCTGTGTCTCCTCATTCTGCTGCCCGTGTACAGTGGGTTTCAGCAAGCCTTCCTCTCGGGTGACTACACGAGGTCGTACG
198	VCAM1	XM_005610265.3	TGACTTTCAGGTACTGAACACTTCAACCCGTGGTGTAATGGTTGGCTGGATTTCTCTGGATGGTACTGACATGGTACGGAGACCTGCTACGATGTTGATT
199	VEGFA	NM_001081821.1	CCCACTGCGGAGTTCAACATCACCATGCAGATTATGCGGATCAAACCTCACCAAAGCCAACACATAGGAGAGATGAGTTTCCTACAGCATAGCAAATGTG

200	ZFR2	XM_014741364.1	TCTGGAAGCCCAGAGCAAGAGGGCAGTGGGCACAGTGGCATCGACCCGTCGCCTCG GATCCTGAAAGGCGTGGTGCGGGTCGGCCTCCTGGCCAGCGGCC

Supplemental Table B2 – Significant genes of interest detected in this preliminary analysis (*Gene Cards Database https://www.genecards.org/*), the expression of which was significant increased compared to the control. LYZ and IL33 were specific to the lysis group, while TBX21 was specific to the sclerosis group. The remaining genes overlapped between these two groups.

Gene	Description
B2M	Encodes a component of MHC class I molecules, which are present on all nucleated cells and involved in presenting peptide antigens to the immune system. It plays a critical role in immune surveillance.
THBS4	Involved in cellular interactions, including cell-to-cell and cell-to-matrix communication. It plays a role in tissue remodeling and response to injury and may contribute to wound healing and angiogenesis.
LYZ	encodes lysozyme, an enzyme with bacteriolytic functions. It is important in the innate immune system and helps to defend against bacterial infections by hydrolyzing the peptidoglycan layer of bacterial cell walls.
CD8A	Encodes a protein that is a component of the CD8 receptor, which is expressed on cytotoxic T cells. The CD8 receptor plays a role in recognizing antigens presented by MHC class I molecules, which is important for immune responses.
CXCL6	A chemokine that plays a role in immune responses by attracting neutrophils to sites of infection or inflammation. It is involved in processes like angiogenesis and inflammation.
TBX21	Encodes a transcription factor critical for the differentiation of Th1 cells, which are important in the immune response to intracellular pathogens. It regulates the expression of IFN-γ and other immune-related genes.
PLVAP	Encodes a protein that plays a key role in the formation of diaphragms in fenestrated endothelia. It is essential for maintaining vascular permeability and is involved in the immune surveillance of tissues
IL33	A cytokine that belongs to the IL-1 family and functions as an alarmin, released upon tissue damage to activate immune responses. It plays a role in allergic inflammation, autoimmune diseases, and various other immune-related processes.